THE UNIVERSITY OF QUEENSLAND

AUSTRALIA

Bio-inspired oil-core silica-shell nanocapsules for controlled-release applications

David Wibowo

A thesis submitted for the degree of Doctor of Philosophy at

The University of Queensland in 2015

Australian Institute for Bioengineering and Nanotechnology

Abstract

Silica nanocapsules having core–shell architecture are of great interest in many current and emerging areas of technology. The core provides high-capacity loading of various actives, while the silica shell serves as protective envelope and diffusion barrier enabling controlled release of the active. Currently, production of silica nanocapsules is mainly based on templating methods using chemical surfactants to stabilize the template and to induce hydrolysis and condensation of silica precursors forming solid silica shell surrounding the template. Major drawbacks with the current methods are extreme pH conditions and/or elevated temperatures involving toxic chemicals that might pose undesirable environmental side effects and require tedious procedures for removing the chemicals. Inspired by Nature, biomimetic approaches have recently been developed to synthesize silica-based nanomaterials under mild physiological conditions through the use of biomolecules (i.e., peptides and proteins). This contrast in processing conditions and the growing demand for benign synthesis methods having minimum environmental risks have spurred much interest in biomimetic approaches. However, their utility is limited to biosilicification in bulk aqueous solution or at solid–liquid interfaces. There is no current biosilicification at oil–water interfaces, and thus fabrication of oil-core silica-shell nanocapsules using biomolecules has not been realized yet.

This thesis addresses the question on benign synthesis method for forming biocompatible oil-core silica-shell nanocapsules, by designing and utilizing biomolecules, in lieu of chemical surfactants, to facilitate formation and stabilization of oil droplets and to direct nucleation and growth of silica shells at the oil–water interfaces. The major outcomes of the work presented in this thesis are: (1) development of a designed bifunctional modular peptide, SurSi, comprising a surface-active module and a biosilicification-active module that led to novel emulsion and biomimetic dual-templating approach for making oil-core silica-shell nanocapsules with tunable silica shell thickness; (2) facile encapsulation and sustained release of model insecticide, fipronil, from the silica nanocapsules *in vitro* in water and *in vivo* against a model insect, termite; (3) development of a designed bifunctional modular protein, D4S2, for making silica nanocapsules, thereby extending conceptual design of SurSi peptide, so that the protein could be produced renewably through biological expression in industrially-relevant, microbial cell-factory *Escherichia coli* (*E. coli*); and (4) large-scale production of D4S2 protein for synthesis of fipronil-encapsulated silica nanocapsules which could then be used for termite field trial.

This work introduces, to the best of our knowledge, the first design and use of bifunctional modular biomolecules for making oil-core silica-shell nanocapsules. The dual-templating method developed in this thesis represents a new strategy for forming silica nanocapsules using components and

processes expected to have minimal environment footprint. Active molecule can be easily encapsulated in silica nanocapsules with high encapsulation efficiency, by directly dissolving the active in the oil core prior to silica shell formation, and then released controllably from the nanocapsules with the release kinetics depending on the silica shell thicknesses. Furthermore, the use of bifunctional modular protein that can be produced through *E. coli* expression system has opened opportunities for sustainable and scalable bioprocess routes to produce oil-filled silica nanocapsules, thus makes the platform developed in this thesis suitable for large-scale applications especially in the fields of biomedical and agricultural applications that demand biocompatibility, high encapsulation efficiency and controlled-release properties.

Declaration by author

This thesis is composed of my original work, and contains no material previously published or written by another person except where due reference has been made in the text. I have clearly stated the contribution by others to jointly-authored works that I have included in my thesis.

I have clearly stated the contribution of others to my thesis as a whole, including statistical assistance, survey design, data analysis, significant technical procedures, professional editorial advice, and any other original research work used or reported in my thesis. The content of my thesis is the result of work I have carried out since the commencement of my research higher degree candidature and does not include a substantial part of work that has been submitted to qualify for the award of any other degree or diploma in any university or other tertiary institution. I have clearly stated which parts of my thesis, if any, have been submitted to qualify for another award.

I acknowledge that an electronic copy of my thesis must be lodged with the University Library and, subject to the policy and procedures of The University of Queensland, the thesis be made available for research and study in accordance with the Copyright Act 1968 unless a period of embargo has been approved by the Dean of the Graduate School.

I acknowledge that copyright of all material contained in my thesis resides with the copyright holder(s) of that material. Where appropriate I have obtained copyright permission from the copyright holder to reproduce material in this thesis.

David Wibowo
January 2015

Publications during candidature

The candidate contributed to the following publications during the course of the candidature.

A. Peer-reviewed papers

1. **Wibowo, D.**, C.-X. Zhao, and A.P.J. Middelberg*, *Emulsion-templated silica nanocapsules formed using bio-inspired silicification.* Chem. Commun., 2014. **50**(77): p. 11325–11328.
2. **Wibowo, D.**, C.-X. Zhao*, B.C. Peters, and A.P.J. Middelberg*, *Sustained release of fipronil insecticide in vitro and in vivo from biocompatible silica nanocapsules*. J. Agric. Food Chem., 2014. **62**(52): p. 12504–12511.
3. **Wibowo, D.**, C.-X. Zhao, and A.P.J. Middelberg*, *Interfacial biomimetic synthesis of silica nanocapsules using a recombinant catalytic modular protein*. Langmuir, 2015. **31**(6): p. 1999–2007.

B. Conference abstracts

1. **Wibowo, D.**, C.-X. Zhao, B.C. Peters, and A.P.J. Middelberg*, *Peptide-directed synthesis of emulsion-templated silica nanocapsules*. 2014 International Conference on Nanoscience and Nanotechnology. 2–6 February 2014. Adelaide, Australia.
2. **Wibowo, D.**, C.-X. Zhao, B.C. Peters, and A.P.J. Middelberg*, *Biomimetic and emulsion dual-templating approach to silica nanocapsules.* 5th International NanoBio Conference. 6–10 July 2014. Brisbane, Australia.
3. Zhao, C.-X., **D. Wibowo**, and A.P.J. Middelberg*, *Sustainable molecular and chemical engineering of soft and hard materials.* 5th International NanoBio Conference. 6–10 July 2014. Brisbane, Australia.

C. Patent

1. Middelberg, A.P.J., C.-X. Zhao, **D. Wibowo**. *Silica micro- and nano-capsules and methods for making them*. PCT Patent Application (PCT/AU2014/050234). Filed: September 18, 2014. Assignee: The University of Queensland.

Publications included in this thesis

1. Wibowo, D., C.-X. Zhao, and A.P.J. Middelberg, *Emulsion-templated silica nanocapsules formed using bio-inspired silicification.* Chem. Commun., 2014. **50**(77): p. 11325–11328.

   – Incorporated as **Chapter 3**.

Contributors	Statement of contributions
Author Wibowo, D. (Candidate)	Designed experiments (60%) Conducted experiments (100%) Wrote the paper (60%)
Author C.-X. Zhao	Designed experiments (20%) Wrote and edited the paper (20%)
Author A.P.J. Middelberg	Designed experiments (20%) Wrote and edited the paper (20%)

2. Wibowo, D., C.-X. Zhao*, B.C. Peters, and A.P.J. Middelberg*, *Sustained release of fipronil insecticide in vitro and in vivo from biocompatible silica nanocapsules*. J. Agric. Food Chem., 2014. **62**(52): p. 12504–12511.

   – Incorporated as **Chapter 4**.

Contributors	Statement of contributions
Author Wibowo, D. (Candidate)	Designed experiments (70%) Conducted experiments (90%) Wrote the paper (65%)
Author C.-X. Zhao	Designed experiments (15%) Wrote and edited the paper (15%)
Author B.C. Peters	Conducted experiments (10%) Edited the paper (5%)
Author A.P.J. Middelberg	Designed experiments (15%) Wrote and edited the paper (15%)

3. Wibowo, D., C.-X. Zhao, and A.P.J. Middelberg. *Interfacial biomimetic synthesis of silica nanocapsules using a recombinant catalytic modular protein*. Langmuir, 2015. **31**(6): p. 1999–2007.

– Incorporated as **Chapter 5**.

Contributors	Statement of contributions
Author Wibowo, D. (Candidate)	Designed experiments (60%) Conducted experiments (100%) Wrote the paper (60%)
Author C.-X. Zhao	Designed experiments (20%) Wrote and edited the paper (20%)
Author A.P.J. Middelberg	Designed experiments (20%) Wrote and edited the paper (20%)

Contributions by others to this thesis

This thesis was drafted and written by the candidate under the supervision of Dr Chun-Xia Zhao and Prof Anton P.J. Middelberg.

Termite collection and devices set-up for termite control experiments, as described in **Chapter 4**, **Chapter 6**, and **Appendix A**, were performed by Dr Brenton C. Peters with the candidate.

All of the data and results presented in the figures of this thesis are solely the work of the candidate with the exception of the following figures in which the data were collected with collaborators:

- **Chapter 1**, Figure 1; **Chapter 3**, Scheme 1; and **Chapter 4**, Figure 1 – figure of SurSi peptide was modelled by Andrea Schaller;
- **Chapter 3**, Figure 2d – energy dispersive X-ray spectrum was taken by Lei Yu;
- **Chapter 4**, Figure 3d – selected area electron diffraction pattern was taken by Lei Yu;
- **Chapter 5**, Figure 1 – figure of D4S2 protein was modelled by Andrea Schaller;
- **Chapter 5**, Figure 3b – mass spectrum was taken by Dr Mirjana Dimitrijev-Dwyer;
- **Chapter 5**, Figure 5 – photographic images of the thin films were taken by Dr Liguang Wang.

Statement of parts of the thesis submitted to qualify for the award of another degree

None.

Acknowledgements

I would like to express my gratitude to the people that have made this thesis possible.

First and foremost, I thank my supervisor Prof Anton P.J. Middelberg for providing plentiful resources, and also his guidance, inspiration, and invaluable mentorship toward my PhD thesis. I appreciate Dr Chun-Xia Zhao, my supervisor, for her unwavering support, patience and kindness, and valuable insight in various aspects of my research.

The nature of research is collaborative. I would also like to thank Dr Brenton C. Peters for his tremendous interest, indispensable help and practical perspective throughout the collaboration. He always had answers for all my questions about termites. Special thanks to Dr Liguang Wang for his superb analytical work in the thin-film experiments.

I acknowledge the financial support provided by the University of Queensland. I also acknowledge the facilities, and the scientific and technical assistance of the Australian Microscopy and Microanalysis Research Facility at the Center for Microscopy and Microanalysis, as well as the Australian National Fabrication Facility at The University of Queensland that have made this thesis possible.

Life in the lab can be frustrating, but I am grateful to work with past and present members in Prof Middelberg's group that helped me in many different ways. I thank Dr Nani Wibowo for her generous help since day one. Her advices in various research aspects especially in biology-related experiments have definitely broadened my horizon. I appreciate the insightful discussions with Dr Mervyn Liew about general research problems and career concerns, and the numerous stimulating intellectual exchanges. I have also enjoyed his sense of humor and benefited from his words of wisdom. I thank Dr Tania Rivera Hernández for her helpful suggestion, encouragement and positive outlook; Dr Mirjana Dimitrijev-Dwyer for teaching me about mass spectrometry theoretically and practically; Dr Frank Sainsbury for his valuable suggestion on techniques for measuring DNA concentrations; as well as Dr Sheng Fang, Bijun Zeng, Melisa Anggraeni, Yuan Yuan Fan, Yang Wu, Arjun Seth and Alemu Tekewe for the discussions about experimental problems and the inspiring exchange of ideas. I very much appreciate Lei Yu for her patience to meticulously teach me with basic experimental techniques down to the smallest details, and her enormous assistance with my experiments. Thanks to Dr Natalie Connors and Andrea Schaller for introducing me with the beauty of computational modeling of biological molecules; Andrea has kindly provided me with the three-dimensional models of peptide and protein used in this thesis.

Thanks also to Doan Thanh Tam for organizing wonderful event for group togetherness during Christmas season in Stradbroke Island. I appreciate Lesley Forest for her gracious help to deal with administrative work. I also cherish her attention to the birthday of each member in the group. Social life in the group exists because of her.

I am thankful for all my friends who have made Brisbane a home away from home for me. They should be credited for balancing my life. Without their cheerfulness, kindness and ever-positive attitude, my PhD journey would not have been so lively, enjoyable and memorable. I look forward to seeing our friendship grow even more as we move on to the next stage of our lives. Finally, and most importantly, I owe much gratitude to my altruistic parents and my admirable brothers kilometers away from Australia. They have always been supportive and appreciative of whatever I do by giving me the freedom to pursue my interest. Their kind love and pray have fueled me to keep me running until the finish line.

Keywords

biosurfactant, bioprocess, biomimetic, interface, recombinant protein, emulsion, capsule, silica, nanocarrier, controlled release

Australian and New Zealand Standard Research Classifications (ANZSRC)

ANZSRC code: 100708, Nanomaterials, 40%

ANZSRC code: 030406, Colloid and Surface Chemistry, 40%

ANZSRC code: 100302, Bioprocessing, Bioproduction and Bioproducts, 20%

Fields of Research (FoR) classification

FoR code: 1007, Nanotechnology, 40%

FoR code: 0306, Physical Chemistry, 40%

FoR code: 1003, Industrial Biotechnology, 20%

Table of contents

List of figures

List of tables

List of abbreviations

ΔA	The change of the contact area between oil and water phases, m^2
ΔG	The change of the interfacial free energy, J or N/m
γ	Interfacial tension at oil–water interfaces, J/m^2 or mN/m
ΔP_L	Laplace pressure, N/m^2
d	Droplet diameter, m
d_n	Number-average diameter
G^f	Free energy of the system in its final state (after emulsification)
G^i	Free energy of the system in its initial state (before emulsification)
ΔG	Difference in free energy between G^f and G^i
ΔG^*	Activation energy that keep the system to be in a kinetically stable state
r	Radius of droplet, m
g	Acceleration due to gravity, m/s^2
ρ	Mass density, kg/m^3
η	Newtonian shear viscosity, kg/m·s
v_{Stokes}	Droplet velocity, m/s
C_f	Fipronil concentration in release medium, mg/mL
V_f	Volume of release medium, mL
C_i	Initial fipronil concentration in the Miglyol® 812 oil, mg/mL
V_i	Volume of the oil phase, mL
n	Number of repeated-release of fipronil
Ac	*N*-terminal acetylation, $-C(O)CH_3$
APTES	(3-Aminopropyl)trimethoxysilane, $H_2N(CH_2)_3Si(OCH_3)_3$
C. acinaciformis	*Coptotermes acinaciformis*
C. lacteus	*Coptotermes lacteus*
CTAB	Cetyltrimethylammonium bromide, $CH_3(CH_2)_5N(Br)(CH_3)_3$
CTAC	Cetyltrimethylammonium chloride, $CH_3(CH_2)_5N(Cl)(CH_3)_3$
CV	Column volume
DLS	Dynamic light scattering
DMDES	Dimethyldiethoxysilane, $(CH_3)_2Si(OC_2H_5)_2$
DMF	*N*, *N*-dimethyl formamide, $HCON(CH_3)_2$
D4S2	Designed bifunctional modular protein comprising a surface-active module and a biosilicification-active module
DNA	Deoxyribonucleic acid
E. coli	*Escherichia coli*
EDTA	Ethylenediaminetetraacetic acid, $(HO_2CCH_2)_2NCH_2CH_2N(CH_2CO_2H)_2$
EDX	Energy dispersive X-ray spectroscopy
FT-IR	Fourier transform-infrared

GABA	γ-Amino butyric acid, $C_4H_9NO_2$
HEPES	sodium 4-(2-Hydroxyethyl)piperazine-1-ethanesulfonic acid, $C_8H_{17}N_2NaO_4S$
HR-TEM	High-resolution transmission electron microscopy
IMAC	Immobilized-metal affinity chromatography
keV	kiloelectron volt
LbL	Layer-by-layer
LC	Liquid chromatography
M	Molecular mass
MBP	Maltose-binding protein
mp	melting point
MS	Mass spectrometry
O/W	Oil-in-water or oil–water
OD_{600}	Optical density at a wavelength of 600 nm measured by using UV-spectroscopy
OTMS	Octadecyltrimethoxysilane, $CH_3(CH_2)_{17}Si(OCH_3)_3$
PDI	Polydispersity index
PEF	Protein Expression Facility
PEO-PPO-PEO	Poly(ethylene oxide)-*b*-poly(propyleneoxide)-*b*-poly(ethylene oxide), $(CH_3(CH_2)_2O)_x((CH_2)_2O)_y(CH_2(CH)CH_3O)_z$
p*I*	Isoelectric point
pK_a	Acid dissociation constant
PS	Poly(styrene), $(C_8H_8)_n$
PTMS	Phenyltrimethoxysilane, $C_6H_5Si(OCH_3)_3$
ReCaMoP	Recombinant catalytic modular protein
RP-HPLC	Reversed-phase high-performance liquid chromatography
RT	Room temperature
SDS	Sodium dodecyl sulfate, $CH_3(CH_2)_{11}OSO_3Na$
SDS-PAGE	Sodium dodecyl sulfate polyacrylamide gel electrophoresis
SAED	Selected area electron diffraction
SEM	Scanning electron microscopy
SurSi	Designed bifunctional modular peptide comprising a surface-active module and a biosilicification-active module
T. aurantia	*Tethya aurantia*
TCPTES	(3-Thiocyanatopropyl)triethoxy silane, $C_{10}H_{21}NO_3SSi$
TEM	Transmission electron microscopy
TEV	Tobacco etch virus
TEVp	Tobacco etch virus protease
TEOS	Tetraethoxysilane, $Si(OC_2H_5)_4$
TMOS	Tetramethoxysilane, $Si(OCH_3)_4$
TFA	Trifluoroacetic acid, CF_3CO_2
TX-100	Triton X-100, $C_{14}H_{22}O(C_2H_4O)_n$
UV	Ultraviolet

Amino acid abbreviation

Amino acid	One-letter abbreviation	Three-letter abbreviation
Alanine	A	Ala
Cysteine	C	Cys
Aspartic acid	D	Asp
Glutamic acid	E	Glu
Phenylalanine	F	Phe
Glycine	G	Gly
Histidine	H	His
Isoleucine	I	Ile
Lysine	K	Lys
Leucine	L	Leu
Methionine	M	Met
Asparagine	N	Asn
Proline	P	Pro
Glutamine	Q	Gln
Arginine	R	Arg
Serine	S	Ser
Threonine	T	Thr
Valine	V	Val
Tryptophan	W	Trp
Tyrosine	Y	Tyr

Chapter 1

Project overview

1.1 Introduction

Utilization of pesticides, including insecticides, herbicides, and fungicides, is indispensable, especially in countries with agriculture-driven economies. Approximately two million metric tons of pesticides are spent annually worldwide (worth US$ 35 billion) [1]. In practice, a significant proportion of pesticides undergo premature degradation (due to wind, sunlight or rain), evaporation or leaching [2], and therefore periodic application is required to achieve satisfactory treatment results. Consequently, excessive use of pesticides occurs which in turn increases the application costs and leads to undesirable environmental side effects including bioaccumulation, death of non-target organisms, development of pest resistance, and pollution of soil, air, ground- and surface-water. Given these harmful impacts that pesticides can cause to the environment, regulatory authorities have banned, or severely restricted, the use of certain pesticides and mandated stringent improvement for registered pesticides prior to their applications [3, 4].

Most pesticide chemistries are designed to have selective toxicity [5] and limited solubility in aqueous solutions [6]. Nanotechnology has emerged to play pivotal roles in agriculture by providing nanocarrier systems [2, 6-11] to encapsulate and deliver such pesticides. The use of nanocarriers is expected to: (1) increase the bioavailability of pesticides; (2) protect the pesticides against rapid degradation; (3) protect the environment from the toxicity of the pesticides; and (4) release the pesticides in a sustained manner which would, in turn, prolong duration of their activity. Through the advances conferred by such nanocarriers, pesticide dosages and its environmental residues can be minimized.

As nanocarriers offer exciting opportunities to address the challenges in agriculture, technology for their development must anticipate their possible harm, whether real or perceived, to people and the environment [12, 13]. Recent studies investigating the toxicity of some nanomaterials in cell cultures and animals have demonstrated that size, surface chemistry, surface area, and possibly shape play a role in determining the toxicity of nanomaterials [14, 15]. However, the degree of toxicity of nanomaterials is a multifaceted issue depending on, for example, their chemical composition, exposure routes and doses. For instance, mesoporous silica nanoparticles that still contained unremoved chemical surfactants originated from the synthetic procedures of the nanoparticles could cause severe cytotoxicity, yet these nanoparticles having complete removal of the bound surfactant

showed low cytotoxicity [16]. Therefore, it is appropriate to implement safe and sustainable nanotechnology during the manufacturing processes [17, 18]. This can be achieved through responsible nanomanufacturing practices which range from minimizing the use of toxic chemicals to selecting processes and materials in a conscious effort to minimize environmental contamination and associated toxicity [18].

In this thesis, a nanoemulsion system is researched and developed to solubilize insecticide having limited water-solubility, and then silica material is encased surrounding the nanoemulsion forming insecticide-encapsulated silica nanocapsules. Encapsulation and delivery of the insecticide *via* silica nanocapsules might be expected to increase its bioavailability in an aqueous-based environment, while also protecting the insecticide and allowing for its controlled release. To comply with stringent regulatory purposes, synthesis of the oil-filled silica nanocapsules should mainly involve biocompatible components. In parallel with biocompatibility, moderate temperature and pressure, and near-neutral pH in the absence of toxic organic solvents are often required.

Nature provides an inspiration for bottom-up design and engineering of hierarchical silica-based nanomaterials in aqueous environments under mild physiological conditions as evident in the biosilicification of biological tissue like cell walls of diatoms and sponges [19, 20]. In Nature, peptides or proteins are the workhorses that control the formation of biological silica structures through their molecular-recognition ability to silica species. Therefore, the underlying biological principles used by the living organisms may inspire the synthesis of oil-filled silica nanocapsules. In the first instance, however, the peptides/proteins should be able to stabilize the oil droplet prior to silica formation. Recognizing these biomolecular and interfacial engineering challenges and opportunities, the central objective of this PhD thesis is to use biomolecules for synthesis of oil-core silica-shell nanocapsules under environmentally-friendly conditions, by stabilizing the nanoemulsion core and forming silica shell surrounding the core, and then to apply the developed silica nanocapsules for encapsulation and controlled release of an insecticide. Termites will be used as a model insect to demonstrate the applicability of the nanocarrier system developed in this thesis.

1.1.1 Silica nanocapsules via emulsion templating

Previous studies have shown the loading and release of various agrochemicals from silica-based nanomaterials, including non-porous silica nanoparticles [21], mesoporous silica nanoparticles [22-25], and hollow-core silica-shell nanoparticles [26-30]. The core–shell morphology of a silica nanocapsule is beneficial as compared to non-porous and porous silica nanoparticles. The core provides higher loading-capacity of the active molecule than non-porous and porous silica nanoparticles [31] (**Figure 1**). With non-porous silica nanoparticles (**Figure 1**, left), the active molecule can only be attached on the nanoparticle surfaces, thus limiting the loading capacity.

Moreover, the active molecule is being exposed to the surrounding environment, thus reducing the flexibility to protect and release the active molecule. With porous silica nanoparticles (**Figure 1**, middle), the active molecule can bind on the nanoparticle surfaces after loading processes (by adsorption), thus increasing the probability of burst release effect and reducing its efficacy. With silica nanocapsules (**Figure 1**, right), the problems highlighted previously can be tackled. This is especially true when oil-in-water (O/W) emulsion is used as a template to synthesize oil-core silica-shell nanocapsule. Emulsion templating facilitates solubilization of the active molecule in the oil core prior to silica shell formation. This avoids attachment of the active molecule on the nanocapsule exterior surfaces, and enables storage and protection of the active molecule in the nanocapsule oil cores. High-capacity loading of the active molecule can be achieved depending on solubility of the active molecule in the oil.

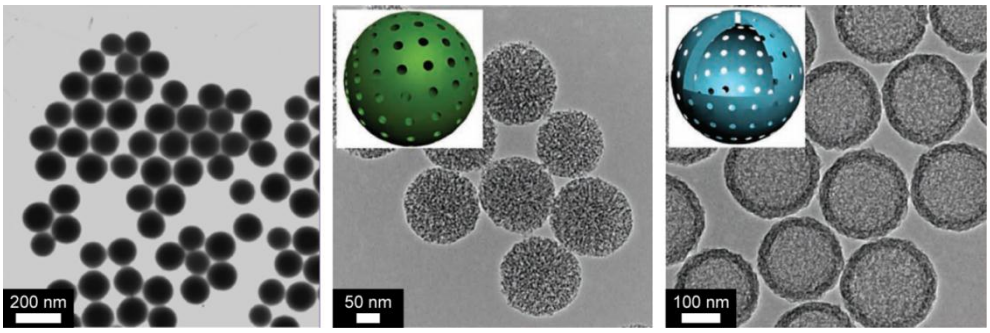

Figure 1. Transmission electron microscopy (TEM) images of common silica nanospherical structures. From left to right, the figures represent non-porous silica nanoparticles, porous silica nanoparticles, and core–shell silica nanocapsules, respectively. Insets show schematic illustrations of the morphology. The figures were adapted from Stöber *et al.* [32] (left) and Chen *et al.* [16] (middle and right).

Silica plays an important role as shell material in nanocapsules. Firstly, silica is biocompatible [33], thus it may impart biocompatibility for the insecticide delivery system. Since the biocompatibility of silica is affected by its concentration [16], silica nanocapsules which have lower silica content (only present at the shell) is clearly more biocompatible than non-porous and porous silica nanoparticles at a given volume (**Figure 1**). Secondly, silica surfaces can be easily functionalized through silane chemistry [34], opening opportunities to combine multiple functionalities in a single nanocapsule, including for bio-labelling, controlled release, and targeted delivery. Thirdly, the kinetics of silica growth is controllable meaning that the size of silica-based nanomaterials can possibly be adjusted by modifying reaction conditions [32]. Finally, silica layers can impart stability to the core materials in an aqueous media through electrostatic repulsion [35].

As previously mentioned, an emulsion can be used as a template material to prepare silica nanocapsules [36-38]. It allows facile encapsulation of poorly-water soluble active molecules through solubilization of the active molecules in the oil cores prior to silica shells formation. However, current synthesis methods suffer from several drawbacks: (1) the reaction conditions for forming silica shells are often not compatible with the active molecules, e.g., elevated temperature and/or extreme pH; (2) the organic solvents and chemical surfactants used for inducing silica formation, as well as the oils are not biocompatible, which would subsequently require stringent monitoring procedures to ensure removal of the chemicals down to the levels that might be considered acceptable to regulatory bodies. It should be emphasized that incomplete removal of chemical surfactants from a final silica product has been shown to cause severe cytotoxicity [16]. Instead of using chemical surfactant, designed proteins/peptides, the key novel contribution of this PhD project, will be used to direct nucleation and growth of silica mimicking the capability of biosilicification-active proteins found in Nature.

1.1.2 Nature as an inspiration for materials chemistry

Hydrated silica (SiO_2) formed in an amorphous state in living organisms [39, 40] serves as a mechanical or structural support, provides protection from predators, or acts as sensors [41] (**Figure 2**). The silica exhibits complex hierarchical organization of particles and pores over several length scales ranging from tens of nanometres to tens or hundreds of micrometres. For example, silica in spicules of sponges has nanoparticle substructure with diameters from about 70 to 200 nm [42]. The biological-mediated assembly of the silica structures in the organisms originates from a similarly simple template: the amino acid sequence that controls nucleation and growth of amorphous silica. Amino acids are the functional building blocks of biological systems. Each amino acid imparts specific functionalities which in concert enable complex processes including biosilicification. Crucial to the processes are the interactions between amino acids and silica species to form amorphous siliceous parts in living organisms. Simply examining how individual amino acids are used by natural systems provides numerous ideas for the utilization of peptides or proteins in synthetic systems. Recently, three model systems have been used to study formation of silica nanostructures *in vitro* [43]: (1) proteins extracted from silica-forming organisms; (2) designed peptides that exhibit similar functionalities to the naturally occurring molecules; and (3) peptides with specific amino acid sequence identified by using combinatorial phage display libraries that can strongly bind to silica [44]. These studies have advanced the bio-inspired synthesis of silica-based nanomaterials.

The use of proteins and peptides to direct the *in vitro* synthesis of silica-based nanomaterials is advantageous as compared to chemical surfactants involved in conventional production methods. This is because: (1) peptides/proteins can facilitate silica synthesis under environmentally-friendly conditions i.e., at or near room temperature and ambient pressure, at or near neutral pH, in aqueous

solutions and in the absence of toxic organic solvents, which makes the bio-inspired silicification inherently “green” processing; (2) the large diversity of amino acid chemistries that composed the biomolecules i.e., polarity, electrostatic, hydrophobicity, hydrophilicity, *etc.* offer the potential to produce materials with multiple functionalities; (3) the biomolecules can be easily processed and prepared through genetic engineering or by chemical synthesis; and (4) they are renewable and biodegradable as well as biocompatible [45].

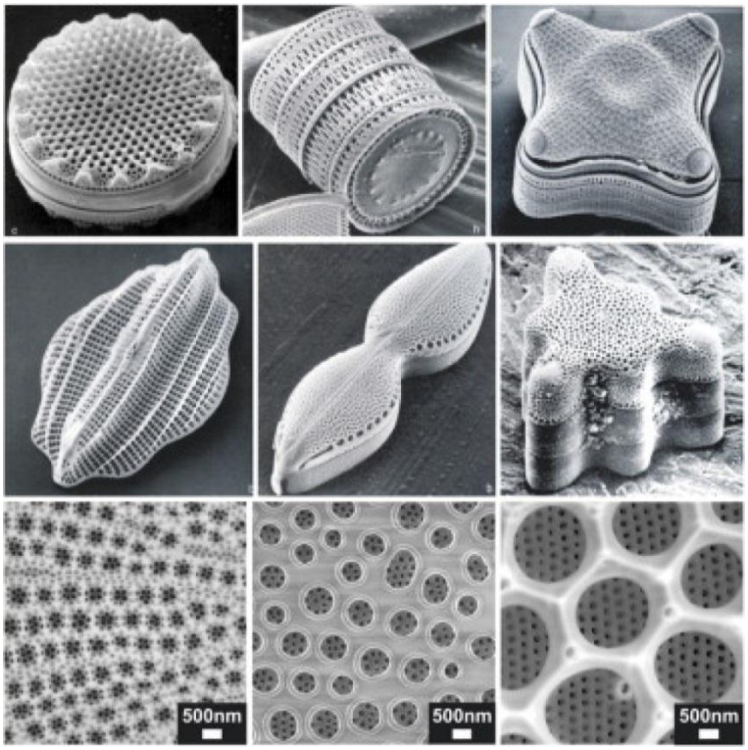

Figure 2. Scanning electron microscopy (SEM) images of nanoscale architectures of cleaned diatom silica cell walls (frustules) from several different diatom species. The assembly of the complex silica structures is controlled under mild physiological conditions by proteins integrated in the cell walls of the living organisms. Scanning electron microscopy (SEM) images of the overall form of the frustule are presented in the top and middle rows, and higher-magnification images of frustule details are presented in the bottom row. The figures were adapted from Kröger [46].

Due to these reasons, peptides and proteins have been widely used to fabricate silica-based nanomaterials [41, 43, 45]. However, there is a gap in their utilities: the bio- inspired silicification has been largely studied on biomolecules that self-assembled in bulk aqueous solution or at solid–liquid interfaces, and there is no current biomimetic approach at oil–water interfaces. Aligned with the major aim of this PhD thesis to produce oil-filled silica nanocapsules, biomolecules able to induce silica formation at oil–water interfaces are required. Obviously, biomolecule-based silica nanocapsules encasing oil droplets should contain an amino acid residue sequence having an ability to facilitate stabilization of O/W emulsion.

Peptide surfactant AM1 (Ac-MKQLADS LHQLARQ VSRLEHA-$CONH_2$) having high surface activity was designed based on biomimetic principles [47]. AM1 is composed of three heptads, and each heptad contains a seven residue repeating motif *abcdefg*, in which the *a* and *d* residues have hydrophobic amino acids (mainly are methionine (M), leucine (L) and valine (V)), while the remaining sites are predominantly hydrophilic. This alternate three and four residue spacing of hydrophobic moieties permits the formation of α-helical structure having distinct hydrophobic and hydrophilic faces that give rise to facial amphiphilicity of AM1. In this regards, AM1 can be rapidly adsorbed and orients parallel to a freshly formed oil–water interface, in which the hydrophobic parts of AM1 face toward the oil phase while the hydrophilic residues orient toward the bulk aqueous phase [48]. AM1 is capable of reversibly and precisely controlling the stability of O/W emulsions [47] and has well characterized interfacial structure [48]. AM1 slows the coalescence of emulsions [49] by forming a cohesive interfacial film that is responsive to metal ion binding to histidine (H) residues in the peptide [50]. AM1-stabilized pharmaceutical grade Miglyol® 812 oil has been formulated to stabilize nanoemulsions loaded with curcumin [51] and ovalbumin [52].

The ability of AM1 peptide surfactant to facilitate the formation of stable O/W nanoemulsions leads to the general question in the context of synthesis of oil-core silica-shell nanocapsules that this research addresses: is AM1 capable of directing nucleation and growth of silica at oil–water interfaces while maintaining nanoemulsion stability? If not, could the AM1 peptide be used for surface activity but be supplemented in such a way that it did drive interfacial silica formation? With this in mind, Professor Middelberg, who is also the supervisor of this PhD project, hypothesized that a modular molecule could be designed by joining a surface-active module (e.g., based on AM1 peptide surfactant) with a module for biosilicification activity. The result would be a bifunctional modular biomolecule that would stabilize a nanoemulsion and also drive silica formation at the interface, thereby forming oil-core silica-shell nanocapsules (**Figure 3**). Specifically, the bifunctional modular biomolecule would undergo interfacial adsorption during emulsification and orient parallel to the nanoemulsion interface through its surface-active module, with the hydrophobic face attached to the oil phase and the hydrophilic face exposed to the bulk aqueous solution, which might then stabilize the nanoemulsion. Upon addition of silica precursors, the biosilicification-active module projecting towards the bulk aqueous phase would catalyze biomimetic silica growth at the oil–water interface hence forming a silica shell encapsulating the nanoemulsion core (**Figure 3**). A main aim of this thesis is to explore this hypothesis through multi-dimensional experimental and theoretical approaches, with a controlled-release application objective.

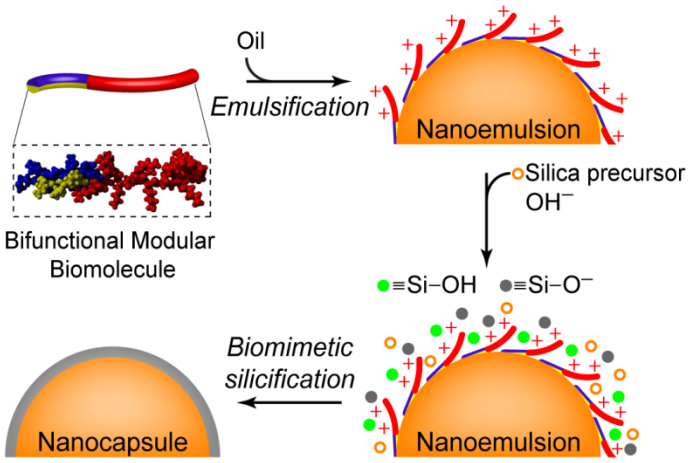

Figure 3. Conceptual design of a bifunctional modular biomolecule for synthesis of oil-core silica-shell nanocapsule under environmentally-friendly conditions. Bifunctional modular biomolecule comprises (1) a surface-active module that incorporates hydrophobic (in yellow) and hydrophilic (in blue) amino acids to impart facial amphiphatic character, hence promoting adsorption at the nanoemulsion interface; and (2) a biosilicification-active module that is rich in cationic amino acid side chains (in red) for directing nucleation and growth of silica at the oil–water interface.

1.1.3 Controlled-release technology for termite control

Termites are the chief decomposers of dead plant materials by digesting the cellulose, and their tunnelling efforts contribute significantly to the nutrient turnover of soil [53]. They are abundant in tropical and subtropical environments where they help in breaking down and recycling one third of the annual production of dead wood [54]. However, termites become economic pests when they feed on structural lumber on houses or man-made structures and most tropical agriculture e.g., forestry, sugar crops, cereal crops, oil crops, beverage crops, pastures, tuber crops, market gardens and fibre crops [55]. Based on the insecticide sales figures of 1999, the worldwide annual control and repair cost were estimated at US$22 billion. A similar estimate with 2010 data showed that the global economic impact of termite pests has increased to US$40 billion with subterranean termites accounting for approximately 80% of the costs [56]. In Australia only, an estimated 130,000 new infestations in houses are reported each year, and the average cost of rectification of termite-damaged properties is in excess of AU$7,000 per house [57].

Current methods to prevent termite infestation rely upon chemical soil barriers. The insecticides used in this method have low durability due to environmental and health concerns [58], which in turn necessitates periodic treatments and hence increases negative environmental side effects. As aforementioned, these consequences have led to the development of nanocarriers for storage, protection, and release of an insecticide in a sustained manner to control termite populations. These

nanocarriers are expected to have high-capacity loading and controlled-release properties capable of carrying high-amount of insecticide, and then releasing the insecticide slowly to achieve an effective local concentration in a prolonged duration. In addition, biocompatibility of the components composing the nanocarriers is substantially important as to minimize environmental risks.

1.2 Thesis objectives

The main goal of this PhD thesis is to synthesize oil-core silica-shell nanocapsules and to examine the application of the nanocapsules for controlled release of insecticide in the context of termite control. Within this central goal, there are four specific objectives of this thesis as described below.

(1) To design a bifunctional modular peptide comprising a surface-active module and a biosilicification-active module for synthesis of oil-core silica-shell nanocapsules;
(2) To evaluate encapsulation and controlled release of fipronil insecticide *in vitro* in water and *in vivo* against termites from biocompatible silica nanocapsules developed in objective (1) in a laboratory scale;
(3) To design a bifunctional modular protein by extrapolating the modular design concept of bifunctional modular peptide developed in objective (1) so that the design can enable the protein to be produced using industrially-relevant microbial cell-factory *Escherichia coli* (*E. coli*) and used for synthesis of oil-core silica-shell nanocapsules;
(4) To produce the bifunctional modular protein developed in objective (3) in a large scale for making fipronil-encapsulated silica nanocapsules and then used them for termite field trial.

The rationale behind each of these research objectives is explained as follows.

1.2.1 Design of a bifunctional modular peptide comprising a surface-active module and a biosilicification-active module for synthesis of oil-core silica-shell nanocapsules

Biomimetic approaches have utilized a variety of amino acid sequences to biosilicification, but none of those have been used for biosilicification at oil–water interfaces [41, 43, 45]. On the other hand, few studies have demonstrated peptide surfactant for facilitating formation and stabilization of O/W emulsions [59], but none of those were used for directing nucleation and growth of silica at the interfaces. The study here aimed to bridging the gap on the utility of peptides that combine emulsification and biosilicification functionalities. Peptide surfactant AM1 was used as a starting peptide to facilitate emulsion stabilization. This then leads to important research questions: could AM1 attract silica precursor species from bulk solution to oil–water interfaces while maintaining its ability to stabilize the nanoemulsions? Could AM1 facilitate the silicification reaction preferentially at the interfaces rather than in bulk solutions? If AM1 then could not be proved to effectively form a

silica shell, bifunctional modular peptide could be designed based on the results of AM1 on interfacial biosilicification. Thence, the following question is: how to arrange amino acid sequences in the peptide so that it could stabilize nanoemulsions and, at the same time, induce silica formation effectively? Thus, this study evaluates AM1 and designed bifunctional modular peptide in order to develop emulsion and biomimetic dual-templating approach for synthesis of oil-core silica-shell nanocapsules.

1.2.2 Applications of insecticide-encapsulated silica nanocapsules for termite control in a laboratory scale

This study is motivated by an increasing need in termite control applications for an effective and efficient pesticide delivery system which left minimal environment footprint [6, 7]. The delivery system requires controlled-release properties to increase bio-efficacy with prolonged duration of activity. Therefore, biocompatible silica nanocapsules developed using bifunctional modular peptide in objective (1) are used to answer these needs. These lead to research questions: could an insecticide be encapsulated and released effectively *in vitro* in water from the silica nanocapsules? Would the insecticide-encapsulated silica nanocapsules demonstrate their efficacy when applied to a number of termites? Thus, this study is a proof-of-concept aimed to evaluate the performance of silica nanocapsules developed in objective (1) to encapsulate an insecticide with high-loading capacity and to release the insecticide in a sustained manner *in vitro* in water and *in vivo* against termites.

1.2.3 Design and microbial-production of a bifunctional modular protein comprising a surface-active module and a biosilicification-active module for synthesis of oil-core silica-shell nanocapsules

This study is motivated by the practical need to develop a scalable and cost-effective method for production of bifunctional modular biomolecule used to make oil-core silica-shell nanocapsules. The development of high cell density culture technique for *E. coli* has made it possible to express modified variants containing bioactive motifs in amounts suitable for research, clinical and industrial purposes [60]. Synthetic DNA encoding amino acid sequence in the bifunctional modular peptide developed in objective (1) can be joined with bacterial DNA, and the resulting recombinant DNA can be inserted into microbial cell-factory *E. coli*, a process known as recombinant DNA technology [61]. However, expression of short recombinant peptides, though possible, is very challenging as it is unstable in bacterial host [62-64] because they may self-associate, be toxic, or be rapidly degraded by proteases within the cell. Therefore, this study addresses these challenges by combining the bifunctional modular peptide with DAMP4 protein (MD(PSMKQLADS-LHQLARQ-VSRLEHAD)$_4$; M = 11.1 kDa) [65] as a protein carrier enabling expression of the recombinant protein in *E. coli*. DAMP4 is selected because it was able to be expressed at high yield as a soluble protein in *E. coli* with ease of

purification procedures, and demonstrated surface activity [65, 66]. This then leads to important questions: would the recombinant protein show dual-functionality that is able to stabilize emulsions and to form silica at the interface for synthesis of oil-core silica-shell nanocapsules? If not, is it possible to cleave the recombinant protein using a chemical or enzymatic reagent and obtain a shorter biomolecule than the recombinant protein, which still contains a surface-active module and biosilicification-active module close to the bifunctional modular peptide developed in objective (1)? This study aims to design a recombinant bifunctional protein comprising a surface-active module and a biosilicification-active module for synthesis of oil-core silica-shell nanocapsules, and develop a sustainable production of the recombinant protein through microbial cell-factory *E. coli* with the potential of process scale-up.

1.2.4 Large-scale production and field application of insecticide-encapsulated silica nanocapsules for termite control

Is it feasible to produce the insecticide-encapsulated silica nanocapsules for a field scale? Could they be cost-effectively applied to treat millions of termites that live in a mound [67]? This study is a combination of objective (2) and (3), but at a larger scale, to demonstrate the large-scale production of the bifunctional modular protein for making fipronil-encapsulated silica nanocapsules which could then be used in combination with α-cellulose as feeding bait for termite field trial (**Figure 4**).

Figure 4. Photographic image of mound of termites from genus *Coptotermes*. The image also shows assembled devices of bait applications for termite field trial.

1.3 Thesis organization

This PhD thesis consists of 6 chapters, in addition to this introductory chapter.

Chapter 2 provides a literature survey on the progress made in chemical methods for synthesis of silica nanocapsules using chemical surfactants. Later in the chapter, biomimetic approaches for making silica-based nanomaterials using peptides and proteins are discussed. Theoretical backgrounds on the silica chemistry, formation and stability of nanoemulsions, microbial production of the peptides/proteins, which are relevant to the aforementioned research objectives, are also presented.

Chapter 3 explores engineering of peptide sequences for their surface activity and biosilicification functionality, and experimentally demonstrates their abilities to stabilize nanoemulsions and to induce silica formation as described in objective (1). Key novel aspects of this thesis are presented in this chapter, including design and use of bifunctional modular peptide in emulsion and biomimetic dual-templating approach for making oil-core silica-shell nanocapsules under benign reaction conditions in the absence of toxic organic solvents.

Chapter 4 centers on the application of the silica nanocapsules to encapsulate fipronil insecticide and to release the insecticide in a sustained manner *in vitro* in water and *in vivo* against termites as specified in objective (2). Two laboratory methods of termite control including direct treatment and feeding treatment are described to evaluate insecticidal effects of the fipronil-encapsulated silica nanocapsules.

Chapter 5 presents the design and production of novel bifunctional modular protein through biological expression as specified in objective (3). It describes the bioprocess routes to obtain the recombinant protein with high purity using biochemical unit operations. Analytical procedures to confirm the identity of the protein are investigated. This chapter also discusses interfacial properties of the protein and demonstrates its capability for both stabilizing nanoemulsions and inducing silica formation surrounding the nanoemulsions.

Chapter 6 concerns the large-scale production and field application of the insecticide-encapsulated silica nanocapsules for termite field trial as described in objective (4).

Chapter 7 draws conclusions from the results accomplished in this project and outlines potential directions for further research.

References

1. Stephenson, G.R., *Pesticide Use and World Food Production: Risks and Benefits*, in *Environmental Fate and Effects of Pesticides*, J.R. Coats and H. Yamamoto, Editors. 2003, American Chemical Society: Washington DC.
2. Ghormade, V., M.V. Deshpande, and K.M. Paknikar, *Perspectives for nano-biotechnology enabled protection and nutrition of plants.* Biotechnol. Adv., 2011. **29**(6): p. 792–803.
3. Thullner, F., *Impact of pesticide resistance and network for global pesticide resistance management based on a regional structure.* World Anim. Rev., 1997. **-**(89): p. 41–47.
4. Lallas, P.L., *Guideline on the Development of National Laws to Implement the Rotterdam Convention*. 2004, Secretariat of the Rotterdam Convention, United Nations Environment Programme (UNEP): Geneva, Switzerland.
5. Moffat, A.S., *Agriculture—new chemicals seek to outwit insect pests.* Science, 1993. **261**(5121): p. 550–551.
6. Kah, M. and T. Hofmann, *Nanopesticide research: current trends and future priorities.* Environ. Int., 2014. **63**(-): p. 224–235.
7. Kah, M., S. Beulke, K. Tiede, and T. Hofmann, *Nanopesticides: state of knowledge, environmental fate, and exposure modeling.* Crit. Rev. Env. Sci. Technol., 2013. **43**(16): p. 1823–1867.
8. Gogos, A., K. Knauer, and T.D. Bucheli, *Nanomaterials in plant protection and fertilization: current state, foreseen applications, and research priorities.* J. Agric. Food Chem., 2012. **60**(39): p. 9781–9792.
9. Pérez-de-Luque, A. and D. Rubiales, *Nanotechnology for parasitic plant control.* Pest Manag. Sci., 2009. **65**(5): p. 540–545.
10. Mulqueen, P., *Recent advances in agrochemical formulation.* Adv. Colloid Interface Sci., 2003. **106**(-): p. 83–107.
11. Kumari, A. and S.K. Yadav, *Nanotechnology in agri-food sector.* Crit. Rev. Food Sci., 2014. **54**(8): p. 975–984.
12. Colvin, V.L., *The potential environmental impact of engineered nanomaterials.* Nature Biotechnology, 2003. **21**(10): p. 1166–1170.
13. Klaine, S.J., P.J.J. Alvarez, G.E. Batley, T.F. Fernandes, R.D. Handy, D.Y. Lyon, S. Mahendra, M.J. McLaughlin, and J.R. Lead, *Nanomaterials in the environment: behavior, fate, bioavailability, and effects.* Environ. Toxicol. Chem., 2008. **27**(9): p. 1825–1851.
14. Oberdörster, G., E. Oberdörster, and J. Oberdörster, *Nanotoxicology: An emerging discipline evolving from studies of ultrafine particles.* Environ. Health Perspect., 2005. **113**(7): p. 823–839.
15. Nel, A., T. Xia, L. Madler, and N. Li, *Toxic potential of materials at the nanolevel.* Science, 2006. **311**(5761): p. 622–627.

16. Chen, Y., H. Chen, and J. Shi, *In vivo bio-safety evaluations and diagnostic/therapeutic applications of chemically designed mesoporous silica nanoparticles.* Adv. Mater., 2013. **25**(23): p. 3144–3176.
17. Albrecht, M.A., C.W. Evans, and C.L. Raston, *Green chemistry and the health implications of nanoparticles.* Green Chem., 2006. **8**(5): p. 417–432.
18. Hull, M.S., M.E. Quadros, R. Born, J. Provo, V.K. Lohani, and R.L. Mahajan, *Sustainable Nanotechnology: A Regional Perspective*, in *Nanotechnology Environmental Health and Safety: Risks, Regulation, and Management*, M. Hull and D. Bowman, Editors. 2014, Elsevier: Oxford.
19. Morse, D.E., *Silicon biotechnology: harnessing biological silica production to construct new materials.* Trends Biotechnol., 1999. **17**(6): p. 230–232.
20. Foo, C.W.P., J. Huang, and D.L. Kaplan, *Lessons from seashells: silica mineralization via protein templating.* Trends Biotechnol., 2004. **22**(11): p. 577–585.
21. Ao, M.M., Y.C. Zhu, S. He, D.G. Li, P.L. Li, J.Q. Li, and Y.S. Cao, *Preparation and characterization of 1-naphthylacetic acid–silica conjugated nanospheres for enhancement of controlled-release performance.* Nanotechnology, 2013. **24**(3): p. 1–8.
22. Chen, J., W. Wang, Y. Xu, and X. Zhang, *Slow-release formulation of a new biological pesticide, pyoluteorin, with mesoporous silica.* J. Agric. Food Chem., 2011. **59**(1): p. 307–311.
23. Popat, A., J. Liu, Q. Hu, M. Kennedy, B. Peters, G.Q. Lu, and S.Z. Qiao, *Adsorption and release of biocides with mesoporous silica nanoparticles.* Nanoscale, 2012. **4**(3): p. 970–975.
24. Wanyika, H., E. Gatebe, P. Kioni, Z. Tang, and Y. Gao, *Mesoporous silica nanoparticles carrier for urea: potential applications in agrochemical delivery systems.* J. Nanosci. Nanotechnol., 2012. **12**(3): p. 2221–2228.
25. Wanyika, H., *Sustained release of fungicide metalaxyl by mesoporous silica nanospheres.* J. Nanopart. Res., 2013. **15**(8): p. 2–9.
26. Wen, L.X., Z.Z. Li, H.K. Zou, A.Q. Liu, and J.F. Chen, *Controlled release of avermectin from porous hollow silica nanoparticles.* Pest Manag. Sci., 2005. **61**(6): p. 583–590.
27. Tan, W.M., N. Hou, S. Pang, X.F. Zhu, Z.H. Li, L.X. Wen, and L.S. Duan, *Improved biological effects of uniconazole using porous hollow silica nanoparticles as carriers.* Pest Manag. Sci., 2012. **68**(3): p. 437–443.
28. Li, Z.Z., S.A. Xu, L.X. Wen, F. Liu, A.Q. Liu, Q. Wang, H.Y. Sun, W. Yu, and J.F. Chen, *Controlled release of avermectin from porous hollow silica nanoparticles: influence of shell thickness on loading efficiency, UV-shielding property and release.* J. Control. Release, 2006. **111**(1–2): p. 81–88.
29. Liu, F., L.-X. Wen, Z.-Z. Li, W. Yu, H.-Y. Sun, and J.-F. Chen, *Porous hollow silica nanoparticles as controlled delivery system for water-soluble pesticide.* Mater. Res. Bull., 2006. **41**(12): p. 2268–2275.

30. Qian, K., T.Y. Shi, S. He, L.X. Luo, X.L. Liu, and Y.S. Cao, *Release kinetics of tebuconazole from porous hollow silica nanospheres prepared by miniemulsion method.* Micropor. Mesopor. Mater., 2013. **169**: p. 1–6.
31. Zhu, Y.F., J.L. Shi, W.H. Shen, X.P. Dong, J.W. Feng, M.L. Ruan, and Y.S. Li, *Stimuli-responsive controlled drug release from a hollow mesoporous silica sphere/polyelectrolyte multilayer core–shell structure.* Angew. Chem., Int. Ed., 2005. **44**(32): p. 5083–5087.
32. Stöber, W., A. Fink, and E. Bohn, *Controlled growth of monodisperse silica spheres in the micron size range.* J. Colloid Interface Sci., 1968. **26**(1): p. 62–69.
33. Asefa, T. and Z. Tao, *Biocompatibility of mesoporous silica nanoparticles.* Chem. Res. Toxicol., 2012. **25**(11): p. 2265–2284.
34. Biju, V., *Chemical modifications and bioconjugate reactions of nanomaterials for sensing, imaging, drug delivery and therapy.* Chem. Soc. Rev., 2014. **43**(3): p. 744–764.
35. Guerrero-Martínez, A., J. Pérez-Juste, and L.M. Liz-Marzán, *Recent progress on silica coating of nanoparticles and related nanomaterials.* Adv. Mater., 2010. **22**(11): p. 1182–1195.
36. Lou, X.W., L.A. Archer, and Z.C. Yang, *Hollow micro-/nanostructures: synthesis and applications.* Adv. Mater., 2008. **20**(21): p. 3987–4019.
37. Liu, J., F. Liu, K. Gao, J.S. Wu, and D.F. Xue, *Recent developments in the chemical synthesis of inorganic porous capsules.* J. Mater. Chem., 2009. **19**(34): p. 6073–6084.
38. Du, X. and J. He, *Spherical silica micro/nanomaterials with hierarchical structures: synthesis and applications.* Nanoscale, 2011. **3**(10): p. 3984–4002.
39. Hildebrand, M., *Diatoms, biomineralization processes, and genomics.* Chem. Rev., 2008. **108**(11): p. 4855–4874.
40. Müller, W.E.G., S.I. Belikov, W. Tremel, C.C. Perry, W.W.C. Gieskes, A. Boreiko, and H.C. Schröder, *Siliceous spicules in marine demosponges (example Suberites domuncula).* Micron, 2006. **37**(2): p. 107–120.
41. Patwardhan, S.V., *Biomimetic and bioinspired silica: recent developments and applications.* Chem. Commun., 2011. **47**(27): p. 7567–7582.
42. Schröder, H.C., X. Wang, W. Tremel, H. Ushijima, and W.E.G. Müller, *Biofabrication of biosilica-glass by living organisms.* Nat. Prod. Rep., 2008. **25**(3): p. 455–474.
43. Dickerson, M.B., K.H. Sandhage, and R.R. Naik, *Protein- and peptide-directed syntheses of inorganic materials.* Chem. Rev., 2008. **108**(11): p. 4935–4978.
44. Naik, R.R., L.L. Brott, S.J. Clarson, and M.O. Stone, *Silica-precipitating peptides isolated from a combinatorial phage display peptide library.* J. Nanosci. Nanotechnol., 2002. **2**(1): p. 95–100.
45. Chen, C.-L. and N.L. Rosi, *Peptide-based methods for the preparation of nanostructured inorganic materials.* Angew. Chem., Int. Ed., 2010. **49**(11): p. 1924–1942.
46. Kröger, N., *Prescribing diatom morphology: toward genetic engineering of biological nanomaterials.* Curr. Opin. Chem. Biol., 2007. **11**(6): p. 662–669.

47. Dexter, A.F., A.S. Malcolm, and A.P.J. Middelberg, *Reversible active switching of the mechanical properties of a peptide film at a fluid–fluid interface.* Nat. Mater., 2006. **5**(6): p. 502–506.
48. Middelberg, A.P.J., L. He, A.F. Dexter, H.H. Shen, S.A. Holt, and R.K. Thomas, *The interfacial structure and Young's modulus of peptide films having switchable mechanical properties.* J. R. Soc. Interface, 2008. **5**(18): p. 47–54.
49. Malcolm, A.S., A.F. Dexter, J.A. Katakdhond, S.I. Karakashev, A.V. Nguyen, and A.P.J. Middelberg, *Tuneable control of interfacial rheology and emulsion coalescence.* ChemPhysChem, 2009. **10**(5): p. 778–781.
50. Dexter, A.F. and A.P.J. Middelberg, *Switchable peptide surfactants with designed metal binding capacity.* J. Phys. Chem. C, 2007. **111**(28): p. 10484–10492.
51. Chuan, Y.P., B.Y. Zeng, B. O'Sullivan, R. Thomas, and A.P.J. Middelberg, *Co-delivery of antigen and a lipophilic anti-inflammatory drug to cells via a tailorable nanocarrier emulsion.* J. Colloid Interface Sci., 2012. **368**(1): p. 616–624.
52. Zeng, B.J., Y.P. Chuan, B. O'Sullivan, I. Caminschi, M.H. Lahoud, R. Thomas, and A.P.J. Middelberg, *Receptor-specific delivery of protein antigen to dendritic cells by a nanoemulsion formed using top-down non-covalent click self-assembly.* Small, 2013. **9**(22): p. 3736–3742.
53. Holt, J.A. and M. Lepage, *Termites and Soil Properties*, in *Termites: Evolution, Sociality, Symbioses, Ecology*, T. Abe, E.D. Bignell, and M. Higashi, Editors. 2000, Kluwer Academic: Dordrecht.
54. Verma, M., S. Sharma, and R. Prasad, *Biological alternatives for termite control: a review.* Int. Biodeter. Biodegr., 2009. **63**(8): p. 959–972.
55. Rouland-Lefevre, C., *Termites as Pests of Agriculture*, in *Biology of Termites: A Modern Synthesis*, D.E. Bignell, Y. Roisin, and N. Lo, Editors. 2011, Springer: London.
56. Rust, M.K. and N.-Y. Su, *Managing social insects of urban importance.* Annu. Rev. Entomol., 2012. **57**(-): p. 355–375.
57. Broadbent, S., *A Stand-Alone Termite Management Technology in Australia*, in *Urban Pest Management: An Environmental Perspective*, P. Dhang, Editor. 2011, CAB International: London.
58. Peters, B.C. and C.J. Fitzgerald, *Developments in termite management in Queensland, Australia: life after cyclodienes (Isoptera).* Sociobiology, 2007. **49**(3): p. 231–249.
59. Dexter, A.F. and A.P.J. Middelberg, *Peptides as functional surfactants.* Ind. Eng. Chem. Res., 2008. **47**(17): p. 6391–6398.
60. Shiloach, J. and R. Fass, *Growing E. coli to high cell density—a historical perspective on method development.* Biotechnol. Adv., 2005. **23**(5): p. 345–357.
61. Sassenfeld, H.M., *Engineering proteins for purification.* Trends Biotechnol., 1990. **8**(4): p. 88–93.

62. Itakura, K., T. Hirose, R. Crea, A.D. Riggs, H.L. Heyneker, F. Bolivar, and H.W. Boyer, *Expression in Escherichia coli of a chemically synthesized gene for hormone somatostatin.* Science, 1977. **198**(4321): p. 1056–1063.
63. Goeddel, D.V., D.G. Kleid, F. Bolivar, H.L. Heyneker, D.G. Yansura, R. Crea, T. Hirose, A. Kraszewski, K. Itakura, and A.D. Riggs, *Expression in Escherichia coli of chemically synthesized genes for human insulin.* Proc. Natl. Acad. Sci. U. S. A., 1979. **76**(1): p. 106–110.
64. Shine, J., I. Fettes, N.C.Y. Lan, J.L. Roberts, and J.D. Baxter, *Expression of cloned β-endorphin gene sequences by Escherichia coli.* Nature, 1980. **285**(5765): p. 456–461.
65. Middelberg, A.P.J. and M. Dimitrijev-Dwyer, *A designed biosurfactant protein for switchable foam control.* ChemPhysChem, 2011. **12**(8): p. 1426–1429.
66. Dimitrijev-Dwyer, M., M. Brech, L. Yu, and A.P.J. Middelberg, *Intensified expression and purification of a recombinant biosurfactant protein.* Chem. Eng. Sci., 2014. **105**(-): p. 12–21.
67. Evans, T.A., M. Lenz, and P.V. Gleeson, *Estimating population size and forager movement in a tropical subterranean termite (Isoptera : Rhinotermitidae).* Environ. Entomol., 1999. **28**(5): p. 823–830.

Chapter 2

Literature review

2.1 Silica nanocapsules

Silica nanocapsules having core–shell architecture have attracted academic and industrial interests [1-3]. Synthesis methods of such engineered silica nanostructure are commonly based on sol–gel reactions of silica precursors on colloidal core templates, i.e., gas bubbles [4, 5], nanoparticles [6-10], and emulsion droplets [11-18], resulting in nucleation and growth of silica at the boundary of gas–liquid, solid–liquid, and liquid–liquid interfaces, respectively. The core–shell morphology of silica nanocapsules allows combination of core material functionalities and silica shell properties on a nanoscopic length scale. Various active materials can be encapsulated in the core of silica nanocapsules with higher loading capacity than solid- and porous-silica nanoparticles [19]. Silica nanocapsules have found diverse applications in fields of chemical, biomedical and agricultural applications depending on the types of the core materials. Encapsulating catalytic metals [7], semiconductor [8], fluorescent [9] and magnetic [17] nanoparticles, and enzymes [11] render silica nanocapsules to act as supports for enhancing long-term activity and/or compatibility of the active molecules in desired environment [20]. In addition, silica nanocapsules can also function as nanocarriers by encapsulating poorly water soluble active molecules, including drugs [14, 19] and pesticides [21], in the oil core for storage, protection, and release.

Silica as a shell material for nanocapsules has a number of advantages, including its stability against aggregation, easy functionalization, biocompatibility, and optical transparency [2, 3]. The stability of silica layer stems from electrostatic repulsion, as the isoelectric point of silica is between 2 and 3 due to the presence of surface hydroxyl groups, hence, the zeta potential of silica is negative under neutral pH [22]. Another benefit of using silica is that the surface chemistry is easily modified (surface functionalization of silica-based nanomaterials is reviewed by Chen and Shi *et al*. [23]). Functionalization of silica surfaces with optical, magnetic, and/or biological functionalities offers bio-labelling, controlled release, and targeted delivery of active molecule [24], as well as allowing detailed surface engineering to circumvent unwanted biological interactions, facilitate bioavailability and cellular uptake [25]. Furthermore, amorphous silica is biocompatible [26-28] as it is considered as “Generally Recognized As Safe (GRAS)” material by the U.S. Food and Drug Administration (FDA) [29], thus suitable for biomedical and agricultural applications. However, it should be emphasized that not all types of silica-based nanomaterials can be considered biocompatible. Several researchers have investigated the level of toxicity of silica-based nanomaterials *in vivo*. It

has been found that their biocompatibility depends on the synthesis processes, particle sizes, morphologies, surface chemistries, doses, and even the administration routes [23, 30-35]. For example, incomplete removal of chemical surfactant, a structure-directing agent, during fabrication of silica-based nanomaterials could cause high cytotoxicity in mice [30, 33, 35]. Therefore, applications that demand biocompatibility of the nanocarriers mandate stringent monitoring procedures when toxic chemical compounds are involved for the synthesis of silica nanocapsules. This is to ensure complete removal of the residual toxic substances from the nanocapsules down to levels that might be considered acceptable by the regulatory authorities.

As outlined in **Chapter 1**, the central objective of this thesis is to develop a novel emulsion and biomimetic dual-templating method for synthesizing oil-core silica-shell nanocapsules, and to examine applications of the nanocapsules for controlled release of active molecules. Fundamental knowledge and available research outcome that are relevant to the synthesis of oil-core silica-shell nanocapsules are reviewed in this chapter. Following significance of silica nanocapsules described in **Section 2.1**, this review systematically surveys the chemical approaches of making silica nanocapsules (**Section 2.2**). Theoretical background of sol–gel chemistry is also introduced to explain reactions of liquid silica precursor to form solid silica. Despite great progresses in the synthesis of silica nanocapsules, the chemical methods variously incorporate toxic chemical catalysts and organic solvents that would pose adverse environmental effects and influence the biocompatibility of the silica product, as previously mentioned. Biomimetic silicification offers an alternative way to produce silica-based nanomaterials under mild physiological conditions using biocompatible components including peptides and proteins. The biomimetic approach would potentially shift the current chemical method to a more environmentally-friendly method for the synthesis of engineered oil-core silica-shell nanostructures. This discussion is covered in **Section 2.3** along with key information on the availability of peptides and proteins for biosilicification, and detailed understanding of the interactions between their functional groups and silica species. Biosilicification has been largely studied in bulk aqueous solutions rather than at oil–water interfaces. Although a number of biomolecules including peptides and proteins has been demonstrated capable of facilitating formation and stabilization of nanoemulsions, they have not been reported to direct nucleation and growth of silica at the interfaces. **Section 2.4** of this review explores the fundamental background on the factors that influence formation and stability of nanoemulsions. Then, the use of designed peptides/proteins as surface-active agents (surfactants) to form nanoemulsions is highlighted in **Section 2.5**, which can provide a key understanding of the design of bifunctional modular peptide/protein developed in this thesis for making oil-core silica-shell nanocapsules. **Section 2.6** describes the biological production methods of peptides/proteins using industrially relevant cell-factory *Escherichia coli* (*E. coli*) which have potential for development of process scale up. This chapter concludes with a short summary about the synthesis of silica nanocapsules

indicating limitation in current methods, and the introduction of the novelty and significance of our work detailed in this thesis (**Section 2.7**).

2.2 Silica nanocapsules based on sol–gel chemistry

The successful deposition of silica species exclusively onto template to form a silica shell surrounding colloidal core template is determined by strong molecular interactions between the silica species and the surface functional groups of the template. In ***Section 2.2.1***, a brief review is provided regarding current chemical approaches on the templating synthesis of silica nanocapsules. Next, ***Section 2.2.2*** provides more detail information of silica chemistry describing that silica formation *via* chemical methods necessitates extreme pH conditions and/or elevated temperature in the presence of toxic organic solvents.

2.2.1 Chemical methods for synthesis of silica nanocapsules

Hard- and soft-templating methods are commonly used for synthesis of silica nanocapsules.

2.2.1.1 Hard templating

Hard-templating approaches have been developed to prepare silica nanocapsules [36, 37] (**Figure 1**). Solid nanoparticles composed of, for example, poly(styrene) (PS) is widely used as hard template and can be prepared *via* emulsion polymerization [38]. The resulting negatively charged PS nanoparticles allow alternate adsorption of oppositely charged polyelectrolytes, and thus result in nanoparticles with multilayer shells surrounding the cores, an approach so-called layer-by-layer (LbL) assembly [39]. Several deposition cycles of poly(diallyl-dimethyl-ammonium chloride), a cationic binder, and negatively charged silica nanoparticles have been employed to form silica nanocapsules with final thickness depending on the number of the cycles [39]. Surface functionalization of PS with amine groups or zwitterionic molecules consisting of amine and carboxylate groups is, in some cases, necessary to facilitate silica growth by *in situ* polycondensation of sodium silicate precursor under alkaline conditions [40]. The classical Stöber synthesis [41] based on the sol–gel chemistry of silicon alkoxide precursor has also been utilized to grow silica layer onto PS template in alcoholic solutions at alkaline conditions [36, 42]. In this regards, cationic surfactants (e.g., cetyltrimethylammonium bromide [42]) or non-ionic surfactants (e.g., polyoxyethylene sorbitan monolaurate [36]) were used to direct the nucleation and growth of silica encapsulating the PS template. Another example of hard templates is calcium carbonate, which can be prepared by using either high gravity reactive precipitation technology [43] or gas diffusion approach [42] to obtain porous or non-porous templates in the nanosized range, respectively. Silica coating of calcium

carbonate template is usually conducted through sodium silicate water-glass methodology [43, 44] or Stöber synthesis [42].

Applications of nanocapsules are often associated with their ability to load and deliver active molecules (**Figure 1**). A common approach to load the active components into the nanocapsules synthesized using the hard template is mainly by tuning pore structure of the silica shell during synthesis, allowing for diffusion of the active molecules from surrounding medium in which the hollow silica nanocapsules are dispersed (i.e., cargo post-loading) (**Figure 1**a). Decomposition of organic compounds, i.e., polymeric [39] or surfactant materials [36, 42], *via* calcinations (at >500 °C) or chemical treatments (e.g., using dimethylsulfoxides) is necessary to remove the template and to subsequently produce hollow nanocapsules with porous silica shells for facilitating diffusion of the cargo into the nanocapsules. However, in most cases, the active molecule can only be deposited at the porous silica shell [44], and high pressure is required to force the active molecule to diffuse into the empty core domain [43]. Moreover, the high temperature applied for template removal, in some cases, could influence the shell integrity, and thus resulted in shell rupture [39]. Another method of encapsulation is to load the desired materials into porous calcium carbonate template prior to silica coating (i.e., cargo pre-loading) (**Figure 1**b) [42]. However, acidic chemicals used for the dissolution of the template could affect the stability of the pre-loaded material, which might be sensitive to such treatment.

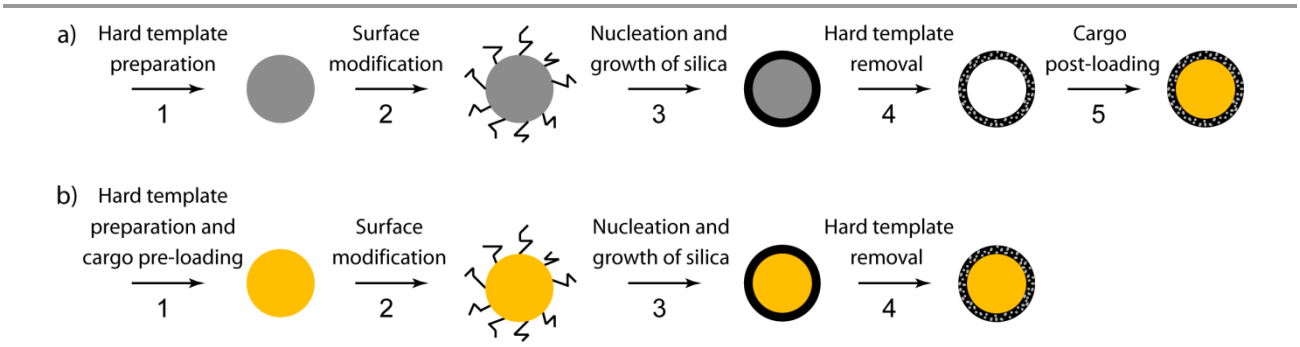

Figure 1. Strategies for synthesis of silica nanocapsules by hard-templating method and their cargo loading techniques. a) Cargo post-loading technique: (1) hard template preparation, (2) template surface modification (optional), (3) nucleation and growth of silica on the template surface, (4) template removal by chemical or thermal means, and (5) cargo loading. b) Cargo pre-loading technique: (1) cargo loading during hard template preparation, (2) template surface modification (optional), (3) nucleation and growth of silica on the template surface, and (4) template removal by chemical means.

2.2.1.2 Soft templating

The hard-templating route suffers from disadvantages associated with template removal and cargo loading. Harsh processes are necessary for ensuring complete template removal in order to minimize potentially destructed template trapped inside the hollow spheres. The cargo loading into hard-templated silica nanocapsules, although possible, is yet challenging. These difficulties have prompted interest in simpler synthetic approaches that exclude template removal step and permit an easy encapsulation of the functional materials. Soft templating by means of oil-in-water (O/W) emulsions seems promising in this context, thereby dissolution of the cargo in the emulsion droplets prior to silica shell formation.

The formation of silica exclusively around the interface between the nanosized oil droplets and the aqueous phase of O/W emulsions has been developed in recent years (**Table 1**). In these approaches, the pre-requisite of co-organization is being fulfilled by electrostatic charge-density matching or hydrogen bonding between silica precursor and cationic [16, 17, 45, 46] or non-ionic [12, 13, 15, 18] surfactant molecules present on the surface of oil droplets, respectively. In addition, an organo-alkoxysilane is often utilized as a co-surfactant to form a thin film at the oil droplet interface and facilitate co-condensation with silicon alkoxide achieving a certain silica shell thickness [12, 13]. Furthermore, self-templating methods have also been reported, in which the oil droplet not only acts as a template but also as a silica precursor itself [14, 47-49]. Reaction time and concentration of an additive (e.g., ammonium hydroxide) are required to be adjusted to produce core–shell nanocapsules instead of solid nanospheres [14]. In another case of self-templating methods [47, 49], the formation of hollow silica nanospheres is achieved by extraction using alcohol to dissolve monomeric or oligomeric units of silica precursor in the core domain.

Oil droplet encased in silica shell can be used directly, for example, as an adsorbent for the uptake of hydrophobic compounds, including bupivacaine [12] and quinoline [13]. However, encapsulation of active molecules can broaden its application. For example, lipase, an enzyme that catalyze the production of biodiesel from vegetable oils, has been immobilized within silica nanoshells to produce a reusable biocatalyst [11]. Rhodamine B (RB), a fluorescent dye molecule used as an imaging agent, or ibuprofen, a non-steroidal anti-inflammatory drug, can be protected by encapsulation with silica shells [14]. The encapsulation of RB or ibuprofen in the oil core of silica nanocapsules involves dissolving the active molecule in the oil phase which also acts as silica precursor (i.e., (3-thiocyanatopropyl)triethoxysilane (TCPTES)). The subsequent hydrolysis and condensation of TCPTES droplets in ammonium hydroxide solutions under 100 °C yielded active molecule-loaded silica nanocapsules. An organic dye molecule, such as pyrene [16], has also been incorporated into the silica nanocapsules by taking advantage of an easy dissolution of the hydrophobic dye in the core domain.

Table 1. Representative soft-templating methods including the components and the conditions used for the formation of silica shells on various oil droplet templates

Template	Surfactant	Silica precursor	Cargo	Reaction conditions				Ref
				T (°C)	pH	P (bar)	Additive	
Ethyl ether	CTAB	TEOS	Pyrene	RT	n/a	n/a	NH_4OH	[16]
TEOS and DMF	CTAC	TEOS	Gold or magnetic nanoparticle	RT	n/a	n/a	Ethanol, Triethanol-amine	[17]
n-Heptane and TEOS	CTAB	TEOS	Gold nanoparticle (post-loaded)	30	3.1–3.9	25–50	Com-pressed CO_2	[46]
Hexadecane	Brij 97	OTMS and TMOS	Bupivacaine	65(E) RT (H, S)	7.0(E) 3.0(H) 7.4(S)	n/a	Saline solutions (E, H, S), HEPES buffer (S)	[12]
Ethyl butyrate	Tween-80 and lecithin	OTMS and TMOS	Quinoline	70 (E) RT (H, S)	n/a(E) 2.5(H) 7.4(S)	n/a	Saline solutions (E, H, S), HEPES buffer (S)	[13]
Supercritical CO_2	PEO-PPO-PEO	TEOS	n/a	40	n/a	200	HCl	[15]
Benzene	TX-100	TEOS	n/a	25 (E) RT (S)	n/a	n/a	NH_4OH	[18]
TCPTES	-	TCPTES	Rhodamine B, or ibuprofen	100 (E, S)	n/a	n/a	NH_4OH	[14]
PTMS	-	PTMS	n/a	60 (E, S)	n/a	n/a	HNO_3 (H) NH_4OH (C)	[47, 49]
DMDES	-	TEOS	n/a	RT	n/a	n/a	NH_4OH	[48]
Oleic acid	-	TEOS and APTES	*Candida antartica-lipase A*	RT (E) 50 (S)	5.3 (E) 9.6 (S)	n/a	-	[11]

E = emulsification; S = silicification; H = hydrolysis; C = condensation; RT = room temperature; TCPTES = (3-thiocyanatopropyl) triethoxysilane; CTAB = cetyltrimethylammonium bromide; CTAC = cetyltrimethylammonium chloride; TMOS = tetramethoxysilane; TEOS = tetraethoxysilane; DMF = *N*, *N*-dimethyl formamide; OTMS = octadecyltrimethoxysilane; PTMS = phenyltrimethoxysilane; PEO-PPO-PEO = poly(ethylene oxide)-*b*-poly(propyleneoxide)-*b*-poly(ethylene oxide); APTES = (3-aminopropyl)trimethoxysilane; DMDES = dimethyldiethoxysilane; HEPES = sodium 4-(2-hydroxyethyl)-1-piperazine ethanesulfonate; TX-100 = Triton X-100; n/a = not available.

Despite the possibility of easy encapsulation of desired materials, most of the soft-templating approaches involve the use of elevated temperatures or pressures and/or extreme pH conditions (**Table 1**), which may affect the stability of active molecules like biomolecules or chemical-sensitive agents. In addition, the inclusion of chemical surfactants, toxic organic solvents, and not-pharmaceutical-graded oils may limit the applicability of soft-templating method for agricultural and biomedical applications which demand biocompatibility. To understand more about conditions and components involved during the reactions for silica formation, silica chemistry is described in detail as follows.

2.2.2 Silica chemistry

Strategies for silica deposition onto a template (**Section 2.2.1**) are basically based on sol–gel chemistry of a silica precursor [50-53], which certainly represents an important parameter in silica formation.

2.2.2.1 Silica precursors

Silicon alkoxides such as tetramethoxysilane (TMOS) and tetraethoxysilane (TEOS) are common silicon-containing precursors used to study silica formation and generate materials for technological applications [53-55]. They are water-insoluble, and their use over aqueous silica precursors (e.g., sodium silicate and silicon catecholate) mainly results from three major aspects [54]. First, silicon alkoxides are available as pure, single molecules of which the hydrolysis kinetics can be efficiently controlled. In contrast, aqueous silica precursors are in the form of metal salt solutions, which can be prepared in a limited range of pH and concentrations and may often contain a mixture of oligomeric species whose reactivity is more difficult to control [56]. Second, silicon alkoxides are mainly neutral species and can remain stable in neutral solutions from days to weeks depending on the water concentration and the length and bulkiness of the alkyl chain [53], whereas metal salts tend to form charged species upon dissolution in water and usually leading to precipitation upon solvent addition [54]. Finally, alkoxides are also available with non-hydrolyzable organic functional group (e.g., phenyl, methyl, and vinyl) allowing modification of surface chemistry of the silica [57]. Overall, the use of silicon alkoxides as precursors to form silica-based nanomaterials is more flexible than using aqueous silica precursors in terms of reaction conditions, functionality and reactivity.

2.2.2.2 Hydrolysis and condensation of silicon alkoxide

In order for solid silica to be produced from silicon alkoxide (*Section 2.2.2.1*), hydrolysis and condensation of the precursor must occur prior to concomitant nucleation and growth of solid silica. In general, the hydrolysis and condensation reactions occur based on bimolecular nucleophilic

substitution (S_N2-type reaction). At the functional group level, three reactions are generally used to describe the sol–gel processes as shown below [52, 53],

Hydrolysis: $Si(OR)_4 + xH_2O \rightleftarrows (RO)_{4-x}–Si–(OH)_x + xROH$ (**Equation 1**)

Condensation: $\equiv Si–OR + HO–Si\equiv \rightleftarrows \equiv Si–O–Si\equiv + ROH$ (**Equation 2**)

$\equiv Si–OH + HO–Si\equiv \rightleftarrows \equiv Si–O–Si\equiv + H_2O$ (**Equation 3**)

where R is an alkyl group (C_xH_{2x+1}).

The hydrolysis reaction (**Equation 1**) replaces alkoxide groups (OR) with hydroxyl groups (OH) producing a monomer containing silanol groups (≡Si–OH). Complete hydrolysis produces silicic acid ($Si(OH)_4$). However, under most conditions, condensation commences before hydrolysis completes [53]. The hydrolysis reaction is specific-acid-[H_3O^+] or specific-base-[$OH^–$] catalyzed [51-53]. It proceeds by bimolecular nucleophilic displacement reactions involving formation of a transition state [53]. In acidic conditions, the alkoxide group is protonated forming a pentacoordinate intermediate molecule in a rapid first step. The protonated species withdraw electron density from the silicon atom within the intermediate molecule, making it more electrophilic, and thus more susceptible to nucleophilic attack by water. The water molecule acquires partial positive charge, and thus the positive charge of the protonated alkoxide within the intermediate molecule is reduced. Then, the transition state decays and followed by displacement of alkoxide with hydroxyl to form monomer containing silanol groups. In basic conditions, water molecule dissociates in a rapid first step to produce nucleophilic hydroxyl anion which then attacks the silicon atom and results in the formation of pentacoordinate intermediate molecule. Both the hydroxyl and the alkoxide within the intermediate molecule acquire partial negative charges. Then the intermediate decays, in which the hydroxyl displaces the alkoxide to form monomer containing silanol groups.

The subsequent condensation reactions involving monomer with silanol groups produce dimer having siloxane bond (≡Si–O–Si≡) and the by-products alcohol (ROH) (**Equation 2**) or water (**Equation 3**). Similar to the hydrolysis reaction, the condensation reactions are also catalyzed by acid or base, and involve formation of a transition state. Below the isoelectric point of silica (< pH 2–4.5, depending on the extent of condensation of the silanol species [53]), some silanol species in monomers are protonated which make the silicon more electrophilic, and thus more susceptible to nucleophilic attack by unionized silanol species. Above the isoelectric point of silica, species containing silanol deprotonate depending on their acidity, and produce negatively charged silicate species (≡Si–$O^–$) which makes the silica species more nucleophilic and enable them to attack unionized silanol species. Overall, the condensation reactions occur through a bimolecular collision between the unionized and ionized monomers [51, 53].

2.2.2.3 Nucleation and growth of silica

As previously mentioned, the molecular mechanism for the condensation reaction involve a bimolecular collision between an ionized and an un-ionized silicic acid molecule (*Section 2.2.2.2*). After the initial condensation, polycondensation of silica species continues in such a way to produce a maximum number of siloxane bonds and a minimum number of uncondensed silanol groups [51]. Therefore, monomers and dimers cyclize and form cyclic trimer and cyclic tetramer, instead of forming linear oligomers. Once the cyclic species dominate, monomers and dimers react preferentially with these species to form higher order rings. The cyclization is due to the proximity of the chain ends and the substantial depletion of the monomer population [53]. Moreover, in the case where the silica species are ionized, the charge distribution in the cyclic species is more symmetrical and thus energetically favourable than the linear species [58]. The presence of the cyclic species during the polycondensation process has been detected experimentally by using various spectroscopy techniques, e.g., Fourier-transform infrared, UV-Raman and ^{29}nuclear magnetic resonance [58-60]. Furthermore, quantum mechanical calculations using ab initio and semi-empirical methods have calculated and compared the structures, charge distributions and energies of the linear and ring structures of the silica species in which the formation of the cyclic species is energetically more favourable [61, 62], consistent with the published experimental results, with a little difference in stability for rings containing 3 and 6 Si atoms i.e., only 4 kcal/mol difference in the heat of formation per silica tetrahedral added [63, 64]. The rings form the basic framework of three-dimensional internally condensed spherical poly(silicic acid) nanoparticles which can also be described as silica nuclei having size of 1–2 nm [51] (**Figure 2**).

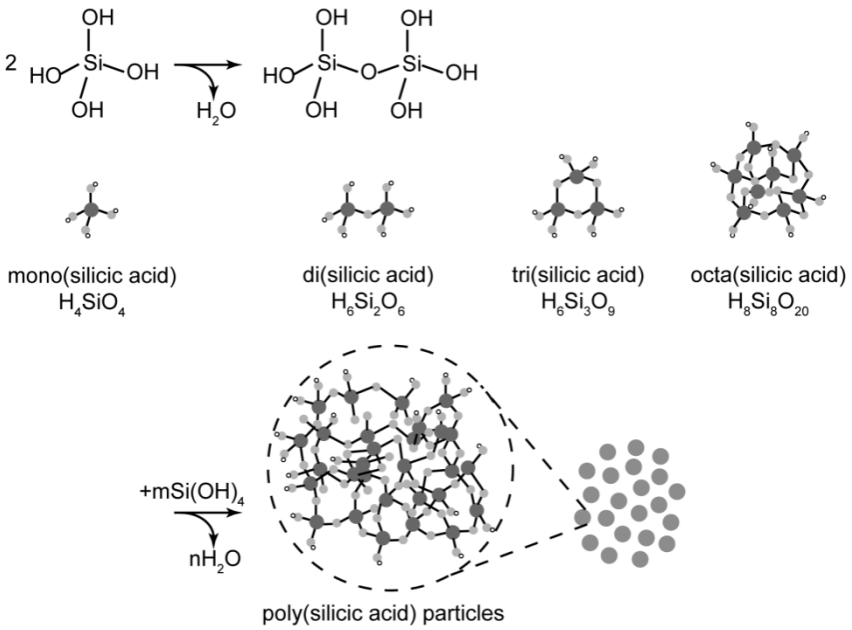

Figure 2. Formation of silica nuclei through polycondensation of silicic acid monomers. Polycondensation of silicic acid monomers yields dimer, cyclic oligomers and subsequently highly condensed, spherical poly(silicic acid) nanoparticles having a homogeneous appearance in aqueous phase. The figure is not drawn to scale.

The poly(silicic acid) nanoparticles (**Figure 2**) can continue growing through Ostwald ripening where the smaller nanoparticles, which are more soluble than the larger ones, dissolve and release silicic acid monomers that re-deposit onto the larger nanoparticles [65]. Silica growth requires both depolycondensation (ring opening) of the poly(silicic acid) nanoparticles and the availability of monomers, which are in solution equilibrium with the oligomeric species and/or generated by depolycondensation (reverse of **Equation 2** and **Equation 3**) [52]. The silica keeps growing until reaching a final size which depends on the temperature, solution pH and ionic strength of the solution [66] (**Figure 3**).

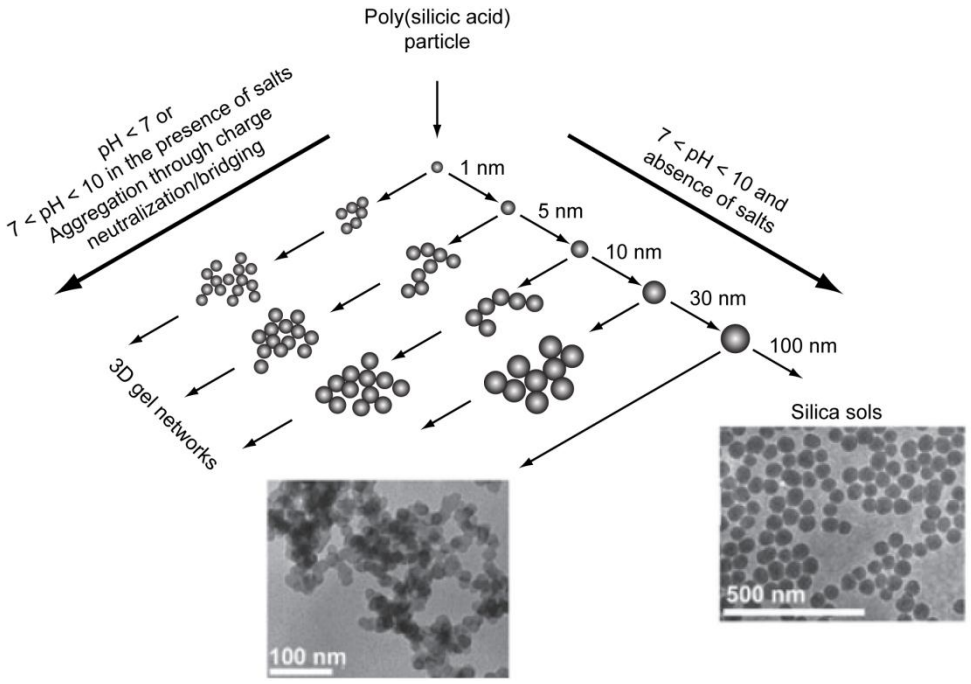

Figure 3. A schematic illustration of silica growth. The schematic describes the formation of nanoparticles and aggregated structures as a function of pH and presence of salts. In basic solution, the nanoparticles grow in size with decrease in number. In acid solution or in the presence of salts, the nanoparticles aggregate into three-dimensional networks and form gels. The transmission electron microscopy (TEM) images were adapted from Belton *et al.* [55].

At pH < 7 and in the absence of salts, the negatively charged silanolate group (Si–O^-) at the surfaces of poly(silicic acid) nanoparticles is protonated, in which the repulsion effect between individual nanoparticles is reduced and cause formation of a gel [51, 53]. At pH between pH 7 and 10 and in the presence of salts, the salts interact with the negatively charged silicate species and screen the surface charge of the nanoparticles which favour their gelation [67]. In both conditions (pH < 7 and 7 < pH < 10 in the presence of salts), the nanoparticles can collide with each other forming dense 3D networks (**Figure 3**). At pH between pH 7 and 10 and in the absence of salts, the nanoparticles become stable toward gelation due to mutual repulsion effects of the negatively charged silanolate groups resulted from deprotonated silanol groups (pK_a 6.7) (**Figure 3**). The nanoparticles can continue growing as isolated nanoparticles until the concentrations of silicic acid approach the solubility limit of amorphous silica. However, the particle size can possibly be increased by supplementing with additional silicic acid monomers that can undergo polycondensation on the surfaces of the nanoparticles [51]. The growth of the nanoparticles stops when majority of the nanoparticles are too large to be re-dissolved and to take part in the Ostwald ripening process [68].

2.2.2.4 Factors governing kinetics of silica growth

Other factors than pH and presence of salts that affect the formation kinetics of solid silica (*Section 2.2.2.3*) include temperatures, presence of additives, identity of precursors, and type of solvents [53, 55].

The solubility of amorphous silica is enhanced with increasing temperature which, in turn, increases the rate of polycondensation and results in a larger particle size at a higher temperature. For example, silica nanoparticles having diameters in a range of 5–10 nm can be obtained at an ambient temperature, whereas silica nanoparticles with diameters up to 150 nm are formed at 350 °C in the same reaction period [68].

Additives such as cationic or hydrogen-bonding polymers can accelerate the condensation reactions leading to a phase separation and forming silica precipitates [51]. The mode of action involves polymer adsorption onto the silica nanoparticle surfaces that contain silanol and negatively charged silanolate groups, which reduces inter-particle electrostatic repulsion and then induces aggregation. If more polymers are adsorbed on the surfaces, the apparent charge of the nanoparticles is reversed to become positive and re-dispersed the aggregates [51]. Long-chain polymers may also bridge the nanoparticles together, which leads to flocculation and precipitation of silica.

The reaction rate of hydrolysis and condensation is affected by the steric factor of silicon alkoxide precursors, i.e., alkyl chain length and degree of branching [53]. For example, the hydrolysis of TMOS ($Si(OCH_3)_4$) completes within minutes whereas the hydrolysis of TEOS ($Si(OC_2H_5)_4$) occurs over several hours under similar conditions [69]. This is because the steric effect of ethoxide is greater than methoxide, as observed by the time needed to convert an emulsion of TEOS in water into a homogeneous solution.

Homogenizing agent including alcohols, tetrahydrofuran or acetone is usually added to facilitate hydrolysis reaction due to the insolubility of silicon alkoxides precursor (*Section 2.2.2.1*) [52, 53]. Because sol–gel processes are hydroxyl or hydronium ion catalyzed, solvent molecules which form hydrogen bonding with hydroxyl ions or hydronium ions can reduce the catalytic activity under basic and acidic conditions, respectively. Therefore aprotic solvents (e.g., tetrahydrofuran and acetone), which do not form hydrogen bonding with hydroxyl ions, have the effect of making hydroxyl ions more nucleophilic, and thus promoting base-catalyzed hydrolysis, whereas protic solvents (e.g., alcohols) make hydronium ions more electrophilic, and thus promoting acid-catalyzed hydrolysis.

2.3 Bio-inspired silicification

Nature's ability to form silica with controlled structure and properties developed over millions years ago provides a new paradigm for developing silica-based nanomaterials. The biological systems in Nature can uptake silicon-containing compounds (in a form yet unknown) from its surrounding environments and organize them into complex, highly ordered structures of defined functionality [70]. There are many types of organisms having an endogenous silica, ranging from aquatic (e.g., diatoms, radiolarian, and sponges) and terrestrial (e.g., horsetail and rice leaves) organisms [71, 72] to plants [72]. The siliceous portions formed in the living organisms are hydrated silica (SiO_2) that is in an amorphous state [73, 74]. They evidence in the cell walls of diatoms, the skeletons of marine sponges, and the leaves of plants, among others [75], which primarily serve as a mechanical or structural support for the organisms. Although silica provides essential life functions for many organisms, it is the inherently green synthesis with precise control of biosilicification that has garnered attention from the academic and industrial communities [71, 76-78]. Specifically, the biosilicification reactions proceed under aqueous conditions at ambient temperatures and pressures, and near-neutral pH in the absence of toxic organic compounds [79]. Successful identification of genes and isolation of the mineralizing proteins from the organisms while still maintaining their biosilicification functionality *in vitro* are crucial for elucidation of the mechanisms governing biosilicification [80, 81]. At the atomic scale, these biomolecules are able to recognize, interact with, and direct the nucleation and growth of silica species [76], thereby transforming silicon-containing compounds in aqueous solution to amorphous solid silica-based nanomaterial under mild physiological conditions [71, 82]. It is thus essential to understand the underlying mechanisms of the biosilicification by understanding the amino acid residue sequences composing those proteins that have molecular recognition to silica species [80, 81]. In turn, the biological principle in biosilicification may inspire "bottom-up" synthesis of silica-based nanomaterials *in vitro* by mimicking functionality of the mineralizing proteins in the organisms [83].

In the following review, the proteins associated with silica formation in diatoms and sponges, the two most prominent source of inspiration for the applications of bio-inspired silicification, are discussed firstly. This provides fundamental understanding of the interactions between silica material and the proteins at the level of amino acids. Then, peptides derived from the naturally occurring mineralizing proteins, peptides obtained from combinatorial biology, and other peptides/proteins rationally designed for the synthesis of silica-based nanomaterials are presented in order to broaden the knowledge of different combinations of amino acid residue sequences that affects the biosilicification.

2.3.1 Silica-precipitating proteins extracted from living organisms

Silicateins (for *silica* pro*teins*), which belong to the cathepsin L class of the papain-like cysteine protease superfamily [84], was demonstrated to have biosilicification activity [80]. The entrapped proteins within the axial channel of the spicule could be isolated from the marine sponge, *Tethya aurantia* (*T. aurantia*) [80]—a sponge whose structure is defined by silica spicules that constitute up to 75% of its dry weight [84]. Three proteins were found by dissolution of the spicule in buffered hydrofluoric acid, and referred to silicatein α, β, γ [84]. The isolated silicatein filaments were observed to initiate hydrolysis and condensation of TEOS *in vitro* at neutral pH and ambient temperature, producing silica precipitates [80]. Biosilicification functionality of silicatein α, which comprises 70% of the silicatein filament mass in *T. aurantia* [84], was explored by first producing it through *E. coli* [80]. Hydrophobic amino acid residues in silicatein α could draw TEOS molecules closer to the protein [85]. Subsequently, the nucleophilic serine–histidine pair in silicatein α attacks silicon atom in TEOS molecule and initiates the hydrolysis and condensation reactions [80, 85, 86] (**Figure 4**). The close juxtaposition of serine-26 and histidine-165 in the active site of silicatein α enhances the efficiency of S_N2-type nucleophilic attack [86]. The catalytic mechanism of silicatein α is similar to the well-characterized catalysis mechanism of the serine–histidine and cysteine–histidine pairs within proteases [87]. In addition to the biosilicification functionality, silicatein α was also found to serve as a scaffold by self-assembled into a fibrous structure that supports silica formation on their surfaces [80]. The acceleration of the hydrolysis and condensation of TEOS and structure-directing activities of silicatein α are also evident when used other silicon alkoxide precursors i.e., organically substituted triethoxysilane precursors having general structure of $R–Si(OC_2H_5)_3$, where R represents phenyl and methyl [80].

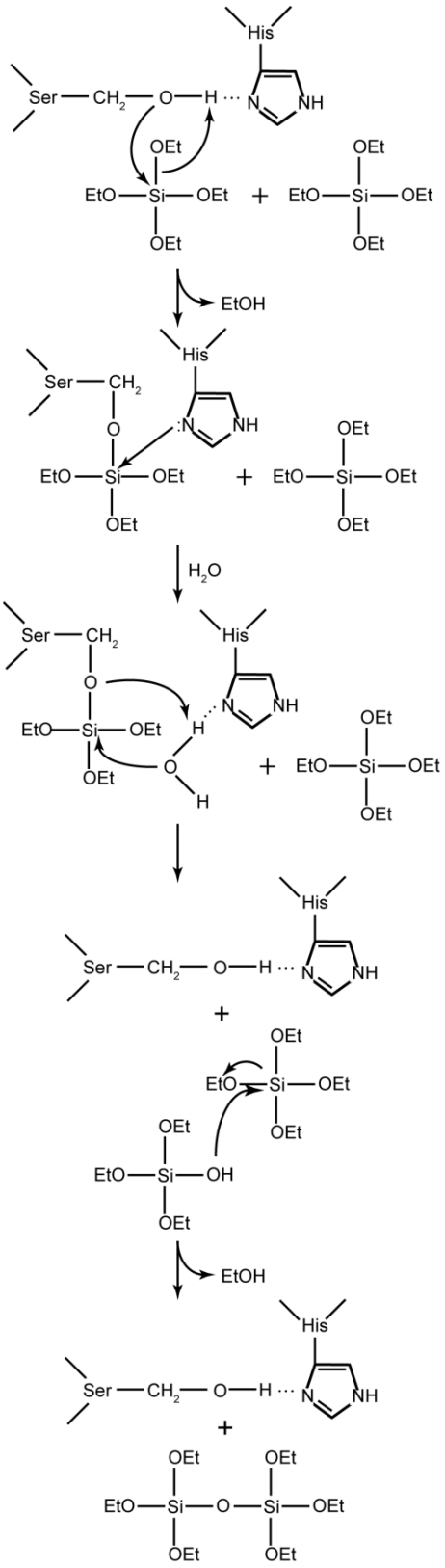

Figure 4. Hydrolysis of tetraethoxysilane (TEOS) through nucleophilic attack of serine–histidine pair within silicatein α on silicon atom and the subsequent condensation reaction, as proposed by Cha *et al.* [80, 85]. Hydrogen bonding between hydroxyl and imidazole side chains of serine-26 and histidine-165, respectively, increases nucleophilicity of the serine oxygen atom to attack silicon atom on TEOS molecule and form a transitory protein–substrate intermediate that

would be stabilized as a pentavalent silicon species through a donor bond from the imidazole nitrogen atom. Hydrolysis of the intermediate releases monomer containing silanol group and regenerates serine–histidine pair. Condensation is initiated by nucleophilic attack of the silanol on the silicon of the second TEOS molecule which then forms dimer.

A completely different type of protein than silicateins which is contributed to the cell walls of a diatom was recently shown to be associated with proteins called silaffins (for *sil*ica *affin*ity) [81]. The mineralizing proteins, silaffin-$1A_1$, -$1A_2$, -1B, were generated *in vivo* through enzymatic cleavage of a single protopolypeptide (sil-1p) and were isolated from the diatom *Cylindrotheca fusiformis* by anhydrous hydrofluoric acid treatment. The silaffins are homologous polypeptides that are highly post-translationally modified and enriched in serine (S), lysine (K) and glycine (G) residues with many of the lysines modified to long-chain polyamine moieties and the serines phosphorylated [81, 88-90]. The silaffins were demonstrated to accelerate polycondensation of silicic acid at pH 5 forming silica nanospheres *in vitro* [81, 89]. The basic amino acid lysine (K) with its modified form, which increases the overall positive charge of the biomolecule at neutral pH, govern the electrostatic interaction with anionic silanolate species (≡Si–O^-) [81]. The hydroxyl-rich domains in silaffins may contribute to form hydrogen bonding with silica species [81]. The potential capability of hydroxyl amino acids in diatom cell walls such as serine (S) and threonine (T), which can interact with the growing silica structure, was also previously suggested for the control of biosilicification [91-93]. Hecky *et al.* proposed that such hydroxyl-rich domains might align silicic acid monomers ($Si(OH)_4$), either by condensing with them (with elimination of water) to form covalent adducts or by hydrogen bonding, thus bringing them into favourable juxtaposition for their condensation to form silica (**Figure 5**) [91]. Furthermore, the silaffins could self-assemble in aqueous solution to function as a template for silica deposition, thus directing spherical structure [89].

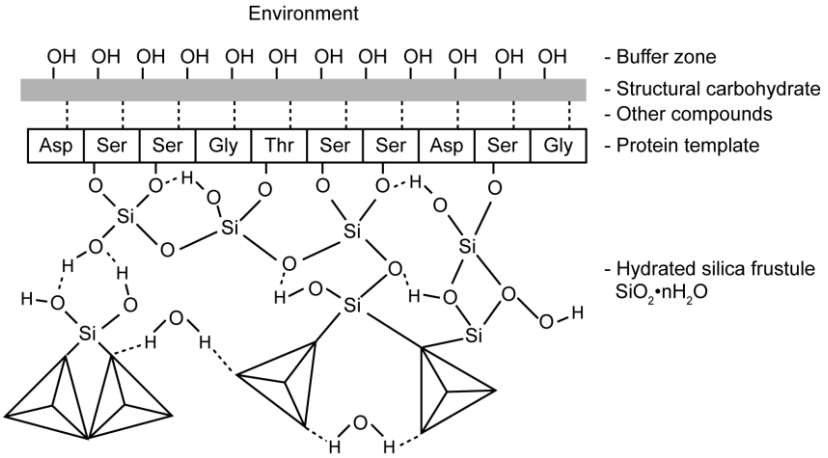

Figure 5. Hypothetical scheme of silicic acid condensation reactions in the diatom cell walls (frustule), as proposed by Hecky *et al.* [91]. A protein template, rich in serine (S), threonine (T) and glycine (G), is proposed to form hydrogen bonding with mono- or orthosilicic acid, followed by a condensation reaction to form initial layer of covalent C–O–Si linkages. This layer would then promote condensation with other silicic acid molecules, thereby "epitaxially" growing silica directly from the template. An outer layer of polysaccharide acts as a buffer against dissolution of the siliceous frustule. Other compounds, including lipids, metal ions, *etc.*, are also present in the cell wall. Hatched lines represent hydrogen bonds. Tetrahedron emphasize the three-dimensionality of the silicic acid (and resulting silica) with Si in four-fold coordination with oxygen atoms at the points of the tetrahedra.

In summary, the specificity of proteins extracted from Nature for silica species may originate from both chemical (nucleophilicity, hydrogen bonding, and charge effects) and structural (morphology) recognition mechanisms. It has been reported that (1) nucleophilic amino acids, including serine (S) and histidine (H) in silicatein α, play roles in the hydrolysis of water-insoluble silicon alkoxide; (2) the hydrolytic activity of serine (S) and histidine (H) in silicatein α necessitates the amino acids to be in the close juxtaposition in order to achieve efficient catalysis and produce high amount of silica precipitates; (3) amino acids having hydroxyl groups and positive charge at near-neutral pH play roles as nucleation sites promoting the interaction with soluble silica species through hydrogen bonding and electrostatic interactions, respectively; and (4) the structural complexity of the protein contributes primarily as a structure-directing agent through polycondensation of silica species forming a layer that follows the contours of the underlying protein structure, thus governing the morphology of the resulted silica-based materials.

2.3.2 Peptide/protein sequences programmed silica formation

Mineralizing proteins obtained from organisms (***Section 2.3.1***) generally involve collection of the organisms, isolation of the siliceous part, and extraction of the proteins using hydrogen fluoride to dissolve silica that associates with the proteins [80, 81]. This extraction technique is a direct method useful for studying the biosilicification processes but limiting for practical applications. Therefore, a number of model systems have been used to study the formation of silica nanostructures (**Table 2**).

Combinatorial phage peptide display and selection technique have been employed to identify consensus binding motifs for peptide–silica interactions [94] (Si*m-n*) (**Table 2**). The inclusion of amino acid residues having hydroxyl, imidazole, and cationic functional groups within the peptides were found effective to bind, nucleate, and grow silica from silicic acid solution at near-neutral pH [94].

Table 2. Amino acid motifs in designed (poly)peptides capable of directing nucleation and growth of silica under mild physiological conditions

Peptide	Sequence	Silica precursor	Morphology	Ref
Si*3-3*; Si*3-4*; Si*3-8*; Si*4-1*; Si*4-3*; Si*4-7*; Si*4-8*; Si*4-10*	APPGHHHWHIHH; MSASSYASFSWS; KPSHHHHHTGAN; MSPHPHPRHHHT; MSPHHMHHSHGH; LPHHHHLHTKLP; APHHHHPHHLSR; RGRRRRLSCRLL	Silicic acid	Spheres	[94]
R5	SSKKSGSYSGSKGSKRRIL	Silicic acid	Spheres	[81, 95, 96]
Mutants of R5	SGSKGSKRRIL; KSGSYSGSKGSKRRIL; SGSKGSKRR; SSKKSGSYSGSKGSK; LIRRSSKKSGSY; SSKKSGSYRRIL;	Silicic acid	Spheres	[96]
(N/A)	NH_2-NSGAITIG-$CONH_2$; NH_2-NTGAITIG-$CONH_2$	TEOS	Fibrils	[97]
P_{11}-3; P_{11}-4	QQRFQWQFQQQ; QQRFEWEFEQQ	TEOS	Fibrils	[98]
(N/A)	YSDQPTQSSQRP; TYHSSQLQRPPL; SPLSIAASSPWP	(N/A)	(N/A)	[99]
SAF[a]	KIAALKQKIASLKQEIDALEYENDALEQ- KIRRLKQKNARLKQEIAALEYEIAALEQ	Silicic acid	Tubes	[100]

Continued Table 2

PA1[b]; PA2[b]	AAAAKKKK; AAAAHHHH	TEOS	Tubes	[101]
Arginine-based surfactant[c]	R	Sodium silicate	Wormhole	[102]
DS202; DS189; DS30; DS250; DS256; DS262	RLNPPSQMDPPF; QTWPPPLWFSTS; LTPHQTTMAHFL; APRDNFNTVNLL; MPAKEWLPKHNN; SVSVGMKPSPRP	TMOS	Highly-porous spheres	[103, 104]
1; 2; 3	RLSKRVSAMQNSGVND; YGGFSKKKFMRF; SGGLHGVG	TEOS	Spheres	[105]
Block copolypeptide[d]	Poly((L-Lys)$_x$-*b*-(L-Cys)$_y$) (x = 200 or 400; y = 10, 30 or 60)	TEOS	Spheres; elongated globules; columns	[106]
	Poly((L-Ala)$_{30}$-*b*-(L-Lys)$_{200}$); Poly((L-Gln)$_{30}$-*b*-(L-Lys)$_{200}$); Poly((L-Ser)$_{30}$-*b*-(L-Lys)$_{200}$); Poly((L-Tyr)$_{30}$-*b*-(L-Lys)$_{200}$); Poly((L-Cys)$_{30}$-*b*-(L-Glu)$_{200}$)	TEOS	Non-ordered	[106]
	Poly((L-Lys)$_x$-*b*-(L-Gly)$_y$) (x = 110, 200, 320 or 340; y = 50, 85, 55 or 160); Poly((L-Lys)$_x$-*b*-(L-Ala)$_y$) (x = 390 or 400; y = 65 or 100); Poly((L-Lys)$_{450}$)	Silicic acid	Platelets; spheres	[107]
	L-Lys$_{23}$-*b*-L-Phe$_{23}$	Silicic acid	Hollow spheres	[108]
K^P_n (see note e)	K^P_{56}; K^P_{300}; K^P_{530}	TMOS	Hexagonal plate	[109]
MAX1; MAX8	VKVKVKVKV^{D}P^{L}PTKVKVKVKV; VKVKVKVKV^{D}P^{L}PTKVEVKVKV	TEOS; TMOS	Tubes	[110]
I_3K	IIIK	TEOS	Tubes	[111]
Lanreotide	NH_2-(D)Naph-Cys-Tyr-(D)Trp-Lys-Val-Cys-Thr-$CONH_2$	TEOS	Tube	[112]
Peptide 1[f]	CKKCKK	TEOS	Silver–silica core–shell spheres	[113]

[a] Self-assembling of SAF to peptide fibers is formed by block A (KIAALKQKIASLKQ) which complements D (EIAALEYEIAALEQ), and B (EIDALEYENDALEQ) which complements C (KIRRLKQKNARLKQ). This leads to sticky-ended dimers that assemble further into fibres. The register of the assembly is partly maintained by the asparagine residues.

[b] The *N*-terminus of PA1 and PA2 are from an alkyl chain, $CH_3(CH_2)_{14}CO^-$, introducing the amphiphilic nature to the peptide.

[c] The *N*-terminus of the arginine-based surfactant is C_nH_{2n-1} introducing the amphiphilic nature to the peptide.

[d] The block copolypeptides were designed to contain covalently linked domains (blocks) of hydrophilic and hydrophobic polypeptides that gave the chains an amphiphilic character. Thus, the copolypeptides could self-assemble into structured aggregates (originated from hydrogen, or covalent bonding, or disulphide linkages forming intra and intermolecular bridges) that act as template for the formation of ordered silica-based nanomaterials. Differences in silica morphologies when using block copolypeptide were observed due to different chemistry of hydrophobic block as well as solution compositions that influence their self-assembly behaviour in solution.

[e] Ethylene glycol-modified polylysine with n represents number of residues.

[f] The two tripeptides (CKK) of Peptide 1 are connected through a disulfide bridge (–S–S–).

The nucleophilic sulfhydryl, amine, and hydroxyl functional groups on the side chains of cysteine (C), glutamine (Q), and tyrosine (Y) amino acid residues, respectively, have been reported able to nucleophilically attack silicon atom in TEOS, and thus initiate TEOS hydrolysis [106] (**Table 2**). Kasotakis and Mitraki [97] had proposed the effect of hydroxyl groups of serine (S) and threonine (T) with an amine group at the *N*-terminus of an octapeptide in initiating TEOS hydrolysis (**Figure 6**), which is close to the mechanism proposed by Cha *et al*. on silicatein α protein [80, 85]. At near-neutral pH, the hydroxyl group of serine (S) or threonine (T) on the peptide undergoes deprotonation caused by the *N*-terminal amino group. The deprotonated hydroxyl group increases nucleophilicity of the serine or threonine oxygen, and allows the attack of the silicon atom in TEOS. Through this process, an ethanol molecule is produced along with the putative formation of a tetrahedral intermediate. The presence of a water molecule completes TEOS hydrolysis producing a monomer containing silanol group (≡Si–OH). A dimer with a siloxane bond (≡Si–O–Si≡) is formed after the attack of the silanol group to the second TEOS molecule. The polycondensation of silica species continues by forming poly(silicic acid) nanoparticles which accumulate and bind to the surfaces of the peptide fibrils *via* hydrogen bonding [97] (**Figure 6**).

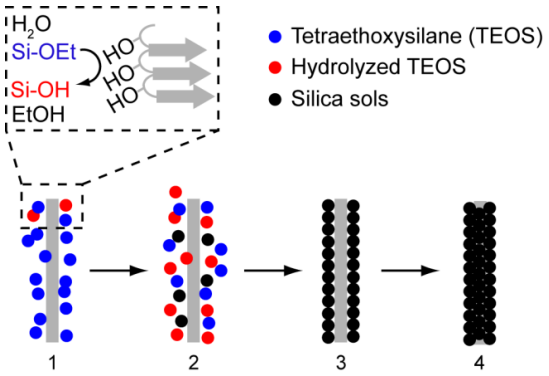

Figure 6. Illustration of the effect of hydroxyl groups on peptide fibril surfaces to nucleophilically attack the silicon atom in tetraethoxysilane (TEOS) molecules, as proposed by Kasotakis and Mitraki [97]. The peptide molecules self-assemble to fibrils in aqueous solution and are shown as gray β-strands with the serine residues located in the loop. (1) TEOS hydrolysis is initiated at the fibrils surfaces by the serine (S) or threonine (T) residues to form silanol species (≡Si–OH). (2) The silanol species diffuse at the vicinity of the fibril where polycondensation begins and silica sols start to form. (3) The silica sols accumulate on the fibril surfaces. (4) In longer incubation times, the silica sols deposit further leading to the complete occlusion of the fibril in a tubular silica sheath.

Amino acid residues with an amine group such as arginine (R) and lysine (K) play important roles in catalyzing silica formation. Example of a peptide composed of cationic amino acids is R5 peptide [114]. R5 peptide is derived from silaffins but lacks of the extensive post-translational modifications (i.e., phosphorylation, polyamine addition, and lysine methylation) that are unique to silaffins. R5 peptide was shown able to initiate the nucleation and growth of silica from aqueous silicic acid at near-neutral pH and room temperature (**Table 2**) [81]. Knecht and Wright investigated a range of R5 peptide variants, in which key amino acid residues within R5 peptide sequence were substituted, deleted, and/or re-arranged [96] (**Table 2**). The analysis of these peptides revealed that the *C*-terminus peptide motif (i.e., RRIL) was important in the biosilicification of the peptide. As suggested by Mizutani *et al*. [115], molecules containing amine functional groups could act as an acid–base catalyst, in which deprotonated residues (base) accepts a proton from silicic acid ($Si(OH)_4$) forming negatively charged silanolate group ($\equiv Si–O^-$), and protonated residues (acid) would drive the release of water by protonation of silicic acid substrates. The positively charged patches along the molecules surfaces would interact electrostatically with the silanolate species to initiate condensation reactions. This hypothesis is supported by other researchers suggesting the effect of cationic amino acid residues in catalyzing polycondensation of silica species [81, 96, 101, 106, 111, 116, 117]. For example, cationic poly(L-cysteine)-*b*-poly(L-lysine) promoted interaction with anionic silanolate to form silica, whereas anionic poly(L-cysteine)-*b*-poly(L-glutamate) was unable to form silica [106]. The various modes of electrostatic interactions between silica species and proteins are illustrated in **Figure 7** [68].

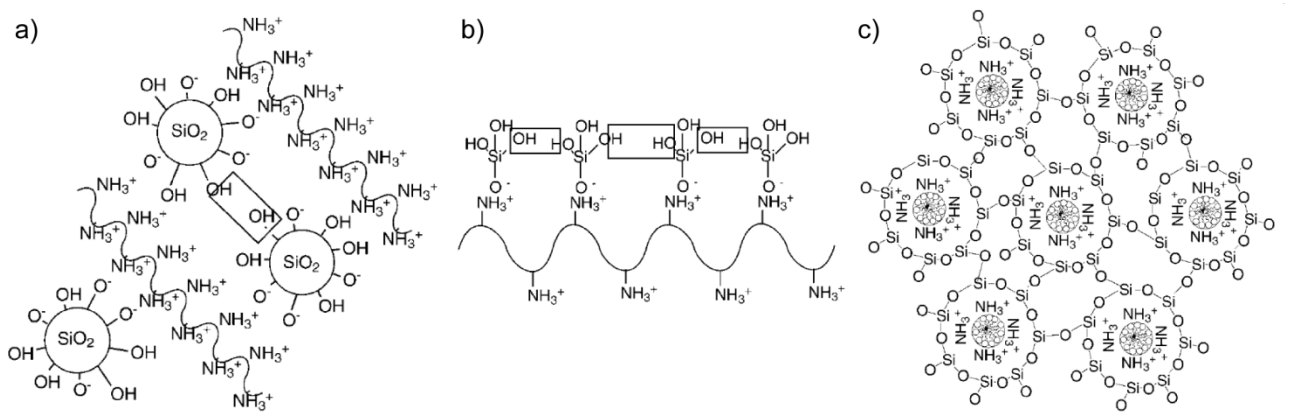

Figure 7. Illustration of the interactions of positively-charged functional groups on amino acid side chains with silica. a) Proteins having cationic functional groups bridge the negatively charged silica particles. b) Cationic patches of a protein interact with anionic silanolate species to initiate condensation reactions. c) Self-assembled proteins forming micelles with positively-charged functional groups on their surfaces act as templates for the formation of mesostructured silica. The figure was adapted from Coradin and Lopez [68].

Some area of applications for biomimetic approach have been developed in the process of making functional silica-based nanomaterials. The applications are mainly intended for enzyme immobilization. It has been achieved by adding aqueous silicic acid, as a silica precursor, and a silica-forming polycationic biomolecules to the solution of enzyme [118-123]. Another way is to fuse a silica-forming peptide, e.g., R5 peptide, with the enzyme before addition of silicic acid [124, 125]. The methods led to entrapment of the enzyme inside the mineral phase, and generally resulted in excellent retention and stabilization of the enzyme activities [126]. In addition, R5 peptide has been incorporated into a hologram to facilitate the formation silica layer, which can improve mechanical and optical properties of the polymeric device [127]. Moreover, anticancer proteins can be autonomously encapsulated within silica nanoparticles to sustain its activity when mixed the proteins with silicic acid solution [128]. The biosilicification activity of the proteins is due to specific sequences in the protein that are mainly composed of cationic amino acid residues, i.e., PTD (YGRKKRRQRRR) and BH3 (LRRFGDKLN). Further applications of designed peptides to mediate silicification are in the area of inorganic coating [113, 123]. Peptide 1 (**Table 2**) was designed to stabilize silver nanoparticles and to subsequently control the growth of a very thin silica layer encasing the silver nanoparticles [113]. The resulting silica layer protects the silver nanoparticles from chemical etching, allows their inclusion in other materials, and renders them biocompatible.

In summary, three important amino acid residues properties that characteristically direct nucleation and growth of silica from silicon alkoxide precursors are nucleophilic, hydrogen-bond donor, and cationic at near-neutral pH. Biosilicification of the peptides/proteins containing these particular amino

acid residues has been developed based on self-assembly of the biomolecules in bulk aqueous solutions or at solid–liquid interfaces producing silica-based nanomaterials with various morphologies. Interactions between silica species and the peptides/proteins at oil–water interfaces have not been reported, and thus there are no current biomimetic routes to oil-filled silica nanocapsules. However, there are peptides that have been designed to be surface active, and capable of facilitating formation and stabilization of O/W nanoemulsions. Understanding the behaviour of such peptides at the interfaces coupled with peptide-directed biosilicification in bulk aqueous solution activity may provide an important knowledge for interfacial biosilicification. Prior to discuss designed peptides/proteins as surfactants, theoretical background of nanoemulsions, including their formation and stability, are described as follows.

2.4 Nanoemulsions

2.4.1 Nanoemulsion formation

Combining oil and water in a container expectedly results in a layer of oil formed over a layer of water due to their density difference. This represents thermodynamically most stable state of a mixture of oil and water as it minimizes the contact area between the two phases, and hence minimizing their free energy. To form nanoemulsions, an input of free energy is required in order to overcome interfacial tension at the oil–water interfaces and to rupture larger droplets down to a smaller size, thereby creating a high total contact area between the two phases [129]. A surface-active agent (surfactant) is usually added to reduce interfacial tension and also to facilitate stabilization of nanoemulsions (see **Section 2.5**). At constant temperature, pressure, and chemical potential, the interfacial free energy can be expressed mathematically as follows [130],

$$\Delta G = \gamma \cdot \Delta A \qquad \textbf{(Equation 4)}$$

where ΔG is the change of the interfacial free energy (J or N/m), ΔA is the change of the contact area between oil and water phases (m^2) and γ is the interfacial tension at oil–water interfaces (J/m^2 or mN/m).

In the absence of any applied external forces, nanoemulsion droplets tend to be spherical because this shape minimizes the energetically unfavourable contact area between the oil and the water phases for a given volume [131]. The forces responsible for holding the droplets together and keep their spherical shape are referred to as interfacial forces. The interfacial forces are characterized by the Laplace pressure (ΔP_L, N/m^2), which is the pressure difference between the inside and the outside of the droplets across the oil–water interfaces. It can be expressed by the following equation [132, 133],

$$\Delta P_L = \frac{4\gamma}{d}$$

(**Equation 5**)

where d is the droplet diameter (m). The equation clearly indicates that it becomes more difficult to disrupt droplets as their interfacial tension increases or their size decreases. A significant disruptive pressure must be generated in order to compensate or overcome the interfacial tension [134].

One of the methods that allow generating intense disruptive forces for the emulsification is by using ultrasonic device. It is beneficial due to its lower energy consumption and its ability to achieve smaller droplet sizes while obtaining more homogeneous batches, as compared to conventional mechanical processes [135]. Ultrasonic devices include focusing horn and pointed tip as transducer that contains piezoelectric crystals. When a high-intensity electrical wave is applied to the transducer, the piezoelectric crystals are rapidly oscillated and generated an ultrasonic wave at ultrasonic frequencies, typically between 20 and 50 kHz [134, 136]. The ultrasonic wave is directed toward the tip of the transducer where it radiates into the surrounding liquids and generates intense pressure, causing extreme shear and cavitation [137-139]. In turn, it causes liquids to be deformed and disrupted into fine droplets [140]. Increasing the intensity or duration of the disruptive energy supplied during sonication can reduce droplets size [135, 141]. Ultrasound method is usually conducted for a period of few minutes in a number of short bursts because it can cause appreciable heating. It should be noted that prolonged exposure of certain proteins to high-intensity ultrasound could promote denaturation of the proteins [136].

2.4.2 Nanoemulsion stability

Nanoemulsions are thermodynamically unstable systems. Thermodynamic stability of nanoemulsions is determined by the free energy between nanoemulsions and the separating phases (i.e., oil and water) [130]. Nanoemulsion systems tend to undergo transition from high free energy state to the lowest free energy state where it is the most thermodynamically stable. The rate at which this transition occurs determines kinetic stability of the nanoemulsion systems; the more stable the nanoemulsions, the longer the nanoemulsions persist. It is affected by (1) height of energy barriers (activation energies) that separates the two states; and (2) mass transport phenomena including diffusion and convection processes that determine how fast components in the nanoemulsion systems can move [130, 136]. Therefore, nanoemulsions are metastable systems as they will ultimately breakdown to separate phases given sufficient time. Difference between the thermodynamic stability and the kinetic stability of a nanoemulsion system is presented in **Figure 8**.

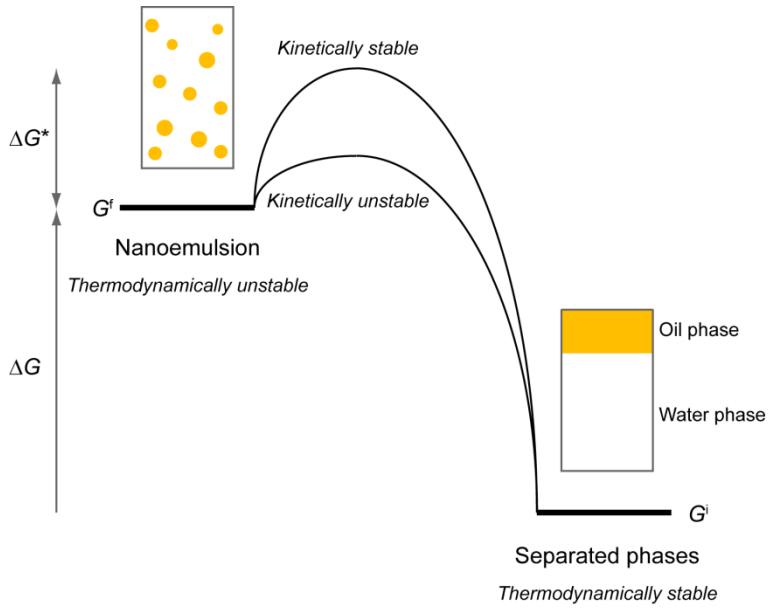

Figure 8. Schematic presentation of the difference between thermodynamic- and kinetic-stability of a nanoemulsion system. Nanoemulsions are thermodynamically unstable and tend to revert to the state with the lowest free energy. Kinetically stable nanoemulsions can be achieved by ensuring that there is a sufficiently high energy barrier between the two states. The higher the energy barrier, the nanoemulsions are more kinetically stable and, hence, the longer the nanoemulsions will persist. G^f and G^i are free energy of the system in its final (after emulsification) and initial (before emulsification) states, respectively. ΔG described the difference in the free energy between G^f and G^i. ΔG^* represents an activation energy that keep the system to be in a kinetically stable state.

The height of energy barrier depends on the physicochemical properties of nanoemulsion surfaces that prevent destabilization of the nanoemulsions. These include repulsive hydrodynamic and colloidal interactions between the nanoemulsion droplets, which are strongly affected by the presence of surfactants [133, 136, 142-147]. The hydrodynamic interactions arise from relative motion of the droplets in a suspending medium. When the droplets approach each other in the suspending medium, the hydrodynamic resistance occurs depending on the interfacial film thickness and interfacial mechanical strength of the thin liquid film between them. On the other hand, the colloidal interactions depend on the surfactant chemistry which may cause steric and/or electrostatic repulsion between nanoemulsion droplets in an aqueous solution. Frequent collisions between droplets, which result from Brownian motion, applied shear or thermal energy, or gravitational forces, can reduce the kinetic stability of the nanoemulsions [131, 136]. To maximize the kinetic stability of nanoemulsion systems, it is necessary to understand physical mechanisms of nanoemulsion instability [136, 148] (**Table 3**).

Table 3. Physical mechanisms of nanoemulsion instability

Type of physical instability of nanoemulsion droplets	Principles
Gravitational separation 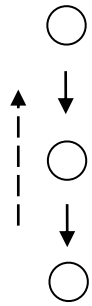	• Gravitational separation results from a density difference between the water (ρ_1) and oil (ρ_2) phases. • If $\rho_1 < \rho_2$, then oil droplets tend to move downward (i.e., sedimentation). • If $\rho_1 > \rho_2$, then oil droplets tend to move upward (i.e., creaming).
Flocculation 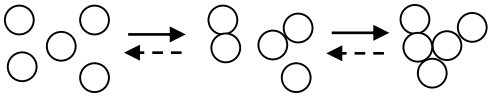	• Flocculation results from collisions between droplets, which is induced by Brownian motion, gravitational separation, or applied forces. The droplets can retain their individual integrity and result in a little change to their total interfacial area. • Droplets flocculation may either be (1) reversible (i.e., weak flocculation) which can be re-dispersed by changing physicochemical conditions (e.g., pH, ionic strength, solvent polarity, or temperature) or by applying mechanical agitation (e.g., stirring or sonication); or (2) irreversible (i.e., strong flocculation or coagulation).
Coalescence 	• Coalescence may result from droplets collisions. As the droplets come to close contact, the thin film separating them is ruptured and the droplets are fused into a larger droplet hence reducing their total surface area. • Coalescence is an irreversible process.
Ostwald ripening 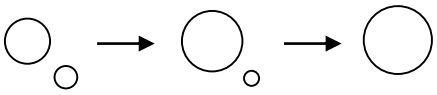	• Ostwald ripening is a process of gradual growth of the larger droplets at the expense of smaller ones due to mass transport of soluble dispersed phase (oil) through the continuous phase (water). • This process causes the small droplets to shrink and eventually disappear, and the large droplets to grow. Once occurred, this process cannot be reversed.

Gravitational separation causes droplets to come into close contact for extended periods which can lead to enhanced aggregation [133, 136], and eventually oiling off, that is, the formation of a layer of oil phase on top of the water phase [136]. According to Stokes [149], when a sphere submerged in a viscous liquid an upward gravitational force would act on it and a downward hydrodynamic frictional force would act retarding its motion. The sphere would accelerate until the forces acting on it are in balance, and thus the velocity rate of the sphere in highly dilute nanoemulsions can be obtained as follows,

$$v_{\text{Stokes}} = -\frac{2gr^2(\rho_2 - \rho_1)}{9\eta_1}$$

(**Equation 6**)

where r is the radius of the droplet (m), g is the acceleration due to gravity (m/s^2), ρ is the mass density (kg/m^3), η is the Newtonian shear viscosity (kg/m·s), and the subscript 1 and 2 refer to the continuous and dispersed phases, respectively. The sign of v_{Stokes} (m/s) determines whether the droplet moves upward (+) or downward (–). **Equation 6** suggests that there are number of ways to reduce the gravitational separation rate: (1) reduction in droplet size (r) by modification of energy input and type, and concentration of surfactants which allow more efficient oil disruption and resistance against droplet coalescence; (2) minimization of phase density difference ($\rho_2 - \rho_1$) by adding an active molecule or a weighting agent to the oil phase to increase the oil density prior to the emulsification; and (3) increase of viscosity of the continuous phase by introducing a thickener or a gelling agent (e.g., biopolymer) in the continuous phase which decreases the velocity of the droplets. The Stoke's equation applies only to highly dilute, non-interacting nanoemulsion system, and therefore is not applicable to concentrated, polydisperse or aggregated nanoemulsion systems. However, the parameters governing gravitational separation rate, as defined by the Stoke's equation, could be applied non-quantitatively to improve nanoemulsion stability against creaming or sedimentation.

Flocculation and coalescence are two types of aggregation. Aggregation occurs due to frequent collision between two or more droplets, and it depends on the nature of the colloidal and hydrodynamic interactions in the systems [133, 136, 142-147]. As the droplets come into close proximity, a relatively thin film of continuous phase is formed at oil–water interfaces. The thin interfacial film generates hydrodynamic resistance to droplets association and, depending on the level of energy barrier that separates the droplets, the thin film continues to thin up to a certain value after which aggregation may occur. At high energy barrier, droplets are finely dispersed in the aqueous phase; at slightly lower energy barrier, droplets are weakly flocculated, as the thin layer still exists; at low energy barrier, droplets are strongly flocculated with a very thin film existing between the droplets. Finally, as the energy barrier is so low, the surfaces between droplets become flattened and the thin film is eventually ruptured, which results in droplets coalescence. The rupture of the thin

film between droplets is caused by thermal energy or applied mechanical forces [150, 151]. The process involves hole formation in any remaining continuous phase between the droplets as well as in the adjacent surfactant layers at the interfaces, which may result in desorption of surfactant from the interfaces to the bulk solutions [133, 136].

In general, aggregation can be prevented through proper selection of nanoemulsion ingredients, including type and concentration of surfactants or presence of additives, that could promote greater repulsive interactions than the attractive forces between droplets [136]. For example, too low concentration of surfactants may result in incomplete surface coverage of droplets and, as a result, the adsorbed surfactants attach to other droplet surfaces which then leads to bridging flocculation [152]. Presence of additives such as multivalent ions that have opposite charge can screen the surface charges and result in bridging flocculation [153]. Surfactants play an important role in reducing the coalescence rate by increasing interfacial film thickness [136] and interfacial mechanical strength [154].

Ostwald ripening occurs when large droplets grow at the expense of smaller ones because of mass transport of dispersed phase from one droplet to another through the intervening continuous phase [155] (**Table 3**). This occurs because concentration gradient exists, which results from higher solubility of the dispersed phase within a small droplet than within a larger droplet [136, 144]. To control Ostwald ripening phenomena in nanoemulsion systems [155, 156], it is important to have nanoemulsion systems with narrow size distribution, low equilibrium solubility of the dispersed phase in the continuous phase, reduced interfacial tension, and high interfacial film thickness to reduce mass transport of molecules from one droplet to another droplet. These factors are largely influenced by surface-active agents.

2.5 Peptides/proteins as surface-active agents

Surface-active agents (surfactants) generally consist of hydrophobic and hydrophilic moieties. Because of their dual nature (amphiphilic), surfactants tend to adsorb at oil–water interfaces. Chemically, the hydrophobic moiety (referred to as the “tail”) is typically hydrocarbon, which can be either straight-chained or branched, or in some specialized surfactants, a fluorocarbon. The hydrophilic moiety (referred to as the “head”) covalently attached to the tail derives from a positive or negative charge (in the case of ionic surfactants), from extensive hydrogen bonding with aqueous phase (in the case of non-ionic surfactants), or from a strong dipole moment (in the case of zwitterionic surfactants) [157]. Besides chemical compounds, biological compounds including peptides/proteins have also been used as surfactants to stabilize O/W emulsions [158, 159]. The hydrophobic and hydrophilic moieties within the peptide surfactants are structurally different from the chemical surfactants [158]. They comprise polyamide backbone chirally decorated with hydrophobic

and hydrophilic side chains. The structural difference between peptide surfactants and conventional surfactants is illustrated in **Figure 9**.

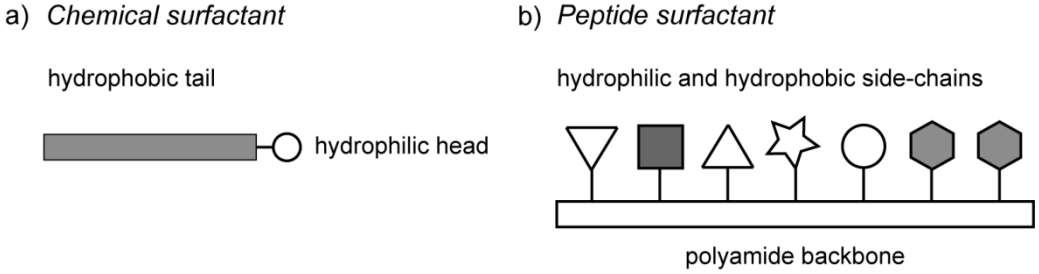

Figure 9. Structural compositions of chemical surfactant compared to peptide surfactant. a) The chemical surfactant comprises hydrophobic tail (shaded dark) and hydrophilic head (shaded light). b) The peptide surfactant composes of polyamide backbone having hydrogen bonding capacity to a defined sequence of hydrophilic (shaded light) and hydrophobic (shaded dark) side-chains. The figure was inspired by Dexter and Middelberg [158].

In this section, designed peptide- and protein-surfactants used as the basis design of bifunctional modular peptide/protein in this study are discussed in detail as follows.

2.5.1 Designed peptide surfactants

A series of peptide surfactants have been designed and investigated in our lab for making oil-in-water (O/W) emulsions including AM1 [160-163] and AFD4 [163]. Other peptides including peptides H, S and R [164], and peptides B-14, B-15, B16 and B17 [165] have also been researched by others (**Table 4**). Among them, AM1 has well characterized interfacial property and structure [166] and is capable of reversibly and precisely controlling the stability of O/W emulsions [160].

Table 4. Examples of peptide surfactants capable of emulsifying oil phase

Peptides	Amino acid sequences	Theoretical net charge at pH 7	Stability mechanism at neutral pH	Ref
AM1[a]	Ac-MKQLADSLHQLARQVSRLEHA-$CONH_2$	+1.2	Cohesive interfacial film; electrostatic repulsion	[160, 161, 167]
AFD4[a]	Ac-MKQLADSLHQLAHKVSHLEHA-$CONH_2$	+0.4	Cohesive interfacial film; electrostatic repulsion	[163, 167]
B-14[b]; B-15[b]; B-16[b]; B-17[b]	Ac-PDFDFDFDP-$CONH_2$; Ac-PHFHFHFHP-$CONH_2$; Ac-PEFEFEFEP-$CONH_2$; Ac-PKFKFKFKP-$CONH_2$	-4.0 +0.02 -4.0 +4.0	Electrostatic repulsion	[165]
H[a]; S[a]; R[a]	LEELLEELLEELLEEL; ELELELELELELELEL; LELLEEELLEEELLEL	-8 -8 -8	Electrostatic repulsion	[164]

- Secondary structures of the respected peptide are α-helix (a) and β-sheet (b). α-helix and β-sheet formation are achieved by manipulating the spacing of the hydrophobic residues within the sequence, i.e., (i, i + 3 and i, i + 4) and (i, i + 2), respectively [168].
- The peptide termini were capped by *N*-acetylation and *C*-amidation to avoid interactions between adjacent peptide termini;

Peptide surfactant AM1 (Ac-MKQLADS LHQLARQ VSRLEHA-$CONH_2$, *M* 2472.86 Da) [160] used in this study was designed based on a 21 amino-acid peptide Lac21 (Ac-MKQLADS LMQLARQ VSRLESA-$CONH_2$) [169] which was derived from sequences contained in the tetramerization domain of the bacterial Lac repressor protein [169]. AM1 and Lac21 contain 21 amino acid residues comprising three repeating seven-residue motif (i.e., heptad), *abcdefg*, in which hydrophobic amino acid residues are located at positions *a* and *d* (mainly methionine (M), leucine (L) and valine (V)), while the remaining residues are predominantly hydrophilic amino acid residues. This alternate three and four residue spacing of hydrophobic moieties permits the formation of an α-helical structure having distinct hydrophobic and hydrophilic faces at the interface. In the presence of oil–water interface, either AM1 [160] or Lac21 [170] could adsorb to the interface; the hydrophobic face interacts with the oil phase and the hydrophilic residues on the opposite face of the helix contact the bulk aqueous phase.

The key difference between AM1 and Lac21 is the inclusion of two metal-binding residues, histidine (H), in AM1 at position 9 and 20. The histidines are incorporated into the AM1 sequence such that they will be orientated toward other interfacially adsorbed peptide molecules, allowing for the formation of metal ion bridges (i.e., Zn^{2+}–histidine) between the adsorbed peptide molecules, hence interfacial peptide network [167]. Such intermolecular crosslinking of the peptide molecules

generates a cohesive interfacial film that contributes significantly to the stability of O/W emulsions [166] (**Figure 10**). Furthermore, the stabilization of emulsions by AM1 can be switched off from film state to detergent state by adding acid (at pH < 4) or chelating ligand (e.g., ethylenediaminetetraacetic acid (EDTA)) in the bulk solutions to sequester the bridging between Zn^{2+} ions and histidine residues [160]. Thus, the histidine residues in AM1 molecules are no longer crosslinked to each other, which results in the reduction of the interfacial mechanical strength, and hence droplets coalescence (**Figure 10**).

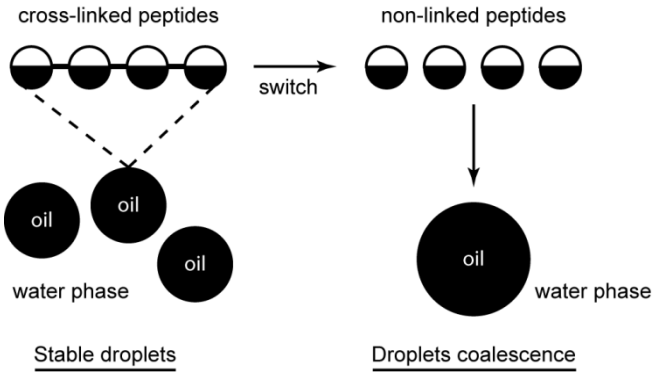

Figure 10. Modulation of the stability of emulsions by peptide surfactant. The peptides self-assemble to α-helix structure at an oil–water interface with the hydrophobic face (shaded dark) oriented toward oil phase and the hydrophilic face (shaded light) oriented toward bulk water phase. In the presence of transition metal ions, crosslinking between the adsorbed peptides occur which increase cohesive monolayer at the interface hence stabilizing the nanoemulsions against coalescence. The cross-links are switched off when metal sequestering compound or acid is added, which result in droplets coalescence. The figure was inspired by Dexter and Middelberg [158].

To obtain better understanding of the interfacial properties of AM1 and the influence of added Zn^{2+} ions, AM1 adsorption at the air–water interface was investigated using Cambridge Interfacial Tensiometer (CIT) [171, 172], and the results showed that the formation of interfacial film (in the presence of Zn^{2+} ions) could transmit significant force in the plane of the interface when compared to its detergent state (in the absence of Zn^{2+} ions) [160]. At film state, the interfacial elasticity modulus and the interfacial tensile stress were 121 mN/m and 6.9 mN/m, respectively. When the interfacial network was switched off, the interfacial elasticity modulus and the interfacial tensile stress dropped significantly to 30 mN/m and 0.5 mN/m, respectively. Furthermore, neutron reflectometer studies demonstrated that AM1 folded into an α-helix structure during interfacial self-assembly, creating a thin, but strong, ordered layer at the interface in the presence of Zn^{2+} [166]. Interfacial film thickness of AM1 was measured to be approximately 15 Å with Young modulus of 80 MPa in the film state and less than 20 MPa in the detergent state [166]. In addition, interfacial molecular area and surface coverage of AM1 at the interface were 380 $Å^2$/molecule and 55%, respectively, as characterized by

the neutron reflectometer [166]. Quantitative determination of the surface activity of AM1 showed a 52.9 mN/m in interfacial tension (from the initial value of 73 mN/m) at AM1 concentration of 5 μM in the presence of added Zn^{2+} [160]. AM1 peptide molecules undergo only minimal self-assembly in bulk solution [167], thus are capable of rapidly adsorbing to the freshly formed air–water interface, and hence reducing interfacial tension. Apparently, switching the film state to the detergent state was not accompanied by significant changes in dynamic interfacial tension (as detergent state of AM1 gave 52.1 mN/m in interfacial tension under the same concentration) [160]. Similar dynamic interfacial tensions of AM1 at film and detergent states was because both states consisted of an approximate monolayer of the peptide with similar surface excess as studied using neutron reflectometer [166]. Therefore, the difference of interfacial properties of AM1 at the film and detergent states is due to changes in the interaction between the peptide molecules at the interface and the formation of cohesive interfacial network [160].

AM1 nanoemulsion has been developed in our lab as nanocarrier of curcumin for biomedical applications [161]. Curcumin, a lipophilic drug, could be co-delivered with bovine serum albumin (BSA), a model protein antigen, for specific inhibition of nuclear factor kappa B (NF-κB), a therapeutic target for treating rheumatoid arthritis disease, in antigen presenting cells [161]. To co-deliver curcumin and BSA, curcumin-loaded nanoemulsions were first formed by directly dissolving curcumin into the oil phase, followed by sonicating the oil phase in AM1 peptide aqueous solution. The resulting nanoemulsions were then surface functionalized through electrostatic deposition of BSA at neutral pH, as positively charged AM1 nanoemulsions (+46 mV) could interact with negatively charged BSA molecules through electrostatic attraction. This resulted in the formation of negatively charged curcumin-loaded nanoemulsions (–40 mV) having BSA decorated on the droplet surfaces [161]. Although the zeta potential of the nanoemulsions was reduced to –13 mV under physiological conditions, the nanoemulsions demonstrated stability as BSA displayed at the interfaces provides steric barrier to flocculation. Further, the nanoemulsions were successfully internalized and well-tolerated by model antigen presenting cells, and were able to suppress NF-κB expression [161].

Use of AM1 nanoemulsions for biomedical applications has also been extended to the development of a targeted and immune-evading nanocarrier formed using “top-down non-covalent click self-assembly” [162]. Ovalbumin was used as a model protein antigen that could be delivered to dendritic cells, a model target cells, in mice. To load ovalbumin into AM1 nanoemulsions, solid-in-oil (S/O) nanodispersion method [173] was used, thereby coating ovalbumin with hydrophobic surfactant *via* homogenization in an aqueous solvent to form protein–surfactant complexes. The complexes were then lyophilized to evaporate the solvent resulting in hydrophobic solid particles which could be dissolved in an oil phase to form S/O nanodispersions. The nanodispersions were mixed with AM1 aqueous solution *via* sonication to form ovalbumin-loaded nanoemulsions. To efficiently deliver ovalbumin to dendritic cells *in vivo*, poly(ethylene glycol), an immune-evading molecule, and

monoclonal antibody Clec9A, a receptor-specific antibody element, conjugated to DAMP4 protein surfactant (detailed in ***Section 2.5.2***) were displayed at the surfaces of the ovalbumin-loaded nanoemulsion resulted from non-covalent integration of DAMP4 present in bulk solution with AM1 at the interfaces (**Figure 11**) [162]. As a result, the nanoemulsions could be uptaken and correctly processed by the target cells in a receptor-targeted fashion.

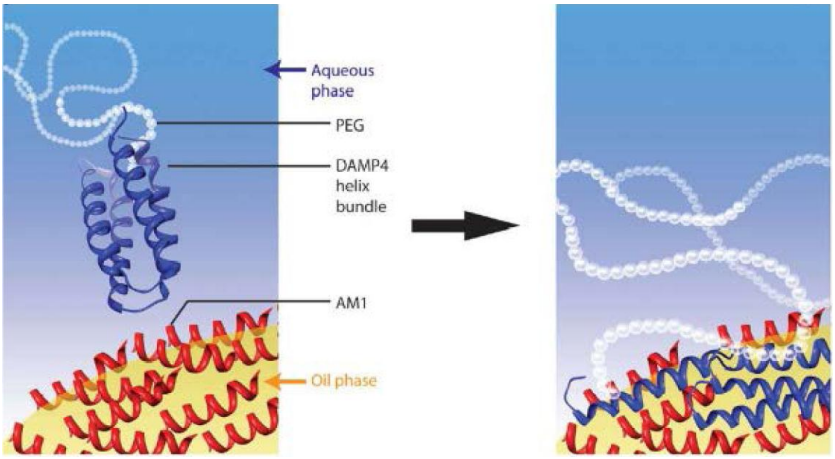

Figure 11. Application of designed AM1 peptide surfactant to facilitate formation of a targeted and immune-evading nanocarrier *via* top-down non-covalent click self-assembly, as proposed by Zeng *et al.* [162]. The figure shows PEG conjugated to DAMP4 protein is integrated onto surfaces of nanoemulsion that has been stabilized with AM1. The non-covalent integration of DAMP4 with AM1 results in the functional display of PEG at the interface separating the oil droplet from the bulk aqueous solution. This figure was adapted from Zeng *et al*. [162]

In summary, AM1 has well characterized interfacial structure, and the stabilization mechanisms of nanoemulsions imparted by AM1 are well understood that is based on a combination of interfacial mechanical strength and charge. The AM1-stabilized nanoemulsions have been demonstrated able to be effectively loaded with either hydrophobic or hydrophilic active agents. With rich chemistry of amino acid residues contained within AM1 peptide, various molecules can be attached to AM1 at the oil–water interfaces, thus enhancing the nanoemulsion performances in biological systems (i.e., stability, immune-evading ability and targeted delivery). Therefore, peptide surfactant AM1-based nanoemulsions could be a promising candidate for performing biosilicification at oil–water interfaces to fabricate peptide-based silica nanocapsules encasing oil droplets.

2.5.2 Designed protein surfactants

It is well known that many naturally occurring proteins including β-lactoglobulin, whey proteins, lysozyme and caseins adsorb spontaneously at oil–water interfaces as a result of their intrinsically amphiphilic nature [159]. The use of these biomolecules as protein surfactants is because of their ability to (1) lower interfacial tension [170]; (2) form interfacial protein network [171, 172]; and (3) generate steric and electrostatic barriers to coalescence [159, 174, 175].

Alternatively, surface active proteins can be rationally designed to contain variants of bioactive motif which can be produced by biological expression using microbial cell-factory (described in **Section 2.6**). A protein surfactant DAMP4 (MD(PSMKQLADS LHQLARQ VSRLEHAD)$_4$, *M* 11157.67 g/mol), was designed in our lab by joining four AM1 peptides through Asp-Pro-Ser (DPS) sequence [176]. The Asp-Pro-Ser linker in DAMP4 was incorporated (1) to promote electrostatic repulsion between adjacent loops through charged residue Asp; (2) to ensure helix termination between loops through Pro residue which has low helical propensity; and (3) to provide rotational freedom through Ser residue. These linkers along with the incorporation of four AM1 peptides give rise to the association of four amphiphilic α-helices interlocking the hydrophobic core, and thus folding into four-helix bundle structure in bulk aqueous solution [176].

Dynamic interfacial tension studies showed that DAMP4 at a concentration of 8 μM and nearly neutral pH was able to lower the interfacial tension of air–water interface to 25 mN/m [176]. DAMP4 was able to facilitate formation of foams, and the foam stability was maintained through electrostatic repulsion at or above pH 8.5 [176], as DAMP4 has isoelectric point (p*I*) of 6.7. Interfacial structure of DAMP4 at the air–water interface was studied using neutron reflectometer. The study suggested that DAMP4 could unfold and adsorb at the interface to form a monolayer of around 10–14 Å in thickness [177], which is approximately the same thickness as that of AM1 [166]. The unfolding behaviour of DAMP4 at the interface allows its hydrophobic face to orient away from the aqueous phase, while the hydrophilic face orients toward the aqueous phase (**Figure 12**) [176, 178].

More importantly, DAMP4 can be produced at high levels of solubility in genetically-modified bacteria, and forms a four-helix bundle structure in bulk aqueous solutions (**Figure 12**a). Initial characterization has demonstrated that the structure of DAMP4 remains stable at high temperature (e.g., 90°C) [179]. This behaviour, which is unusual for a protein, confers a unique manufacturing advantage. Basically, after making the protein in genetically modified bacteria, simply heating the cells to high temperature in the solution used to grow the cells releases product into the solution phase and deposits cellular contaminants into a solid phase, allowing very simple centrifugal or filtration separation. This discovery opens the way to a unique and very cheap manufacturing method (detailed in **Section 2.6**).

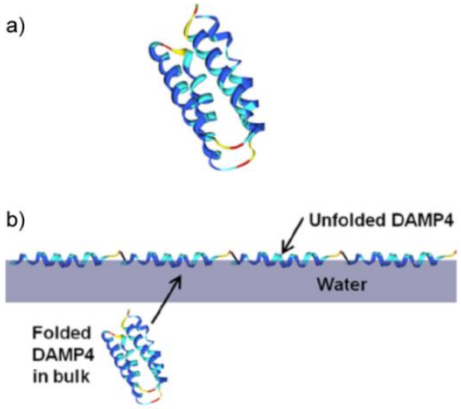

Figure 12. The interfacial behaviours of DAMP4 providing its surfactant properties as determined based on neutron reflectrometry study by Dimitrijev-Dwyer *et al.* [177]. a) Four-helix bundle motif of DAMP4 that fold in bulk aqueous solution. b) Unfolding of DAMP4 at air–water interfaces with the hydrophobic face oriented toward air phase and the hydrophilic face oriented toward water phase. This figure was adapted from Dimitrijev-Dwyer *et al.* [179].

2.6 Microbial bio-production of functional peptides/proteins

(Poly)peptides having biosilicification activity (**Table 2**) and peptide surfactants with surface activity (**Table 4**) are mainly synthesized by using chemical methods. The chemical synthesis methods are rapid and effective for the production of specialized peptides in relatively small quantities [180, 181]. However, it is technically difficult and costly when large scale chemical production of the peptides is needed [182]. Recombinant DNA technology provides a way to produce biomolecules from bacteria, e.g., *E. coli* [180, 183] at low cost. One example of the widely and commercially used recombinant protein produced by genetically engineered *E. coli* is insulin [184], which has been proved to be safe enough to be injected in human [185].

In general, recombinant DNA method involves insertion of a fragment of DNA containing gene of interest into a circular DNA molecule (i.e., vector) by cutting and joining the DNA using enzyme to produce a recombinant DNA molecule [186]. This recombinant DNA molecules are then transformed into a host cell, e.g., *E. coli*, so when the cell divides it will replicate the recombinant DNA molecules to the progenies; the process is so-called cloning. The cell then transcribes the recombinant DNA into messenger RNA as sets of three-nucleotide sequences (i.e., codons), each of which is translated to a particular amino acid. Cloning of genes that encode specific peptides/proteins having biosilicification or surface-active functionality, thus, permits their production through *E. coli*, which can provide assured and consistent source of the peptides/proteins.

Production of peptides/proteins through recombinant DNA technology is beneficial because it is more sustainable than the chemical synthesis. The development of high cell density culture technique for

E. coli has made it possible to express modified variants containing bioactive motifs in amounts suitable for research, clinical and industrial purposes [187]. In addition, the use of recombinant DNA allows molecular design and hence the introduction of new function, allowing for engineering-based solutions to problems of yield, cost and process scale-up. A number of studies have used *E. coli* to produce recombinant peptides/proteins having either biosilicification functionality or surface activity (**Table 5**).

Several challenges exist when expressing and purifying biomolecules in *E. coli*. It is especially the case when producing short recombinant peptides (10–30 amino acids). It has been shown that short recombinant peptide will be unstable in bacterial host [184, 188, 189] because they may self-associate, be toxic, or be rapidly degraded by proteases within the cell. Therefore, peptide is usually fused to a larger carrier protein to mask the self-assembly characteristic and to improve the intracellular stability. The resulting recombinant biomolecules should be determined for their activity whether the additional amino acid residue sequences might have negative impact. When the additional amino acid residue sequence influence the activity of the target peptides/proteins, then purification methods involve cleavage and separation of the peptides/proteins of interest from the carrier protein.

Table 5. Production of recombinant peptides/proteins having biosilicification or surface-active functionality in *E. coli* and their purification techniques

Target peptide/ protein	Expressed proteins	Amino acids length	*M* (kDa)	Purification processes	Final product and activity	Ref
15mer + R5 peptide	$(His)_6$-MaSp1-R5	561	46.5	Immobilized-metal affinity chromatography[a]	- $(His)_6$-MaSp1-R5 - Biosilicification activity	[190]
284[b]	$(His)_6$-284	214	24.2	Immobilized-metal affinity chromatography[c]	- $(His)_6$-284 - Biosilicification activity	[128, 191]
Silicatein α	Silicatein α-MBP[d]		29	1. Maltose-affinity chromatography[e]; 2. Enzymatic cleavage; 3. Ion exchange chromatography; 4. Size-exclusion chromatography	- Silicatein α - Biosilicification activity	[86, 192]
GAM1[f]	MBP-s-TEV-GAM1	22	2.5	1. Maltose-affinity chromatography[e]; 2. Enzymatic cleavage; 3. Acid precipitation; 4. Desalting	- GAM1 - Surface activity	[193]
DAMP4	DAMP4	98	11.1	- Chromatography method: 1. Immobilized-metal affinity chromatography[a]; 2. Ion-exhange chromatography; 3. Reversed-phase chromatography Or - Bake-to-break and precipitate method: 1. Heating/cell lysis and contaminant precipitation using sodium sulfate; 2. Dilute precipitation; 3. Membrane filtration	- DAMP4 - Surface activity	[176, 179]

[a] The IMAC process uses nickel-charged affinity resin. It uses a chelating ligand nitrilotriacetic acid coupled to a cross-linked agarose. It allows for the specific binding of the 6×Histidine fusion tag. MaSp1 is major ampullate spidroin protein 1 of *Nephila clavipes* spider dragline silk.

[b] 284 protein is an anticancer protein containing two PTD (YGRKKRRQRRR) and three BH3 (LRRFGDKLN) peptide motifs. The recombinant 284 proteins have demonstrated biosilicification functionality in bulk aqueous solution when reacted in a silicic acid solution at ambient temperature [128].

[c] The IMAC method uses cobalt-charged TALON® resin which is coupled to a cross-linked agarose. It allows binding to 6×Histidine fusion tag at the N-terminal of the protein.

[d] MBP is a maltose binding protein with an amino acid length of 387 and a molecular mass of ~41 kDa.

[e] Maltose-affinity chromatography uses amylose resin to capture maltose-binding protein (MBP).

[f] MBP-s-TEV-GAM1 is composed of maltose-binding protein (MBP), a spacer (s), tobacco etch virus (TEV), glycine (G) and AM1 sequences.

One recombinant peptide GAM1, which is surface active, was produced in *E. coli* [193]. It has a sequence equivalent to AM1 peptide surfactant [160] but with an *N*-terminal appended glycine residue and without *N*- and *C*-terminal capping (**Table 5**). Since the length of GAM1 (~2.5 kDa) is less than 30 amino acids, special design of the peptide is required to ensure successful expression of the peptide in *E. coli* and to enable its ease of purification. Maltose binding protein (MBP) having molecular mass of ~46 kDa was fused to the peptide in order to enhance solubility and enable high expression levels of the target peptide. The tagged protein is also useful to facilitate the purification by binding to the amylose resin through maltose-affinity chromatography. Tobacco etch virus (TEV) sequence (ENLYFQ) was added after MBP sequence to facilitate the release of the peptide from the fusion tag through the addition of tobacco etch virus protease (TEVp). Furthermore, a 14 amino acid unstructured spacer sequence (QTNSITSLYKSAGS) was inserted at the *C*- and *N*-terminal of the MBP sequence and TEVp cleavage site, respectively, to open the accessibility of the TEVp cleavage site. Additionally, glycine was introduced at the N-terminal of the original AM1 sequence to ensure more efficient cleavage by TEVp. Pure GAM1 peptides (>95% purity) were obtained after acid precipitation and desalting processes. In the presence of Zn^{2+}, GAM1 was demonstrated to yield characteristic stress–strain curves of the tension-compression cycle to 300% strain indicating that they have assembled into a mechanically strong cohesive film state at air–water interfaces, and thus capable of stabilizing foams [193].

DAMP4 protein surfactant can be expressed in *E. coli* at high levels and solubility, and easily purified (**Table 5**) due to the four-helix bundle structure of DAMP4, as described previously (***Section 2.5.2***). Protein having four helix bundle structures are known to have good post-expression stability [194] and, due to this design, DAMP4 was expressed successfully without a fusion partner [176]. To purify DAMP4, chromatography-based purification processes, i.e., immobilized-metal affinity chromatography (IMAC), ion exchange chromatography and reversed phase chromatography, can

be conducted [176]. Although DAMP4 does not carry hexahistidine tag, it can be captured to the IMAC column through binding between histidine residues in DAMP4 and nickel ions in IMAC system. Another purification method, which is cheaper than chromatography, is by using bake-to-break precipitation method [179], thereby mixing the *E. coli* cells in a buffer containing high Na_2SO_4 concentrations (up to 1 M) under high temperature (above 90 °C) to disrupt cell walls of *E. coli* containing DAMP4 and simultaneously precipitate the majority of contaminant proteins of *E. coli* while maintaining DAMP4 solubility. The thermal- and chemical denaturant-stability properties of DAMP4 are due to its four-helix bundle structure in bulk aqueous solution. Importantly, this simple purification still allows DAMP4 to maintain its surface activity [179]. Furthermore, the possibility to cleave DAMP4 at its DP sequence *via* acid hydrolysis opens opportunity to use DAMP4 as a carrier protein to potentially express a target peptide in *E. coli* at high levels and solubility and subsequently facilitate simple purification of the target peptide from the carrier DAMP4 protein.

In summary, recombinant DNA technology allows manipulation of bacterial genetic material in order to express designed peptides/proteins of interest using *E. coli*. It is desirable that peptides/proteins are designed with special considerations prior to expression and purification in order to enhance solubility, ease of cleavage (when applicable), and purification. Availability of fusion tag protein, spacer, and cleavage sites are the factors that need to be considered, together with the sequence specific for surface activity and biosilicification functionality. More importantly, the functionalities of the final products of recombinant peptides/proteins should be tested whether all those additional sequences and processes affect the surface activity and/or biosilicification functionality of the biomolecules.

2.7 Concluding remarks

Silica nanocapsules have attracted considerable attention due to their core–shell morphology which provides feasible way to combine multiple functionalities of the core and the silica shell on a nanoscopic length scale (**Section 2.1**). Templating-based methods using hard and soft templates are commonly used to synthesize silica nanocapsules (**Section 2.2**). Soft template-based synthetic approaches are more advantageous as compared to hard-templating methods. Loading of an active cargo in soft template is simplified as it can be directly dissolved in the core prior to silica shell formation without the need for template removal. However, the methods contain several drawbacks associated with harsh reaction conditions including extreme pH conditions and elevated temperatures in the presence of toxic organic solvents. The drawbacks can potentially be overcome by using biomimetic approaches that utilize peptides or proteins to induce silica formation under environmentally-friendly conditions including at near-neutral pH and room temperature in the absence of toxic organic solvents (**Section 2.3**). In addition, peptides/proteins have advantages of renewability and high biodegradability, as well as a likely high biocompatibility. Literature shows

various amino acid residue motifs in peptides and proteins that have been used to induce nucleation and growth of silica from silica precursor to silica-based nanomaterials. However, peptides and proteins available in the biomimetic approaches are limited for the biosilicification in bulk aqueous solution or at solid–liquid interfaces. As a result, the fabrication of oil-core silica-shell nanocapsules using peptides/proteins has not been realized yet.

In order to synthesize oil-core silica-shell nanocapsules, designed peptide and protein would be actively developed in this PhD project so that they have dual-functionality i.e., to facilitate formation and stabilization of nanoemulsion and to direct nucleation and growth of silica shell encapsulating the nanoemulsion core. Literatures suggest that only a few peptides with a surface activity that have been developed to emulsify oils (**Section 2.5**). Among designed surface-active peptides that are capable of stabilizing O/W nanoemulsions, AM1 designed in our lab has well characterized interfacial structure. The incorporation of specifically oriented functional groups in this helical peptide allows control over interfacial properties including charge and interfacial mechanical strength, resulting in the formation of switchable peptide-based emulsions. Building on the known surface-active peptide sequence of AM1 coupled with the knowledge of amino acid sequence specific for biosilicification (reviewed in this chapter), a bifunctional modular peptide would be designed to contain surface-active module and biosilicification-active module. The modular combination design would allow stabilization of nanoemulsion core and formation of silica shell, thus emulsion and biomimetic dual-templating approach for making oil-core silica-shell nanocapsules could be developed. This novel approach for making silica nanocapsules, as hypothesized in **Chapter 1**, will be experimentally researched and described in detail in **Chapter 3**.

References

1. Lou, X.W., L.A. Archer, and Z. Yang, *Hollow micro-/nanostructures: synthesis and applications.* Adv. Mater., 2008. **20**(21): p. 3987–4019.
2. Guerrero-Martínez, A., J. Pérez-Juste, and L.M. Liz-Marzán, *Recent progress on silica coating of nanoparticles and related nanomaterials.* Adv. Mater., 2010. **22**(11): p. 1182–1195.
3. Schärtl, W., *Current directions in core–shell nanoparticle design.* Nanoscale, 2010. **2**(6): p. 829–843.
4. Rana, R.K., Y. Mastai, and A. Gedanken, *Acoustic cavitation leading to the morphosynthesis of mesoporous silica vesicles.* Adv. Mater., 2002. **14**(19): p. 1414–1418.
5. Prouzet, E., F. Cot, C. Boissiere, P.J. Kooyman, and A. Larbot, *Nanometric hollow spheres made of MSU-X-type mesoporous silica.* J. Mater. Chem., 2002. **12**(5): p. 1553–1556.
6. Ung, T., L.M. Liz-Marzán, and P. Mulvaney, *Redox catalysis using Ag@SiO_2 colloids.* J. Phys. Chem. B, 1999. **103**(32): p. 6770–6773.

7. Joo, S.H., J.Y. Park, C.-K. Tsung, Y. Yamada, P. Yang, and G.A. Somorjai, *Thermally stable Pt/mesoporous silica core–shell nanocatalysts for high-temperature reactions.* Nat. Mater., 2009. **8**(2): p. 126–131.
8. Correa-Duarte, M.A., M. Giersig, and L.M. Liz-Marzán, *Stabilization of CdS semiconductor nanoparticles against photodegradation by a silica coating procedure.* Chem. Phys. Lett., 1998. **286**(5-6): p. 497–501.
9. Ow, H., D.R. Larson, M. Srivastava, B.A. Baird, W.W. Webb, and U. Wiesner, *Bright and stable core–shell fluorescent silica nanoparticles.* Nano Lett., 2005. **5**(1): p. 113–117.
10. Graf, C., D.L.J. Vossen, A. Imhof, and A. van Blaaderen, *A general method to coat colloidal particles with silica.* Langmuir, 2003. **19**(17): p. 6693–6700.
11. Kuwahara, Y., T. Yamanishi, T. Kamegawa, K. Mori, M. Che, and H. Yamashita, *Lipase-embedded silica nanoparticles with oil-filled core–shell structure: stable and recyclable platforms for biocatalysts.* Chem. Commun., 2012. **48**(23): p. 2882–2884.
12. Underhill, R.S., A.V. Jovanovic, S.R. Carino, M. Varshney, D.O. Shah, D.M. Dennis, T.E. Morey, and R.S. Duran, *Oil-filled silica nanocapsules for lipophilic drug uptake: implications for drug detoxification therapy.* Chem. Mater., 2002. **14**(12): p. 4919–4925.
13. Jovanovic, A.V., R.S. Underhill, T.L. Bucholz, and R.S. Duran, *Oil core and silica shell nanocapsules: toward controlling the size and the ability to sequester hydrophobic compounds.* Chem. Mater., 2005. **17**(13): p. 3375–3383.
14. Hayashi, K., M. Nakamura, and K. Ishimura, *In situ synthesis and photoresponsive rupture of organosilica nanocapsules.* Chem. Commun., 2011. **47**(5): p. 1518–1520.
15. Wang, J.W., Y.D. Xia, W.X. Wang, R. Mokaya, and M. Poliakoff, *Synthesis of siliceous hollow spheres with large mesopore wall structure by supercritical CO_2-in-water interface templating.* Chem. Commun., 2005. **-**(2): p. 210–212.
16. Chen, H., J. He, H. Tang, and C. Yan, *Porous silica nanocapsules and nanospheres: dynamic self-assembly synthesis and application in controlled release.* Chem. Mater., 2008. **20**(18): p. 5894–5900.
17. Li, J., J. Liu, D. Wang, R. Guo, X. Li, and W. Qi, *Interfacially controlled synthesis of hollow mesoporous silica spheres with radially oriented pore structures.* Langmuir, 2010. **26**(14): p. 12267–12272.
18. Zhao, M., L. Zheng, X. Bai, N. Li, and L. Yu, *Fabrication of silica nanoparticles and hollow spheres using ionic liquid microemulsion droplets as templates.* Colloids Surf., A, 2009. **346**(1–3): p. 229–236.
19. Zhu, Y.F., J.L. Shi, W.H. Shen, X.P. Dong, J.W. Feng, M.L. Ruan, and Y.S. Li, *Stimuli-responsive controlled drug release from a hollow mesoporous silica sphere/polyelectrolyte multilayer core–shell structure.* Angew. Chem., Int. Ed., 2005. **44**(32): p. 5083–5087.
20. Schärtl, W., *Crosslinked spherical nanoparticles with core–shell topology.* Adv. Mater., 2000. **12**(24): p. 1899–1908.

21. Qian, K., T.Y. Shi, S. He, L.X. Luo, X.L. Liu, and Y.S. Cao, *Release kinetics of tebuconazole from porous hollow silica nanospheres prepared by miniemulsion method.* Micropor. Mesopor. Mater., 2013. **169**: p. 1–6.
22. Parida, S.K., S. Dash, S. Patel, and B.K. Mishra, *Adsorption of organic molecules on silica surface.* Adv. Colloid Interface Sci., 2006. **121**(1–3): p. 77–110.
23. Chen, Y., H. Chen, and J. Shi, *In vivo bio-safety evaluations and diagnostic/therapeutic applications of chemically designed mesoporous silica nanoparticles.* Adv. Mater., 2013. **25**(23): p. 3144–3176.
24. Rosenholm, J.M., C. Sahlgren, and M. Linden, *Towards multifunctional, targeted drug delivery systems using mesoporous silica nanoparticles – opportunities & challenges.* Nanoscale, 2010. **2**(10): p. 1870–1883.
25. Mamaeva, V., C. Sahlgren, and M. Linden, *Mesoporous silica nanoparticles in medicine—recent advances.* Adv. Drug Deliv. Rev., 2013. **65**(5): p. 689–702.
26. Mahkam, M., *Synthesis and characterization of pH-sensitive silica nanoparticles for oral-insulin delivery.* Curr. Drug Deliv., 2011. **8**(6): p. 607–611.
27. Rigby, S.P., M. Fairhead, and C.F. van der Walle, *Engineering silica particles as oral drug delivery vehicles.* Curr. Pharm. Design, 2008. **14**(18): p. 1821–1831.
28. Rosenholm, J.M., V. Mamaeva, C. Sahlgren, and M. Linden, *Nanoparticles in targeted cancer therapy: mesoporous silica nanoparticles entering preclinical development stage.* Nanomedicine, 2012. **7**(1): p. 111–120.
29. U.S. Food and Drug Administration's Website, *GRN No. 321: Synthetic amorphous silica*. Available from: http://www.accessdata.fda.gov/scripts/fcn/gras_notices/GRN000321.pdf. Cited 21 May 2014.
30. He, Q., Z. Zhang, F. Gao, Y. Li, and J. Shi, *In vivo biodistribution and urinary excretion of mesoporous silica nanoparticles: effects of particle size and PEGylation.* Small, 2011. **7**(2): p. 271–280.
31. He, Q., J. Shi, M. Zhu, Y. Chen, and F. Chen, *The three-stage in vitro degradation behavior of mesoporous silica in simulated body fluid.* Micropor. Mesopor. Mat., 2010. **131**(1-3): p. 314–320.
32. Huang, X., X. Teng, D. Chen, F. Tang, and J. He, *The effect of the shape of mesoporous silica nanoparticles on cellular uptake and cell function.* Biomaterials, 2010. **31**(3): p. 438–448.
33. He, Q., Z. Zhang, Y. Gao, J. Shi, and Y. Li, *Intracellular localization and cytotoxicity of spherical mesoporous silica nano- and microparticles.* Small, 2009. **5**(23): p. 2722–2729.
34. Barbé, C., J. Bartlett, L.G. Kong, K. Finnie, H.Q. Lin, M. Larkin, S. Calleja, A. Bush, and G. Calleja, *Silica particles: a novel drug-delivery system.* Adv. Mater., 2004. **16**(21): p. 1959–1966.

35. He, Q., J. Shi, F. Chen, M. Zhu, and L. Zhang, *An anticancer drug delivery system based on surfactant-templated mesoporous silica nanoparticles.* Biomaterials, 2010. **31**(12): p. 3335–3346.
36. Kong, S.D., W. Zhang, J.H. Lee, K. Brammer, R. Lal, M. Karin, and S. Jin, *Magnetically vectored nanocapsules for tumor penetration and remotely switchable on-demand drug release.* Nano Lett., 2010. **10**(12): p. 5088–5092.
37. Chen, Y., Y. Gao, H. Chen, D. Zeng, Y. Li, Y. Zheng, F. Li, X. Ji, X. Wang, F. Chen, Q. He, L. Zhang, and J. Shi, *Engineering inorganic nanoemulsions/nanoliposomes by fluoride-silica chemistry for efficient delivery/co-delivery of hydrophobic agents.* Adv. Funct. Mater., 2012. **22**(8): p. 1586–1597.
38. Xia, Y.N., B. Gates, Y.D. Yin, and Y. Lu, *Monodispersed colloidal spheres: old materials with new applications.* Adv. Mater., 2000. **12**(10): p. 693–713.
39. Caruso, F., R.A. Caruso, and H. Mohwald, *Nanoengineering of inorganic and hybrid hollow spheres by colloidal templating.* Science, 1998. **282**(5391): p. 1111–1114.
40. Cornelissen, J.J.L.M., E.F. Connor, H.-C. Kim, V.Y. Lee, T. Magibitang, P.M. Rice, W. Volksen, L.K. Sundberg, and R.D. Miller, *Versatile synthesis of nanometer sized hollow silica spheres.* Chem. Commun., 2003. **-**(8): p. 1010–1011.
41. Stöber, W., A. Fink, and E. Bohn, *Controlled growth of monodisperse silica spheres in the micron size range.* J. Colloid Interface Sci., 1968. **26**(1): p. 62–69.
42. Zhao, Y., L.-N. Lin, Y. Lu, S.-F. Chen, L. Dong, and S.-H. Yu, *Templating synthesis of preloaded doxorubicin in hollow mesoporous silica nanospheres for biomedical applications.* Adv. Mater., 2010. **22**(46): p. 5255–5259.
43. Li, Z.Z., L.X. Wen, L. Shao, and J.F. Chen, *Fabrication of porous hollow silica nanoparticles and their applications in drug release control.* J. Control. Release, 2004. **98**(2): p. 245–254.
44. Chen, J.F., H.M. Ding, J.X. Wang, and L. Shao, *Preparation and characterization of porous hollow silica nanoparticles for drug delivery application.* Biomaterials, 2004. **25**(4): p. 723–727.
45. Wang, H.G., P. Chen, and X.M. Zheng, *Hollow permeable polysiloxane capsules: a novel approach for fabrication, guest encapsulation and morphology studies.* J. Mater. Chem., 2004. **14**(10): p. 1648–1651.
46. Zhao, Y., J. Zhang, W. Li, C. Zhang, and B. Han, *Synthesis of uniform hollow silica spheres with ordered mesoporous shells in a CO_2 induced nanoemulsion.* Chem. Commun., 2009. **-**(17): p. 2365–2367.
47. Hah, H.J., J.S. Kim, B.J. Jeon, S.M. Koo, and Y.E. Lee, *Simple preparation of monodisperse hollow silica particles without using templates.* Chem. Commun., 2003. **-**(14): p. 1712–1713.
48. Zoldesi, C.I. and A. Imhof, *Synthesis of monodisperse colloidal spheres, capsules, and microballoons by emulsion templating.* Adv. Mater., 2005. **17**(7): p. 924–928.

49. Wang, Q., Y. Liu, and H. Yan, *Mechanism of a self-templating synthesis of monodispersed hollow silica nanospheres with tunable size and shell thickness.* Chem. Commun., 2007. **-**(23): p. 2339–2341.
50. Iler, R.K., *The Colloid Chemistry of Silica and Silicates*. 1955, Ithaca, New York: Cornell University Press.
51. Iler, R.K., *The Chemistry of Silica: Solubility, Polymerization, Colloid and Surface Properties, and Biochemistry*. 1979, New York: Wiley.
52. Brinker, C.J., *Hydrolysis and condensation of silicates: effects on structure.* J. Non-Cryst. Solids, 1988. **100**(1-3): p. 31–50.
53. Brinker, C.J. and G.W. Scherrer, *Sol–Gel Science: The Physics and Chemistry of Sol–Gel Processing*. 1990, London: Academic Press.
54. Coradin, T. and J. Livage, *Aqueous silicates in biological sol–gel applications: new perspectives for old precursors.* Acc. Chem. Res., 2007. **40**(9): p. 819–826.
55. Belton, D.J., O. Deschaume, and C.C. Perry, *An overview of the fundamentals of the chemistry of silica with relevance to biosilicification and technological advances.* FEBS J., 2012. **279**(10): p. 1710–1720.
56. Jolivet, J.P., *Metal Oxides Chemistry and Synthesis: From Solution to Solid State*. 2000, Chichester: Wiley.
57. Sanchez, C. and F. Ribot, *Design of hybrid organic–inorganic materials synthesized via sol–gel chemistry.* New J. Chem., 1994. **18**(10): p. 1007–1047.
58. Wijnen, P.W.J.G., T.P.M. Beelen, J.W. Dehaan, L.J.M. Vandeven, and R.A. Vansanten, *The structure directing effect of cations in aqueous silicate solutions. A ^{29}NMR study.* Colloids Surf., 1990. **45**: p. 255–268.
59. Depla, A., D. Lesthaeghe, T.S. van Erp, A. Aerts, K. Houthoofd, F.T. Fan, C. Li, V. Van Speybroeck, M. Waroquier, C.E.A. Kirschhock, and J.A. Martens, *^{29}Si NMR and UV–Raman investigation of initial oligomerization reaction pathways in acid-catalyzed silica sol–gel chemistry.* J. Phys. Chem. C, 2011. **115**(9): p. 3562–3571.
60. Hench, L.L. and J.K. West, *Molecular orbital models of silica.* Annu. Rev. Mater. Sci., 1995. **25**: p. 37–68.
61. Pereira, J.C.G., C.R.A. Catlow, and G.D. Price, *Ab initio studies of silica-based clusters. Part I. Energies and conformations of simple clusters.* J. Phys. Chem. A, 1999. **103**(17): p. 3252–3267.
62. Pereira, J.C.G., C.R.A. Catlow, and G.D. Price, *Ab initio studies of silica-based clusters. Part II. Structures and energies of complex clusters.* J. Phys. Chem. A, 1999. **103**(17): p. 3268–3284.
63. West, J.K. and L.L. Hench, *A PM3 molecular-orbital model of silica rings and their vibrational-spectra.* J. Non-Cryst. Solids, 1994. **180**(1): p. 11–16.

64. West, J.K. and L.L. Hench, *Molecular-orbital models of silica rings and their vibrational-spectra.* J. Am. Ceram. Soc., 1995. **78**(4): p. 1093–1096.
65. Perry, C.C. and T. Keeling-Tucker, *Biosilicification: the role of the organic matrix in structure control.* J. Biol. Inorg. Chem., 2000. **5**(5): p. 537–550.
66. Kröger, N. and M. Sumper, *Biomineralization: From Biology to Biotechnology and Medical Application*, in *The Molecular Basis of Diatom Biosilica Formation*, E. Baeuerlein, Editor. 2004, Wiley: Weinheim.
67. Allen, L.H. and Matijevic.E, *Stability of colloidal silica: II. Ion exchange.* J. Colloid Interface Sci., 1970. **33**(3): p. 420–429.
68. Coradin, T. and P.J. Lopez, *Biogenic silica patterning: simple chemistry or subtle biology?* ChemBioChem, 2003. **4**(4): p. 251–259.
69. Hubert, D.H.W., M. Jung, P.M. Frederik, P.H.H. Bomans, J. Meuldijk, and A.L. German, *Vesicle-directed growth of silica.* Adv. Mater., 2000. **12**(17): p. 1286–1290.
70. Lowenstam, H.A. and S. Weiner, *On Biomineralization*. 1989, New York: Oxford University Press.
71. Patwardhan, S.V., *Biomimetic and bioinspired silica: recent developments and applications.* Chem. Commun., 2011. **47**(27): p. 7567–7582.
72. Patwardhan, S.V., S.J. Clarson, and C.C. Perry, *On the role(s) of additives in bioinspired silicification.* Chem. Commun., 2005. **-**(9): p. 1113–1121.
73. Hildebrand, M., *Diatoms, biomineralization processes, and genomics.* Chem. Rev., 2008. **108**(11): p. 4855–4874.
74. Müller, W.E.G., S.I. Belikov, W. Tremel, C.C. Perry, W.W.C. Gieskes, A. Boreiko, and H.C. Schröder, *Siliceous spicules in marine demosponges (example Suberites domuncula).* Micron, 2006. **37**(2): p. 107–120.
75. Simpson, T.L. and B.E. Volcani, *Silicon and Siliceous Structures in Biological Systems*. 1981, New York: Springer.
76. Dickerson, M.B., K.H. Sandhage, and R.R. Naik, *Protein- and peptide-directed syntheses of inorganic materials.* Chem. Rev., 2008. **108**(11): p. 4935–4978.
77. Sarikaya, M., C. Tamerler, A.K.Y. Jen, K. Schulten, and F. Baneyx, *Molecular biomimetics: nanotechnology through biology.* Nat. Mater., 2003. **2**(9): p. 577–585.
78. Chen, C.-L. and N.L. Rosi, *Peptide-based methods for the preparation of nanostructured inorganic materials.* Angew. Chem., Int. Ed., 2010. **49**(11): p. 1924–1942.
79. Mann, S., *Biomineralization and biomimetic materials chemistry.* J. Mater. Chem., 1995. **5**(7): p. 935–946.
80. Cha, J.N., K. Shimizu, Y. Zhou, S.C. Christiansen, B.F. Chmelka, G.D. Stucky, and D.E. Morse, *Silicatein filaments and subunits from a marine sponge direct the polymerization of silica and silicones in vitro.* Proc. Natl. Acad. Sci. U. S. A., 1999. **96**(2): p. 361–365.

81. Kröger, N., R. Deutzmann, and M. Sumper, *Polycationic peptides from diatom biosilica that direct silica nanosphere formation.* Science, 1999. **286**(5442): p. 1129–1132.
82. Bäuerlein, E., *Biomineralization: From Biology to Biotechnology and Medical Application*. 2nd ed. 2004, Weinheim: Wiley.
83. Mann, S., *Biomineralization: Principles and Concepts in Bioinorganic Materials Chemistry*. 2001, New York: Oxford University Press.
84. Shimizu, K., J. Cha, G.D. Stucky, and D.E. Morse, *Silicatein α: Cathepsin L-like protein in sponge biosilica.* Proc. Natl. Acad. Sci. U. S. A., 1998. **95**(11): p. 6234–6238.
85. Cha, J.N., *Lessons from Nature: Novel Routes to Biomimetic Synthesis of Silica Based Materials*, in *Chemistry*. 2000, University of California, Santa Barbara.
86. Zhou, Y., K. Shimizu, J.N. Cha, G.D. Stucky, and D.E. Morse, *Efficient catalysis of polysiloxane synthesis by silicatein α requires specific hydroxy and imidazole functionalities.* Angew. Chem., Int. Ed., 1999. **38**(6): p. 780–782.
87. Karp, G., *Cell Biology*. 1984, New York: McGraw-Hill.
88. Kröger, N., R. Deutzmann, and M. Sumper, *Silica-precipitating peptides from diatoms—the chemical structure of silaffin-1A from Cylindrotheca fusiformis.* J. Biol. Chem., 2001. **276**(28): p. 26066–26070.
89. Kröger, N., S. Lorenz, E. Brunner, and M. Sumper, *Self-assembly of highly phosphorylated silaffins and their function in biosilica morphogenesis.* Science, 2002. **298**(5593): p. 584–586.
90. Sumper, M. and N. Kröger, *Silica formation in diatoms: the function of long-chain polyamines and silaffins.* J. Mater. Chem., 2004. **14**(14): p. 2059–2065.
91. Hecky, R.E., K. Mopper, P. Kilham, and E.T. Degens, *Amino-acid and sugar composition of diatom cell-walls.* Mar. Biol., 1973. **19**(4): p. 323–331.
92. Swift, D.M. and A.P. Wheeler, *Evidence of an organic matrix from diatom biosilica.* J. Phycol., 1992. **28**(2): p. 202–209.
93. Harrison, C.C., *Evidence for intramineral macromolecules containing protein from plant silicas.* Phytochemistry, 1996. **41**(1): p. 37–42.
94. Naik, R.R., L.L. Brott, S.J. Clarson, and M.O. Stone, *Silica-precipitating peptides isolated from a combinatorial phage display peptide library.* J. Nanosci. Nanotechnol., 2002. **2**(1): p. 95–100.
95. Naik, R.R., P.W. Whitlock, F. Rodriguez, L.L. Brott, D.D. Glawe, S.J. Clarson, and M.O. Stone, *Controlled formation of biosilica structures in vitro.* Chem. Commun., 2003. **-**(2): p. 238–239.
96. Knecht, M.R. and D.W. Wright, *Functional analysis of the biomimetic silica precipitating activity of the R5 peptide from Cylindrotheca fusiformis.* Chem. Commun., 2003. **-**(24): p. 3038–3039.
97. Kasotakis, E. and A. Mitraki, *Silica biotemplating by self-assembling peptides via serine residues activated by the peptide amino terminal group.* Biopolymers, 2012. **98**(6): p. 501–509.
98. Meegan, J.E., A. Aggeli, N. Boden, R. Brydson, A.P. Brown, L. Carrick, A.R. Brough, A. Hussain, and R.J. Ansell, *Designed self-assembled β-sheet peptide fibrils as templates for silica nanotubes.* Adv. Funct. Mater., 2004. **14**(1): p. 31–37.

99. Sarikaya, M., C. Tamerler, D.T. Schwartz, and F.O. Baneyx, *Materials assembly and formation using engineered polypeptides.* Annu. Rev. Mater. Res., 2004. **34**(-): p. 373–408.
100. Holmstrom, S.C., P.J.S. King, M.G. Ryadnov, M.F. Butler, S. Mann, and D.N. Woolfson, *Templating silica nanostructures on rationally designed self-assembled peptide fibers.* Langmuir, 2008. **24**(20): p. 11778–11783.
101. Yuwono, V.M. and J.D. Hartgerink, *Peptide amphiphile nanofibers template and catalyze silica nanotube formation.* Langmuir, 2007. **23**(9): p. 5033–5038.
102. Coradin, T., C. Roux, and J. Livage, *Biomimetic self-activated formation of multi-scale porous silica in the presence of arginine-based surfactants.* J. Mater. Chem., 2002. **12**(5): p. 1242–1244.
103. Tamerler, C. and M. Sarikaya, *Molecular biomimetics: utilizing naturels molecular ways in practical engineering.* Acta Biomater., 2007. **3**(3): p. 289–299.
104. Tamerler, C., T. Kacar, D. Sahin, H. Fong, and M. Sarikaya, *Genetically engineered polypeptides for inorganics: a utility in biological materials science and engineering.* Mat. Sci. Eng. C-Bio. S., 2007. **27**(3): p. 558–564.
105. Sudheendra, L. and A.R. Raju, *Peptide-induced formation of silica from tetraethylorthosilicate at near-neutral pH.* Mater. Res. Bull., 2002. **37**(1): p. 151–159.
106. Cha, J.N., G.D. Stucky, D.E. Morse, and T.J. Deming, *Biomimetic synthesis of ordered silica structures mediated by block copolypeptides.* Nature, 2000. **403**(6767): p. 289–292.
107. Jan, J.-S. and D.F. Shantz, *Biomimetic silica formation: effect of block copolypeptide chemistry and solution conditions on silica nanostructure.* Adv. Mater., 2007. **19**(19): p. 2951–2956.
108. Jan, J.S., S.J. Lee, C.S. Carr, and D.F. Shantz, *Biomimetic synthesis of inorganic nanospheres.* Chem. Mater., 2005. **17**(17): p. 4310–4317.
109. Bellomo, E.G. and T.J. Deming, *Monoliths of aligned silica-polypeptide hexagonal platelets.* J. Am. Chem. Soc., 2006. **128**(7): p. 2276–2279.
110. Altunbas, A., N. Sharma, M.S. Lamm, C. Yan, R.P. Nagarkar, J.P. Schneider, and D.J. Pochan, *Peptide–silica hybrid networks: biomimetic control of network mechanical behavior.* ACS Nano, 2010. **4**(1): p. 181–188.
111. Wang, S., X. Ge, J. Xue, H. Fan, L. Mu, Y. Li, H. Xu, and J.R. Lu, *Mechanistic processes underlying biomimetic synthesis of silica nanotubes from self-assembled ultrashort peptide templates.* Chem. Mater., 2011. **23**(9): p. 2466–2474.
112. Pouget, E., E. Dujardin, A. Cavalier, A. Moreac, C. Valery, V. Marchi-Artzner, T. Weiss, A. Renault, M. Paternostre, and F. Artzner, *Hierarchical architectures by synergy between dynamical template self-assembly and biomineralization.* Nat. Mater., 2007. **6**(6): p. 434–439.
113. Graf, P., A. Mantion, A. Haase, A.F. Thuenemann, A. Masic, W. Meier, A. Luch, and A. Taubert, *Silicification of peptide-coated silver nanoparticles—a biomimetic soft chemistry approach toward chiral hybrid core-shell materials.* ACS Nano, 2011. **5**(2): p. 820–833.

114. Belton, D., G. Paine, S.V. Patwardhan, and C.C. Perry, *Towards an understanding of (bio)silicification: the role of amino acids and lysine oligomers in silicification.* J. Mater. Chem., 2004. **14**(14): p. 2231–2241.
115. Mizutani, T., H. Nagase, N. Fujiwara, and H. Ogoshi, *Silicic acid polymerization catalyzed by amines and polyamines.* Bull. Chem. Soc. Jpn, 1998. **71**(8): p. 2017–2022.
116. van Bommel, K.J.C. and S. Shinkai, *Silica transcription in the absence of a solution catalyst: the surface mechanism.* Langmuir, 2002. **18**(12): p. 4544–4548.
117. van Bommel, K.J.C., J.H. Jung, and S. Shinkai, *Poly(L-lysine) aggregates as templates for the formation of hollow silica spheres.* Adv. Mater., 2001. **13**(19): p. 1472–1476.
118. Ivnitski, D., K. Artyushkova, R.A. Rincon, P. Atanassov, H.R. Luckarift, and G.R. Johnson, *Entrapment of enzymes and carbon nanotubes in biologically synthesized silica: glucose oxidase-catalyzed direct electron transfer.* Small, 2008. **4**(3): p. 357–364.
119. Luckarift, H.R., M.B. Dickerson, K.H. Sandhage, and J.C. Spain, *Rapid, room-temperature synthesis of antibacterial bionanocomposites of lysozyme with amorphous silica or titania.* Small, 2006. **2**(5): p. 640–643.
120. Luckarift, H.R., J.C. Spain, R.R. Naik, and M.O. Stone, *Enzyme immobilization in a biomimetic silica support.* Nat. Biotechnol., 2004. **22**(2): p. 211–213.
121. Neville, F., M.J.F. Broderick, T. Gibson, and P.A. Millner, *Fabrication and activity of silicate nanoparticles and nanosilicate-entrapped enzymes using polyethyleneimine as a biomimetic polymer.* Langmuir, 2011. **27**(1): p. 279–285.
122. Swartz, J.D., L.F. Deravi, and D.W. Wright, *Bottom-up synthesis of biologically active multilayer films using inkjet-printed templates.* Adv. Funct. Mater., 2010. **20**(9): p. 1488–1492.
123. Naik, R.R., M.M. Tomczak, H.R. Luckarift, J.C. Spain, and M.O. Stone, *Entrapment of enzymes and nanoparticles using biomimetically synthesized silica.* Chem. Commun., 2004. **-**(15): p. 1684–1685.
124. Chien, L.-J. and C.-K. Lee, *Biosilicification of dual-fusion enzyme immobilized on magnetic nanoparticle.* Biotechnol. Bioeng., 2008. **100**(2): p. 223–230.
125. Marner, W.D., II, A.S. Shaikh, S.J. Muller, and J.D. Keasling, *Enzyme immobilization via silaffin-mediated autoencapsulation in a biosilica support.* Biotechnol. Progr., 2009. **25**(2): p. 417–423.
126. Betancor, L. and H.R. Luckarift, *Bioinspired enzyme encapsulation for biocatalysis.* Trends Biotechnol., 2008. **26**(10): p. 566–572.
127. Brott, L.L., R.R. Naik, D.J. Pikas, S.M. Kirkpatrick, D.W. Tomlin, P.W. Whitlock, S.J. Clarson, and M.O. Stone, *Ultrafast holographic nanopatterning of biocatalytically formed silica.* Nature, 2001. **413**(6853): p. 291–293.
128. Sano, K.-I., T. Minamisawa, and K. Shiba, *Autonomous silica encapsulation and sustained release of anticancer protein.* Langmuir, 2010. **26**(4): p. 2231–2234.

129. Meleson, K., S. Graves, and T.G. Mason, *Formation of concentrated nanoemulsions by extreme shear.* Soft Mater., 2004. **2**(2-3): p. 109–123.
130. McClements, D.J., *Nanoemulsions versus microemulsions: terminology, differences, and similarities.* Soft Matter, 2012. **8**(6): p. 1719–1729.
131. Israelachvili, J.N., *Intermolecular and Surface Force*. 2nd ed. 1992, London: Academic Press.
132. Lucassenreynders, E.H. and K.A. Kuijpers, *The role of interfacial properties in emulsification.* Colloids Surf., 1992. **65**(2–3): p. 175–184.
133. Walstra, P., *Physical Chemistry of Foods*. 2003, New York: Marcel Dekker.
134. Mason, T.G., J.N. Wilking, K. Meleson, C.B. Chang, and S.M. Graves, *Nanoemulsions: formation, structure, and physical properties.* J. Phys.: Condens. Matter, 2006. **18**(41): p. R635–R666.
135. Abismail, B., J.P. Canselier, A.M. Wilhelm, H. Delmas, and C. Gourdon, *Emulsification by ultrasound: drop size distribution and stability.* Ultrason. Sonochem., 1999. **6**(1-2): p. 75–83.
136. McClements, D.J., *Food Emulsions: Principles, Practices, and Techniques*. 2nd ed. 2005, Boca Raton: CRC Press.
137. Behrend, O., K. Ax, and H. Schubert, *Influence of continuous phase viscosity on emulsification by ultrasound.* Ultrason. Sonochem., 2000. **7**(2): p. 77–85.
138. Mason, T.J., *Sonochemistry*. 1999, New York: Oxford University Press.
139. Povey, M.J.W. and T.J. Mason, *Ultrasound in Food Processing*. 1998, New York: Blackie Academic & Professional.
140. Canselier, J.R., H. Delmas, A.M. Wilhelm, and B. Abismail, *Ultrasound emulsification—an overview.* J. Dispersion Sci. Technol., 2002. **23**(1-3): p. 333–349.
141. Jafari, S.M., E. Assadpoor, Y. He, and B. Bhandari, *Re-coalescence of emulsion droplets during high-energy emulsification.* Food Hydrocolloid, 2008. **22**(7): p. 1191–1202.
142. Dickinson, E., *Hydrocolloids and Emulsion Stability*, in *Handbook of Hydrocolloids*, G.O. Phillips and P.A. Williams, Editors. 2009, CRC Press: Washington, DC.
143. Dukhin, S.S., J. Sjoblom, and O. Saether, *An Experimental and Theoretical Approach to the Dynamic Behavior of Emulsions*, in *Emulsions and Emulsion Stability*, J. Sjoblom, Editor. 2006, CRC Press: New York.
144. Schramm, L.L., *Emulsions, Foams and Suspensions: Fundamentals and Applications*. 2005, Weinheim: Wiley.
145. Petsev, D.N., *Theoretical analysis of film thickness transition dynamics and coalescence of charged miniemulsion droplets.* Langmuir, 2000. **16**(5): p. 2093–2100.
146. Dukhin, S.S., J. Sjoblom, D.T. Wasan, and O. Saether, *Coalescence coupled with either coagulation or flocculation in dilute emulsions.* Colloids Surf., A, 2001. **180**(3): p. 223–234.
147. Mishchuk, N.A., R. Miller, A. Steinchen, and A. Sanfeld, *Conditions of coagulation and flocculation in dilute mini-emulsions.* J. Colloid Interface Sci., 2002. **256**(2): p. 435–450.

148. Becher, P., *Emulsions: Theory and Practice*. 3rd ed. 2001, Washington, DC: Oxford University Press.
149. Stokes, G.G., *On the effect of the internal friction of fluids on the motion of pendulums.* Trans. Cambridge Phil. Soc., 1851. **9**(-): p. 8–106.
150. Evans, D.F. and H. Wennerstrom, *The Colloidal Domain: Where Physics, Chemistry, Biology, and Technology Meet*. 2nd ed. 1994, New York: Wiley.
151. van Aken, G.A., *Coalescence Mechanisms in Protein-Stabilized Emulsions*, in *Food Emulsions*, S. Friberg, K. Larsson, and J. Sjoblom, Editors. 2004, Marcel Dekker: New York.
152. Dickinson, E. and M. Golding, *Rheology of sodium caseinate stabilized oil-in-water emulsions.* J. Colloid Interface Sci., 1997. **191**(1): p. 166–176.
153. Ye, A.Q. and H. Singh, *Interfacial composition and stability of sodium caseinate emulsions as influenced by calcium ions.* Food Hydrocolloids, 2001. **15**(2): p. 195–207.
154. Kabalnov, A., *Coalescence in Emulsions*, in *Modern Aspects of Emulsion Science*, B.P. Binks, Editor. 1998, The Royal Society of Chemistry: Cambridge.
155. Weers, J.G., *Molecular Diffusion in Emulsions and Emulsions Mixtures*, in *Modern Aspects of Emulsions Science*, B.P. Binks, Editor. 1998, The Royal Society of Chemistry: Cambridge.
156. Taylor, P., *Ostwald ripening in emulsions.* Adv. Colloid Interface Sci., 1998. **75**(2): p. 107–163.
157. Israelachvili, J.N., *Intermolecular and Surface Forces: With Applications to Colloidal and Biological Systems*. 1985, Orlando: Academic Press.
158. Dexter, A.F. and A.P.J. Middelberg, *Peptides as functional surfactants.* Ind. Eng. Chem. Res., 2008. **47**(17): p. 6391–6398.
159. McClements, D.J., *Protein-stabilized emulsions.* Curr. Opin. Colloid Interface Sci., 2004. **9**(5): p. 305–313.
160. Dexter, A.F., A.S. Malcolm, and A.P.J. Middelberg, *Reversible active switching of the mechanical properties of a peptide film at a fluid–fluid interface.* Nat. Mater., 2006. **5**(6): p. 502–506.
161. Chuan, Y.P., B.Y. Zeng, B. O'Sullivan, R. Thomas, and A.P.J. Middelberg, *Co-delivery of antigen and a lipophilic anti-inflammatory drug to cells via a tailorable nanocarrier emulsion.* J. Colloid Interface Sci., 2012. **368**(1): p. 616–624.
162. Zeng, B.J., Y.P. Chuan, B. O'Sullivan, I. Caminschi, M.H. Lahoud, R. Thomas, and A.P.J. Middelberg, *Receptor-specific delivery of protein antigen to dendritic cells by a nanoemulsion formed using top-down non-covalent click self-assembly.* Small, 2013. **9**(22): p. 3736–3742.
163. Malcolm, A.S., A.F. Dexter, J.A. Katakdhond, S.I. Karakashev, A.V. Nguyen, and A.P.J. Middelberg, *Tuneable control of interfacial rheology and emulsion coalescence.* ChemPhysChem, 2009. **10**(5): p. 778–781.
164. Saito, M., M. Ogasawara, K. Chikuni, and M. Shimizu, *Synthesis of a peptide emulsifier with an amphiphilic structure.* Biosci. Biotech. Biochem., 1995. **59**(3): p. 388–392.

165. Dexter, A.F., *Interfacial and emulsifying properties of designed β-strand peptides.* Langmuir, 2010. **26**(23): p. 17997–18007.
166. Middelberg, A.P.J., L. He, A.F. Dexter, H.H. Shen, S.A. Holt, and R.K. Thomas, *The interfacial structure and Young's modulus of peptide films having switchable mechanical properties.* J. R. Soc. Interface, 2008. **5**(18): p. 47–54.
167. Dexter, A.F. and A.P.J. Middelberg, *Switchable peptide surfactants with designed metal binding capacity.* J. Phys. Chem. C, 2007. **111**(28): p. 10484–10492.
168. Degrado, W.F. and J.D. Lear, *Induction of peptide conformation at apolar water interfaces. 1. A study with model peptides of defined hydrophobic periodicity.* J. Am. Chem. Soc., 1985. **107**(25): p. 7684–7689.
169. Fairman, R., H.G. Chao, L. Mueller, T.B. Lavoie, L.Y. Shen, J. Novotny, and G.R. Matsueda, *Characterization of a new four-chain coiled-coil: influence of chain-length on stability.* Protein Sci., 1995. **4**(8): p. 1457–1469.
170. Middelberg, A.P.J., C.J. Radke, and H.W. Blanch, *Peptide interfacial adsorption is kinetically limited by the thermodynamic stability of self association.* Proc. Natl. Acad. Sci. U. S. A., 2000. **97**(10): p. 5054–5059.
171. Jones, D.B. and A.P.J. Middelberg, *Micromechanical testing of interfacial protein networks demonstrates ensemble behavior characteristic of a nanostructured biomaterial.* Langmuir, 2002. **18**(14): p. 5585–5591.
172. Jones, D.B. and A.P.J. Middelberg, *Direct determination of the mechanical properties of an interfacially adsorbed protein film.* Chem. Eng. Sci., 2002. **57**(10): p. 1711–1722.
173. Tahara, Y., S. Honda, N. Kamiya, H. Piao, A. Hirata, E. Hayakawa, T. Fujii, and M. Goto, *A solid-in-oil nanodispersion for transcutaneous protein delivery.* J. Control. Release, 2008. **131**(1): p. 14–18.
174. Malcolm, A.S., A.F. Dexter, and A.P.J. Middelberg, *Mechanical properties of interfacial films formed by lysozyme self-assembly at the air-water interface.* Langmuir, 2006. **22**(21): p. 8897–8905.
175. Wilde, P.J., *Interfaces: their role in foam and emulsion behaviour.* Curr. Opin. Colloid Interface Sci., 2000. **5**(3-4): p. 176–181.
176. Middelberg, A.P.J. and M. Dimitrijev-Dwyer, *A designed biosurfactant protein for switchable foam control.* ChemPhysChem, 2011. **12**(8): p. 1426–1429.
177. Dimitrijev-Dwyer, M., L. He, M. James, A. Nelson, and A.P.J. Middelberg, *Insights into the role of protein molecule size and structure on interfacial properties using designed sequences.* J. R. Soc. Interface, 2013. **10**(80): p. 20120987.
178. Dimitrijev-Dwyer, M., L. He, M. James, A. Nelson, L. Wang, and A.P.J. Middelberg, *The effects of acid hydrolysis on protein biosurfactant molecular, interfacial, and foam properties: pH responsive protein hydrolysates.* Soft Matter, 2012. **8**(19): p. 5131–5139.

179. Dimitrijev-Dwyer, M., M. Brech, L. Yu, and A.P.J. Middelberg, *Intensified expression and purification of a recombinant biosurfactant protein.* Chem. Eng. Sci., 2014. **105**(-): p. 12–21.
180. Kyle, S., A. Aggeli, E. Ingham, and M.J. McPherson, *Production of self-assembling biomaterials for tissue engineering.* Trends Biotechnol., 2009. **27**(7): p. 423–433.
181. Sato, A.K., M. Viswanathan, R.B. Kent, and C.R. Wood, *Therapeutic peptides: technological advances driving peptides into development.* Curr. Opin. Biotechnol., 2006. **17**(6): p. 638–642.
182. Latham, P.W., *Therapeutic peptides revisited.* Nat. Biotechnol., 1999. **17**(8): p. 755–757.
183. Sassenfeld, H.M., *Engineering proteins for purification.* Trends Biotechnol., 1990. **8**(4): p. 88–93.
184. Goeddel, D.V., D.G. Kleid, F. Bolivar, H.L. Heyneker, D.G. Yansura, R. Crea, T. Hirose, A. Kraszewski, K. Itakura, and A.D. Riggs, *Expression in Escherichia coli of chemically synthesized genes for human insulin.* Proc. Natl. Acad. Sci. U. S. A., 1979. **76**(1): p. 106–110.
185. Keen, H., A. Glynne, J.C. Pickup, G.C. Viberti, R.W. Bilous, R.J. Jarrett, and R. Marsden, *Human insulin produced by recombinant DNA technology: safety and hypoglycemic potency in healthy men.* Lancet, 1980. **2**(8191): p. 398–401.
186. Miller, W.L., *Cell Substrates: Their Use in the Production of Biologicals*, in *Use of Recombinant DNA Technology for the Production of Polypeptides*, C. Petriccinai, H.E. Hopps, and P.S. Chapple, Editors. 1979, Plenum Press: New York.
187. Shiloach, J. and R. Fass, *Growing E. coli to high cell density—a historical perspective on method development.* Biotechnol. Adv., 2005. **23**(5): p. 345–357.
188. Itakura, K., T. Hirose, R. Crea, A.D. Riggs, H.L. Heyneker, F. Bolivar, and H.W. Boyer, *Expression in Escherichia coli of a chemically synthesized gene for hormone somatostatin.* Science, 1977. **198**(4321): p. 1056–1063.
189. Shine, J., I. Fettes, N.C.Y. Lan, J.L. Roberts, and J.D. Baxter, *Expression of cloned β-endorphin gene sequences by Escherichia coli.* Nature, 1980. **285**(5765): p. 456–461.
190. Foo, C.W.P., S.V. Patwardhan, D.J. Belton, B. Kitchel, D. Anastasiades, J. Huang, R.R. Naik, C.C. Perry, and D.L. Kaplan, *Novel nanocomposites from spider silk-silica fusion (chimeric) proteins.* Proc. Natl. Acad. Sci. U. S. A., 2006. **103**(25): p. 9428–9433.
191. Saito, H., T. Honma, T. Minamisawa, K. Yamazaki, T. Noda, T. Yamori, and K. Shiba, *Synthesis of functional proteins by mixing peptide motifs.* Chem. Biol., 2004. **11**(6): p. 765–773.
192. Lebendiker, M. and T. Danieli, *Purification of Proteins Fused to Maltose-Binding Protein*, in *Protein Chromatography: Methods and Protocols*, D. Walls and S.T. Loughran, Editors. 2011.
193. Kaar, W., B.M. Hartmann, Y. Fan, B. Zeng, L.H.L. Lua, A.F. Dexter, R.J. Falconer, and A.P.J. Middelberg, *Microbial bio-production of a recombinant stimuli-responsive biosurfactant.* Biotechnol. Bioeng., 2009. **102**(1): p. 176–187.

194. Hecht, M.H., J.S. Richardson, D.C. Richardson, and R.C. Ogden, *Denovo design, expression, and characterization of felix – a four-helix bundle protein of native-like sequence.* Science, 1990. **249**(4971): p. 884–891.

Chapter 3

Emulsion-templated silica nanocapsules formed using bio-inspired silicification

The research in this chapter consists of the peer-reviewed paper published as:

Wibowo, D., C.-X. Zhao, and A.P.J. Middelberg*, *Emulsion-templated silica nanocapsules formed using bio-inspired silicification.* Chem. Commun., 2014. **50**(77): p. 11325–11328.

The following modifications were made to the article:

- Page numbers of the original article were crossed-out; and
- Page numbers consistent with those on the remainder of the thesis pages were inserted.

Abstract

This chapter described a method for the synthesis of oil-core silica-shell nanocapsules using designed peptides, in lieu of chemical surfactants. This was motivated by the need to develop environmentally-friendly processes—i.e., nearly neutral pH and room temperature without using any toxic organic solvents—for making silica nanocapsules composed of biocompatible components, including pharmaceutically-grade oil (i.e., Miglyol® 812), peptide and amorphous silica. Surface-active peptide, AM1, and a rationally-designed bifunctional modular peptide comprising a surface-active module and a biosilicification-active module, as mentioned in **Chapter 1**, were evaluated for the effective formation of oil-core silica-shell nanocapsules. This was achieved by testing their abilities to facilitate formation and stabilization of nanoemulsions and to induce hydrolysis and polycondensation of silica precursor tetraethoxysilane at the oil–water interfaces. Reaction parameters for the interfacial biosilicification of the peptide were explored by controlling reaction pH, reaction times and silica precursor concentrations in order to obtain silica nanocapsules with different controlled-release properties. Additionally, characterizations of the resulting silica nanocapsules, including using dynamic light scattering and transmission electron microscopy, were discussed. Important for the studies in subsequent chapters, high-capacity loading of an active material in silica nanocapsules and its controlled release from the oil core to water phase were demonstrated.

ChemComm

COMMUNICATION

View Article Online
View Journal | View Issue

Cite this: *Chem. Commun.*, 2014, **50**, 11325

Received 27th June 2014,
Accepted 7th August 2014

DOI: 10.1039/c4cc04904g

www.rsc.org/chemcomm

Emulsion-templated silica nanocapsules formed using bio-inspired silicification†

David Wibowo, Chun-Xia Zhao and Anton P. J. Middelberg*

A novel, bio-inspired templating platform technology is reported for the synthesis of biocompatible oil-core silica-shell nanocapsules with tunable shell thickness by utilizing a designed bifunctional peptide. Furthermore, facile encapsulation of an active molecule and its sustained release are demonstrated.

Templated core–shell silica nanocapsule structures promise great impact from the intersection of molecular and inorganic chemistry.[1] They allow encapsulation of fluorescent materials,[2] magnetic nanoparticles,[3] and active agents[4] in the core domain for imaging, sensing, and delivery, with a higher loading-capacity than an equivalent solid nanoparticle. The silica shell is engineered around the core to provide: (1) a protective envelope with chemical and mechanical stability for storage and delivery; (2) accessible pathways for adsorption, separation and sustained release; and (3) ease of surface modification with optical, magnetic, and/or biological functionalities enhancing the performance of nanocapsules for applications including biolabelling, controlled release and targeted delivery. Therefore, the fabrication of silica nanocapsules has attracted much research and industrial interest.

Hard- and soft-templating approaches are commonly employed to construct silica nanocapsules. Soft-templating methods offer a number of advantages. Thermal decomposition or chemical dissolution necessary for complete removal of the solid core is avoided, and the loading of an active cargo is simplified as it can be solubilized in the core prior to silica shell formation.[5] Sol–gel routes,[5,6] including self-templating of an alkoxysilane[5b,6a] and interfacial poly-condensation of hydrolyzed silicon alkoxide on ionic[5a] and non-ionic surfactants,[6b] have been developed to synthesize silica shells on oil-in-water (O/W) emulsions in the nanometer range. However, these soft-templating approaches variously incorporate the use of elevated temperature or extreme pH, or involve chemicals that have limited biocompatibility. An alternative pathway using more benign reaction conditions and biocompatible components would, for some applications, remove limitations embedded in current approaches.

Biomimetic templating offers mild routes to silica nanostructures using biomolecules.[7] Identification of amino acid sequences from nature[8] and combinatorial biology[9] capable of catalyzing silica formation has led to new strategies.[10] These involve biosilicification of the biomolecules in bulk aqueous solution[10a–c] and at solid–fluid interfaces.[10d] Erni *et al.* reported the synthesis of silica capsules at a scale of hundreds of micrometers by silicification of cross-linked coacervate of gelatin and *Acacia* gum around oil droplets.[11] To the best of our knowledge, peptides or proteins with modularized amino acid sequences capable of both stabilizing an emulsion and inducing biosilicification at the oil–water interface have not been reported, especially for the fabrication of silica capsules of nanometer dimension. Here, we designed a bifunctional peptide comprising one module capable of forming a stable nanoemulsion core and another module that induces biosilicification at oil–water interface to facilitate formation of oil-filled silica nanocapsule. This work opens new environmentally-friendly strategies for bio-inspired oil-core silica-shell nanocapsule formation having wide potential utility.

We designed a bifunctional peptide (SurSi, Ac-*MKQLAHSVSRLEHA* RKKRKKRKKRKKGGGY-$CONH_2$) by modularizing part of peptide surfactant AM1 (Ac-MKQLADSLHQLARQVSRLEHA-$CONH_2$) for surface activity[12] (*i.e.*, Sur module, *MKQLAHSVSRLEHA*) with a sequence for biosilicification (*i.e.*, Si module, RKKRKKRKKRKKGGGY). Peptide surfactant AM1 is capable of reversibly and precisely controlling the stability of O/W emulsions[12] by forming a cohesive interfacial film responsive to metal ion binding to histidine (H) residues.[13] Sur was designed based on heptads of AM1 but without the second heptad (*i.e.*, LHQLARQ) and with the replacement of aspartic acid (D) with histidine (H) in the first heptad. It is known that the molecular weight of adsorbing peptide molecules at oil–water interfaces is inversely proportional to the square of the interfacial adsorption rate constant.[14] Therefore, the incorporation of only two heptads, instead of three heptads, of AM1 in Sur would promote more rapid adsorption of the peptide at a freshly formed oil–water interface.

Australian Institute for Bioengineering and Nanotechnology, The University of Queensland, Brisbane, QLD 4072, Australia.
E-mail: a.middelberg@uq.edu.au

† Electronic supplementary information (ESI) available: Experimental details and additional figures. See DOI: 10.1039/c4cc04904g

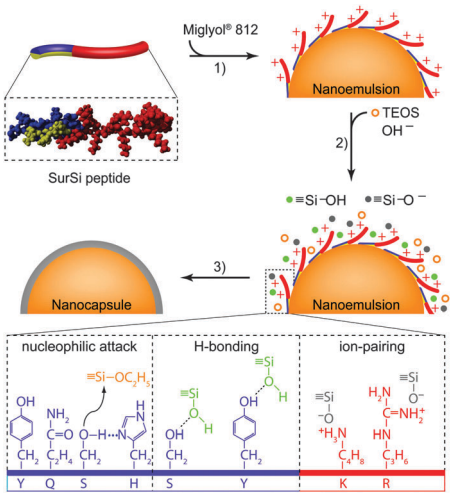

Scheme 1 Synthesis strategy of silica nanocapsule based on bio-inspired silicification at an oil–water interface. Step (1) sonication of Miglyol® 812 oil in a SurSi solution followed by dialysis at pH 7.5; step (2) addition of tetraethoxysilane (TEOS) to nanoemulsion; and step (3) interfacial poly-condensation of silica species. SurSi peptide operates synergistically by (1) stabilizing a nanoemulsion core through a "Sur" module incorporating hydrophobic amino acids (in yellow) to impart facial amphiphatic character hence promoting adsorption at the nanoemulsion interface; and (2) directing nucleation and growth of silica at the oil–water interface through a "Si" module.

Rapid interfacial adsorption facilitates efficient coverage of peptide molecules onto oil droplets and hence formation and stabilization of nanoscale emulsions.[15] The replacement of aspartic acid (D) with histidine (H) was designed to have the same number of histidine residues as AM1, thus allowing the metal-ion-mediated crosslinking between interfacially adsorbed peptide molecules and the formation of a cohesive film state at the interface[16] (Scheme 1). Proteins and peptides having positively-charged amino acids arginine (R) and lysine (K) can induce formation of silica under mild conditions.[8b,9a,10a] The R- and K-rich Si module, based on a sequence known to precipitate titania in bulk,[17] is discovered here to promote biosilicification at the oil–water interface when modularized with Sur. A number of peptide- or protein-based biomineralization mechanisms have been proposed in literature, including nucleophilic attack, hydrogen bonding, and electrostatic attraction or ion-pairing. Cha *et al.* reported that polar amino acid residues, including serine (S), tyrosine (Y), histidine (H) and glutamine (Q), can promote nucleophilic attack, in which the nucleophilicity of hydroxyl oxygen of serine can be enhanced by the formation of hydrogen bond between serine and adjacent histidine, on the silicon atom within tetraethoxysilane[8a,10a] (TEOS) and thus may facilitate its hydrolysis to produce silanol and negatively-charged silanolate (Scheme 1). Moreover, positively-charged arginine (R) and lysine (K) may interact electrostatically with silanolate at near-neutral pH, while the hydroxyls of serine (S) and tyrosine (Y) promote hydrogen bonding with silanol[8b] (Scheme 1), which in turn act as nucleation sites and direct silica growth through poly-condensation of the silica species at the interface. Under these possible mechanisms, SurSi peptide would thus be expected to make silica nanocapsules at room temperature and near-neutral pH without using any chemical-based catalysts.

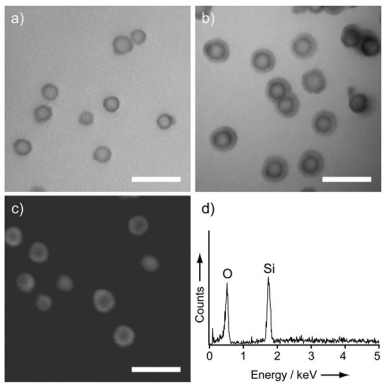

Fig. 1 Silica nanocapsules formed using bio-inspired silicification. (a and b) Transmission electron microscopy (TEM) images confirming the formation of a nanostructured core–shell architecture after a 20 h biosilicification reaction of SurSi-stabilized nanoemulsion with 32 μmol TEOS in 25 mM HEPES buffer at pH 7.5 (a) or at pH 8 (b). (c and d) Representative TEM dark-field image (c) and the corresponding energy-dispersive X-ray spectrum (d) of the nanocapsule confirming existence of a silica shell. Scale bars are 200 nm.

Nanoemulsion was formed by sonication of Miglyol® 812 oil in SurSi solution, confirming surface activity due to the amphiphilic Sur module. The addition of 32 μmol TEOS to dialyzed nanoemulsion at pH 7.5 or 8 led to successful formation of silica nanocapsule after 20 h, as evidenced by an electron-dense shell (Fig. 1a and b). The outer diameter and the shell thickness of nanocapsules formed at pH 7.5 as measured by transmission electron microscopy (TEM) were 66 ± 5 nm and 12 ± 2 nm, respectively (Fig. 1a). Dynamic light scattering (DLS) confirmed a size increase in comparison with base nanoemulsion (Fig. S1a, ESI†). Additionally, the ζ-potential of both the nanoemulsion templates and the nanocapsules were measured. In contrast to the nanoemulsions which had a positive zeta potential of +35 ± 5 mV because of the positively-charged SurSi peptide, the silica nanocapsules exhibited a highly negative charge of −30 ± 5 mV as a result of silanolate groups on the silica surface. Furthermore, formation of a silica shell was confirmed by presence of silicon and oxygen in the thick layer surrounding the oil core using energy-dispersive X-ray spectroscopy (EDX) (Fig. 1c and d). As a control experiment, AM1 was unable to demonstrate an effective dual functionality of emulsion stabilization and silica shell formation, as the silica was largely formed in bulk solutions rather than at oil–water interfaces (Fig. S2, ESI†). Thus modularization of a partial AM1 sequence with a specialized Si sequence was considered essential for acceptable practical formation of nanocapsules. The results confirm this is the case, with the desired result achieved in a way not possible with AM1.

The silica shell thickness is tunable. Compared to reaction at pH 7.5, reaction at pH 8 with 32 μmol TEOS for 20 h gave a remarkable increase in silica shell thickness (27 ± 6 nm) (Fig. 1b). DLS also confirmed a size increase with increasing reaction pH (Fig. S1b, ESI†). As increasing reaction pH assists TEOS hydrolysis and generates a higher concentration of reactive silica species, we hypothesized that increasing the concentration of negatively-charged silanolate-rich species would favor their attraction to the positively-charged nanoemulsion surface.

Then the positively-charged amino acids enriched at the oil–water interface would generate highly localized electrostatic forces to the silica species. Another silica species, silanol, could also interact with hydrogen-bond donor amino acids at the interface through hydrogen-bonding (Scheme 1). The attracted silica species then could act as nucleation sites for further silica growth forming the shell with thickness solely depending on the local concentration of the silica species.

To further investigate silica formation and methods for control of silica shell thickness, reaction time and TEOS concentration were varied at pH 7.5 (Fig. 2a). Shell thicknesses increased regularly with increasing reaction time and TEOS concentration, as reflected by an increase in nanocapsule diameter (Fig. 2b) shown in TEM. The boundary between core and shell by TEM was more obvious after 30 h reaction (Fig. 2a), and the silica shell thicknesses, as measured by TEM, were 5 ± 1 nm, 10 ± 2 nm and 16 ± 3 nm following reaction with 8 μmol, 16 μmol and 32 μmol TEOS, respectively. The surface of the silica shell was rough, especially during the first 20 h, as observed from TEM images (Fig. 2a). This roughness might be due to the fact that the silica species were still undergoing poly-condensation at the interface as the reaction proceeded.[18] The silica shell kept on growing through further interfacial biosilicification and poly-condensation, and became thicker over time until TEOS was depleted (Fig. 2c–e). The evolution of the silica growth during biosilicification reaction was also monitored using DLS. An increase of the nanocapsule diameter was observed at different reaction times (Fig. S3, ESI†). These results demonstrate the possibility of obtaining well-dispersed nanocapsules (see PDIs in Table S1, ESI†) having different silica shell thicknesses by controlling TEOS concentration and reaction time.

Silica nanocapsules can be used to encapsulate an active material in the oil core for protection and/or to provide a diffusion barrier through the silica shell for slow release of the active,[5] thus enabling applications in biomedical and agricultural domains. We demonstrate facile encapsulation and sustained release profile associated with the core–shell structure of a silica nanocapsule using fipronil as a model of oil-soluble active molecules. Fipronil is a phenylpyrazole insecticide that controls a broad spectrum of insect pests and provides long-term protection for crops.[19] Fipronil can be solubilized in Miglyol® 812 oil at high loading capacity (up to 10 mg mL^{-1}). We loaded 10 mg mL^{-1} fipronil in oil to form a SurSi-stabilized nanoemulsion. After a 30 h reaction with TEOS at pH 7.5, TEM images (Fig. 3a–c) suggested the successful formation of silica nanocapsules. The encapsulation efficiencies of fipronil in the silica nanocapsules obtained at TEOS concentrations of 16 μmol, 32 μmol and 96 μmol were 69.3%, 70.6% and 71.1%, respectively (see ESI†). With a fipronil-loaded nanoemulsion, the silica shell thickness can also be controlled by varying TEOS concentration (Fig. 3a–c). Increase in TEOS concentration (16 μmol, 32 μmol and 96 μmol) resulted in loaded nanocapsules with higher average diameters (140 ± 13 nm, 198 ± 15 nm and 288 ± 24 nm, respectively) and thicker silica shells (8 ± 2 nm, 25 ± 3 nm and 44 ± 7 nm, respectively) (Fig. 3a–c).

We further investigated the sustained release of fipronil from silica nanocapsules in water. Fig. 3 shows the fipronil release profiles (Fig. 3d) for silica nanocapsules with shell thickness of 8 nm, 25 nm and 44 nm (Fig. 3a–c). The concentration of fipronil in solution resulting from release from the silica nanocapsules to water was normalized against the saturated concentration of fipronil in water (2 μg mL^{-1}) to allow normalized comparison of different nanocapsule designs. We observed the effect of silica shell thickness on the release profile of fipronil. Silica nanocapsules with 8 nm shell thickness showed 3.1 ± 0.6% release of fipronil at 2 h.

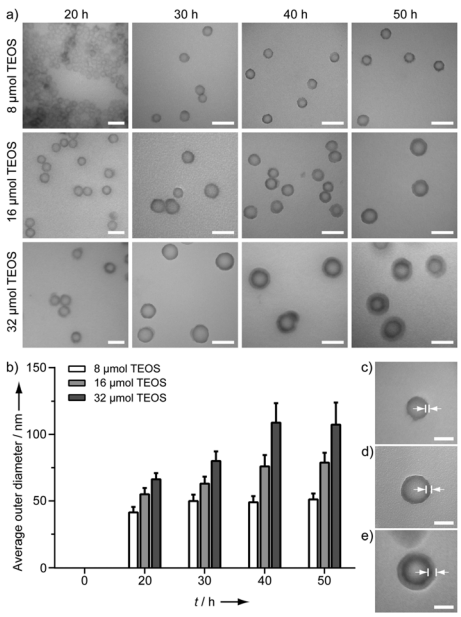

Fig. 2 Tunable silica shell thickness through control of biosilicification reaction time (t) and TEOS concentration. (a) TEM images showing silica nanocapsules produced at different reaction times and TEOS concentrations at pH 7.5 (scale bars are 100 nm). (b) Increases in the average outer diameter of nanocapsules reflected increases in silica shell thicknesses as calculated from TEM based on the average value of at least 100 individual nanocapsules. (c–e) Representative TEM images of individual nanocapsules after a 50 h biosilicification reaction with 8 μmol (c), 16 μmol (d) and 32 μmol (e) TEOS (scale bars are 50 nm).

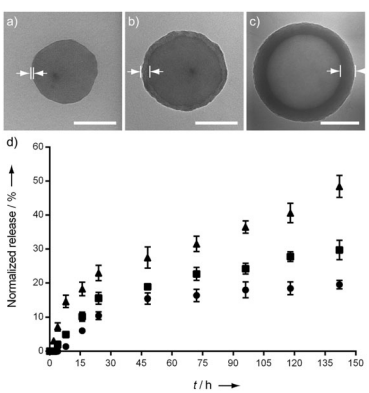

Fig. 3 Encapsulation of fipronil in silica nanocapsules and its sustained release profile. (a–c) TEM images showing fipronil-loaded silica nanocapsules with 8 nm (a), 25 nm (b) and 44 nm (c) shell thicknesses (scale bars are 100 nm). (d) Release profiles of fipronil-encapsulated nanocapsules with 8 nm (▲), 25 nm (■) and 44 nm (●) silica shell thicknesses.

Nanocapsules with a thicker shell, *i.e.* 25 nm and 44 nm, demonstrated slower fipronil release which occurred at 4 h and 8 h at 1.9 ± 1.0% and 1.4 ± 0.2%, respectively. The fipronil release then gradually increased with time. The release of fipronil decreased with increasing silica shell thickness, with 48.4 ± 3.2%, 29.8 ± 2.9% and 19.6 ± 1.2% of fipronil released from silica nanocapsules having 8 nm, 25 nm and 44 nm shell thicknesses, respectively, at 142 h. TEM images (Fig. S4, ESI†) showed that the shell morphology of the nanocapsules was still intact before and after 142 h of study, indicating that the release of fipronil from silica nanocapsules in water was governed mainly by diffusion rather than by physical changes to the silica nanoshell. This study demonstrated that the core–shell structure of silica nanocapsules formed using bio-inspired silicification can be used for encapsulation of active components and thus their sustained release, and the release profile can be controlled by the silica shell thickness.

To conclude, we demonstrated a novel and facile method for the fabrication of silica nanocapsules using emulsion templating based on bio-inspired silicification. Our approach was based on the novel design of a bifunctional peptide by modularizing a surface-active peptide sequence with a sequence having biosilicification activity, thus achieving the formation of stable nanoemulsions followed by the nucleation and growth of a defined and controllable silica shell at the oil–water interface under benign conditions, including room temperature, neutral pH and without use of toxic reagents. Moreover, the silica shell thickness could be tuned simply by controlling pH, reaction time and silica precursor concentration. Active ingredient was encapsulated effectively in the oil core of silica nanocapsules with a high loading capacity, and was shown to have a sustained release profile dependent on shell thickness. Therefore, the emulsion and biomimetic dual-templating technology developed in this work represents a new strategy for forming nanomaterials having core–shell structure using components and processes expected to have minimal environment footprint, opening opportunities for further applications that demand biocompatibility, facile manufacture and high loading capacity coupled with slow release of an active agent.

This work was supported by the Australian Research Council (ARC) (grants DP1093056 and 120103683). DW acknowledges a scholarship from The University of Queensland (UQ). CXZ acknowledges financial support from ARC (Australian Post-doctoral Fellow DP110100394). APJM acknowledges support from the Queensland Government through award of the 2010 Queensland Premier's Science Fellowship. We thank Lei Yu for support with EDX analyses as well as the facilities, and the scientific and technical assistance of the Australian Microscopy & Microanalysis Research Facility at the Centre for Microscopy and Microanalysis, UQ.

Notes and references

1 (*a*) X. W. Lou, L. A. Archer and Z. C. Yang, *Adv. Mater.*, 2008, **20**, 3987–4019; (*b*) A. Guerrero-Martínez, J. Pérez-Juste and L. M. Liz-Marzán, *Adv. Mater.*, 2010, **22**, 1182–1195; (*c*) W. Schärtl, *Nanoscale*, 2010, **2**, 829–843.
2 A. Burns, H. Ow and U. Wiesner, *Chem. Soc. Rev.*, 2006, **35**, 1028–1042.
3 (*a*) A.-H. Lu, E. L. Salabas and F. Schüth, *Angew. Chem., Int. Ed.*, 2007, **46**, 1222–1244; (*b*) Y. Chen, C. Chu, Y. Zhou, Y. Ru, H. Chen, F. Chen, Q. He, Y. Zhang, L. Zhang and J. Shi, *Small*, 2011, **7**, 2935–2944.
4 (*a*) J. F. Chen, H. M. Ding, J. X. Wang and L. Shao, *Biomaterials*, 2004, **25**, 723–727; (*b*) Y. Zhao, L.-N. Lin, Y. Lu, S.-F. Chen, L. Dong and S.-H. Yu, *Adv. Mater.*, 2010, **22**, 5255–5259.
5 (*a*) H. Chen, J. He, H. Tang and C. Yan, *Chem. Mater.*, 2008, **20**, 5894–5900; (*b*) K. Hayashi, M. Nakamura and K. Ishimura, *Chem. Commun.*, 2011, **47**, 1518–1520.
6 (*a*) C. I. Zoldesi and A. Imhof, *Adv. Mater.*, 2005, **17**, 924–928; (*b*) R. S. Underhill, A. V. Jovanovic, S. R. Carino, M. Varshney, D. O. Shah, D. M. Dennis, T. E. Morey and R. S. Duran, *Chem. Mater.*, 2002, **14**, 4919–4925.
7 (*a*) M. B. Dickerson, K. H. Sandhage and R. R. Naik, *Chem. Rev.*, 2008, **108**, 4935–4978; (*b*) C.-L. Chen and N. L. Rosi, *Angew. Chem., Int. Ed.*, 2010, **49**, 1924–1942; (*c*) S. V. Patwardhan, *Chem. Commun.*, 2011, **47**, 7567–7582; (*d*) S. V. Patwardhan, S. J. Clarson and C. C. Perry, *Chem. Commun.*, 2005, 1113–1121.
8 (*a*) J. N. Cha, K. Shimizu, Y. Zhou, S. C. Christiansen, B. F. Chmelka, G. D. Stucky and D. E. Morse, *Proc. Natl. Acad. Sci. U. S. A.*, 1999, **96**, 361–365; (*b*) N. Kröger, R. Deutzmann and M. Sumper, *Science*, 1999, **286**, 1129–1132.
9 (*a*) R. R. Naik, L. L. Brott, S. J. Clarson and M. O. Stone, *J. Nanosci. Nanotechnol.*, 2002, **2**, 95–100; (*b*) M. Sarikaya, C. Tamerler, A. K. Y. Jen, K. Schulten and F. Baneyx, *Nat. Mater.*, 2003, **2**, 577–585.
10 (*a*) J. N. Cha, G. D. Stucky, D. E. Morse and T. J. Deming, *Nature*, 2000, **403**, 289–292; (*b*) H. R. Luckarift, J. C. Spain, R. R. Naik and M. O. Stone, *Nat. Biotechnol.*, 2004, **22**, 211–213; (*c*) R. R. Naik, M. M. Tomczak, H. R. Luckarift, J. C. Spain and M. O. Stone, *Chem. Commun.*, 2004, 1684–1685; (*d*) P. Graf, A. Mantion, A. Haase, A. F. Thünemann, A. Mašić, W. Meier, A. Luch and A. Taubert, *ACS Nano*, 2011, **5**, 820–833.
11 P. Erni, G. Dardelle, M. Sillick, K. Wong, P. Beaussoubre and W. Fieber, *Angew. Chem., Int. Ed.*, 2013, **52**, 10334–10338.
12 A. F. Dexter, A. S. Malcolm and A. P. J. Middelberg, *Nat. Mater.*, 2006, **5**, 502–506.
13 A. F. Dexter and A. P. J. Middelberg, *J. Phys. Chem. C*, 2007, **111**, 10484–10492.
14 A. P. J. Middelberg, C. J. Radke and H. W. Blanch, *Proc. Natl. Acad. Sci. U. S. A.*, 2000, **97**, 5054–5059.
15 Y. P. Chuan, B. Y. Zeng, B. O'Sullivan, R. Thomas and A. P. J. Middelberg, *J. Colloid Interface Sci.*, 2012, **368**, 616–624.
16 A. P. J. Middelberg, L. He, A. F. Dexter, H. H. Shen, S. A. Holt and R. K. Thomas, *J. R. Soc. Interface*, 2008, **5**, 47–54.
17 M. B. Dickerson, S. E. Jones, Y. Cai, G. Ahmad, R. R. Naik, N. Kröger and K. H. Sandhage, *Chem. Mater.*, 2008, **20**, 1578–1584.
18 (*a*) L. M. Liz-Marzán, M. Giersig and P. Mulvaney, *Langmuir*, 1996, **12**, 4329–4335; (*b*) Y. Lu, J. McLellan and Y. N. Xia, *Langmuir*, 2004, **20**, 3464–3470.
19 (*a*) F. Colliot, K. A. Kukorowski, D. W. Hawkins and D. A. Roberts, *Proc. Brighton Crop Prot. Conf. Pest Dis.*, Brighton, UK, 1992; (*b*) C. C. D. Tingle, J. A. Rother, C. F. Dewhurst, S. Lauer and W. J. King, *Rev. Environ. Contam. Toxicol.*, 2003, **176**, 1–66.

Electronic Supplementary Information (ESI)

Emulsion-templated silica nanocapsules formed using bio-inspired silicification

D. Wibowo,[a] C.-X. Zhao[a] and Anton P. J. Middelberg*[a]

[a]*Australian Institute for Bioengineering and Nanotechnology, The University of Queensland, Brisbane, QLD 4072, Australia*

*Corresponding author: Phone: (+61) 7 3346 4189; Fax: (+61) 7 3346 4197; E-mail: a.middelberg@uq.edu.au.

Experimental section

Synthesis of silica nanocapsules: To synthesize silica nanocapsules, lyophilized SurSi peptide (Peptide 2.0 Inc., VA) was dissolved in sodium 4-(2-hydroxyethyl)-1-piperazine ethanesulfonate (HEPES) buffer (25 mM, pH 7) in the presence of $ZnCl_2$ (800 μM) to give a final peptide concentration of 400 μM. Then Miglyol® 812 (20 μL) was added into 1 mL of the solution. The mixture was sonicated at 10 W (Branson Sonifier 450 ultrasonicator) for four 30 s burst and interspersed in an ice bath for 60 s. Nanoemulsion (1 mL) was dialyzed against HEPES buffer (25 mM, 500 mL, pH 7.5) at 4°C for 20 h. An aliquot of the nanoemulsion (400 μL) was transferred into a 4-mL glass vial for biosilicification reaction with tetraethoxysilane (TEOS) under magnetic stirring for up to 50 h at room temperature. To investigate the effects of reaction time and silica precursor concentration, TEOS concentration was varied and samples were taken at various times for characterization. A control vial demonstrated stability of the nanoemulsion for the reaction period.

Encapsulation efficiency: Encapsulation efficiency of fipronil (%*EE*) was characterized by the percentage between mass of fipronil in silica nanocapsules after the final TEOS removal step and initial mass of fipronil dissolved in the oil phase. To calculate %*EE*, silica nanocapsules containing fipronil were prepared as previously described. After TEOS removal step, the suspensions of silica nanocapsules were freeze-dried at 0.08 mbar and –55 °C for 20 h. The freeze-dried samples were mixed with water, finely dispersed by sonication at 20 W

(Branson Sonifier 450 ultrasonicator) for 60 s, and subsequently added into acetonitrile with final acetonitrile concentration of 60 v/v%, as fipronil is soluble in acetonitrile (60 v/v%) as high as 71.5 mg mL^{-1}, under vigorous stirring at room temperature for up to 72 h. The suspensions were centrifuged at an interval 24 h and the supernatants were collected, then fresh acetonitrile (60 v/v%) was added to the pellets. The releases of fipronil in the acetonitrile solutions were repeated until no residual fipronil in supernatants was detected. The fipronil concentrations in the supernatants were measured by RP-HPLC as described in the following section. Then, the encapsulation efficiencies of fipronil were calculated by using Eq. S1, where C_f is the fipronil concentration in release medium (mg mL^{-1}), V_f is the volume of release medium (mL), C_i is the initial fipronil concentration in the Miglyol® 812 oil (10 mg mL^{-1}), V_i is the volume of the oil phase (mL) and n is the number of repeated-release of fipronil.

$$\text{Encapsulation Efficiency: } \%EE = \frac{\sum_{j=1}^{n} (C_f V_f)_j}{C_i V_i} \times 100\% \qquad \text{(Eq. S1)}$$

Sustained release study: To encapsulate fipronil, fipronil was first dissolved in Miglyol® 812 (10 mg mL^{-1}) used to form a nanoemulsion. Fipronil-loaded silica nanocapsules were then prepared by a reaction of dialyzed fipronil-loaded nanoemulsions with TEOS at concentration of 16 μmol, 32 μmol, or 96 μmol in 25 mM HEPES buffer at pH 7.5 for 30 h. The 10 mg mL^{-1} fipronil-loaded nanocapsules with different silica shell thicknesses were then dialyzed in water at 4°C for 20 h to remove residual TEOS. Then, the release study was started by stirring the nanocapsules aqueous solution at room temperature. At different time intervals, aliquots of 200 μL were taken, replaced with water, and the aliquots were centrifuged to obtain clear supernatant. Fipronil in the supernatant was assayed by high-performance liquid chromatography (HPLC) using a Shimadzu system equipped with a reversed-phase C18 column (Jupiter, 5 μm, 300 Å, 150 × 4.6 mm). Phosphoric acid 0.1 v/v% (A) and 90 v/v% acetonitrile, 0.1 v/v% phosphoric acid (B) were used as the mobile phases. A linear gradient from 50 to 70% B in 20 min at a flow rate of 1 mL min^{-1} was used with a monitoring wavelength set at 220 nm. The concentrations of fipronil released were reported relative to the saturation limit of fipronil in water (2 μg mL^{-1}). To determine the concentration of fipronil, a standard curve was obtained by dissolving weighted amounts of fipronil powder in 60 v/v% acetonitrile.

Characterization: Dynamic light scattering (DLS) was performed on Malvern Zetasizer Nano ZS at a scattering angle of 173° and a temperature of 25°C. Samples were diluted by a factor of 100 prior to the size and zeta potential measurements. Transmission electron microscopy (TEM) was carried out on a JEOL 1010 operated at 100 kV. Samples (2 µL) were deposited onto Formvar-coated copper grids, washed with water and left to air-dry prior to TEM examination, without the need for staining or cryopreservation. Energy dispersive X-ray spectroscopy (EDX) spectrum were obtained by using high-resolution (HR) TEM (JEOL 2100, 200 kV accelerating voltage) equipped with an EDX detector.

Supplementary figures

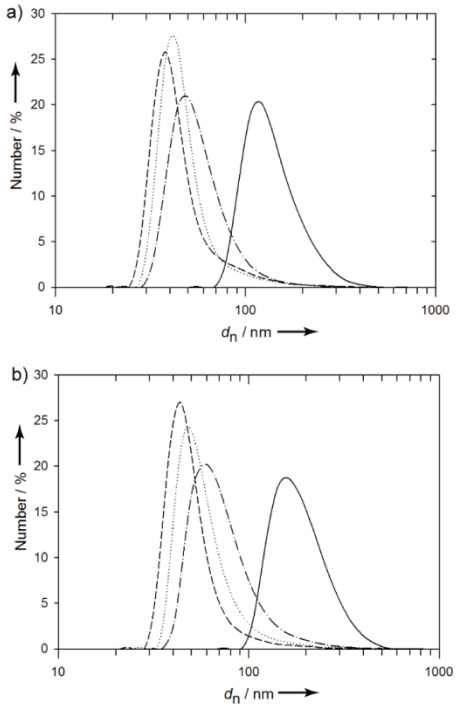

Fig. S1 (a–b) Size distribution of SurSi-stabilized nanoemulsions and nanocapsule formed at pH 7.5 (a) and pH 8 (b) as determined by dynamic light scattering (DLS), after emulsification at pH 7 (– – –), after 20 h of dialysis at pH 7.5 (a) or pH 8 (b) (·····), after 20 h of reaction with 32 µmol tetraethoxysilane (TEOS) at pH 7.5 (a) or pH 8 (b) (——), and control SurSi-stabilized nanoemulsion after 40 h of incubation at pH 7.5 (a) or pH 8 (b) (–·–·–·).

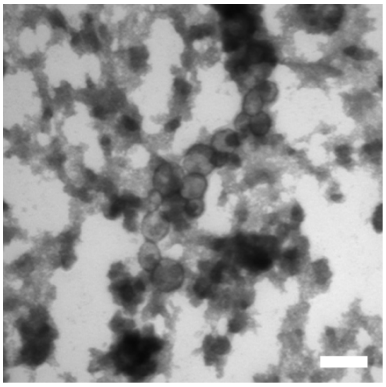

Fig. S2 Transmission electron microscopy (TEM) image taken after a 20-h reaction of the dialyzed AM1-stabilized nanoemulsions with 32 μmol tetraethoxysilane (TEOS) in 25 mM HEPES buffer pH 7.5 at room temperature. Scale bar is 200 nm.

The procedure for the synthesis of silica nanocapsules by templating AM1-stabilized nanoemulsions was described in the *Synthesis of silica nanocapsules* (**Experimental section**) except that AM1 peptide was used instead of SurSi peptide. Despite the formation of silica nanocapsules by templating AM1-stabilized nanoemulsions, it led mainly to the formation of bulk silica nanoparticles (Fig. S2) indicating that the dual functionality of emulsion stabilization and silica shell formation cannot be effectively achieved by using AM1 as its surface activity is sacrificed during biosilicification reactions resulting in formation of silica largely in bulk solutions (Fig. S2).

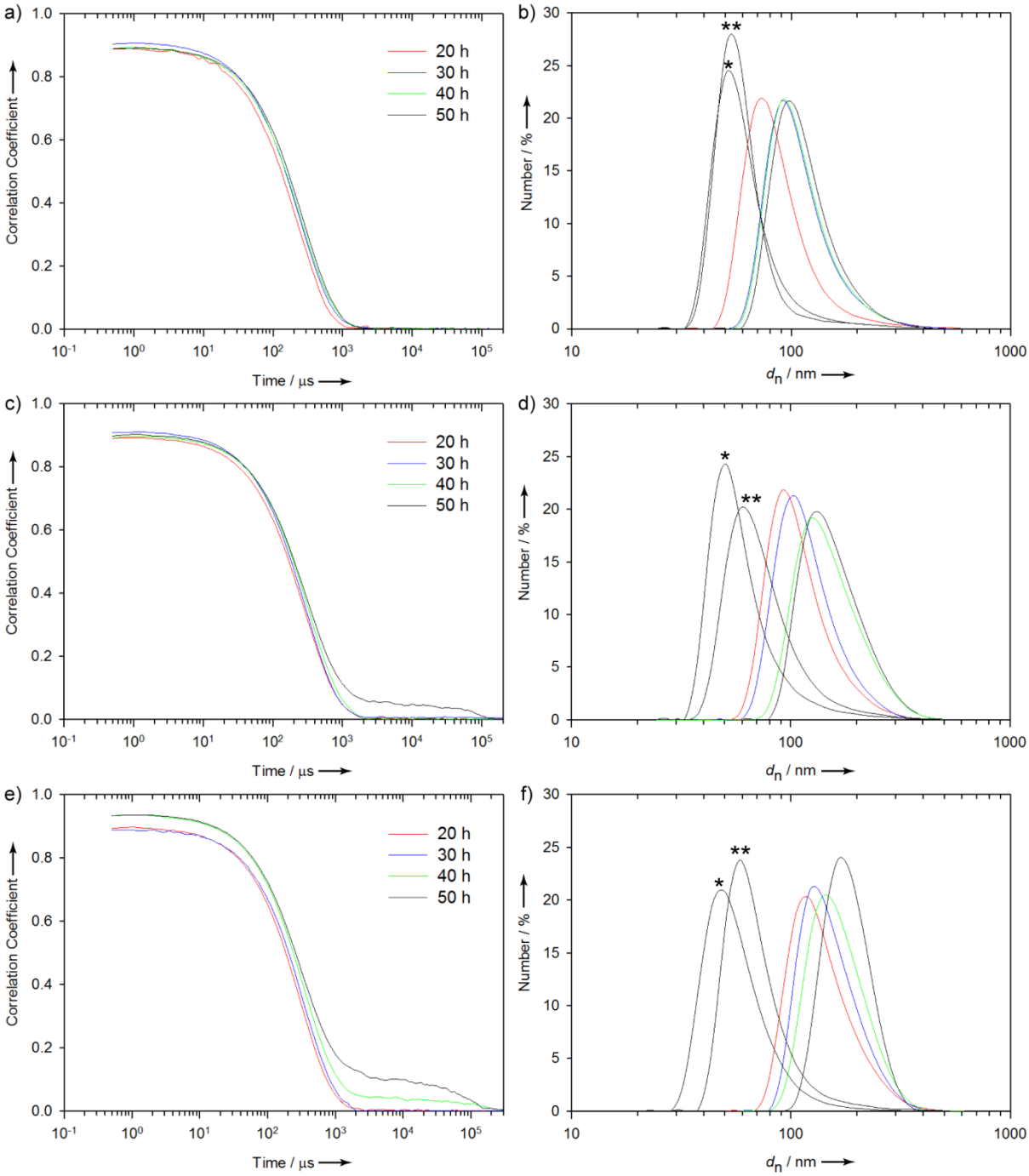

Fig. S3 Dynamic light scattering (DLS) results presenting the correlograms (left) and the associated number-weighted size distributions (right). (a–f) DLS data of the silica nanocapsules were taken after reaction of SurSi-stabilized nanoemulsions with tetraethoxysilane (TEOS) at concentrations of 8 µmol (a, b), 16 µmol (c, d) and 32 µmol (e, f) in 25 mM HEPES buffer pH 7.5 for up to 50 h at room temperature. Samples of SurSi-stabilized nanoemulsions before reaction with TEOS (*) and dialyzed SurSi-stabilized nanoemulsions incubated for 50 h (**) are included in the size distribution profiles (right) for comparison.

The correlograms show a typical single exponential decay of the scattered intensities over time due to the Brownian motion of the nanocapsules (Fig. S3a, c, e). However, the correlograms of the samples of silica nanocapsules obtained after reactions with 16 µmol TEOS for 50 h (Fig. S3c), and 32 µmol TEOS for 40 h and 50 h (Fig. S3e) show multiple peaks, i.e., substantial tail and non-flat baseline at the end of the decay, indicating the presence of aggregates. The decays of these samples show more extended slope suggesting their polydispersities. These are confirmed by the polydispersity index (PDI) values presented in Table S1. The number-weighted size distributions, which were calculated from the correlation functions by the zetasizer software, show only single peaks suggesting that the corresponding aggregates were present in trace amounts (Fig. S3b, d, f). Furthermore, the time at which the correlation function starts to decay over time gives an indication of the mean size of the nanocapsules in the suspensions. Increasing reaction times between SurSi-stabilized nanoemulsions and TEOS produces larger silica nanocapsules which move more slowly in the suspensions and thus the correlation functions persist for longer time prior to the decay (Fig. S3a, c, e). The number-weighted size distributions show more clearly the increase in size as the reaction times were increased (Fig. S3b, d, f).

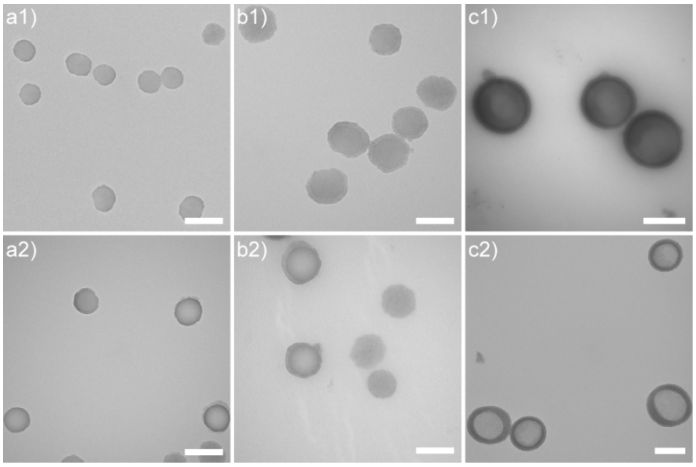

Fig. S4 (a–c) Transmission electron microscopy (TEM) images of the silica nanocapsules having shell thickness of 8 nm (a), 25 nm (b) and 44 nm (c) before (1) and after (2) fipronil-release study. Scale bars are 200 nm.

Supplementary table

Table S1 Polydispersity index of nanocapsules as a function of reaction time and tetratethoxysilane (TEOS) concentration.

Time / **mol_{TEOS}**	**0 h**	**20 h**	**30 h**	**40 h**	**50 h**
0 µmol	0.293	0.318	-	-	-
8 µmol	-	0.216	0.184	0.150	0.140
16 µmol	-	0.168	0.140	0.154	0.345
32 µmol	-	0.146	0.180	0.468	0.651

Chapter 4

Sustained release of fipronil insecticide *in vitro* and *in vivo* from biocompatible silica nanocapsules

The research in this chapter consists of the peer-reviewed paper published as:

Wibowo, D., C.-X. Zhao*, B.C. Peters, and A.P.J. Middelberg*, *Sustained release of fipronil insecticide in vitro and in vivo from biocompatible silica nanocapsules*. J. Agric. Food Chem., 2014. **62**(52): p. 12504–12511.

The following modifications were made to the article:

- Page numbers of the original article were crossed-out; and
- Page numbers consistent with those on the remainder of the thesis pages were inserted.

Abstract

This chapter describes the applications of the bio-inspired oil-core silica-shell nanocapsules developed in **Chapter 3**, which include facile encapsulation of fipronil insecticide and its sustained release *in vitro* as well as *in vivo* against termites. Facile encapsulation of fipronil in the silica nanocapsules was demonstrated by first solubilizing fipronil in Miglyol® 812 oil (0.5 or 1 mg/mL), and then emulsifying the oil phase through sonication. Subsequently, the resulted fipronil-loaded nanoemulsions were dialyzed and then reacted with tetraethoxysilane (TEOS) by 30-h stirring at pH 7.5 and room temperature for the biosilicification process. The resulted fipronil-encapsulated silica nanocapsules were characterized using dynamic light scattering, transmission electron microscopy, Fourier-transform infrared spectroscopy, and selected area electron diffraction. Tunability of silica shell thicknesses was easily achieved by varying TEOS concentrations. Controlled-release profiles of fipronil associated with the core–shell structure of the silica nanocapsules having different silica shell thicknesses were demonstrated *in vitro* in water. Two laboratory methods of termite control (i.e., direct- and feeding-treatment) were conducted for the *in vivo* experiments against economically important subterranean termites *Coptotermes acinaciformis* to further demonstrate the controlled-release properties and insecticidal effect of the fipronil-encapsulated silica nanocapsules. Photographic images regarding termite collection and the *in vivo* studies against termites in this chapter were presented in **Appendix A**.

JOURNAL OF AGRICULTURAL AND FOOD CHEMISTRY

Article

pubs.acs.org/JAFC

Sustained Release of Fipronil Insecticide *in Vitro* and *in Vivo* from Biocompatible Silica Nanocapsules

David Wibowo,[†] Chun-Xia Zhao,*[,†] Brenton C. Peters,[‡] and Anton P. J. Middelberg*[,†]

[†]Australian Institute for Bioengineering and Nanotechnology, The University of Queensland, St Lucia, QLD 4072, Australia

[‡]Brenton Peters Consulting, Jindalee, QLD 4074, Australia

ABSTRACT: A pesticide delivery system made of biocompatible components and having sustained release properties is highly desirable for agricultural applications. In this study, we report a new biocompatible oil-core silica-shell nanocapsule for sustained release of fipronil insecticide. Silica nanocapsules were prepared by a recently reported emulsion and biomimetic dual-templating approach under benign conditions and without using any toxic chemicals. The loading of fipronil was achieved by direct dissolution in the oil core prior to biomimetic growth of a layer of silica shell surrounding the core, with encapsulation efficiency as high as 73%. Sustained release of fipronil *in vitro* was tunable through control of the silica-shell thickness (i.e., 8−44 nm). *In vivo* laboratory tests showed that the insecticidal effect of the fipronil-encapsulated silica nanocapsules against economically important subterranean termites could be controlled by tuning the shell thickness. These studies demonstrated the effectiveness and tunability of an environmentally friendly sustained release system for insecticide, which has great potential for broader agricultural applications with minimal environmental risks.

KEYWORDS: *silica, nanocapsules, sustained release, insecticides, fipronil, subterranean termites*

INTRODUCTION

Over recent decades, there has been an increasing interest in the development of pesticide delivery systems to prevent and control pest populations, especially in countries with agriculture-driven economies.[1−5] Encapsulation and delivery of active ingredients such as pesticides using carriers offer substantial advantages, including protection of the actives against premature decomposition (e.g., photolysis, hydrolysis, microbial, or oxidation/reduction) and loss (e.g., evaporation or leaching), protection of the environment against toxicity of the actives, enhanced bioavailability especially for hydrophobic actives, and the possibility of delivering high amounts of actives in a sustained manner. Sustained release of pesticides is highly desirable in agriculture as it likely reduces periodic applications by maintaining an effective local concentration in a prolonged duration, thereby lowering potential for development of pest resistance and undesirable environmental side effects. Polymeric matrices,[6−8] solid lipid particles[9] and composites[10,11] are among commonly investigated carriers in pesticide delivery systems.

Silica-based nanomaterials mainly evaluated for biomedical applications[12] have emerged as relatively new nanocarriers for agricultural applications.[13−25] Silica materials can offer distinct advantages over other materials, as they provide more mechanically stable structures than polymeric materials[15] and have structural flexibility in forming nanomaterials with high-capacity loading of actives.[26] Furthermore, silica in an amorphous structure is biocompatible as it is categorized as a "Generally Recognized As Safe (GRAS)" material by the U.S. Food and Drug Administration.[27] Previous studies have shown the loading and release of various agrochemicals from silica-based nanomaterials, including nonporous silica nanoparticles,[16] mesoporous silica nanoparticles[17−20] and hollow-core silica-shell nanoparticles.[21−25] The latter are more advantageous as the core provides higher loading capacity of actives than nonporous and mesoporous silica nanoparticles.[28] Generally, there are two techniques of active-loading in core−shell silica nanoparticles, i.e., postloading and preloading. The postloading is based on diffusion of actives into the interior space via immersion[21,22] or high-pressure supercritical fluid.[22−24] The drawback with this method is that it promotes initial burst release in aqueous-based environments due to the presence of surface-associated active molecules,[21−24] especially when water-soluble actives were used.[24] On the other hand, the preloading technique is based on the solubilization of actives in template materials prior to formation of silica shells,[25] which is more advantageous as to reduce the possibility of attachment of actives at the external surfaces of the shells, thus increasing the flexibility to protect and release the actives. Despite these benefits, synthesis of the core−shell silica nanoparticles most commonly involves chemical surfactants, templates and toxic organic solvents which must then be completely removed from the product.[25] It has been shown that residual chemical surfactants embedded in the silica-based nanomaterials can cause severe cytotoxicity[12] which would pose significant environmental risks. In this respect, a superior strategy for synthesis of nanocarriers should enable the preloading of actives with high loading capacity and involve only biocompatible components, thus avoiding time-consuming and tedious monitoring-procedures for ensuring complete removal of residual toxic components down to the levels that might be considered as environmentally safe.

Received: September 15, 2014
Revised: December 2, 2014
Accepted: December 5, 2014
Published: December 5, 2014

Recently, we developed a novel emulsion and biomimetic dual-templating approach to synthesize oil-core silica-shell nanocapsules with tunable shell thickness.[29] Bifunctional SurSi peptide (Ac-MKQLAHSVSRLEHARKKRKKRKKRKKGGGY-$CONH_2$) was designed by modularizing a surface active peptide sequence (Sur module, MKQLAHSVSRLEHA) with a sequence for biosilicification (Si module, RKKRKKRKKR KKGGGY). Typically, oil-in-water (O/W) nanoemulsions are formed with a pharmaceutically safe oil, Miglyol 812, dispersed in the SurSi aqueous solution. Then a silica precursor tetraethoxysilane (TEOS) is added to facilitate the biosilicification at the O/W interfaces forming the oil-core silica-shell nanocapsules under room temperature, and at nearly neutral pH without use of any toxic chemicals. In contrast to the chemical methods mentioned above, our method is more biocompatible and environmentally friendly. An additional advantage of using peptide biosurfactant is the ability to be produced renewably at large scale and relatively low cost using biological expression.[30,31] Furthermore, our dual-templating approach offers easy preloading of active components by simply dissolving in the oil phase with a high loading capacity. It has been demonstrated that fipronil saturated in Miglyol 812 (at 10 $mg{\cdot}mL^{-1}$) was easily encapsulated in silica nanocapsules by a preloading technique and without the need for template removal.[29]

Fipronil (5-amino-1-[2,6-dichloro-4-(trifluoromethyl)-phenyl]-4-[(trifluoromethyl)sulfinyl] pyrazole-3-carbonitrile) is a systemic insecticide commonly used as soil treatment, seed coating, or baits[32] due to its nonrepellent property, broad-spectrum activity against agricultural, forest, pastoral, domestic and veterinary pests,[33] and high specificity for insect pests over mammalians.[34] The biochemical mode of action of fipronil is by blocking γ-aminobutyric acid (GABA) receptor of the GABA-gated chloride channel, thereby disrupting central nervous system activity and, at a sufficient dose, causing death.[34] It has low water solubility (~2 $\mu g{\cdot}mL^{-1}$ at 25 °C) and low Henry's constant (6.6×10^{-6} $m^3{\cdot}atm{\cdot}mol^{-1}$ at 25 °C), suggesting low volatility, and its soil organic carbon partition coefficient (K_{oc}) of 727 indicates low mobility in soil and, hence, low potential for groundwater contamination.[32,35]

In this study, sustained release of fipronil *in vitro* and *in vivo* from biocompatible oil-core silica-shell nanocapsules were investigated and compared. Fipronil-encapsulated silica nanocapsules with different shell thicknesses were synthesized using the dual-templating approach aforementioned. The *in vitro* release of fipronil was studied in water. The efficacy of the fipronil-encapsulated silica nanocapsules was evaluated by conducting *in vivo* laboratory tests, i.e., direct- and feeding-treatments, against economically important subterranean termites (i.e., *Coptotermes acinaciformis*). Subterranean termites cause substantial damages to cultivated plants, wooden structures, pastures, forests and other agricultural crops.[36] Based on the sales estimation of insecticides in 2010, the worldwide annual control and repair costs can reach US$40 billion with subterranean termites accounted for 80% of the costs.[37] This study would thus be expected to bring significant impact in agricultural fields.

MATERIALS AND METHODS

Chemicals. SurSi peptide (Ac-MKQLAHSVSRLEHARKKRKK RKKRKKGGGY-$CONH_2$, M_w 3632 $g{\cdot}mol^{-1}$) was custom synthesized by Peptide 2.0 Inc. (Chantilly, VA, USA) with purity >95% and was lyophilized prior to use. Fipronil in a powder form ($C_{12}H_4Cl_2F_6N_4OS$, M_w 437.15 $g{\cdot}mol^{-1}$, mp 196−201 °C, and d 1.55 $g{\cdot}cm^{-3}$) was of analytical standard obtained from Sigma-Aldrich. Miglyol 812 was purchased from AXO Industry S.A. (Wavre, Belgium) and was passed through heat-activated silica gel (Sigma-Aldrich) prior to use. Termidor (9.1% fipronil in a form of suspension concentrate) was obtained from BASF Australia Ltd. Water with >18.2 MΩ·cm resistivity was obtained from a Milli-Q (Millipore, Australia) system with a 0.22 μm filter. Other chemicals were of analytical grade purchased from either Sigma-Aldrich or Merck and used as received.

Synthesis. Oil-core silica-shell nanocapsules were synthesized using an emulsion and biomimetic dual-templating approach as we previously reported.[29] Briefly, fipronil was dissolved in Miglyol 812 oil at a concentration of 0.05 $mg{\cdot}mL^{-1}$ or 1 $mg{\cdot}mL^{-1}$, and then the fipronil-loaded oil was added into a solution of SurSi peptide (400 μM) containing $ZnCl_2$ (800 μM) in sodium 4-(2-hydroxyethyl)-1-piperazine ethanesulfonate (HEPES) buffer (25 mM, pH 7), and the mixture was sonicated at 10 W (Branson Sonifier 450 ultrasonicator) to obtain O/W nanoemulsions which were dialyzed against HEPES buffer (25 mM, pH 7.5) at 4 °C for 20 h to remove residual peptide in the bulk solution. Then the nanoemulsions (pH 7.5) were mixed with tetraethoxysilane (TEOS) at a concentration of 16 μmol, 32 μmol or 96 μmol under stirring at room temperature for 30 h to form fipronil-encapsulated silica nanocapsules having three different shell thicknesses. Subsequently, the nanocapsules were dialyzed against water at 4 °C for 20 h to remove the residual TEOS and prevent further growth of the silica shell.

Characterization. *Encapsulation Efficiency.* The suspensions of fipronil-encapsulated silica nanocapsules were freeze-dried for 20 h, subsequently mixed with water and sonicated at 20 W (Branson Sonifier 450 ultrasonicator) for 60 s to finely disperse the nanocapsules. Subsequently, acetonitrile was added into the suspensions with final acetonitrile concentration of 60 v/v%, and vigorously stirred at room temperature for up to 72 h. At different time intervals, the supernatants were collected by centrifugation, then fresh acetonitrile (60 v/v%) was added to the pellets to repeat the release of fipronil from the nanocapsules until no residual fipronil in the supernatants was detected via reversed-phase high-performance liquid chromatography (RP-HPLC).

Reversed-Phase High-Performance Liquid Chromatography (RP-HPLC). Concentrations of fipronil were assayed by RP-HPLC using a Shimadzu system equipped with a Jupiter C18 column (5 μm, 300 Å, 150 mm × 4.6 mm). Mobile phase A was water containing 0.1 v/v% phosphoric acid, while phase B contained 90 v/v% acetonitrile and 0.1 v/v% phosphoric acid. The elution gradient was increased from 50% B to 70% B over 20 min at a monitoring wavelength of 220 nm. The concentration of fipronil was determined based on the peak area at retention time of approximately 14.5 min according to calibration curve obtained from standard solution of fipronil in acetonitrile solution (60 v/v%).

Fourier Transform-Infrared (FT-IR) Spectroscopy. Silica nanocapsules without and with fipronil in the oil cores were prepared as described previously. The nanocapsules were washed twice with water and subsequently freeze-dried. FT-IR spectra of lyophilized SurSi peptide and the nanocapsules were determined by using a PerkinElmer Spectrum 100 FT-IR Spectrometer equipped with a universal attenuated total reflection (ATR) attachment. Spectra data were collected in the transmission mode by averaging 135 scans over wavenumber range 4000−600 cm^{-1} at a spectral resolution of 4 cm^{-1}.

Dynamic Light Scattering (DLS). Size distributions of nanoemulsions and nanocapsules were determined by DLS using Malvern Zetasizer Nano ZS (Malvern Instrument Ltd., UK) at a scattering angle of 173° and a temperature of 25 °C. Samples were diluted by a factor of 100 prior to the measurements to avoid multiple scattering effects.

Transmission Electron Microscopy (TEM). Morphology of the fipronil-encapsulated silica nanocapsules was characterized by depositing the suspension (2 μL) onto Formvar-coated copper grids (ProSciTech Pty Ltd., Australia) and was then visualized via TEM (JEOL 1010, accelerating voltage of 100 kV). Size of the nanocapsules was analyzed using iTEM software (version 3.2, Soft Imaging System

GmbH) equipped with the TEM. Structure of the silica shell was determined using selected area electron diffraction (SAED) technique via high-resolution (HR) TEM (JEOL 2100, accelerating voltage of 200 kV).

***In Vitro* Release Study of Fipronil into Water.** Silica nanocapsules with three different shell thicknesses encapsulating 1 mg·mL^{-1} fipronil in Miglyol 812 were used to study the release profile of fipronil *in vitro*. The releases of fipronil from the silica nanocapsules to water were carried out by stirring the suspensions at room temperature for up to 142 h. At different time intervals, aliquots were taken, replaced with fresh water and centrifuged to obtain clear supernatants which were then analyzed using RP-HPLC.

***In Vivo* Study against Termites.** Termites (*C. acinaciformis*) were collected from field site in Esk (Queensland, Australia). Plastic containers filled with moist wood were inverted (lid off) onto a timber-filled trench known to contain termite infestation, and each container was then covered with insulating material secured with soil. After harvesting, actively moving termites were carefully selected from the containers for *in vivo* tests.

Direct Treatment. Six samples, including water, nanoemulsions, silica nanocapsules (encapsulating 0.05 mg·mL^{-1} fipronil in Miglyol 812) with three different shell thicknesses (8, 25, and 44 nm), and Termidor were used in the direct treatment, and they all contained the same final fipronil concentration except for the water sample. Water was used as control, and nanoemulsion was used as nanocapsules with zero silica-shell thickness. All six samples were used in five replicates for the direct treatment. Prior to the treatment, termites were placed in a group of ten termites in a Petri dish (92 mm × 16 mm), and incubated at 2 °C for 2 min to slow their movement. Each of the fipronil formulations or water (5.5 μL) was topically applied on the dorsal thorax of the worker termite. The termites were then transferred to clean Petri dishes containing a filter paper (42.5 mm, Whatman). The Petri dishes were placed into a controlled-environment chamber (65 cm × 47 cm × 37.5 cm) containing a thermometer, a lid and a 11.5-L metal container with water and heater to maintain the temperature at 28 ± 1 °C and high humidity, and, once covered with insulating material, total darkness (except during observation). At different time intervals, the Petri dishes were removed from the chamber, and the lids were opened with the least possible disturbance in order to examine termite response (mortality). A termite was considered dead when it was on its back or side (not supported by legs) and not able to move even after prodding with a soft brush.

Feeding Treatment. Silica nanocapsules (encapsulating 1 mg·mL^{-1} fipronil in Miglyol 812) with the thickest shell (44 nm) were used in the feeding treatment. Termidor with the same final fipronil concentration and water were used as controls. Each fipronil formulation and water samples were used in four and two replicates for the feeding treatment, respectively. To mimic natural environment of termite colonies, a 750 mL container was filled with *Nasutitermes magnus* mound material (150 g) which was roasted (200 °C, 60 min), ground and mixed with water (50 g) prior to use. A clear vinyl tubing (150 mm × 6 mm) was connected from the container to a 70 mL feeding vial containing α-cellulose (20 g) bait with a moisture content of 70 w/w%. Then termites (7.5 g ≈ 1500 worker and soldier termites) were placed into the container. Each of the assembled feeding devices was placed into a controlled-environment chamber having dimensions and conditions similar to that in the direct treatment (described above). The termites in the ten assemblies were allowed to acclimatize to these conditions for 4 days and began feeding on the baits as indicated by the presence of enclosed tunnels and chambers built in the baits. Then, 0.5 mL of the sample (water, Termidor or the nanocapsule) was transferred into each feeding vial. The assemblies were removed from the chamber and observed daily with the least possible disturbance in order to detect movement of living termites using a TermatracT3i device (Termatrac Pty Ltd., Australia). Lack of movement indicated 100% mortality of termites and inspections in the containers were conducted to confirm. During the treatment, termite groups in one container connected to Termidor-treated bait and in two containers connected to nanocapsule-treated baits remained alive for up to 8 days as the tube entrances to the vials were blocked with mud built by the termites. These containers were not considered for further study. Therefore, three treatment results were included in the analysis for the Termidor-treated baits and two treatment results for the nanocapsule-treated baits. The termites in two containers connected to water-treated baits survived throughout the study.

RESULTS AND DISCUSSION

Encapsulation of Fipronil in Silica Nanocapsules. Fipronil was easily dissolved in Miglyol 812 due to its high solubility in the oil (i.e., 10 mg·mL^{-1}).[29] The fipronil-loaded oil was emulsified in the presence of SurSi peptide via sonication, and nanoemulsions with narrow droplet size distribution were obtained due to the presence of the surface active Sur module[29] (Figure 1) in the emulsifying peptide. Following addition of the

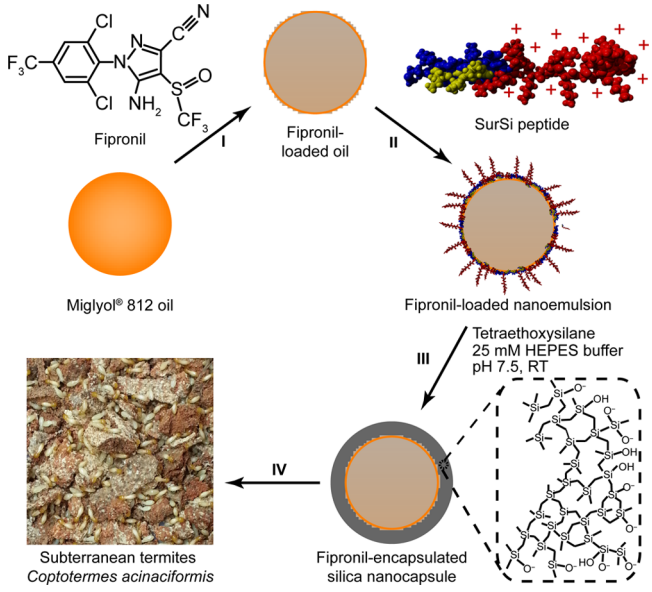

Figure 1. Illustration of the synthesis of fipronil-encapsulated silica nanocapsules formed using an emulsion and biomimetic dual-templating approach for sustained-release agroformulations against termites. Step (I), solubilization of fipronil in Miglyol 812 oil; step (II), sonication of the oil in SurSi peptide solution to form fipronil-loaded nanoemulsions; step (III), addition of tetraethoxysilane (TEOS) in the nanoemulsions to form a silica shell encapsulating the nanoemulsion core; step (IV), *in vivo* efficacy tests of the fipronil-encapsulated silica nanocapsules against economically important subterranean termites.

silica precursor tetraethoxysilane (TEOS) to the nanoemulsions, silica shell encasing the nanoemulsion core was formed at near-neutral pH and room temperature without using any toxic chemicals. The biosilicification process at the oil–water interface was due to the catalytic role of densely packed cationic arginine (R) and lysine (K) residues of Si module (RKKRKKRKKRKKGGGY) as well as polar residues of Sur module exposed toward the bulk aqueous solution that could induce hydrolysis of TEOS and interfacial polycondensation of the hydrolysis products i.e., silanol (≡Si–OH) and negatively charged silanolate (≡Si–O$^-$)[29] (Figure 1).

In this study, fipronil dissolved in Miglyol 812 oil at a concentration of 0.05 mg·mL^{-1} or 1 mg·mL^{-1} was encapsulated in silica nanocapsules and used for the sustained release study *in vitro* and *in vivo*. The amount of fipronil encapsulated in silica nanocapsules was determined based on the lethal dose of

fipronil sufficient to eliminate a termite for the *in vivo* tests. It has been reported that the lethal dose of fipronil for *Coptotermes* spp. is in the range of 2−10 ng per termite.[38,39] Based on this consideration, the encapsulated fipronil which was dissolved in Miglyol 812 at concentrations of 0.05 mg·mL^{-1} and 1 mg·mL^{-1} was equivalent to 1 ppm and 20 ppm in the silica nanocapsule suspensions and, at an applied volume, would give fipronil dose of around 6 ng/termite in the direct- and feeding treatments, respectively.

The encapsulation efficiencies (%*EE*) of fipronil in silica nanocapsules were determined by monitoring the concentration of fipronil released in acetonitrile solution (60 v/v%) over a period of time compared to initial concentration of fipronil dissolved in Miglyol 812 oil. Higher solubility of fipronil in acetonitrile (60 v/v%) i.e., 71.5 mg·mL^{-1} than in Miglyol 812 i.e., 10 mg·mL^{-1} promotes easy partition of the fipronil and its diffusion out of the silica nanocapsules. The results of practical encapsulation efficiencies of fipronil were calculated using eq 1:[29]

$$\%EE = \frac{\sum_{j=1}^{n} (C_f V_f)_j}{C_i V_i} \times 100\% \quad (1)$$

where C_f (mg·mL^{-1}) and V_f (mL) are the fipronil concentration released in acetonitrile solution and volume of the acetonitrile solution, respectively, C_i (mg·mL^{-1}) and V_i (mL) are the initial fipronil concentration in Miglyol 812 and volume of the Miglyol 812, respectively, and n is the number of repeated-release of fipronil. At an initial fipronil concentration of 0.05 mg·mL^{-1}, %*EE* of fipronil in silica nanocapsules obtained at reactions with 16 μmol, 32 μmol and 96 μmol of TEOS were 72.8%, 73.2%, and 73.6%, respectively, while similar %*EE* of 71.6%, 72.2%, and 72.9%, respectively, were obtained when initial fipronil concentration of 1 mg·mL^{-1} was used. The encapsulation of fipronil in the silica nanocapsules demonstrated high encapsulation efficiency which is suitable for agricultural applications.

Characterization of Silica Nanocapsules Containing Fipronil. To determine the molecular components of fipronil-encapsulated silica nanocapsules, SurSi peptide and silica nanocapsules without and with fipronil in the oil cores were analyzed using Fourier transform-infrared (FT-IR) spectroscopy, and the results were compared in Figure 2. For SurSi peptide, four characteristic peaks of the peptide backbone were observed (Figure 2a) which are assigned to amide A (N−H stretch), amide B (N−H stretch), amide I (C═O stretch), and amide II (C−N stretch and N−H in-plane bend) at 3284, 3071, 1648, and 1542 cm^{-1}, respectively.[40] The functional groups of peptide side chains can also be identified (Figure 2a) i.e., peak at 1298 cm^{-1} corresponds to O−H deformation of hydroxyl group of serine (S), shoulder at 1248 cm^{-1} and doublet at 837 and 800 cm^{-1} are associated with C−O stretch and phenyl ring of tyrosine (Y), respectively, and doublet at 1180 and 1130 cm^{-1} can be attributed to NH_3^+ rocking of lysine (K).[40,41] FT-IR spectrum of the silica nanocapsules without fipronil (Figure 2b) shows a broad signal centered at 3330 cm^{-1} which reflects the vibration of O−H stretching of silanol group Si−OH. A strong absorption band at about 1060 cm^{-1}, with a shoulder at 1160 cm^{-1}, and a band at 780 cm^{-1} correspond to asymmetric and symmetric Si−O−Si stretching vibrations of siloxane group, respectively. An absorption shoulder at 960 cm^{-1} arises from the Si−O$^-$ stretching of Si−OH. The major peaks of N−H stretch of peptide and other peptide side chains are

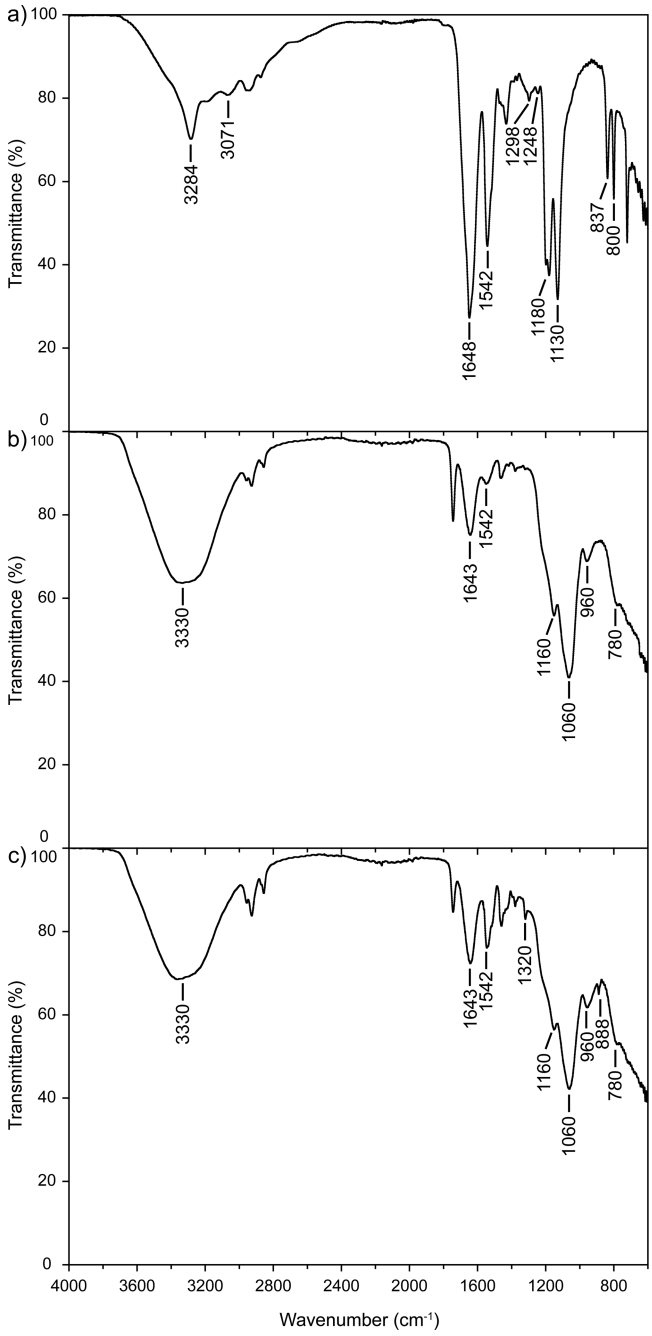

Figure 2. FT-IR spectra of (a) SurSi peptide, (b) silica nanocapsules without fipronil in the oil cores, and (c) fipronil-encapsulated silica nanocapsules.

overlapped by the characteristic bands of silica and thus are unobserved (Figure 2b). However, the presence of peptide in the silica nanocapsules can still be characterized by the absorption bands of amide I and amide II although the intensities are significantly reduced. The FT-IR spectrum of fipronil-encapsulated silica nanocapsules (Figure 2c) retained most of the major peaks of the silica nanocapsules without fipronil (Figure 2b). Additionally, new absorption bands appear and are clearly discernible at 1320 and 888 cm^{-1} which can be attributed to $-CF_3$ stretching of trifluoromethyl group and C−H out-of-plane bending of benzene ring[42] of the fipronil molecule, respectively (Figure 2c). These vibrational frequen-

dx.doi.org/10.1021/jf504455x | J. Agric. Food Chem. 2014, 62, 12504−12511

cies further verify the incorporation of fipronil into silica nanocapsules.

Morphology of silica nanocapsules can be visualized by using TEM without the need for staining or cryo-preservation. The TEM images showed morphology of a core−shell structure of fipronil-encapsulated silica nanocapsules having three different shell thicknesses (Figure 3a−c). In contrast, fipronil-loaded

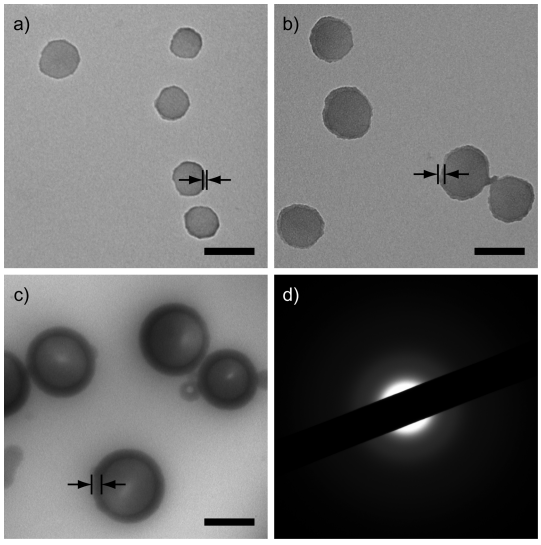

Figure 3. Fipronil-encapsulated silica nanocapsules with tunable shell thickness. (a−c) Representative transmission electron microscopy (TEM) images of fipronil-encapsulated silica nanocapsules having (a) 8 nm, (b) 25 nm, and (c) 44 nm shells. Scale bars are 200 nm. Arrows indicate the boundary of the silica shell. (d) Representative selected area electron diffraction (SAED) pattern of silica nanocapsules confirmed the amorphous state of the silica shell.

nanoemulsion having no silica shell was hardly observed in TEM as its structure was prone to disintegrate under high vacuum and electron beam irradiation (data not shown). The measured shell thicknesses, as determined by using TEM, of silica nanocapsules obtained at TEOS concentrations of 16 μmol, 32 μmol and 96 μmol were 8 nm, 25 nm, and 44 nm, respectively, while the outer diameters were 140 nm, 198 nm, and 288 nm, respectively. These values are consistent with our previously reported silica nanocapsules that encapsulated fipronil at concentration of 10 mg·mL^{-1} in Miglyol 812.[29] Additionally, the representative selected area electron diffraction (SAED) of silica nanocapsules shows diffuse ring pattern (Figure 3d), indicating the amorphous structure of the silica shell. The formation of amorphous silica via peptides has also been reported for natural biogenic silica[43,44] and biomimetic silica.[45]

Dynamic light scattering (DLS) confirmed a size increase for silica nanocapsules in comparison with the nanoemulsion template (Figure 4). Furthermore, increasing TEOS concentrations corresponded to an increase in number-averaged diameters of the nanocapsules (Figure 4a−c). The number-weighted size distribution results showed that silica nanocapsules having 8, 25, and 44 nm shells have narrow size distributions (polydispersity index, PDI < 0.350).

Fipronil Release Study *in Vitro*. The release profiles of fipronil *in vitro* from silica nanocapsules with three different shell thicknesses encapsulating 1 mg·mL^{-1} fipronil in Miglyol 812 i.e., 1F-NC8, 1F-NC25 and 1F-NC44 are shown in Figure

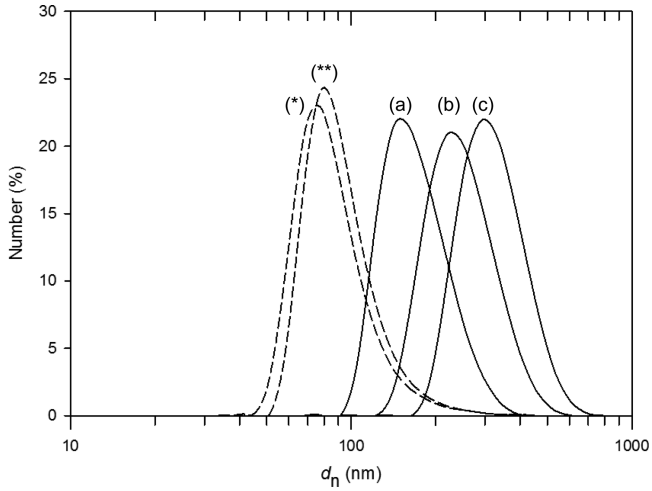

Figure 4. Number-weighted size distributions of fipronil-encapsulated silica nanocapsules and the nanoemulsion template. The measured number-averaged diameters (d_n) include silica nanocapsules having (a) 8 nm, (b) 25 nm, and (c) 44 nm shells, (*) fipronil-loaded nanoemulsions before reaction with TEOS, and (**) control fipronil-loaded nanoemulsions incubated over the reaction period.

5. The concentration of fipronil released in the water phase was normalized against the saturated concentration of fipronil in

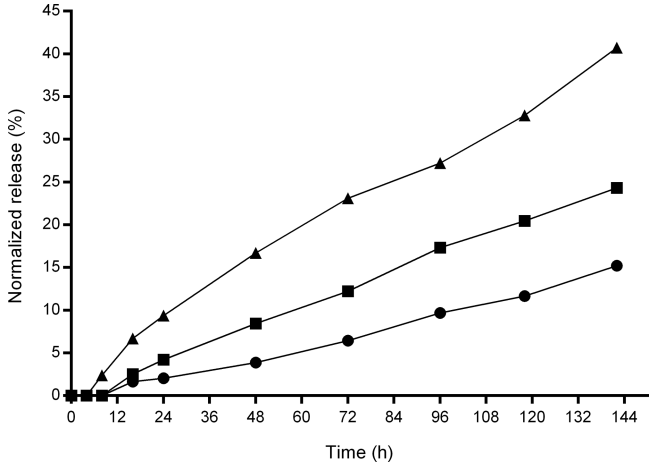

Figure 5. *In vitro* release profile of fipronil from silica nanocapsules having 8 nm (1F-NC8, ▲), 25 nm (1F-NC25, ■), and 44 nm (1F-NC44, ●) shells into water.

water considering the low solubility of fipronil in water (2 μg·mL^{-1}). The release of fipronil from 1F-NC8 was detected after 8 h of release study at 2.4%, while a longer lag time of 16 h was observed for fipronil released at 2.5% and 1.6% from silica nanocapsules having thicker shells i.e., 1F-NC25 and 1F-NC44, respectively (Figure 5). After 142 h, fipronil was released at percentages of 40.7%, 24.3% and 15.2% from 1F-NC8, 1F-NC25 and 1F-NC44, respectively. The rates of fipronil released in water show the order of 1F-NC8 > 1F-NC25 > 1F-NC44, demonstrating that increasing shell thickness resulted in an increased diffusion pathway and hence enhanced barrier to diffusion of fipronil across the silica shell, thus the slower release of fipronil.

Fipronil Release Study *in Vivo*. Sustained release of fipronil from silica nanocapsules was also investigated *in vivo*

against termites. Two experiments were carried out, including direct treatment and feeding treatment.

Direct treatment was demonstrated by topical application of six different formulations including water, Termidor, nanoemulsions (0.05F-NE), silica nanocapsules with three different shell thicknesses of 8 nm (0.05F-NC8), 25 nm (0.05F-NC25) and 44 nm (0.05F-NC44), on the dorsal thorax of worker termite *C. acinaciformis* (Figure 6). Rapid mortality was

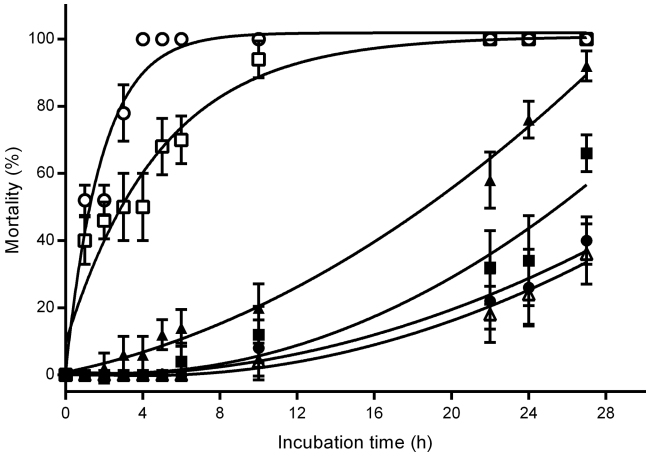

Figure 6. *In vivo* efficacy test via topical application on the dorsal thorax of worker termites. Fipronil-encapsulated silica nanocapsules having 8 nm (0.05F-NC8, ▲), 25 nm (0.05F-NC25, ■), and 44 nm (0.05F-NC44, ●) shells are tested in comparison with fipronil-loaded nanoemulsions without silica shells (0.05F-NE, □), Termidor (○), and water containing no fipronil (control, Δ). The lines are drawn to assist in reading the trends.

observed when termites were treated with commercial Termidor or fipronil-loaded nanoemulsions having no silica shells (0.05F-NE). The fipronil penetrated through the cuticle layer on the body surface of worker termites and eventually caused death depending the fipronil doses.[39] Termidor gave burst release of fipronil resulting in 50% mortality within the first hour and 100% mortality at 4 h (Figure 6). Fipronil-loaded nanoemulsions having no silica shells (0.05F-NE) exhibited a two-step release profile; a significant initial burst effect, with mortality of almost 50% within the first 4 h, and then more sustained release over 22 h (Figure 6). In contrast, silica nanocapsules showed sustained release as a result of the silica shell. First mortality was at 4 h (6%), 6 h (4%), and 10 h (8%) for silica nanocapsules having 8 nm (0.05F-NC8), 25 nm (0.05F-NC25) and 44 nm (0.05F-NC44) shells, respectively (Figure 6). Further, the termite mortality gradually increased in a way dependent on shell thickness suggesting that the silica shell provided an effective barrier for the controlled diffusion of the encapsulated fipronil, which corresponds well with the *in vitro* release study. The lag time, which was also observed in *in vitro* experiments, prior to termite mortality in the topical applications of silica nanocapsules strongly evidenced the sustained release of fipronil from the nanocapsules with no indication of burst release. Fipronil-encapsulated silica nanocapsules having 44 nm shell demonstrated the most significant delay in termite mortality and thus was chosen for the subsequent *in vivo* test.

We further evaluated the sustained release performance of fipronil-encapsulated silica nanocapsule having 44 nm shell (1F-NC44) *in vivo* by remote feeding treatment against *C. acinaciformis*. Prior to the treatment, groups of orphaned worker and soldier termites (≈1500) were allowed to adapt to the living conditions maintaining their biological activities in a container filled with nutritious materials at set temperature.[46] Food in the form of α-cellulose was supplied in peripheral feeding vials which were accessible through clear vinyl tubes. After 4 days, we observed that termites built mud and cellulose surrounding the interior space of the connector tubes as well as galleries within the baits, indicating that termites were responding to the α-cellulose. The α-cellulose in the feeding vials was then treated with water containing no fipronil, Termidor or 1F-NC44. As termites foraged in the feeding vials, they acquired and carried the α-cellulose back to the container, and inadvertently transferred it to other termites within the groups. These interactions could be through trophallaxis in which foraging worker termites feed other termites that do not or cannot forage on their own including soldier termites due to their anatomical and behavioral specializations.[47] Termidor-treated α-cellulose caused 100% mortality to termite groups after 3 days, whereas more delayed 100% mortality (6 days) was observed after treatment using nanocapsule-treated α-cellulose (Figure 7). The α-cellulose treated with water

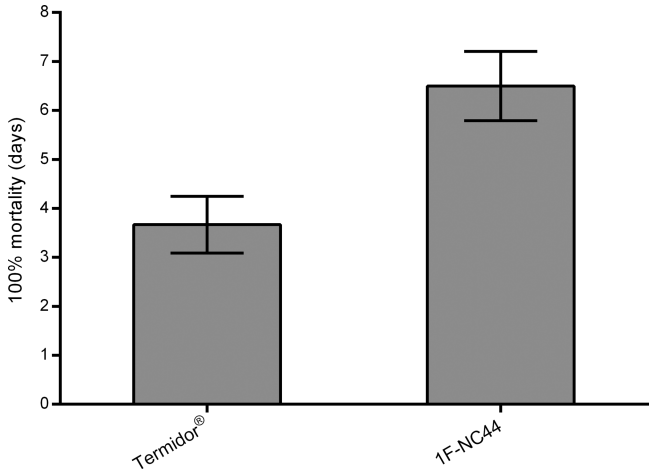

Figure 7. *In vivo* efficacy test via feeding treatment against groups of ≈1500 worker and soldier termites. The delayed 100% mortality of the termite groups caused by fipronil-encapsulated silica nanocapsules having a 44 nm shell (1F-NC44) is presented as compared to Termidor.

containing no fipronil in the feeding vials caused negligible termite mortality during the 8 days of the test. The feeding experiment results further confirmed the sustained release property of silica nanocapsules as a result of the presence of silica shell which plays a role as barrier to diffusion of fipronil.

Dead and decaying bodies of termites can elicit avoidance behavior of other termites,[48,49] and consequently any transmission through those termites is ineffective.[39] Therefore, the sustained release property of the fipronil-encapsulated silica nanocapsules is important to ensure constant exposure of fipronil to the termites in the colony until 100% mortality of the colony can be achieved. Furthermore, the more delaying insecticidal effect demonstrated by the silica nanocapsules as compared to the commercial fipronil formulation would be highly desirable, as it increases the likelihood of horizontal transfer of fipronil, hence allowing improved areawide control of larger populations of termite colonies.

dx.doi.org/10.1021/jf504455x | J. Agric. Food Chem. 2014, 62, 12504−12511

CONCLUSION

Biocompatible oil-core silica-shell nanocapsules synthesized using an emulsion and biomimetic dual-templating approach under environmentally friendly conditions were investigated as nanocarriers for the sustained release of fipronil insecticide. *In vitro* release studies of fipronil showed decreased release rate with increasing the shell thickness. *In vivo* direct treatment experiments using silica nanocapsules with three different shell thicknesses (8, 25, and 44 nm) against worker termites demonstrated that the time interval between the application of the nanocapsules and the occurrence of the termite mortality could be prolonged in a way dependent on silica-shell thickness as compared to the commercial formulation Termidor and fipronil-loaded nanoemulsions having no silica shells. The *in vivo* efficacy of 44-nm-shell nanocapsules against orphaned groups of ≈1500 worker and soldier termites by dispersing the nanocapsules in α-cellulose feeding bait proved that the silica nanocapsules could be taken up from the bait vials by foraging workers, transmitted to recipient termites in the groups probably through horizontal transfer, and eventually caused 100% mortality of the termite groups in 6 days after the application, which was 3 days longer than the commercial Termidor. Both the *in vitro* and *in vivo* fipronil-released studies presented in this paper demonstrated the effectiveness of a pesticide delivery system having biocompatibility, high encapsulation efficiency, and sustained release property, which open potential utilities of the silica nanocapsules for other agricultural applications.

AUTHOR INFORMATION

Corresponding Authors

* Phone: +61-7-3346-4189. Fax: +61-7-3346-4197. E-mail: z.chunxia@uq.edu.au.

* Phone: +61-7-3346-4189. Fax: +61-7-3346-4197. E-mail: a.middelberg@uq.edu.au.

Funding

This work was supported by the Australian Research Council (grants DP1093056 and 120103683). D.W. acknowledges a scholarship from The University of Queensland. C.X.Z. acknowledges financial support from the Australian Research Council in the form of an Australian Postdoctoral Fellow (DP110100394). A.P.J.M. acknowledges support from the Queensland Government through award of the 2010 Queensland Premier's Science Fellowship.

Notes

The authors declare no competing financial interest.

ACKNOWLEDGMENTS

The authors thank Lei Yu for taking the SAED images as well as the facilities and the scientific and technical assistance of the Australian Microscopy & Microanalysis Research Facility at the Centre for Microscopy and Microanalysis, The University of Queensland. Termatrac Pty Ltd., Beenleigh QLD (Australia), is thanked for the use of the Termatrac T3i device.

ABBREVIATIONS USED

Ac, acetyl; M, methionine; K, lysine; Q, glutamine; L, leucine; A, alanine; H, histidine; S, serine; V, valine; R, arginine; E, glutamic acid; G, glycine; Y, tyrosine; O/W, oil-in-water; M_w, molecular weight; mp, melting point; *d*, density; TEOS, tetraethoxysilane; HEPES, sodium 4-(2-hydroxyethyl)-1-piperazine ethanesulfonate; 0.05F-NE, nanoemulsions loaded with 0.05 mg·mL^{-1} fipronil in Miglyol 812 oil; *x*F-NC*y*, silica nanocapsules (encapsulating *x* mg·mL^{-1} fipronil in Miglyol 812 oil) with shell thickness of *y* nm; TEM, transmission electron microscopy; HR-TEM, high-resolution transmission electron microscopy; SAED, selected area electron diffraction; DLS, dynamic light scattering; FT-IR, Fourier transform-infrared; RP-HPLC, reversed-phase high-performance liquid chromatography

REFERENCES

(1) Mulqueen, P. Recent advances in agrochemical formulation. *Adv. Colloid Interface Sci.* **2003**, *106*, 83−107.

(2) Ghormade, V.; Deshpande, M. V.; Paknikar, K. M. Perspectives for nano-biotechnology enabled protection and nutrition of plants. *Biotechnol. Adv.* **2011**, *29*, 792−803.

(3) Gogos, A.; Knauer, K.; Bucheli, T. D. Nanomaterials in plant protection and fertilization: current state, foreseen applications, and research priorities. *J. Agric. Food Chem.* **2012**, *60*, 9781−9792.

(4) Rai, M.; Ingle, A. Role of nanotechnology in agriculture with special reference to management of insect pests. *Appl. Microbiol. Biotechnol.* **2012**, *94*, 287−293.

(5) Kah, M.; Hofmann, T. Nanopesticide research: current trends and future priorities. *Environ. Int.* **2014**, *63*, 224−235.

(6) Asrar, J.; Ding, Y. W.; La Monica, R. E.; Ness, L. C. Controlled release of tebuconazole from a polymer matrix microparticle: release kinetics and length of efficacy. *J. Agric. Food Chem.* **2004**, *52*, 4814−4820.

(7) Sopena, F.; Cabrera, A.; Maqueda, C.; Morillo, E. Controlled release of the herbicide norflurazon into water from ethylcellulose formulations. *J. Agric. Food Chem.* **2005**, *53*, 3540−3547.

(8) Stloukal, P.; Kucharczyk, P.; Sedlarik, V.; Bazant, P.; Koutny, M. Low molecular weight poly(lactic acid) microparticles for controlled release of the herbicide metazachlor: preparation, morphology, and release kinetics. *J. Agric. Food Chem.* **2012**, *60*, 4111−4119.

(9) Frederiksen, H. K.; Kristenson, H. G.; Pedersen, M. Solid lipid microparticle formulations of the pyrethroid gamma-cyhalothrin-incompatibility of the lipid and the pyrethroid and biological properties of the formulations. *J. Controlled Release* **2003**, *86*, 243−252.

(10) Garrido-Herrera, F. J.; Gonzalez-Pradas, E.; Fernandez-Perez, M. Controlled release of isoproturon, imidacloprid, and cyromazine from alginate-bentonite-activated carbon formulations. *J. Agric. Food Chem.* **2006**, *54*, 10053−10060.

(11) Ziv, D.; Mishael, Y. G. Herbicide solubilization in micelle-clay composites as a basis for controlled release sulfentrazone and metolachlor formulations. *J. Agric. Food Chem.* **2008**, *56*, 9159−9165.

(12) Chen, Y.; Chen, H.; Shi, J. *In vivo* bio-safety evaluations and diagnostic/therapeutic applications of chemically designed mesoporous silica nanoparticles. *Adv. Mater.* **2013**, *25*, 3144−3176.

(13) Hussain, H. I.; Yi, Z.; Rookes, J. E.; Kong, L. X.; Cahill, D. M. Mesoporous silica nanoparticles as a biomolecule delivery vehicle in plants. *J. Nanopart. Res.* **2013**, *15*.

(14) Martin-Ortigosa, S.; Valenstein, J. S.; Lin, V. S. Y.; Trewyn, B. G.; Wang, K. Gold functionalized mesoporous silica nanoparticle mediated protein and DNA codelivery to plant cells via the biolistic method. *Adv. Funct. Mater.* **2012**, *22*, 3576−3582.

(15) Torney, F.; Trewyn, B. G.; Lin, V. S. Y.; Wang, K. Mesoporous silica nanoparticles deliver DNA and chemicals into plants. *Nat. Nanotechnol.* **2007**, *2*, 295−300.

(16) Ao, M. M.; Zhu, Y. C.; He, S.; Li, D. G.; Li, P. L.; Li, J. Q.; Cao, Y. S. Preparation and characterization of 1-naphthylacetic acid-silica conjugated nanospheres for enhancement of controlled-release performance. *Nanotechnology* **2013**, *24*, 1−8.

(17) Chen, J.; Wang, W.; Xu, Y.; Zhang, X. Slow-release formulation of a new biological pesticide, pyoluteorin, with mesoporous silica. *J. Agric. Food Chem.* **2011**, *59*, 307−311.

(18) Popat, A.; Liu, J.; Hu, Q.; Kennedy, M.; Peters, B.; Lu, G. Q.; Qiao, S. Z. Adsorption and release of biocides with mesoporous silica nanoparticles. *Nanoscale* **2012**, *4*, 970−975.

(19) Wanyika, H.; Gatebe, E.; Kioni, P.; Tang, Z.; Gao, Y. Mesoporous silica nanoparticles carrier for urea: potential applications in agrochemical delivery systems. *J. Nanosci. Nanotechnol.* **2012**, *12*, 2221−2228.
(20) Wanyika, H. Sustained release of fungicide metalaxyl by mesoporous silica nanospheres. *J. Nanopart. Res.* **2013**, *15*.
(21) Wen, L. X.; Li, Z. Z.; Zou, H. K.; Liu, A. Q.; Chen, J. F. Controlled release of avermectin from porous hollow silica nanoparticles. *Pest. Manag. Sci.* **2005**, *61*, 583−590.
(22) Tan, W. M.; Hou, N.; Pang, S.; Zhu, X. F.; Li, Z. H.; Wen, L. X.; Duan, L. S. Improved biological effects of uniconazole using porous hollow silica nanoparticles as carriers. *Pest. Manag. Sci.* **2012**, *68*, 437−443.
(23) Li, Z. Z.; Xu, S. A.; Wen, L. X.; Liu, F.; Liu, A. Q.; Wang, Q.; Sun, H. Y.; Yu, W.; Chen, J. F. Controlled release of avermectin from porous hollow silica nanoparticles: influence of shell thickness on loading efficiency, UV-shielding property and release. *J. Controlled Release* **2006**, *111*, 81−88.
(24) Liu, F.; Wen, L.-X.; Li, Z.-Z.; Yu, W.; Sun, H.-Y.; Chen, J.-F. Porous hollow silica nanoparticles as controlled delivery system for water-soluble pesticide. *Mater. Res. Bull.* **2006**, *41*, 2268−2275.
(25) Qian, K.; Shi, T. Y.; He, S.; Luo, L. X.; Liu, X. L.; Cao, Y. S. Release kinetics of tebuconazole from porous hollow silica nanospheres prepared by miniemulsion method. *Microporous Mesoporous Mater.* **2013**, *169*, 1−6.
(26) Lou, X. W.; Archer, L. A.; Yang, Z. C. Hollow micro-/nanostructures: synthesis and applications. *Adv. Mater.* **2008**, *20*, 3987−4019.
(27) U.S. Food and Drug Administration's Website. *GRN No. 321: Synthetic amorphous silica*, http://www.accessdata.fda.gov/scripts/fcn/gras_notices/GRN000321.pdf (21 May 2014).
(28) Zhu, Y. F.; Shi, J. L.; Shen, W. H.; Dong, X. P.; Feng, J. W.; Ruan, M. L.; Li, Y. S. Stimuli-responsive controlled drug release from a hollow mesoporous silica sphere/polyelectrolyte multilayer core-shell structure. *Angew. Chem., Int. Ed.* **2005**, *44*, 5083−5087.
(29) Wibowo, D.; Zhao, C.-X.; Middelberg, A. P. J. Emulsion-templated silica nanocapsules formed using bio-inspired silicification. *Chem. Commun.* **2014**, *50*, 11325−11328.
(30) Kyle, S.; Aggeli, A.; Ingham, E.; McPherson, M. J. Production of self-assembling biomaterials for tissue engineering. *Trends Biotechnol.* **2009**, *27*, 423−433.
(31) Morreale, G.; Lee, E. G.; Jones, D. B.; Middelberg, A. P. J. Bioprocess-centered molecular design (BMD) for the efficient production of an interfacially active peptide. *Biotechnol. Bioeng.* **2004**, *87*, 912−923.
(32) Tingle, C. C. D.; Rother, J. A.; Dewhurst, C. F.; Lauer, S.; King, W. J. Fipronil: environmental fate, ecotoxicology, and human health concerns. *Rev. Environ. Contam. Toxicol.* **2003**, *176*, 1−66.
(33) Colliot, F.; Kukorowski, K. A.; Hawkins, D. W.; Roberts, D. A. *Fipronil: A New Soil and Foliar Broad Spectrum Insecticide*; British Crop Protection Council: 2000.
(34) Cole, L. M.; Nicholson, R. A.; Casida, J. E. Action of phenylpyrazole insecticides at the gaba-gated chloride channel. *Pestic. Biochem. Physiol.* **1993**, *46*, 47−54.
(35) Ngim, K. K.; Crosby, D. G. Abiotic processes influencing fipronil and desthiofipronil dissipation in California, USA, rice fields. *Environ. Toxicol. Chem.* **2001**, *20*, 972−977.
(36) Rouland-Lefevre, C. Termites as Pests of Agriculture. In *Biology of Termites: A Modern Synthesis*; Bignell, D. E., Roisin, Y., Lo, N., Eds.; Springer: London, U.K., 2011; pp 499−517.
(37) Rust, M. K.; Su, N.-Y. Managing social insects of urban importance. *Annu. Rev. Entomol.* **2012**, *57*, 355−375.
(38) Song, D. L.; Hu, X. P. Effects of dose, donor-recipient interaction time and ratio on fipronil transmission among the Formosan subterranean termite nestmates (Isoptera: Rhinotermitidae). *Sociobiology* **2006**, *48*, 237−246.
(39) Ibrahim, S. A.; Henderson, G.; Fei, H. X. Toxicity, repellency, and horizontal transmission of fipronil in the formosan subterranean termite (Isoptera: Rhinotermitidae). *J. Econ. Entomol.* **2003**, *96*, 461−467.
(40) Krimm, S.; Bandekar, J. Vibrational spectroscopy and conformation of peptides, polypeptides, and proteins. *Adv. Protein Chem.* **1986**, *38*, 181−364.
(41) Hernandez, B.; Pfluger, F.; Derbel, N.; De Coninck, J.; Ghomi, M. Vibrational Analysis of Amino Acids and Short Peptides in Hydrated Media. VI. Amino Acids with Positively Charged Side Chains: L-Lysine and L-Arginine. *J. Phys. Chem. B* **2010**, *114*, 1077−1088.
(42) Gauglitz, G.; Moore, D. S. *Handbook of Spectroscopy*, 2nd ed.; Wiley-VCH: Germany, 2014; Vol. *1*.
(43) Hildebrand, M. Diatoms, biomineralization processes, and genomics. *Chem. Rev.* **2008**, *108*, 4855−4874.
(44) Müller, W. E. G.; Belikov, S. I.; Tremel, W.; Perry, C. C.; Gieskes, W. W. C.; Boreiko, A.; Schröder, H. C. Siliceous spicules in marine demosponges (example *Suberites domuncula*). *Micron* **2006**, *37*, 107−120.
(45) Patwardhan, S. V. Biomimetic and bioinspired silica: recent developments and applications. *Chem. Commun.* **2011**, *47*, 7567−7582.
(46) Spomer, N. A.; Kamble, S. T.; Warriner, R. A.; Davis, R. W. Influence of temperature on rate of uptake and subsequent horizontal transfer of (14)C Fipronil by eastern subterranean termites (Isoptera: Rhinotermitidae). *J. Econ. Entomol.* **2008**, *101*, 902−908.
(47) Buczkowski, G.; Wang, C.; Bennett, G. Immunomarking reveals food flow and feeding relationships in the eastern subterranean termite, Reticulitermes flavipes (Kollar). *Environ. Entomol.* **2007**, *36*, 173−182.
(48) Su, N. Y.; Tamashiro, M.; Yates, J. R.; Haverty, M. I. Effect of behavior on the evaluation of insecticides for prevention of or remedial control of the formosan subterranean termite (Isoptera, Rhinotermitidae). *J. Econ. Entomol.* **1982**, *75*, 188−193.
(49) Fei, H.; Henderson, G. Repellency of formosan subterranean termites (Isoptera: Rhinotermitidae) to dead termites and attraction to 2-phenoxyethanol with and without nonrepellent insecticides. *J. Agr. Urban Entomol.* **2005**, *22*, 159−172.

Chapter 5

Interfacial biomimetic synthesis of silica nanocapsules using a recombinant catalytic modular protein

The research in this chapter consists of the peer-reviewed paper published as:

Wibowo, D., C.-X. Zhao, A.P.J. Middelberg*, *Interfacial biomimetic synthesis of silica nanocapsules using a recombinant catalytic modular protein*. Langmuir, 2015. **31**(6): p. 1999–2007.

The following modifications were made to the article:

- Page numbers of the original article were crossed-out; and
- Page numbers consistent with those on the remainder of thesis pages were inserted.

Abstract

This chapter describes the design of a bifunctional modular protein, D4S2, by extrapolating the design principle of the bifunctional modular peptide developed in **Chapter 3**, for the synthesis of oil-core silica-shell nanocapsules. The 116-residue protein was designed by fusing the Si module rich in cationic amino acids known for biosilicification activity derived from SurSi peptide (**Chapter 3**), with a four-helix bundle structure DAMP4 variant module as carrier protein derived from recombinant DAMP4 protein which has known surface activity. The modular combination design would enable expression of D4S2 in industrially-relevant, microbial cell-factory *Escherichia coli* at high solubility while potentially allowing for easy process-scale manufacture as in DAMP4. Moreover, it also allowed simplified purification process conferred by its thermal- and chemical-stability properties. Purification methods to obtain high purity D4S2 and analyses of the purified protein were discussed. Protein behaviors at the macroscopic interface were investigated using dynamic interfacial tension and thin film pressure balance. Finally, functionalities of D4S2 for making silica nanocapsules were demonstrated through synergistic activities of surface-active and biosilicification-active modules within D4S2. This chapter introduces biomolecular protein design for the development of sustainable production of bifunctional modular protein, which is important for the subsequent chapter.

Langmuir

Article

pubs.acs.org/Langmuir

Interfacial Biomimetic Synthesis of Silica Nanocapsules Using a Recombinant Catalytic Modular Protein

David Wibowo, Chun-Xia Zhao, and Anton P. J. Middelberg*

Australian Institute for Bioengineering and Nanotechnology, The University of Queensland, St. Lucia QLD 4072, Australia

Supporting Information

ABSTRACT: This paper reports interfacially driven synthesis of oil-core silica-shell nanocapsules using a rationally designed recombinant catalytic modular protein (ReCaMoP), in lieu of a conventional chemical surfactant. A 116-residue protein, D4S2, was designed by modularizing a surface-active protein module having four-helix bundle structure in bulk and a biosilicification-active peptide module rich in cationic residues. This modular combination design allowed the protein to be produced via the industrially relevant cell factory *Escherichia coli* with simplified purification conferred by thermostability engineered in design. Dynamic interfacial tension and thin film pressure balance were used to gain an overview of the protein behavior at macroscopic interfaces. Functionalities of D4S2 to make silica nanocapsules were demonstrated by facilitating formation and stabilization of pharmaceutically grade oil droplets through its surface-active module and then by directing nucleation and growth of a silica shell at the oil−water interface through its biosilicification-active module. Through these synergistic activities in D4S2, silica nanocapsules could be formed at near-neutral pH and ambient temperature without using any organic solvents that might have negative environmental and sustainability impacts. This work introduces parallelization of biomolecular, scale-up and interfacial catalytic design strategies for the ultimate development of sustainable and scalable production of a recombinant modular protein that is able to catalyze synthesis of oil-filled silica nanocapsules under environmentally friendly conditions, suitable for use as controlled-release nanocarriers of various actives in biomedical and agricultural applications.

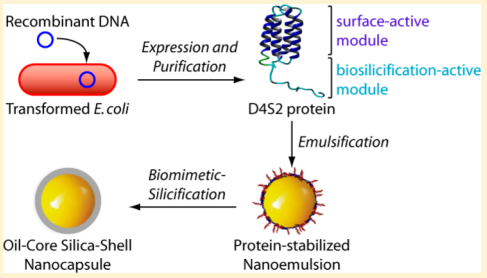

INTRODUCTION

Advances in interfacial chemistry have enabled synthesis of silica nanocapsules having core−shell architecture.[1,2] The synthesis methods involve sol−gel reactions of aqueous silica precursor on colloidal core templates, i.e., gas bubbles,[3,4] nanoparticles,[5−11] and emulsion droplets,[12−20] resulting in nucleation and growth of silica at the boundary of gas−liquid, solid−liquid, and liquid−liquid interfaces, respectively. With silica shells encapsulating the core materials, the nanocapsules combine properties of silica, i.e., biocompatibility, easy functionalization, mechanical stability, and optical transparency,[1,21] and tunable functionalities of the core. Depending on the core's type, silica nanocapsules have found diverse applications in fields of chemical, biomedical, and agricultural applications, for example, as nanoreactors;[5] as supports of catalytic metals,[6] semiconductor,[7] fluorescent[8] and magnetic[9] nanoparticles, and enzymes[12] for their long-term activity and/or dispersibility in aqueous environment; as adsorbents;[13,14] and as nanocarriers of drugs[15] and pesticides[16] for their storage, protection, and release.

Surface chemistry of the colloidal core templates plays important roles for the synthesis of silica nanocapsules,[1,2] thereby maintaining template stability and concurrently catalyzing silica formation preferentially at the interface. Therefore, various chemicals have been decorated surrounding the template surfaces via adsorption, including cationic surfactants (e.g., tetradecyltrimethylammonium bromide,[6] cetyltrimethylammonium bromide,[3,18] and cetyltrimethylammonium chloride[19]), nonionic surfactants (e.g., Brij 97,[13] Tween 80,[14] and Triton X-100[20]), and polymers (e.g., poly(acrylic acid),[5] poly(vinylpyrrolidone),[10] and poly(ethylene oxide)-*b*-poly(propylene oxide)-*b*-poly(ethylene oxide)[17]). Despite great progress in the interfacial synthesis of silica nanocapsules, the aforementioned chemical methods[12−15,17−20] variously incorporate toxic chemical catalysts and organic solvents that would pose adverse environmental effects. An alternative way to construct silica nanocapsules using biocompatible components and benign conditions is still highly desired especially for biomedical and agricultural applications.

Nature's ability to form silica using biomolecules as in cell walls of diatoms[22] and spicules of sponges[23] provides an example for "green" synthesis of silica-based nanomaterials. The biomolecules play important roles in biosilicification by inducing nucleation and growth of silica species in aqueous solution under physiological conditions.[24] To mimic the naturally occurring biomolecules, many studies have used short peptides for biosilicification in bulk aqueous solutions,[25−28] but very few studies report biosilicification at biphasic interfaces.[11,16] Graf et al. used two tripeptides (CKK) connected with a disulfide bridge to facilitate formation of silica

Received: December 2, 2014
Revised: January 11, 2015
Published: January 20, 2015

DOI: 10.1021/la504684g
Langmuir 2015, 31, 1999−2007

shell encapsulating a silver nanoparticle core.[11] We recently reported synthesis of oil-core silica-shell nanocapsules via a novel emulsion and biomimetic dual-templating approach[16] using bifunctional SurSi peptide (Ac-MKQLAHS VSRLEHA RKKRKKRKKRKKGGGY-CONH$_2$) that modularized a surface-active sequence (Sur module, MKQLAHS VSRLEHA) capable of stabilizing pharmaceutically grade oil droplets with a sequence for catalyzing biosilicification at the oil−water interfaces (Si module, RKKRKKRKKRKKGGGY).

Synthesis of oil-core silica-shell nanocapsules using biomolecular engineering[16] instead of chemical surfactant approaches[12−20] may contribute substantially to the development of an environmentally friendly approach to produce biocompatible nanocarriers having controlled-release properties. Various hydrophobic actives could potentially be encapsulated in the nanocapsules' core with high encapsulation efficiency, thus broadening opportunities to wide range of applications especially in biomedical and agricultural fields. In turn, sustainable and scalable processes of making such nanocapsules would be highly demanded. Peptide surfactant, a key ingredient in the synthesis of silica nanocapsules using this new approach,[16] is currently produced based on solid-phase chemistry[29] which is useful for research but limiting for large-scale production.[30] Recombinant peptide production offers the potential of process scale-up using established bioprocess unit operations,[31] for example, by expression of recombinant DNA encoding expression of the peptide via the low-cost "cell factory" *Escherichia coli* (*E.coli*).[32] Significant challenges may exist during peptide expression as peptides may self-associate forming insoluble aggregated materials[33] and undergo intracellular degradation.[34] To counter these problems, peptides are commonly fused to carrier proteins to mask the self-assembly characteristic and improve the intracellular stability.[35] Design of fusion protein combining the peptide with a carrier protein should enable its expression in *E. coli*, allowing peptide cleavage from the carrier protein if necessary, to facilitate simplified purification.

In this study, we designed a-116 residue protein, D4S2, by fusing the Si module of the SurSi peptide, known for its biosilicification activity,[16] with a helical DAMP4 variant module as carrier protein derived from recombinant DAMP4 protein which has known surface activity.[36] This modular combination design would enable expression of D4S2 in *E. coli* at high solubility while potentially allowing easy process-scale manufacture as demonstrated for DAMP4.[37] We hypothesized that this strategy would allow the purified D4S2 to be directly used for making silica nanocapsules without the need for peptide cleavage from the carrier protein. In addition, the recombinant D4S2 would be expected capable of (1) facilitating formation and stabilization of nanoemulsions through its surface-active module and (2) catalyzing biosilicification at the oil−water interfaces through its biosilicification-active module, forming oil-core silica-shell nanocapsules at room temperature and nearly neutral pH in the absence of any toxic organic solvents. To the best of our knowledge, this is the first report of parallel biomolecular, scale-up, and interfacial catalytic design strategies for the development of a sustainable and scalable production route to a recombinant catalytic modular protein (ReCaMoP) that is able to catalyze interfacial synthesis of silica nanocapsules under environmentally friendly conditions.

EXPERIMENTAL SECTION

Materials. Miglyol 812 purchased from AXO Industry S.A. (Wavre, Belgium) was passed through heat-activated silica gel (Sigma-Aldrich) prior to use. Water with >18.2 MΩ cm resistivity was obtained from a Milli-Q system with a 0.22 μm filter (Millipore, Australia). Other chemicals were of analytical grade purchased from either Sigma-Aldrich or Merck and used as received unless otherwise stated.

Protein Expression, Purification, and Characterization. Plasmid pET-48b(+) composed of nucleotide sequence encoding for D4S2 protein (Protein Expression Facility, The University of Queensland) was transformed into chemically competent *E. coli* BL21(DE3) (Novagen, Merck KGaA, Germany). Production of D4S2 protein was through expression of recombinant DNA in *E. coli* controlled by the T7 promoter. Purification was based on the reported precipitation process for DAMP4 protein[37] (Figures S1 and S2) and chromatography techniques (Figure S3) to obtain high purity of D4S2. Detailed transformation, expression, and purification can be found in the Supporting Information.

Sodium Dodecyl Sulfate Polyacrylamide Gel Electrophoresis (SDS-PAGE). Qualitative analysis of protein samples was performed using NuPAGE 4−12% Bis-Tris gels (Life Technologies, Australia) mounted in a Bio-Rad XCell 3 system (Bio-Rad, Hercules, CA). Procedures for sample preparation, gel staining and destaining, and gel imaging are provided in the Supporting Information.

Reversed-Phase High-Performance Liquid Chromatography (RP-HPLC). To determine concentration of D4S2 protein, RP-HPLC equipped with a Jupiter C_{18} column (5 μm, 300 Å, 150 mm × 4.6 mm) (Phenomenex, Torrance, CA) and connected to an LC-10AVP series HPLC system (Shimadzu, Japan) was used. Buffer A was 0.1% v/v trifluoroacetic acid (TFA) in water, and buffer B was 90% v/v acetonitrile and 0.1% v/v TFA in water. Gradient conditions applied in the analysis were from 30 to 65% of buffer B in 35 min at a flow rate of 1 mL/min and a set detection wavelength of 214 nm.

Liquid Chromatography−Mass Spectrometry (LC-MS). LC-MS was performed using a Waters Alliance HPLC system (Waters, Milford, MA) linked with a Quattro Micro API Quadrupole system to determine molecular mass of D4S2. The LC was equipped with a Kinetex C_{18} column (2.6 μm, 100 Å, 100 mm × 4.6 mm) (Phenomenex, Torrance, CA) with a mobile phase A, 0.01% v/v TFA in water, and mobile phase B, 90% v/v acetonitrile, 0.01% v/v TFA in water. An applied gradient from 30 to 65% B in 35 min at a flow rate of 0.6 mL/min was used. For mass analysis, an electrospray mass spectrometry in positive-ion mode was performed with capillary, cone, extractor, and a radio frequency lens voltages set at 3 kV, 24 V, 3 V, and 0 V, respectively.

Circular Dichroism (CD). To determine the secondary structure of D4S2, CD spectroscopy (Jasco 810, Easton, MD) was performed on 0.025 mg/mL D4S2 filled in a 1 cm path length quartz cell (Starna, Australia) at 20 and 90 °C. Water was used to dissolve D4S2 in order to eliminate the effect of buffer salts on the CD signal. Far-UV CD spectra were recorded from 260 to 190 nm using 0.1 nm data pitch, 50 nm/s scan speed, 2 s response time, 1 nm bandwidth, and 10 accumulations. The obtained raw ellipticity was converted to molar ellipticity by the equation[38]

$$[\theta] = \frac{\theta M_{\mathrm{mrm}}}{10cl}$$

where $[\theta]$ is molar ellipticity (deg cm^2/dmol), θ is raw ellipticity (mdeg), c is protein concentration (mg/mL), l is cell path length (cm), and M_{mrm} is mean residue molecular mass, i.e., protein molecular mass/number of residues.

Interfacial Tension. Oil−water interfacial tension studies employed droplet tensiometry with a Krüss drop shape analysis system DSA-10 (Krüss GmbH, Germany). Protein solution of either D4S2 or DAMP4 (8 mL, 0.1 mg/mL) in HEPES buffer (25 mM, pH 7.5) was filled in an 8 mL quartz cuvette (Hellma, Germany), and an oil droplet (Miglyol 812) was formed manually via a glass syringe connected to a U-shaped stainless steel capillary of known diameter submerged in the protein solution. Measurements of the interfacial

DOI: 10.1021/la504684g
Langmuir 2015, 31, 1999−2007

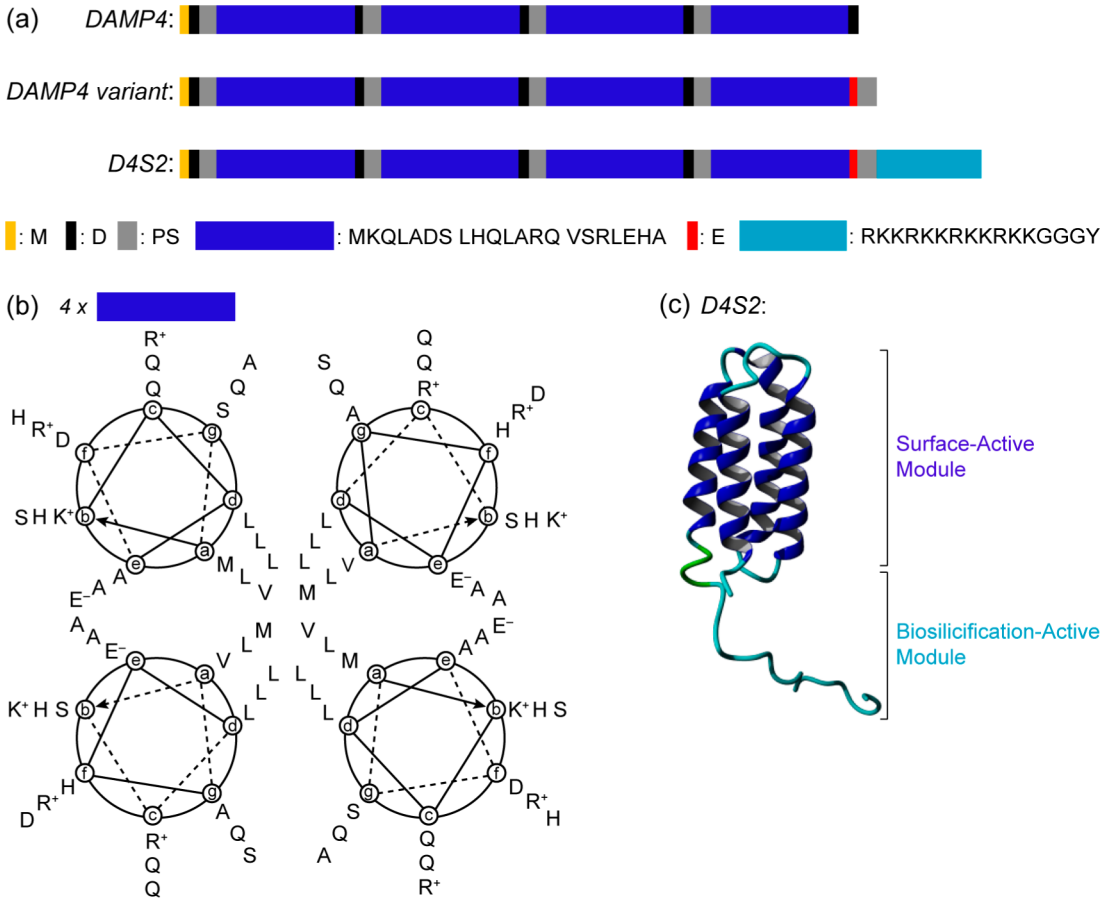

Figure 1. Design of recombinant catalytic modular protein (ReCaMoP), D4S2. (a) Schematic amino acid sequence of DAMP4, DAMP4 variant, and D4S2 proteins. The proteins consist of four AM1 peptides[42] (dark blue rectangle) comprising three heptads with repeating motif abcdefg in each, in which the alternate three and four spacing residues (a and d) have hydrophobic side chains (mainly methionine (M), leucine (L), and valine (V)), while the remaining sites are predominantly hydrophilic, allowing formation of α-helix structure. (b) End-on view helical wheel projection of DAMP4 variant module in D4S2 with its four-α-helical structure interlocking of hydrophobic residues at the core that might be expected to give rise to the protein stability. (c) Molecular D4S2 modularizing DAMP4 variant module (dark blue) forming four-helix bundle in bulk and Si module (light blue) projecting toward bulk aqueous phase.

tension were made automatically over 1000 s following initial oil droplet formation. Prior to measurement, the interfacial tension of Miglyol 812 oil in the buffer was measured at approximately 30 mN/m and remained constant for at least 10 min to ensure correct functioning, focusing, and cleanliness of the instrument.

Thin Film Experiment. The thin film pressure balance technique[39] was used to determine the surface forces in a liquid film stabilized by either D4S2 or DAMP4 (1.53 mg/mL) in HEPES buffer (25 mM, pH 7.5) under controlled capillary pressure. A liquid film was formed using a microfabricated bike-wheel microcell, designed for uniform radial drainage,[40] with diameter of the central hole inside the microcell of 0.75 mm. A vapor-saturated chamber inserted with the film holder was placed on an inverted microscopic stage (Olympus IX51). Temperature was maintained at 22 ± 0.1 °C using a water jacket, and the air pressure inside the chamber was controlled by using a 100 mL gastight syringe (SGE, Australia) driven by a micropositioner (M4454, Parker) as described by Wang and Yoon.[41] To record images of the films, a digital video camera was used at a rate of 30 frames/s.

Synthesis and Characterization of Oil-Core Silica-Shell Nanocapsules. Lyophilized D4S2 protein was dissolved in HEPES buffer (25 mM, pH 7.5) to prepare D4S2 solutions from 0.47 to 2.5 mg/mL. Miglyol 812 (10% v/v) was added to the D4S2 solutions (1 mL) and homogenized using a Branson Sonifier 450 ultrasonicator for four 30 s bursts at 20 W and interspersed in an ice bath for 60 s. The nanoemulsion aliquot (400 μL) was transferred into a 4 mL glass vial containing weighed tetraethoxysilane (TEOS, 32 μmol). Interfacially catalyzed reaction with TEOS was conducted under magnetic stirring at room temperature for 20 h.

Dynamic Light Scattering (DLS). Size distribution and zeta potential were determined by DLS using a Malvern Zetasizer Nano ZS (Malvern Instrument, UK) at a scattering angle of 173° and a temperature of 25 °C. Samples were diluted by a factor of 100 prior to measurement to avoid multiple scattering effects.

Transmission Electron Microscopy (TEM). Morphology of the silica nanocapsules was visualized by TEM using a JEOL 1010 (JEOL, Japan) operated at 100 kV. Samples (2 μL) were deposited onto Formvar-coated copper grids (ProSciTech, Australia). The size of the nanocapsules was analyzed by using iTEM software (version 3.2, Soft Imaging System GmbH).

RESULTS AND DISCUSSION

Protein Design. The aim of the reported research was to synthesize oil-core silica-shell nanocapsules based on protein supramolecular chemistry allowing sustainable and scalable protein production via expression in the cell factory *E. coli*. Design of the protein followed the concept of our recently reported bifunctional SurSi peptide, thereby modularizing a surface-active module with a module for biosilicification.[16] Synergistic combination of both modules was considered essential to stabilize nanoemulsions and concurrently induce nucleation and growth of silica forming silica nanocapsules.

DOI: 10.1021/la504684g
Langmuir 2015, 31, 1999−2007

This was confirmed by the fact that AM1 peptide (Ac-MKQLADS LHQLARQ VSRLEHA-$CONH_2$)—known for its surface activity[42] and ability to stabilize nanoemulsions[43]—was unable to effectively produce silica nanocapsules as the silica was largely form in bulk solution rather than at oil−water interfaces.[16]

D4S2 protein (M *DP*S MKQLADSLHQLARQVSRLEHA *DP*S MKQLADSLHQLARQVSRLEHA *DP*S MKQLADSLHQLARQVSRLEHA *DP*S MKQLADSLHQLARQVSRLEHA EPS RKKRKKRKKRKKGGGY), having theoretical molecular mass 13.3 kDa and p*I* 10.9, was designed by modularizing DAMP4 variant module (M *DP*S MKQLADSLHQLARQVSRLEHA *DP*S MKQLADSLHQLARQVSRLEHA *DP*S MKQLADSLHQLARQVSRLEHA *DP*S MKQLADSLHQLARQVSRLEHA EPS) with Si peptide module (RKKRKKRKKRKKGGGY) (Figure 1). Si peptide rich in cationic amino acid side chains known for its biosilicification activity was derived from SurSi peptide.[16] DAMP4 variant module was derived from four-helix bundle DAMP4 protein (MD(PS MKQLADS LHQLARQ VSRLEHAD)$_4$) known for its surface activity,[36] except that the aspartic acid (D) residue at C-terminal DAMP4 was replaced with glutamic acid (E) residue followed by addition of proline (P) and serine (S) residues in order to provide molecular flexibility to the Si module projecting toward the bulk aqueous phase (Figure 1c).

DAMP4, designed by connecting four surface-active AM1 peptide[42] via Asp-Pro-Ser (DPS) linkers, has been shown to have surface activity similar to the AM1 peptide[36] and was used as a basis for the design of surface-active module of D4S2. Several other reasons were also considered when selected DAMP4. First, DAMP4 has been proved to be successfully produced in *E. coli* at high levels and solubility.[36,37] Second, DAMP4 has demonstrated stability at high temperature (above 90 °C) and Na_2SO_4 concentrations (up to 1 M)[37] due to its four-helix bundle structure in bulk (Figure 1b), useful for disruption of the cell walls releasing the intracellular proteins and precipitation of the contaminant proteins while maintaining DAMP4 solubility, respectively. These properties allow simple separation of DAMP4 from contaminant proteins without losing its surface activity.[37] Finally, DAMP4 could be cleaved, if necessary or desired, at its DP sequence via acid hydrolysis,[44] and the resulting individual DAMP1 peptide (PS MKQLADS LHQLARQ VSRLEHA D) has been demonstrated to have surface activity as well.[44] In the case where peptide cleavage from the carrier protein is required for D4S2, acid digestion of D4S2 would cleave the *DP* sequence while the EP sequence would be more stable against the acid, thus resulting in a sequence comprising DAMP1 variant peptide (*PS* MKQLADS LHQLARQ VSRLEHA EPS RKKRKKRKKRKKGGGY), expected to have surface activity close to DAMP1 peptide,[44] and biosilicification-active Si peptide.[16]

Based on these considerations, incorporation of DAMP4 variant module in D4S2 would be expected to form four-helix bundle protein structure and impart surface activity, while the Si module would provide biosilicification activity for D4S2 (Figure 1). We hypothesized that the surface-active module of D4S2 would undergo interfacial adsorption to the freshly formed droplet (Miglyol 812 oil) surfaces upon sonication, during which the four-helix bundle of D4S2 unfolds at the interface, causing the hydrophobic residues to face the oil phase while the hydrophilic residues face toward bulk aqueous phase and stabilize the droplets. This hypothesis is based on extrapolation of the known physical chemistry of DAMP4.[45] Upon addition of silica precursor tetraethoxysilane (TEOS) molecules, the biosilicification module of D4S2 oriented within the subinterfacial region toward bulk solution would act as a catalytic site for nucleation and growth of silica layer surrounding the droplets forming oil-core silica-shell nanocapsules at near neutral pH and room temperature and without using any toxic organic solvents.

Protein Production and Characterization. To recover D4S2 from *E. coli* cell pellet, a purification process was developed based on the bake-to-break and precipitate method of the DAMP4 purification process,[37] thereby heating the resuspended cell pellet in a buffer containing 1 M Na_2SO_4 at 90 °C for 30 min (Figure S1). Under such high temperature, the cell walls disrupted and the intracellular proteins including D4S2 released into the bulk phase. In the presence of Na_2SO_4, most proteins precipitated (Figure 2, lane 2), whereas D4S2

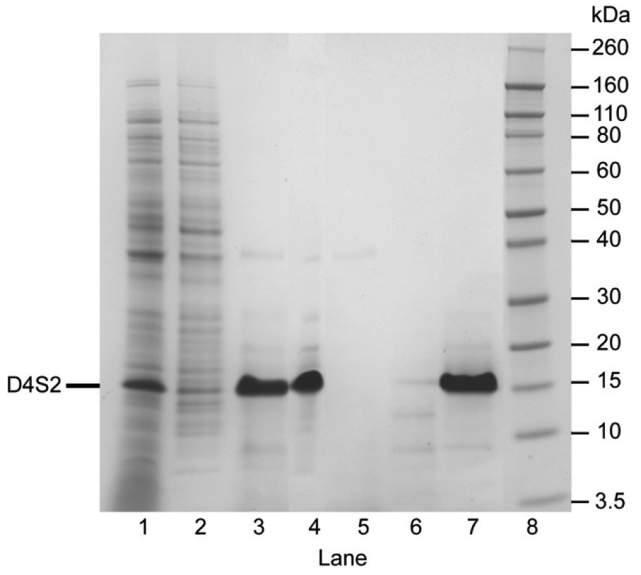

Figure 2. SDS-PAGE analysis of D4S2 protein after heating/cell lysis, contaminant precipitation and dilute precipitation steps, and IMAC purification step: (lane 1) total protein; (lane 2) resuspended precipitate and (lane 3) supernatant after heating/cell lysis and contaminant precipitation step; (lane 4) solubilized precipitate after dilute precipitation step; (lane 5) passed-through fraction, (lane 6) washed fraction, and (lane 7) eluted fraction after IMAC process; (lane 8) Novex sharp prestain protein standard.

remained soluble (Figure 2, lane 3) as concentrated Na_2SO_4 salted-in the four-helix bundle structure[37] of D4S2. The protein solution contained high levels DNA (Table S1) which derived from either the expression construct or the genomic DNA.[46] Protein and DNA may form noncovalent complexes via electrostatic interactions between anionic phosphate groups on the DNA and cationic functional groups on protein at physiological pH.[47,48] Binding of DNA to protein could alter protein properties (e.g., charge and size) and may cause increased viscosity of the protein solution. To separate D4S2 from DNA, the solution was diluted with water to lower Na_2SO_4 concentration and adjusted to pH 3.5 (i.e., dilute precipitation process), which is well below the isoelectric points of both D4S2 and DNA,[49] thus inducing charge−charge repulsion between D4S2 and DNA. Under this condition, D4S2 precipitated from the solution as the Na_2SO_4 concentration was

DOI: 10.1021/la504684g
Langmuir 2015, 31, 1999−2007

insufficient to salt-in D4S2, while most DNA separated from the precipitate and remained in the aqueous phase. At this stage, DNA concentration of the solubilized D4S2 (Figure 1, lane 4) reduced by approximately 95% (Table S1). Prior to the functionality test of D4S2, the protein solution was filtered and passed through desalting chromatography. Then, purified D4S2 was used to form nanoemulsions via sonication in HEPES buffer (25 mM, pH 7.5). Although D4S2 is rich in cationic amino acids (theoretical p*I* 10.9), the resulting nanoemulsions unexpectedly had negative zeta potentials at pH 7.5. This is probably because the anionic DNA residues were still present in an amount sufficient to cover the cationic protein side chains at the oil–water interfaces. As a consequence, the nanoemulsions were unable to react with silica precursor tetraethoxysilane (TEOS) molecules and form a silica shell at pH 7.5 as both nanoemulsion surfaces and silica species[50] bore negative charges.

To further remove DNA from D4S2, immobilized-metal affinity chromatography (IMAC) was used applying high salt concentration (1.2 M NaCl) (Figure S4a) followed by desalting chromatography (Figure S4b). D4S2 bound to the IMAC column through its high intrinsic histidine content by forming coordination bonds with Ni^{2+} ions immobilized on the column. DNA dissociated from the bound D4S2 and passed through the column as the electrostatic interactions between D4S2 and DNA were screened under the high salt concentration. D4S2 could then be eluted from the column using imidazole (Figure 2, lane 7) and passed through desalting chromatography to obtain high-purity D4S2 protein (Figure 3a), with a reduction of DNA concentration by approximately 97% as compared to the sample before load to the IMAC column. The calculated molecular mass of D4S2 protein based on the mass spectrum is 13308.2 Da (Figure 3b), which is very close to its theoretical molecular mass, i.e., 13299.3 Da, confirming the correct protein sequence. The far-UV circular dichroism (CD) measurements for D4S2 at 20 and 90 °C showed nearly identical spectra (Figure 3c) dominated by a double minimum at 208 and 222 nm and a maximum near 195 nm, typical of α-helical conformation.[51] The ability of D4S2 to maintain the helical structure at a temperature up to 90 °C suggests that D4S2 has thermal stability properties likely due to the four-helix bundle structure that formed through association of four amphiphilic α-helices interlocking the hydrophobic core within D4S2 (Figure 1b). Proteins having four-helix bundle structure have been recognized for their high molecular stability including to temperature[52] and chemical denaturants,[53] and their design and utility have been an area of intense and expanding research.[54]

Surface Activity. Initial surface-active studies focused on the interfacial tension of D4S2 solution against a Miglyol 812 oil droplet and in comparison with DAMP4. Oil–water dynamic interfacial tension data were recorded at the low weight concentration of 0.1 mg/mL in HEPES buffer (25 mM) at pH 7.5, corresponding to the pH value for biosilicification reaction,[16] to follow adsorption events at an earlier period (Figure 4). It is clear that D4S2 is surface-active as it spontaneously adsorbed to the oil–water interface and lowered the interfacial tension (γ), despite the high temperature and high salt concentrations applied for its purification. The surface activity of D4S2 was likely due to α-helical structure of D4S2 (Figure 3c) giving rise to its amphiphilic character that allowed D4S2 to unfold upon interfacial adsorption, thus oriented the hydrophobic residues toward the oil phase, while the hydrophilic sites faced toward the bulk aqueous phase. The

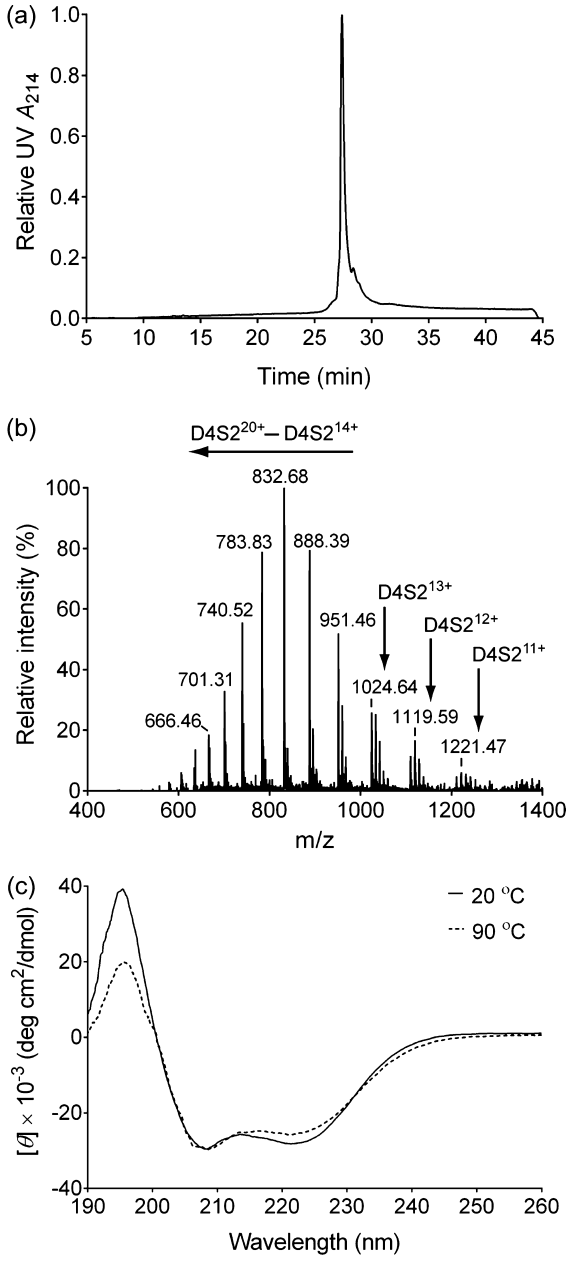

Figure 3. Characterization of D4S2. (a) Reversed-phase high-performance liquid chromatography showing high purity of D4S2. (b) Mass spectrum determining D4S2 molecular mass of 13 308.2 Da. (c) Circular dichroism spectra showing secondary structure of D4S2 in water (0.025 mg/mL) at 20 and 90 °C.

interfacial tension of D4S2 approached equilibrium at 18.6 ± 0.3 mN/m, while DAMP4 showed increased interfacial adsorption as the equilibrium interfacial tension reached 16.5 ± 0.4 mN/m. D4S2 showed approximately 81% of the decrease in interfacial tension occurred after 50 s, while DAMP4 gave more rapid adsorption, with 93% of the decrease in interfacial tension seen in the first 50 s. The slower interfacial adsorption indicates existence of energy barriers to protein adsorption that can be affected by molecular mass[45] and net electrical charge of the protein.[55] D4S2 has higher molecular mass (M 13 308.2 Da) (Figure 3b) than DAMP4 (M 11 116.5 Da)[36] which results in a lower bulk diffusion coefficient (D) of D4S2, since $D \sim M^{-1/3}$,[45,56] hence lowering the relative adsorption rate. With the D4S2 theoretical isoelectric point being 10.9 in bulk solution,

DOI: 10.1021/la504684g
Langmuir 2015, 31, 1999–2007

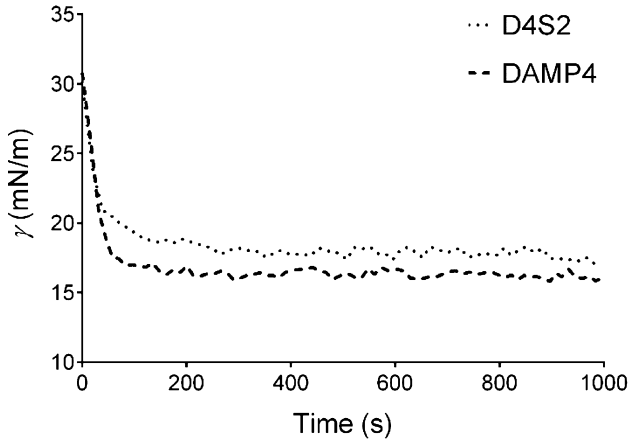

Figure 4. Dynamic interfacial tension of protein solutions vs Miglyol 812 oil. Proteins were 0.1 mg/mL in 25 mM HEPES buffer at pH 7.5.

D4S2 would be expected to carry more positive charges than DAMP4 (theoretical p*I* 6.7) at pH 7.5, thus yielding an increased charge−charge repulsion causing slower interfacial saturation and conformational changes at the oil−water interfaces upon interfacial adsorption.

To understand macroscopic stability of a colloidal system, it is important to understand surface forces of the building blocks, i.e., a single thin liquid film that separates the dispersed phase in a continuous phase.[57] In this study, the thin liquid film was studied by using a thin film pressure balance technique[39] on a free-standing horizontal liquid foam film, as a model system, that is compressed under controlled-capillary pressure (P_c). Typical images of D4S2 films (Figure 5a) were placed side by side to indicate visual changes in the thin films as the capillary pressure were increased progressively to reach instrument-limit pressure of 2500 Pa, as compared to DAMP4 films (Figure 5b). A weight concentration of 1.53 mg/mL protein solution in 25 mM buffer pH 7.5 was used similar to that used for emulsion preparation using D4S2. Both D4S2 and DAMP4 films exhibited heterogeneous film thickness as evident from the presence of dark and bright area. The bright phase regions are indicative of thicker surface materials, which can be due to the presence of protein aggregates at the film surfaces,[58] while the black areas can be considered as domains with a reduced thickness. D4S2 films were stable as the shape integrity remained intact at increasing pressure even when pressure reached 2500 Pa (Figure 5a). In contrast, increasing capillary pressure on DAMP4 films triggered formation of a dark hole at the top edge of the surface films that grew larger occupying half of the film, an initiation of film rupture, upon increasing the pressure to 2500 Pa (Figure 5b). It is evident that surface films of D4S2 demonstrated higher stability than of DAMP4, which bears a positive charge and a near-zero charge, respectively, at pH 7.5, during film compression as a result of higher charge−charge repulsion of positively charged D4S2 at the investigated pH and hence increased mechanical resistance of the film. DAMP4 protein bearing near-zero charge has been reported to have low film stability[44] and that the film stability could be enhanced by increasing its positive charges through addition of Zn^{2+} ions which bound to histidine (H) residues within DAMP4.

Emulsification Activity. The surface activity of D4S2 was tested further for emulsifying Miglyol 812 oil, i.e., whether D4S2 is able to facilitate disruption of the oil phase into small emulsion droplets upon sonication and stabilization of the droplets from aggregating with neighboring droplets. Emulsions of 10% v/v Miglyol 812 oil were prepared in various concentrations of D4S2 protein solutions (0.47−2.50 mg/mL) in HEPES buffer (25 mM, pH 7.5) via sonication that yielded emulsions having different physical properties (Figure 6). The size of emulsions produced at a D4S2 concentration of 0.47 mg/mL was 555 ± 25 nm with a dispersity ($Đ$) of 0.822, and the size decreased to 415 ± 8 nm ($Đ$ = 0.440) when D4S2 concentration was increased to 0.93 mg/mL. The high $Đ$'s indicate aggregation probably because the protein was insufficiently available to adsorb at oil−water interfaces, thus leaving gaps at the interfaces and, when two gaps on different droplets came into close proximity, resulting in droplet coalescence. Increasing D4S2 concentration to 1.53 mg/mL substantially decreased the droplet size to 203 ± 3 nm ($Đ$ = 0.210). Further increase of D4S2 concentration resulted in only a slight decrease in size. Overall, D4S2 formed sufficiently stable emulsions at 1.53 mg/mL with highly positive charges (zeta potential = +38 mV), suggesting that electrostatic repulsion is a key mode of stabilization for D4S2.

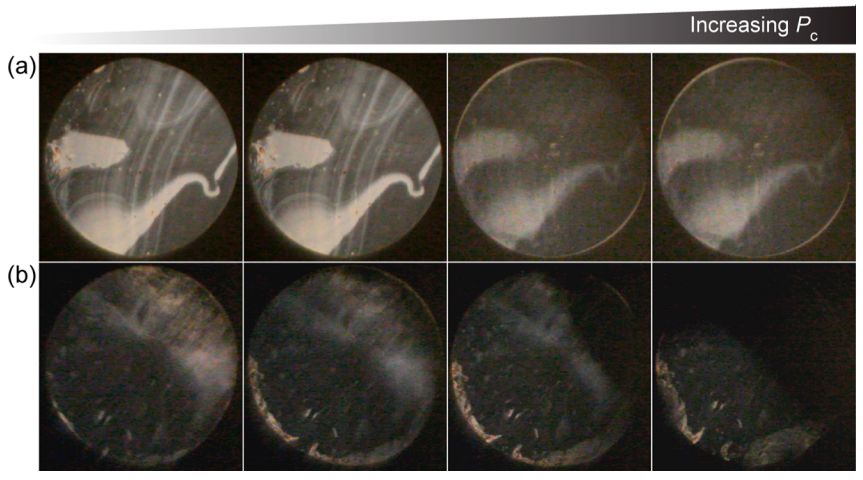

Figure 5. Surface visualization of thin liquid films: (a) D4S2 films; (b) DAMP4 films. Proteins were 1.53 mg/mL in 25 mM HEPES buffer pH 7.5. P_c is the capillary pressure applied to compress the films with maximum pressure reached at 2500 Pa.

DOI: 10.1021/la504684g
Langmuir 2015, 31, 1999−2007

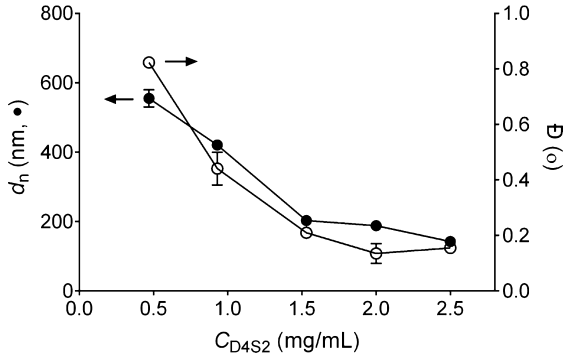

Figure 6. Dependence of number-averaged diameter (d_n, ●) and the corresponding dispersity (Đ, ○) of emulsion droplets formed at various concentration of D4S2 in HEPES buffer (25 mM, pH 7.5) as determined by using dynamic light scattering (DLS).

Biomimetic Silicification Activity. To determine the effectiveness of D4S2 for making silica nanocapsules, the nanoemulsions formed using 1.53 mg/mL D4S2 in HEPES buffer (25 mM, pH 7.5) were reacted with silica precursor tetraethoxysilane (TEOS) molecules. Following addition of TEOS to the nanoemulsions, silica nanocapsule was formed after 20 h reaction at pH 7.5 and room temperature (Figure 7).

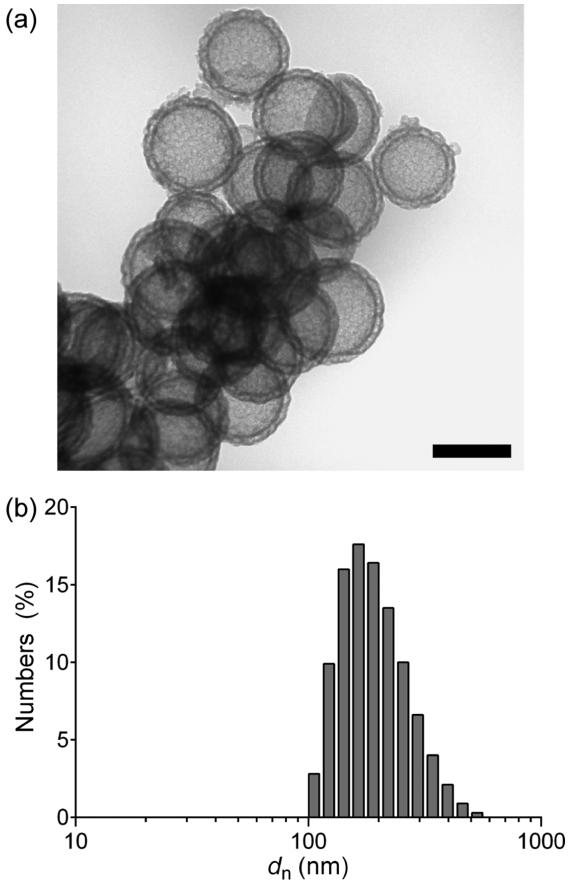

Figure 7. Silica nanocapsules formed after reaction of nanoemulsions stabilized by D4S2 (1.53 mg/mL) with TEOS (32 μmol) in HEPES buffer (25 mM) at pH 7.5 and room temperature for 20 h. (a) Transmission electron microscopy (TEM) image of the silica nanocapsules (scale bar is 200 nm). (b) Dynamic light scattering (DLS) showing size distribution profiles of the silica nanocapsules.

The outer diameter and shell thickness of the nanocapsules as measured by TEM were 249 ± 29 and 26 ± 2 nm, respectively. The biosilicification process at the oil−water interface was due to the catalytic role of Si module, which comprises densely packed cationic arginine (R) and lysine (K) residues, projecting toward bulk aqueous phase as well as polar residues of DAMP4 variant module that induced hydrolysis of TEOS and polycondensation at the oil−water interfaces forming silica shell encapsulating the oil core.

■ CONCLUSIONS

This study demonstrates the parallel biomolecular, scale-up, and interfacial catalytic design strategies for development of a 116-residue protein, D4S2, to catalyze interfacial synthesis of silica nanocapsules. D4S2 was designed, at the molecular level, by modularizing a DAMP4 variant protein, expected to have four-helix bundle structure and surface activity as imparted by DAMP4 protein, with a Si peptide rich in cationic amino acids known for biosilicification activity derived from SurSi peptide. This modular protein could be synthesized in cell factory *Escherichia coli* and extracted from the cells by heating and mixing with a suitably high concentration of Na_2SO_4 to disrupt the cells and precipitate most protein contaminants while maintaining D4S2 solubility, respectively. The stability of D4S2 to high temperature and chemical denaturant was related to its four-helix bundle structure in bulk, as designed. D4S2 protein was further purified by means of immobilized-metal affinity chromatography and then desalting chromatography to remove DNAs and salts. Properties of the purified D4S2 including molecular mass (13.3 kDa) and secondary structure (α-helix) were confirmed by using mass spectrometry and circular dichroism spectroscopy, respectively. Surface activity of D4S2 was evidenced as it substantially lowered the dynamic interfacial tension of freshly formed Miglyol 812 oil droplet upon interfacial adsorption. Thin film of D4S2 demonstrated stability against rupture when compressed at increasing pressure likely due to high electrostatic repulsion of D4S2 at the pH that imparted mechanical resistance to the film. Finally, D4S2 was shown able to facilitate formation and stabilization of nanoemulsions through its surface-active module and, upon addition of silica precursor tetraethoxysilane (TEOS), direct nucleation and growth of a silica layer encasing the nanoemulsion core through its biosilicification-active module under near-neutral pH and ambient temperature without using any toxic organic solvents. The present work provides an environmentally friendly approach to synthesize biocompatible oil-core silica-shell nanocapsules using a recombinant catalytic modular protein (ReCaMoP) offering the advantages of sustainable and scalable bioproduction, suitable for use as controlled-release nanocarrier of various actives in biomedical and agricultural fields.

■ ASSOCIATED CONTENT

Supporting Information

Qualitative analysis of protein, quantitation of DNA, transformation of recombinant DNA encoded for D4S2 protein into *E. coli*, expression of recombinant D4S2 protein in *E. coli*, and the subsequent purification processes as well as Figures S1−S4. This material is available free of charge via the Internet at http://pubs.acs.org.

DOI: 10.1021/la504684g
Langmuir 2015, 31, 1999−2007

AUTHOR INFORMATION

Corresponding Author

*Phone +61-7-3346-4189; Fax +61-7-3346-4197; e-mail a.middelberg@uq.edu.au (A.P.J.M.).

Notes

The authors declare no competing financial interest.

ACKNOWLEDGMENTS

This work was supported by the Australian Research Council (grants DP1093056 and 120103683). D.W. acknowledges a scholarship from The University of Queensland. C.X.Z. acknowledges financial support from the Australian Research Council in the form of an Australian Postdoctoral Fellow (DP110100394). A.P.J.M. acknowledges support from the Queensland Government through award of the 2010 Queensland Premier's Science Fellowship. The authors acknowledge the facilities, and the scientific and technical assistance, of the Australian Microscopy & Microanalysis Research Facility at the Centre for Microscopy and Microanalysis, The University of Queensland. The authors also acknowledge the Australian National Fabrication Facility at The University of Queensland for access to the LC-MS, Andrea Schaller for molecular modeling of D4S2 protein, and Dr Liguang Wang for assistance with thin film pressure balance experiment.

ABBREVIATIONS

A, alanine; D, aspartic acid; E, glutamic acid; G, glycine; H, histidine; K, lysine; L, leucine; M, methionine; P, proline; Q, glutamine; R, arginine; S, serine; V, valine; Y, tyrosine; CD, circular dichroism; Da, Dalton; DLS, dynamic light scattering; DNA, deoxyribonucleic acid; HEPES, sodium 4-(2-hydroxyethyl)-1-piperazine ethanesulfonate; IMAC, immobilized-metal affinity chromatography; LC, liquid chromatography; MS, mass spectrometry; *M*, molecular mass; *Đ*, dispersity; p*I*, isoelectric point; ReCaMoP, recombinant catalytic modular protein; RP-HPLC, reversed-phase high-performance liquid chromatography; SDS-PAGE, sodium dodecyl sulfate polyacrylamide gel electrophoresis; TEM, transmission electron microscopy; TEOS, tetraethoxysilane; TFA, trifluoroacetic acid; UV, ultraviolet.

REFERENCES

(1) Guerrero-Martínez, A.; Pérez-Juste, J.; Liz-Marzán, L. M. Recent Progress on Silica Coating of Nanoparticles and Related Nanomaterials. *Adv. Mater.* **2010**, *22*, 1182−1195.

(2) Li, W.; Yue, Q.; Deng, Y. H.; Zhao, D. Y. Ordered Mesoporous Materials Based on Interfacial Assembly and Engineering. *Adv. Mater.* **2013**, *25*, 5129−5152.

(3) Rana, R. K.; Mastai, Y.; Gedanken, A. Acoustic Cavitation Leading to the Morphosynthesis of Mesoporous Silica Vesicles. *Adv. Mater.* **2002**, *14*, 1414−1418.

(4) Prouzet, E.; Cot, F.; Boissiere, C.; Kooyman, P. J.; Larbot, A. Nanometric Hollow Spheres Made of MSU-X-type Mesoporous Silica. *J. Mater. Chem.* **2002**, *12*, 1553−1556.

(5) Ung, T.; Liz-Marzán, L. M.; Mulvaney, P. Redox Catalysis Using Ag@SiO_2 Colloids. *J. Phys. Chem. B* **1999**, *103*, 6770−6773.

(6) Joo, S. H.; Park, J. Y.; Tsung, C.-K.; Yamada, Y.; Yang, P.; Somorjai, G. A. Thermally Stable Pt/Mesoporous Silica Core−Shell Nanocatalysts for High-Temperature Reactions. *Nat. Mater.* **2009**, *8*, 126−131.

(7) Correa-Duarte, M. A.; Giersig, M.; Liz-Marzán, L. M. Stabilization of CdS Semiconductor Nanoparticles against Photodegradation by a Silica Coating Procedure. *Chem. Phys. Lett.* **1998**, *286*, 497−501.

(8) Ow, H.; Larson, D. R.; Srivastava, M.; Baird, B. A.; Webb, W. W.; Wiesner, U. Bright and Stable Core−Shell Fluorescent Silica Nanoparticles. *Nano Lett.* **2005**, *5*, 113−117.

(9) Lu, A.-H.; Salabas, E. L.; Schüth, F. Magnetic Nanoparticles: Synthesis, Protection, Functionalization, and Application. *Angew. Chem., Int. Ed.* **2007**, *46*, 1222−1244.

(10) Graf, C.; Vossen, D. L. J.; Imhof, A.; van Blaaderen, A. A General Method to Coat Colloidal Particles with Silica. *Langmuir* **2003**, *19*, 6693−6700.

(11) Graf, P.; Mantion, A.; Haase, A.; Thuenemann, A. F.; Mašic, A.; Meier, W.; Luch, A.; Taubert, A. Silicification of Peptide-Coated Silver Nanoparticles—A Biomimetic Soft Chemistry Approach toward Chiral Hybrid Core−Shell Materials. *ACS Nano* **2011**, *5*, 820−833.

(12) Kuwahara, Y.; Yamanishi, T.; Kamegawa, T.; Mori, K.; Che, M.; Yamashita, H. Lipase-Embedded Silica Nanoparticles with Oil-Filled Core−Shell Structure: Stable and Recyclable Platforms for Biocatalysts. *Chem. Commun.* **2012**, *48*, 2882−2884.

(13) Underhill, R. S.; Jovanovic, A. V.; Carino, S. R.; Varshney, M.; Shah, D. O.; Dennis, D. M.; Morey, T. E.; Duran, R. S. Oil-Filled Silica Nanocapsules for Lipophilic Drug Uptake: Implications for Drug Detoxification Therapy. *Chem. Mater.* **2002**, *14*, 4919−4925.

(14) Jovanovic, A. V.; Underhill, R. S.; Bucholz, T. L.; Duran, R. S. Oil Core and Silica Shell Nanocapsules: Toward Controlling the Size and the Ability to Sequester Hydrophobic Compounds. *Chem. Mater.* **2005**, *17*, 3375−3383.

(15) Hayashi, K.; Nakamura, M.; Ishimura, K. *In situ* Synthesis and Photoresponsive Rupture of Organosilica Nanocapsules. *Chem. Commun.* **2011**, *47*, 1518−1520.

(16) Wibowo, D.; Zhao, C.-X.; Middelberg, A. P. J. Emulsion-Templated Silica Nanocapsules Formed Using Bio-Inspired Silicification. *Chem. Commun.* **2014**, *50*, 11325−11328.

(17) Wang, J. W.; Xia, Y. D.; Wang, W. X.; Mokaya, R.; Poliakoff, M. Synthesis of Siliceous Hollow Spheres with Large Mesopore Wall Structure by Supercritical CO_2-in-Water Interface Templating. *Chem. Commun.* **2005**, 210−212.

(18) Chen, H.; He, J.; Tang, H.; Yan, C. Porous Silica Nanocapsules and Nanospheres: Dynamic Self-Assembly Synthesis and Application in Controlled Release. *Chem. Mater.* **2008**, *20*, 5894−5900.

(19) Li, J.; Liu, J.; Wang, D.; Guo, R.; Li, X.; Qi, W. Interfacially Controlled Synthesis of Hollow Mesoporous Silica Spheres with Radially Oriented Pore Structures. *Langmuir* **2010**, *26*, 12267−12272.

(20) Zhao, M.; Zheng, L.; Bai, X.; Li, N.; Yu, L. Fabrication of Silica Nanoparticles and Hollow Spheres Using Ionic Liquid Microemulsion Droplets as Templates. *Colloids Surf., A* **2009**, *346*, 229−236.

(21) Chen, Y.; Chen, H.; Shi, J. *In Vivo* Bio-Safety Evaluations and Diagnostic/Therapeutic Applications of Chemically Designed Mesoporous Silica Nanoparticles. *Adv. Mater.* **2013**, *25*, 3144−3176.

(22) Kröger, N.; Deutzmann, R.; Sumper, M. Polycationic Peptides from Diatom Biosilica that Direct Silica Nanosphere Formation. *Science* **1999**, *286*, 1129−1132.

(23) Cha, J. N.; Shimizu, K.; Zhou, Y.; Christiansen, S. C.; Chmelka, B. F.; Stucky, G. D.; Morse, D. E. Silicatein Filaments and Subunits from a Marine Sponge Direct the Polymerization of Silica and Silicones *In Vitro*. *Proc. Natl. Acad. Sci. U. S. A.* **1999**, *96*, 361−365.

(24) Patwardhan, S. V. Biomimetic and Bioinspired Silica: Recent Developments and Applications. *Chem. Commun.* **2011**, *47*, 7567−7582.

(25) Meegan, J. E.; Aggeli, A.; Boden, N.; Brydson, R.; Brown, A. P.; Carrick, L.; Brough, A. R.; Hussain, A.; Ansell, R. J. Designed Self-Assembled *β*-Sheet Peptide Fibrils as Templates for Silica Nanotubes. *Adv. Funct. Mater.* **2004**, *14*, 31−37.

(26) Yuwono, V. M.; Hartgerink, J. D. Peptide Amphiphile Nanofibers Template and Catalyze Silica Nanotube Formation. *Langmuir* **2007**, *23*, 5033−5038.

(27) Holmstrom, S. C.; King, P. J. S.; Ryadnov, M. G.; Butler, M. F.; Mann, S.; Woolfson, D. N. Templating Silica Nanostructures on Rationally Designed Self-Assembled Peptide Fibers. *Langmuir* **2008**, *24*, 11778−11783.

DOI: 10.1021/la504684g
Langmuir 2015, 31, 1999−2007

(28) Altunbas, A.; Sharma, N.; Lamm, M. S.; Yan, C.; Nagarkar, R. P.; Schneider, J. P.; Pochan, D. J. Peptide−Silica Hybrid Networks: Biomimetic Control of Network Mechanical Behavior. *ACS Nano* **2010**, *4*, 181−188.
(29) Merrifield, R. B. Solid Phase Peptide Synthesis. 1. Synthesis of a Tetrapeptide. *J. Am. Chem. Soc.* **1963**, *85*, 2149−2154.
(30) Latham, P. W. Therapeutic Peptides Revisited. *Nat. Biotechnol.* **1999**, *17*, 755−757.
(31) Lee, S. Y. High Cell-Density Culture of *Escherichia coli*. *Trends Biotechnol.* **1996**, *14*, 98−105.
(32) Morreale, G.; Lee, E. G.; Jones, D. B.; Middelberg, A. P. J. Bioprocess-Centered Molecular Design (BMD) for the Efficient Production of an Interfacially Active Peptide. *Biotechnol. Bioeng.* **2004**, *87*, 912−923.
(33) Kyle, S.; Aggeli, A.; Ingham, E.; McPherson, M. J. Production of Self-Assembling Biomaterials for Tissue Engineering. *Trends Biotechnol.* **2009**, *27*, 423−433.
(34) Itakura, K.; Hirose, T.; Crea, R.; Riggs, A. D.; Heyneker, H. L.; Bolivar, F.; Boyer, H. W. Expression in *Escherichia coli* of a Chemically Synthesized Gene for Hormone Somatostatin. *Science* **1977**, *198*, 1056−1063.
(35) Kaar, W.; Hartmann, B. M.; Fan, Y.; Zeng, B.; Lua, L. H. L.; Dexter, A. F.; Falconer, R. J.; Middelberg, A. P. J. Microbial Bio-Production of a Recombinant Stimuli-Responsive Biosurfactant. *Biotechnol. Bioeng.* **2009**, *102*, 176−187.
(36) Middelberg, A. P. J.; Dimitrijev-Dwyer, M. A Designed Biosurfactant Protein for Switchable Foam Control. *ChemPhysChem* **2011**, *12*, 1426−1429.
(37) Dimitrijev-Dwyer, M.; Brech, M.; Yu, L.; Middelberg, A. P. J. Intensified Expression and Purification of a Recombinant Biosurfactant Protein. *Chem. Eng. Sci.* **2014**, *105*, 12−21.
(38) Pain, R. Determining the CD Spectrum of a Protein. In *Current Protocols in Protein Science*; Coligan, J. E., Hidde, L., Ploegh, B. M. D., Speicher, D. W., Wingfield, P. T., Taylor, S. E. G., Eds.; John Wiley & Sons, Inc.: New York, 2005; pp 7.6.1−7.6.24.
(39) Sheludko, A. Thin Liquid Films. *Adv. Colloid Interface Sci.* **1967**, *1*, 391−464.
(40) Pereira, L. G. C.; Johansson, C.; Blanch, H. W.; Radke, C. J. A Bike-Wheel Microcell for Measurement of Thin-Film Forces. *Colloids Surf., A* **2001**, *186*, 103−111.
(41) Wang, L.; Yoon, R. H. Effects of Surface Forces and Film Elasticity on Foam Stability. *Int. J. Miner. Process.* **2008**, *85*, 101−110.
(42) Dexter, A. F.; Malcolm, A. S.; Middelberg, A. P. J. Reversible Active Switching of the Mechanical Properties of a Peptide Film at a Fluid−Fluid Interface. *Nat. Mater.* **2006**, *5*, 502−506.
(43) Chuan, Y. P.; Zeng, B. Y.; O'Sullivan, B.; Thomas, R.; Middelberg, A. P. J. Co-Delivery of Antigen and a Lipophilic Anti-Inflammatory Drug to Cells via a Tailorable Nanocarrier Emulsion. *J. Colloid Interface Sci.* **2012**, *368*, 616−624.
(44) Dimitrijev-Dwyer, M.; He, L.; James, M.; Nelson, A.; Wang, L.; Middelberg, A. P. J. The Effects of Acid Hydrolysis on Protein Biosurfactant Molecular, Interfacial, and Foam Properties: pH Responsive Protein Hydrolysates. *Soft Matter* **2012**, *8*, 5131−5139.
(45) Dimitrijev-Dwyer, M.; He, L.; James, M.; Nelson, A.; Middelberg, A. P. J. Insights into the Role of Protein Molecule Size and Structure on Interfacial Properties using Designed Sequences. *J. R. Soc. Interface* **2013**, *10*, 20120987.
(46) Gregory, C. A.; Rigg, G. P.; Illidge, C. M.; Matthews, R. C. Quantification of *Escherichia coli* Genomic DNA Contamination in Recombinant Protein Preparations by Polymerase Chain Reaction and Affinity-Based Collection. *Anal. Biochem.* **2001**, *296*, 114−121.
(47) Harrison, S. C.; Aggarwal, A. K. DNA Recognition by Proteins with the Helix-Turn-Helix Motif. *Annu. Rev. Biochem.* **1990**, *59*, 933−969.
(48) Kalodimos, C. G.; Biris, N.; Bonvin, A.; Levandoski, M. M.; Guennuegues, M.; Boelens, R.; Kaptein, R. Structure and Flexibility Adaptation in Nonspecific and Specific Protein-DNA Complexes. *Science* **2004**, *305*, 386−389.
(49) Sherbet, G. V.; Lakshmi, M. S.; Cajone, F. Isoelectric Characteristics and the Secondary Structure of Some Nucleic Acids. *Biophys. Struct. Mech.* **1983**, *10*, 121−128.
(50) Brinker, C. J.; Scherrer, G. W. *Sol−Gel Science: The Physics and Chemistry of Sol−Gel Processing*; Academic Press: San Diego, CA, 1990; pp 108−150.
(51) Johnson, W. C. Protein Secondary Structure and Circular Dichroism: A Practical Guide. *Proteins: Struct., Funct., Bioinf.* **1990**, *7*, 205−214.
(52) Akanuma, S.; Matsuba, T.; Ueno, E.; Umeda, N.; Yamagishi, A. Mimicking the Evolution of a Thermally Stable Monomeric Four-Helix Bundle by Fusion of Four Identical Single-Helix Peptides. *J. Biochem.* **2010**, *147*, 371−379.
(53) Regan, L.; Degrado, W. F. Characterization of a Helical Protein Designed from First Principles. *Science* **1988**, *241*, 976−978.
(54) Baltzer, L.; Broo, K. S.; Nilsson, H.; Nilsson, J. Designed Four-Helix Bundle Catalysts—the Engineering of Reactive Sites for Hydrolysis and Transesterification Reactions of p-Nitrophenyl Esters. *Bioorg. Med. Chem.* **1999**, *7*, 83−91.
(55) Beverung, C. J.; Radke, C. J.; Blanch, H. W. Protein Adsorption at the Oil/Water Interface: Characterization of Adsorption Kinetics by Dynamic Interfacial Tension Measurements. *Biophys. Chem.* **1999**, *81*, 59−80.
(56) Young, M. E.; Carroad, P. A.; Bell, R. L. Estimation of Diffusion-Coefficients of Proteins. *Biotechnol. Bioeng.* **1980**, *22*, 947−955.
(57) Stubenrauch, C.; von Klitzing, R. Disjoining Pressure in Thin Liquid Foam and Emulsion Films—New Concepts and Perspectives. *J. Phys.: Condens. Matter* **2003**, *15*, R1197−R1232.
(58) Bergeron, V. Measurement of Forces and Structure between Fluid Interfaces. *Curr. Opin. Colloid Interface Sci.* **1999**, *4*, 249−255.

DOI: 10.1021/la504684g
Langmuir 2015, 31, 1999−2007

Supporting Information

Interfacial biomimetic synthesis of silica nanocapsules using a recombinant catalytic modular protein

*David Wibowo, Chun-Xia Zhao, and Anton P. J. Middelberg**

Australian Institute for Bioengineering and Nanotechnology, The University of Queensland, St Lucia QLD 4072, Australia.

*To whom correspondence should be addressed. Phone: +61-7-3346-4189; Fax: +61-7-3346-4197; E-mail: a.middelberg@uq.edu.au.

EXPERIMENTAL SECTION

Analytical methods. Qualitative analysis of protein was performed using sodium dodecyl sulfate polyacrylamide gel electrophoresis (SDS-PAGE). Protein samples (15 μL) were mixed with 5× sample buffer (3 μL) (225 mM Tris–HCl pH 6.8, 50 v/v% glycerol, 173 mM SDS, 0.746 mM bromophenol blue, 250 mM dithiothreitol), heated to 95 °C for 5 min, and then filled into the NuPAGE® 4–12% Bis-Tris gels (Life Technologies, Australia). Novex® sharp pre-stained protein standard was used as a marker. Then, electrophoresis was performed using a Bio-Rad XCell 3 system (Bio-Rad, CA, USA) at 200 V for 35 min. Following electrophoresis, the gel was stained in staining buffer (45 v/v% methanol, 45 v/v% water, 10 v/v% acetic acid, 2.4 mM coomassie brilliant blue R-250) for 1 h. Subsequently, the gel was destained in destaining buffer (45 v/v% methanol, 45 v/v% water, 10 v/v% acetic acid) for 1 h, incubated overnight in water, and imaged with a ChemiDoc™ MP Imaging System (Bio-Rad, CA, USA).

DNA concentrations in D4S2 protein samples were determined by fluorescence measurement using Infinite® M200 Pro plate reader (Tecan, Switzerland). SYBR® Safe (Life Technologies, Australia) was used as the fluorescent dye. It is a cyanine-based dye having cationic core structure with *N*-*n*-propyl on the quinolinium ring system.[1] The binding modes of the dye and DNA are by intercalation of the dye into the base pair stack at the core of the DNA, and by insertion of the dye into the minor groove of the DNA.[2] For DNA quantitation, each solution (standards, sample and blank) was prepared in a volume of 100 μL in a 96-well plate with flat bottom and white polystyrol (Greiner Bio-One, Germany). Subsequently, a 100 μL SYBR® Safe (available commercially in concentration of 10 000×) with concentration of 1× was added into each individual well. The plate was then incubated for 5 min in a dark room at room temperature, followed by fluorescence measurement at excitation and emission wavelengths of 502 nm and

530 nm, respectively. As standard DNA, plasmid pET-48b(+) with inserted D4S2 nucleotide sequence (Protein Expression Facility, University of Queensland) was used. It was obtained after transformation in *E. coli* XL1-Blue competent cells (Novagen, Merck KGaA, Germany). Extraction and purification of the DNA was performed using PureLink™ Quick Plasmid Miniprep Kit (Invitrogen, CA, USA) following instructions from the manufacturer. Existence of the pure plasmid DNA was confirmed by A_{260}/A_{280} ratio value of 1.8 as measured by UV absorbance at 260 nm using NanoDrop 1000 Spectrophotometer (Thermo Fisher Scientific, DE, USA). A serial dilution of pre-determined concentration of the standard DNA (0–50 ng/mL) was used, and the mean fluorescence intensity across a duplicate for each concentration of the DNA was corrected by subtracting the fluorescence intensity of the blank (i.e., the relative fluorescent units (RFU)) to construct a calibration curve (i.e., relationship of RFU to concentration) having a regression linear of $y = 822.5x + 1500$ and a coefficient of determination (R^2) of 0.9948. DNA concentration in a protein sample can then be calculated by inserting its RFU into the regression linear equation.

Recombinant DNA transformation. Plasmid pET-48b(+) with nucleotide sequence encoding for D4S2 protein (1 μL) (Protein Expression Facility, The University of Queensland) was added into *E. coli* BL21(DE3) competent cells (50 μL) (Novagen, Merck KGaA, Germany) and incubated on ice for 30 min, heat-shocked at 42 °C for 45 s, and incubated on ice for further 2 min. Then, 0.95 mL Luria Bertani (LB) medium (10 g/L NaCl, 10 g/L tryptone, 5 g/L yeast extract, water) was added into the cell suspension and incubated at 37 °C, 220 rpm for 1 h. The cell suspension (100 μL) was plated on LB agar (10 g/L NaCl, 10 g/L tryptone, 5 g/L yeast extract, 15 g/L agar, water) and incubated at 37 °C, 180 rpm for 16 h. Following transformation, a single colony was picked from the plate, placed in 5 mL 2× yeast extract and tryptone (2YT)

medium (5 g/L NaCl, 16 g/L tryptone, 10 g/L yeast extract, water), and incubated at 37 °C, 180 rpm for 16 h. The LB agar and 2YT media were supplemented with 15 μg/mL antibiotic (i.e., kanamycin sulfate) (Life Technologies, CA, USA). To preserve the clones, the overnight culture (0.5 mL) and 60 v/v% glycerol (0.5 mL) were mixed well, frozen in liquid nitrogen, and stored at –80 °C for later use.

Protein expression. A single colony from a freshly streaked plate was inoculated into 5 mL 2YT medium and incubated at 30 °C, 180 rpm for 16 h. After overnight culture, an optical density at a wavelength of 600 nm (OD_{600}) was obtained at approximately 2 by using UV-visible spectrophotometer (UV-2450) (Shimadzu, Japan). 2YT medium (800 mL) was inoculated with 800 μL of the overnight culture in a 2.5 L-baffled shake flask and incubated at 37 °C, 180 rpm until OD_{600} reached approximately 0.5. Protein expression was induced by adding isopropyl β-D-1-thiogalactopyranoside (IPTG) (Astral Scientific, Australia) to a final concentration of 1 mM, and then incubated at 37 °C, 180 rpm for a further 4 h. A final OD_{600} of approximately 2 was routinely obtained. Cell pellet was harvested by centrifugation at 4 °C, 6250 ×*g* for 10 min, washed with the supernatant (40 mL) and then centrifuged at 4 °C, 4700 ×*g* for 10 min. The cell pellet was stored at –80 °C until further processing. All media for cultures were supplemented with 15 μg/mL kanamycin sulfate.

Protein purification. To purify D4S2 protein from *E. coli*, a precipitation-based process i.e., heating/cell lysis, contaminant precipitation, and dilute precipitation (Figure S1) was conducted based on intensified purification process of DAMP4.[3]

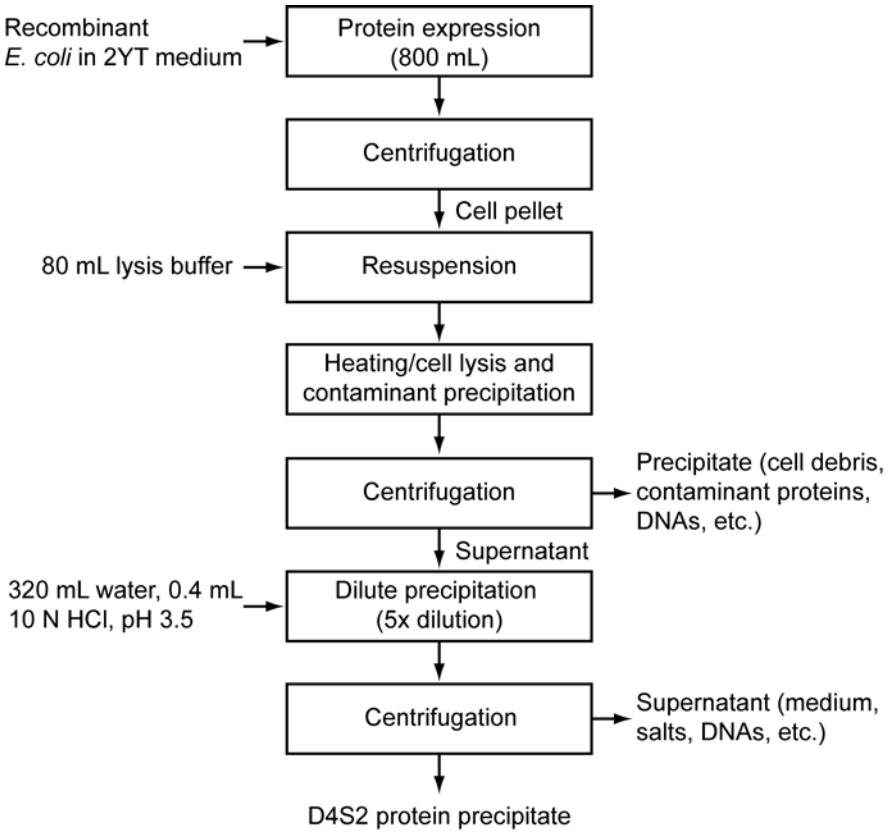

Figure S1. Block flow diagram of precipitation-based purification process of D4S2.

Initial heating/cell lysis and contaminant precipitation tests: To determine optimum concentration of Na_2SO_4 precipitating cellular protein contaminants, initial heating/cell lysis and contaminant precipitation tests were performed on cell pellet containing expressed D4S2. The cell pellet was re-suspended in 80 mL buffer (25 mM sodium phosphate, 1.2 M NaCl, pH 7.5), and five samples of 500 μL were taken. To one of these samples, 500 μL of water was added and used as the reference for soluble and insoluble cell contents. To the remaining four samples, Na_2SO_4 solution was added to achieve Na_2SO_4 concentrations of 0.3 M, 0.5 M, 0.8 M, and 1 M, respectively, with a final volume of 1 mL in each. All samples were heated in a heating block (model DBH20D, Ratek Instruments, Australia) at 90 °C for 30 min, and then centrifuged. SDS-PAGE was performed to qualitatively analyze the supernatant and the pellet fractions which

were denoted as soluble protein and insoluble cell content, respectively. The SDS-PAGE result (Figure S2) showed that heating/cell lysis and contaminant precipitation using 1 M Na_2SO_4, at 90 °C for 30 min yield more pure D4S2 protein as indicated by a clearer background on the gel (Figure S2, lane 9) than using lower Na_2SO_4 concentrations at the same incubation temperature and time period (Figure S2, lanes 3, 5, and 7). Therefore, Na_2SO_4 with a concentration of 1 M was used in the lysis buffer for future process of heating/cell lysis and contaminant precipitation.

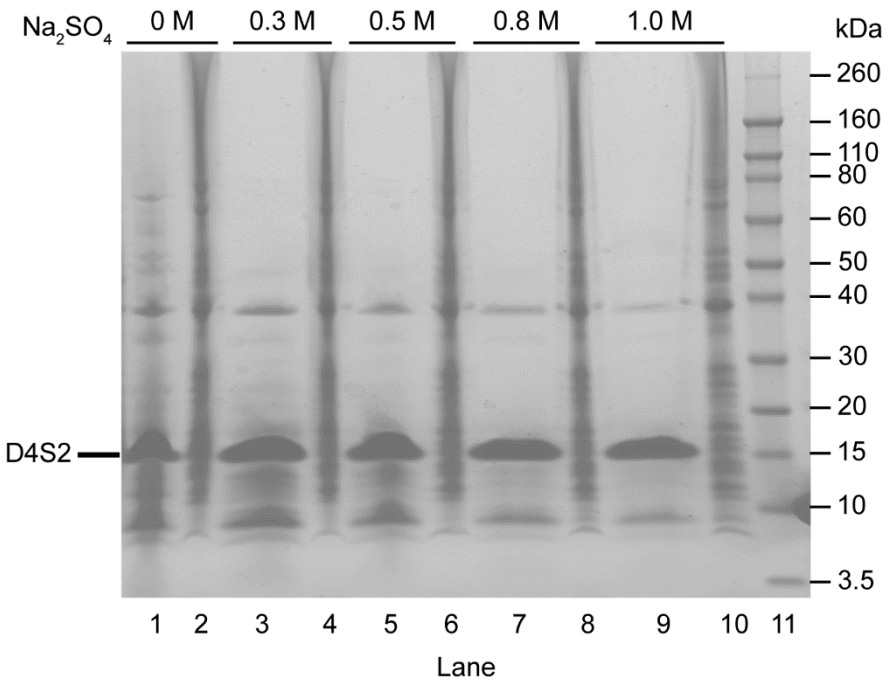

Figure S2. SDS-PAGE analysis after initial test of heating/cell lysis and contaminant precipitation using different Na_2SO_4 concentrations at 90 °C for 30 min. (Lane 1) Soluble protein and (Lane 2) insoluble cell content in the absence of Na_2SO_4; (Lane 3) Soluble protein and (Lane 4) insoluble cell content at 0.3 M Na_2SO_4; (Lane 5) Soluble protein and (Lane 6) insoluble cell content at 0.5 M Na_2SO_4; (Lane 7) Soluble protein and (Lane 8) insoluble cell content at 0.8 M Na_2SO_4; (Lane 9) Soluble protein and (Lane 10) insoluble cell content at 1 M Na_2SO_4; (Lane 11) Novex® sharp pre-stain protein standard.

Heating/cell lysis, contaminant precipitation, and dilute precipitation: The cell pellet was re-suspended in 80 mL lysis buffer (25 mM sodium phosphate, 1.2 M NaCl, 1 M Na_2SO_4, pH 7.5). The mixture was transferred into a 250 mL-conical flask and then incubated at 90 °C with stirring at 1000 rpm for 30 min in a thermostatic bath equipped with an electronic contact thermometer (IKA®-Werke GmbH & Co. KG, Germany). During the heating, the opening of the flask and the bath were covered with aluminium foil to minimize evaporation. The cell lysate was then centrifuged at 20 °C, 51500 ×*g* for 5 min. The supernatant was collected and diluted 5-fold with water, and pH was adjusted to pH 3.5 by adding 10 N HCl to allow precipitation of D4S2 protein. Then, the mixture was centrifuged at 4 °C, 33750 ×*g* for 30 min. The precipitated sample was re-suspended in equilibrium buffer (25 mM sodium phosphate, 1.2 M NaCl, 20 mM imidazole, pH 7.5) and solubilized by adjusting the pH to pH > 10 using 5 N NaOH. Further purification was conducted to remove DNA contaminant (Table S1) by applying chromatography-based purification process (Figure S3).

Table S1. Mass balance of the purification processes of D4S2.

Process	**D4S2 conc.[a] (mg/mL)**	**Volume (mL)**	**D4S2 yield (mg)**	**DNA conc. (ng/mg D4S2)**
Heating/cell lysis and contaminant precipitation	0.26	140.0	36.40	1261 ± 38
Dilute precipitation	0.56	22.0	12.32	63.18 ± 6.14
Filtration	0.61	20.1	12.26	62.87 ± 5.62
IMAC	0.66	14.0	9.24	1.90 ± 0.48
Desalting	0.38	19.0	7.22	1.82 ± 0.46

[a]D4S2 concentration was determined by reversed-phase high-performance liquid chromatography (RP-HPLC), except for D4S2 protein obtained after heating/cell lysis and

contaminant precipitation in which the concentration was measured by SDS-PAGE semi quantitation using ImageJ software.[4]

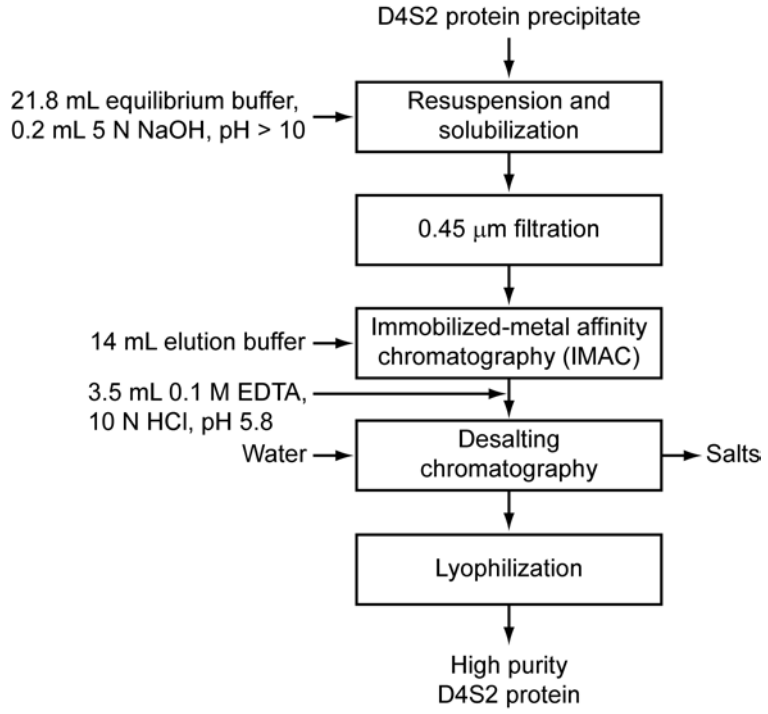

Figure S3. Block flow diagram of chromatography-based purification process following the precipitation-based process to obtain high purity D4S2 protein.

Chromatography: Immobilized-metal affinity chromatography (IMAC) was conducted by using an ÄKTA Explorer 10 system (GE Healthcare, Sweden) with Ni^{2+} charged IMAC Sepharose High Performance resin (GE Healthcare, UK) packed into a 15 mm diameter Omnifit glass column (Omnifit, NJ, USA) to a bed height of 75 mm which is equivalent to 5.5 mL column volume (CV). Prior to loading, the protein solution from a previous process was filtered using a 0.45 μm syringe filter with MF-Millipore® mixed cellulose ester membrane (Millipore, Australia), and the column was equilibrated with 3 CV of equilibrium buffer (25 mM sodium

phosphate, 1.2 M NaCl, 20 mM imidazole, pH 7.5). The protein solution was then loaded into the column at a flow rate of 1 mL/min, and set wavelengths of 280 nm and 260 nm to detect the presence of protein and DNA, respectively. Unbound components including DNAs as indicated by higher UV absorbance at 260 nm than at 280 nm were passed-through the column and then washed out with 2 CV of equilibrium buffer. Bound protein was then eluted using 2.5 CV of elution buffer (25 mM sodium phosphate, 1.2 M NaCl, 500 mM imidazole, pH 7.5) (Figure S4a). The flow-through fraction (Figure 1, lane 5) and wash fraction (Figure 1, lane 6) did not contain D4S2 protein, whereas the eluted fraction was mainly D4S2 protein (Figure 1, lane 7) based on the SDS-PAGE analysis. After the IMAC process, concentration of DNA in the eluted fraction was reduced significantly by 97% to 1.90 ± 0.48 ng DNA/mg D4S2 (Table S1). To chelate Ni^{2+} ions that might be leaked and bound to histidine (H) residues within D4S2 after the IMAC process, the pH of the collected fractions was adjusted to pH 5.8 by adding 10 N HCl to protonate the histidine (H) residues, and a chelating agent ethylenediaminetetraacetic acid disodium salt (EDTA) was added to a final concentration of 20 mM. Then, desalting of the protein solution with water was conducted by using an ÄKTA Explorer 10 system with a Sephadex G-25 resin (GE Healthcare, UK) packed into a 20 mm diameter Omnifit glass column to a bed height of 129 mm (CV = 22.8 mL). The protein solution was loaded into the column pre-equilibrated with water at a flow rate of 1 mL/min and a set wavelength of 280 nm coupled with a conductivity detector. The protein fraction after the desalting process was collected (Figure S4b) and lyophilized at –55°C, 0.08 mbar for 16 h. After the desalting process, the DNA fraction in D4S2 protein solution was 1.82 ± 0.46 ng DNA/mg D4S2 with a final yield of D4S2 protein of approximately 7.22 mg (Table S1).

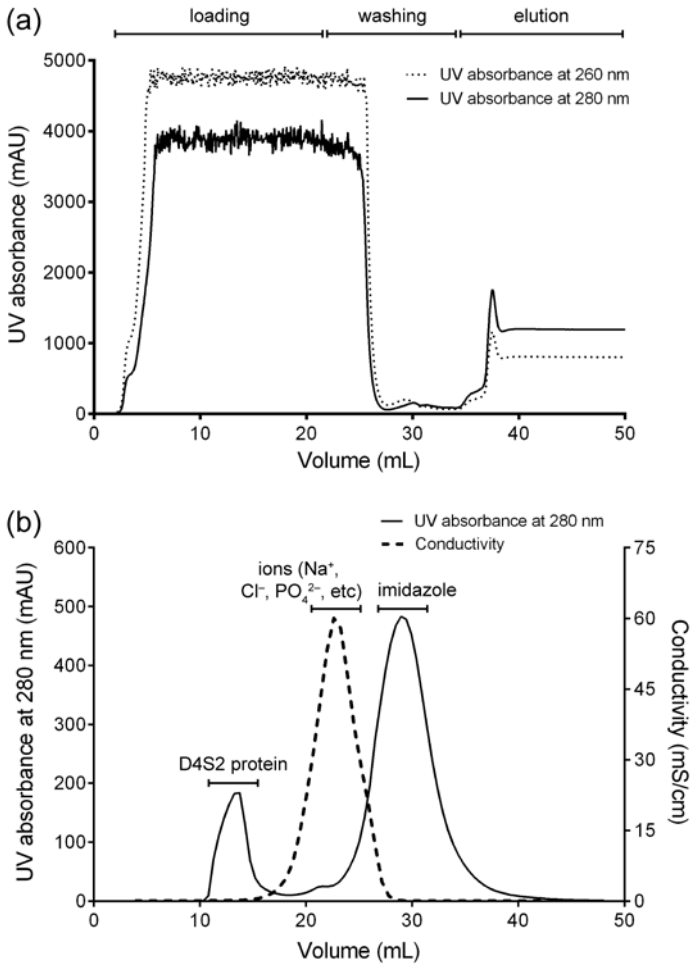

Figure S4. Representative chromatography profiles to obtain high purity of D4S2 protein. (a) Immobilized-metal affinity chromatography (IMAC). (b) Desalting chromatography.

References

(1) Evenson, W.E.; Boden, L. M.; Muzikar, K. A.; O'Leary, D. J. ^{1}H and ^{13}C NMR Assignments for the Cyanine Dyes SYBR Safe and Thiazole Orange. *J. Org. Chem.* **2012**, *77*, 10967–10971.

(2) Armitage, B.A. Cyanine Dye-DNA Interactions: Intercalation, Groove Binding, and Aggregation. In *DNA Binders and Related Subjects*; Waring, M.J., Chaires, J.B., Eds.; Springer-Verlag: Berlin, 2005; pp 55–76.

(3) Dimitrijev-Dwyer, M.; Brech, M.; Yu, L.; Middelberg, A. P. J. Intensified Expression and Purification of a Recombinant Biosurfactant Protein. *Chem. Eng. Sci.* **2014**, *105*, 12–21.

(4) Schneider, C.A.; Rasband, W.S.; Eliceiri, K.W. NIH Image to ImageJ: 25 Years of Image Analysis. *Nat. Methods*. **2012**, *9*, 671–675.

Chapter 6

Large-scale production of fipronil-encapsulated silica nanocapsules for termite field trial

Abstract

Development of the bifunctional modular protein, D4S2, for making oil-core silica-shell nanocapsules as described in **Chapter 5** provided an opportunity for sustainable and cost-effective production of the protein *via* microbial cell-factory *Escherichia coli*. In this chapter, D4S2 was produced at approximately 1.4 g using the biological expression and purification methods developed in **Chapter 5**. Prior to the emulsification using D4S2, fipronil (≈0.9 g) was dissolved in Miglyol® 812 oil at a concentration of 10 mg/mL. D4S2 (1.53 mg/mL) was used to emulsify the fipronil-loaded oil (10 v/v%), and the resulted nanoemulsions were reacted with silica precursor tetraethoxysilane to form fipronil-encapsulated silica nanocapsules. The silica nanocapsules could then be used in combination with α-cellulose as feeding baits for termite field trial. The feeding baits placed in treatment-units were attached separately in mounds of termite *Coptotermes lacteus*. The activities of foraging worker termites toward the baits were examined. As the field trial entered the six week after treatment-units installation and is still on-going, this chapter presents preliminary results indicated that the termites responded well to the treated baits as they readily removed the baits from the treatment-units within three weeks of treatments, providing a chance that the baits would be transmitted to other termites within the mounds through horizontal transfer which could then lead to potential elimination of the termite colonies.

6.1 Introduction

Termites are prevalent in tropical and subtropical environments where they assist in breaking down and recycling dead plant materials [1]. However, some termite species become pests when they feed on any plant materials and structural lumber causing substantial crop losses and building damages, hence economic losses [2]. In Australia only, an estimated 130,000 new infestations in houses are reported each year, and the average cost of rectification of termite-damaged properties is in excess of AU$7,000 per house [3]. The worldwide annual control and repair cost were estimated at US$40 billion in 2010 with subterranean termites accounting for approximately 80% of the costs [4]. Therefore, controlling termite pest populations are urgently important as to control global economic impact caused by the termite infestations.

Preventative treatments against termite infestations have been conducted using chemical soil barriers [5, 6], in which an insecticide is applied to the soil forming an insecticide-treated layer of soil surrounding and under buildings [7]. Cyclodienes, including chlordane, heptachlor, aldrin and dieldrin, were used as the main active ingredients of the insecticides [8]. However, cyclodienes were withdrawn from the market due to increasing environmental and public-health concerns, primarily in relation to their persistence in the environment and their tendency to accumulate in the fat of animals and humans [9]. Insecticides used for termite control must undergo a rigorous approval and registration processes, including an assessment for possible effects on human health and the environment. In Australia, for example, use of insecticides is authorized by Australian Pesticides and Veterinary Medicines Authority (APVMA). Currently, several insecticides for termite control have been formulated as alternatives to the cyclodienes and approved for use under different commercial brands [9]. Various main active ingredients can be collectively classified based on their particular chemical structure, including pyrethroids (e.g., alpha-cypermethrin, permethrin, bifenthrin, deltamethrin), organophosphates (e.g., chlorpyrifos), neonicotinoid (e.g., imidacloprid), and phenylpyrazole (e.g., fipronil). These insecticides are less persistent than the cyclodienes, as they have shorter lifetime which can break down relatively quickly [9], and thus their periodic applications on the soils are necessary to provide long-term protection against termites [10]. Consequently, this action could cause enormous waste of the active molecules and allows non-target organisms, householders and pest control operators to be frequently exposed to the chemicals [5, 9]. Therefore, there has been an increasing emphasis in formulation development and application methods for the remedial treatments [11].

Baiting technologies offer an alternative way for treating subterranean termites [4, 12, 13]. Several insecticides have been used in baiting systems including chitin synthesis inhibitor (e.g., hexaflumuron [14], chlorfluazuron [15, 16], noviflumuron [17], and diflubenzuron [16]), avermectins (e.g., ivermectin [18]), and phenylpyrazole (e.g., fipronil [19]). The methods have a number of

advantages as compared to the chemical soil barriers aforementioned: (1) baiting uses small amounts of active molecules that are administered in localized sites [10, 12, 20-22]; (2) active molecules are contained in a food matrix, e.g., paper, cardboard [23], wooden blocks [14, 23-25], cellulose powders [15], and straw pulp and white sugar [19]; (3) baits are usually confined within an impervious bait station; and (4) any remaining baiting materials can be removed and properly disposed after the control actions have been completed [26]. Termite control using baiting technologies exploits termite eusociality to deliver the insecticide from the site where it is applied to the sites where the termites live in colonies [27]. Termites live in complex societies and engage in constant, close-contact interactions with each other within the colonies. These interactions include mutual grooming, cooperative nest construction, larval care, and trophallaxis in which foraging worker termites feed other termites that do not or cannot forage on their own including larvae, reproductive, and soldier termites [28]. Ideally, when termites forage in insecticide-treated areas, they acquire and carry the insecticide, and inadvertently share it with their nestmates during grooming, trophallaxis or both (i.e., horizontal transfer). Subsequently, the horizontal transfer results in mortality at a situation where a lethal dose of the insecticide is transferred from the exposed donor termites to an unexposed recipient termite, and the insecticide is then consumed by the recipient termites. This horizontal transfer could cause colony elimination [26, 29], which is a strategy commonly being exploited for an effective termite control [30].

In recent years, nanotechnology has been developed to manufacture nanocarrier systems for the encapsulation and delivery of insecticides [31-37]. The benefits of using such nanocarriers include: (1) protection of the insecticides from premature decomposition and loss; (2) enhancement of bioavailability especially for hydrophobic insecticides; and (3) delivery of high amounts of insecticides in a sustained manner. As mentioned in **Chapter 1**, some nanomaterials could possibly exert toxicity in the environment depending on many factors, e.g., chemical compositions, physical properties, exposure routes and doses [38, 39]. In order to minimize the risks of nanomaterials in the environment, it is imperative to ensure the development of nanomaterials through responsible nanomanufacturing practices, including minimizing the use of toxic chemicals and using benign conditions for the synthesis of nanomaterials [40, 41]. Previous chapters of this thesis have demonstrated the development of oil-core silica-shell nanocapsules in environmentally friendly conditions without using toxic organic solvents (**Chapters 3–5**). In the context of termite control, **Chapter 4** has investigated the use of the silica nanocapsules as biocompatible nanocarriers of fipronil insecticide in a combination with α-cellulose as the feeding baits against termites. Orphaned colonies of ≈1500 termites comprising workers and soldiers were placed in a container. To deliver fipronil to the colonies, the fipronil-encapsulated silica nanocapsules were mixed with α-cellulose and then used as feeding baits which were connected to the container *via* a clear tube. The results proved that the treated baits could be taken up by foraging workers and brought back to the container. Eventually, the termite colonies were eliminated, probably through horizontal transfer of

the treated baits within the colonies, in 6 days after the applications, while the control group using water-treated baits showed negligible termite mortality during the 8 days of the tests.

Although it has been established that fipronil-encapsulated silica nanocapsules mixed with cellulosic bait matrices can be used to eliminate termite colonies as demonstrated in **Chapter 4**, there is a need to implement termite controls at their natural feeding-sites. Termite species that build epigeal mounds, e.g., *Coptotermes lacteus* (*C. lacteus*) [42], can be useful for examining the efficacy of fipronil-encapsulated silica nanocapsules under field conditions due to easy access to their mounds. The mounds are characterized by an outer earthen wall enclosing a dense woody mass moulded to form an intricate system of galleries [42] containing all castes and stages of termites, including the reproductive, eggs and larvae, soldiers, and workers [25]. Number of termites in a mound was estimated around two millions or more [43]. In this chapter, the designed bifunctional modular protein, D4S2, developed in **Chapter 5** is used for making fipronil-encapsulated silica nanocapsules. This study aims to demonstrate large-scale production of D4S2 protein (≈1.4 g) for making silica nanocapsules encapsulated fipronil (≈0.9 g) which could then be used for termite field trial on three *C. lacteus* mounds in tropical northern Queensland, Australia. The activities of foraging worker termite to remove the treated baits and bring the baits back to their mounds were examined.

6.2 Materials and Methods

6.2.1 Materials

Miglyol® 812 purchased from AXO Industry S.A. (Wavre, Belgium) was passed through heat-activated silica gel (Sigma-Aldrich) prior to use. Fipronil in a form of powder was obtained from Gulmohar Pty. Ltd. (Australia). Water with >18.2 MΩ cm resistivity was obtained from a Milli-Q system with a 0.22 μm filter (Millipore, Australia). Other chemicals were of analytical grade purchased from either Sigma-Aldrich or Merck and used as received unless otherwise stated.

6.2.2 Production of bifunctional modular protein

6.2.2.1. Protein expression and purification

Expression of the bifunctional modular protein, D4S2, in *Escherichia coli* (*E. coli*) BL21(DE3) and subsequent purification were conducted according to the methods described in **Chapter 5** and briefly explained as follows.

Expression: A single colony of *E. coli* containing plasmid DNA, pET-48(+), with inserted nucleotide sequence encoded for D4S2 protein was selected from a freshly-streaked plate and then inoculated

into 5 mL 2x yeast extract and tryptone (2YT) medium (5 g/L NaCl, 16 g/L tryptone, 10 g/L yeast extract, water) and incubated at 30 °C, 180 rpm for 16 h. Main culture of 800 mL was inoculated with 800 µL of overnight culture and incubated at 37 °C, 180 rpm. When the OD_{600} reached approximately 0.5, isopropyl β-D-1-thiogalactopyranoside (IPTG) (Astral Scientific, Australia) was added to the culture to a final concentration of 1 mM, and then incubated at 37 °C, 180 rpm for a further 4 h. A final OD_{600} of approximately 2 was routinely obtained. Cell pellet was harvested by centrifugation at 4 °C, 6250 x*g* for 10 min, washed with the supernatant (40 mL) and then centrifuged at 4 °C, 4700 x*g* for 10 min. The cell-pellet was collected and stored at –80 °C until further processing. All media for cultures were supplemented with 15 µg/mL kanamycin sulfate (Life Technologies, CA, USA).

Purification: To recover D4S2, two cell-pellets were re-suspended and combined in 160 mL lysis buffer (25 mM sodium phosphate, 1.2 M NaCl, 1 M Na_2SO_4, pH 7.5). The mixture was transferred into a 250 mL-conical flask and then incubated at 90 °C with stirring at 1000 rpm for 30 min. The cell lysate was then centrifuged at 20 °C, 51500 x*g* for 5 min. The supernatant was collected and diluted 5-fold with water, and pH was adjusted to pH 3.5 by adding 10 N HCl to allow precipitation of D4S2 protein. Then, the mixture was centrifuged at 4 °C, 33750 x*g* for 30 min. The precipitated sample was re-suspended in equilibrium buffer (25 mM sodium phosphate, 1.2 M NaCl, 20 mM imidazole, pH 7.5) and solubilized by adjusting the pH to pH > 10 using 5 N NaOH.

To remove DNA contaminations, the protein solution was purified through immobilized-metal affinity chromatography (IMAC). Prior to loading, the solution was filtered using a 0.45 µm syringe filter with MF-Millipore® mixed cellulose ester membrane (Millipore, Australia). The filtered solution was then loaded into IMAC column (Ni^{2+} charged IMAC Sepharose High Performance resin, GE Healthcare, UK) pre-equilibrated with 3 column volumes (CV) of equilibrium buffer (25 mM sodium phosphate, 1.2 M NaCl, 20 mM imidazole, pH 7.5) at a flow-rate of 1 mL/min. The column was washed with 2 CV of equilibrium buffer to remove unbound contaminants before the purified D4S2 was eluted with 3 CV of elution buffer (25 mM sodium phosphate, 1.2 M NaCl, 500 mM imidazole, pH 7.5). The pH of the collected fractions was adjusted to pH 5.8 by adding 10 N HCl and ethylenediaminetetraacetic acid disodium salt (EDTA) was added to a final concentration of 20 mM in order to chelate Ni^{2+} ions that might be leaked and bound to histidine residues within D4S2 after the IMAC process.

Following IMAC process, desalting chromatography of the protein solution was conducted using a Sephadex G-25 resin (GE Healthcare, UK). The protein solution was loaded into the column pre-equilibrated with water at a flow rate of 1 mL/min. The protein fraction after the desalting process was collected and lyophilized at –55°C, 0.08 mbar for 16 h.

6.2.2.2 Protein analysis

Qualitative analysis of D4S2 and measurement of D4S2 concentration were conducted by using sodium dodecyl sulfate polyacrylamide gel electrophoresis (SDS-PAGE) and reversed-phase high performance liquid chromatography (RP-HPLC), respectively. SDS-PAGE was performed using NuPAGE Bis-Tris 4–12% gels (Invitrogen), and Novex® sharp pre-stained ladder, using standard methods and staining. RP-HPLC equipped with a Jupiter C_{18} column (5 µm, 300 Å, 150 mm x 4.6 mm) (Phenomenex, CA, USA) and connected to an LC-10AVP series HPLC system (Shimadzu, Japan) was used. Buffer A was 0.1 v/v% trifluoroacetic acid (TFA) in water, and buffer B was 90 v/v% acetonitrile and 0.1 v/v% TFA in water. Gradient conditions applied in the analysis were from 30 to 65% of buffer B in 35 min at a flow rate of 1 mL/min and a set detection wavelength of 214 nm.

6.2.3 Synthesis and characterization of fipronil-encapsulated silica nanocapsules

6.2.3.1 Synthesis

Lyophilized D4S2 protein was dissolved in HEPES buffer (25 mM, pH 7.5) to prepare D4S2 solutions having a concentration of 1.53 mg/mL. Miglyol® 812 was added to the D4S2 solutions (3 mL) with an oil fraction of 10 v/v%, and homogenized using a Branson Sonifier 450 ultrasonicator for four 30 s bursts at 20 W and interspersed in an ice bath for 60 s. The emulsification was repeated and the resulting nanoemulsions were combined to obtain a total of 900 mL nanoemulsion. The nanoemulsion (50 mL) was transferred into a beaker glass containing silica precursor tetraethoxysilane (TEOS, 96 µmol). Biosilicification reaction of the nanoemulsion with TEOS was conducted under magnetic stirring at room temperature for 20 h. The suspension of fipronil-encapsulated silica nanocapsules was washed three times with water by centrifugation at 4 °C, 4500 x*g* for 10 min, and the pellet was kept at 4 °C. Prior to the field trial, the pellet was re-suspended with water through sonication and subjected to characterization for quality control.

6.2.3.2 Characterization

Size distribution was determined by dynamic light scattering (DLS) using Malvern Zetasizer Nano ZS (Malvern Instrument, UK) at a scattering angle of 173° and a temperature of 25 °C. Samples were diluted by a factor of 100 prior to measurement to avoid multiple scattering effects.

Morphology of the silica nanocapsules was visualized by transmission electron microscopy (TEM) using a JEOL 1010 (JEOL, Japan) operated at 100 kV. Samples (2 µL) were deposited onto Formvar-coated copper grids (ProSciTech, Australia). Size of the nanocapsules was analyzed by using iTEM software (version 3.2, Soft Imaging System GmbH).

6.2.4 Field trial

6.2.4.1 Field site

The termite field trial was conducted in an area located near to Compartment 47, State Forest 589, Twins Logging Area at Beerburrum (26°58'S., 152°54'E.), south east Queensland, which contains *C. lacteus* mounds (epigeous nests).

6.2.4.2 Initial field trial

On the 17 October 2014, six *C. lacteus* mounds were selected for field trial. Prior to the field trial, feeding-bait stations were installed to the mounds, aiming to heighten consistency of termite acceptance to the baits. In each mound, two holes having a diameter of 25 mm were drilled, and then two feeding-bait stations were attached to the mound *via* these holes (**Figure 1**a). Each feeding station (**Figure 1**b) consisted of a rectangular plastic container filled with two sapwoods of pine (200 g each), a corrugated cardboard, and lidless plastic vial (100 mL) containing moist α-cellulose baits (15 g dry α-cellulose and 35 g water). The container was drilled (25 mm) so that a plastic conduit (400 mm x 25 mm) can be attached through the container's holes with the open end of the conduit closed (distal from the mound). The conduit was filled with moist corrugated cardboard (450 mm x 15 mm). Then, the container was closed with lid and covered with a black plastic with the conduit protruding toward the mound. Inspections were conducted to the feeding-bait stations after two-week of installation. Live termites were found in most of the feeding stations and termite activity was noticed as the containers contained mud materials built by the termites (**Figure 1**c).

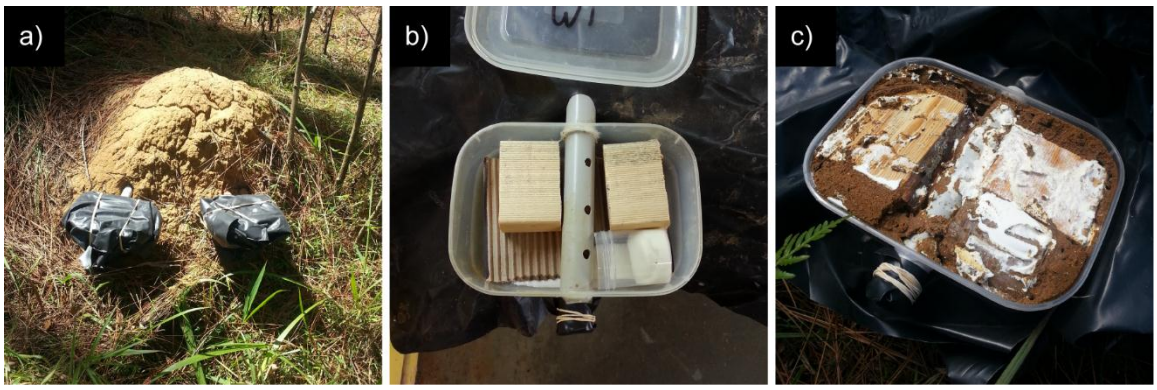

Figure 1. Photographic images describing initial field trial. a) Typical assembly of feeding-bait stations near termite mound. b) A typical container of a feeding-bait station consisted of two sapwoods, a plastic vial containing moist α-cellulose bait, and a plastic conduit sealed at distal end. The conduit had three drill-holes which allowed termites for entering the container. c) Inspection of the container after two weeks of installation of the feeding-bait station confirmed the presence of live termites and termite activity.

6.2.4.3 Field assay and treatment-units installation

From the six *C. lacteus* mounds aforementioned, three mounds were used for controls (Mounds 1–3) and the other three mounds were for treatment (Mounds 4–6) with the fipronil-encapsulated silica nanocapsules (*Section 6.2.3.1*). With the treatment-mounds, two assay chambers labelled as treatment- and monitoring-unit were attached to each mound (Mounds 4–6) *via* drill-holes (25 mm) on the 27 November 2014. Each unit of the assay chambers consisted of a plastic conduit (500 mm x 25 mm) attached through the lid to a clear plastic vial (100 mL) and secured with glue. The conduit and vial were filled with corrugated cardboard and moist α-cellulose, respectively, and the vial was closed with lid and covered with a black plastic with the conduit protruding. The treatment-units contained treated moist α-cellulose baits (15 g dry α-cellulose and 35 g fipronil-encapsulated silica nanocapsules), while the monitoring-units contained untreated moist α-cellulose baits (15 g dry α-cellulose and 35 g water). The untreated baits were replaced, as necessary, at each inspection to keep the termites feeding on the untreated baits. After the treatment-units installation, inspections to the assay chambers were conducted weekly.

6.2.4.4 Monitoring colony health

During the treatment, a hole (25 mm) was drilled into the side of each mound using a portable drill, and a plastic conduit (300 mm x 20 mm) was inserted about two-thirds of its length into the hole. A 400 mm-long hardwood dowel was inserted into the conduit, in which fresh dowels were used at each inspection. The presence of termites, faecal mottling, and feeding on the dowel was used as

an indicator of an active colony. Commencing at the second inspection (10 December 2014), a hole (25 mm) was drilled into the side of each mound using a portable drill. The hole was left open, and repairs by the termites were noted at the next inspection indicating an active colony.

A Termatrac®T3i (Termatrac® Pty. Ltd., Australia) was used during each inspection to detect movement of live termites in the plastic units attached to the treatment-mounds. A wooden platform was clipped to the plastic conduit to stabilize the T3i sensor unit.

The temperature in the termite mounds was monitored to track colony health as healthy termite colonies maintain relatively constant temperature in their mounds [44-46]. Ten iButton temperature loggers (Thermochron DS1920) (Alfa-Tek Australia Pty. Ltd.) were used to monitor temperature variation at two locations i.e., inside and outside the mounds. An iButton was secured into a plastic conduit (300 mm x 25 mm) and inserted proximal to each of the 6 mounds, whereas the other four temperature loggers were affixed to trees near the mounds to measure ambient temperature. The iButtons were programmed to record temperature once an hour.

6.3 Results and Discussion

In this study, three mounds were used for the termite field trial. Amount of fipronil needed for termite elimination in one mound was estimated at approximately 300 mg [47], and thus a total of 900 mg was required to treat three termite mounds. It was known that solubility of fipronil in Miglyol® 812 oil used to make nanoemulsions was 10 mg/mL (**Chapter 3**), and as much as 1.53 mg/mL of D4S2 can be used to stabilize nanoemulsions having Miglyol® 812 oil fraction of 10 v/v% (**Chapter 5**). Therefore, to load 900 mg fipronil in D4S2-stabilized nanoemulsions having oil fraction of 10 v/v%, 900 mL of nanoemulsion was required, with total D4S2 of approximately 1.4 g. The nanoemulsions can then be encapsulated with silica shell forming fipronil-encapsulated silica nanocapsules upon addition of silica precursor tetraethoxysilane.

6.3.1 Large-scale preparation of fipronil-encapsulated silica nanocapsules

Bifunctional modular protein, D4S2, was used in this study for making silica nanocapsules that encapsulated fipronil insecticide. D4S2 was produced through biological expression in *E. coli*, as developed in **Chapter 5**. The expression of D4S2 in *E. coli* was induced by adding isopropyl β-D-1-thiogalactopyranoside (IPTG) at 37 °C when optical density of the microbial culture at 600 nm (OD_{600}) reached at approximately 0.5. After the expression at 37 °C for about 4 h ($OD_{600} \approx 2$) (**Figure 2**, lane 3), the *E. coli* cells containing D4S2 protein were harvested, washed, and stored in a form of cell pellets at –80 °C for further use.

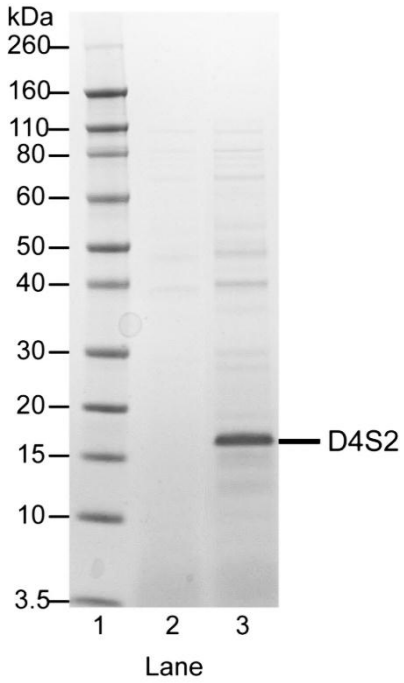

Figure 2. Sodium dodecyl sulfate polyacrylamide gel electrophoresis (SDS-PAGE) result for the expression of D4S2 protein in *E. coli*. (Lane 1) Novex® sharp pre-stain protein standard; (Lane 2) total protein before induction; and (Lane 3) total protein after induction at 37 °C for 4 h.

Two-step purification processes were conducted to obtain D4S2 with high purity. At the first purification step, D4S2 was recovered from the *E. coli* cell pellets by heating/cell lysis and contaminant precipitation, and dilute precipitation. The heating/cell lysis and contaminant precipitation was conducted by firstly re-suspending the cell pellet in lysis buffer (25 mM sodium phosphate buffer pH 7.5, 1.2 M NaCl, 1 M Na_2SO_4) and then heating the suspension at 90 °C under constant stirring for 30 min. The heating process disrupted the cell walls and released the intracellular proteins including D4S2 and other contaminants (e.g., DNA) into the bulk phase, while precipitated most of the proteins and cell debris except D4S2 that remained soluble as concentrated Na_2SO_4 salted-in the protein. Simple centrifugation step removed almost all protein contaminants (**Figure 3**, lane 1) and yielded supernatant solution containing most of the D4S2 protein with little contamination (**Figure 3**, lane 2). The supernatant solution was then diluted five times with water and adjusted the solution pH to 3.5 to precipitate D4S2 protein, as such a low Na_2SO_4 concentration was insufficient to salt-in D4S2, and separate most medial salts and DNA contaminants that remained in the supernatant solution.

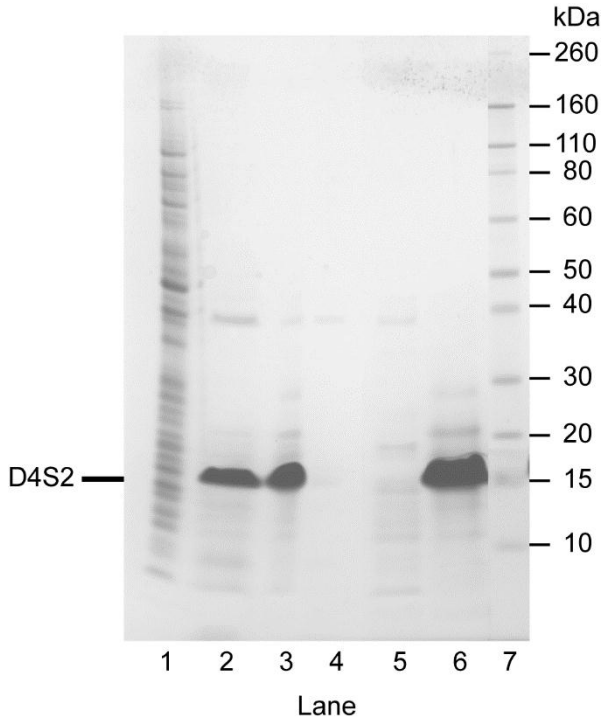

Figure 3. Sodium dodecyl sulfate polyacrylamide gel electrophoresis (SDS-PAGE) result after precipitation-based purification and immobilized-metal affinity chromatography (IMAC) processes. (Lane 1) Re-suspended precipitate and (Lane 2) supernatant after heating/cell lysis and contaminant precipitation step; (Lane 3) Solubilized precipitate after dilute precipitation step; (Lane 4) Passed-through fraction, (Lane 5) washed fraction and (Lane 6) eluted fraction after IMAC process; (Lane 7) Desalted D4S2; (Lane 7) Novex® sharp pre-stain protein standard.

At the second purification step, immobilized-metal affinity chromatography (IMAC) and desalting chromatography were conducted to obtain high purity of D4S2 (**Figure 4**). The precipitated sample was re-suspended in equilibrium buffer (25 mM sodium phosphate, 1.2 M NaCl, 20 mM imidazole, pH 7.5) and solubilized by adjusting the pH to pH > 10 using 5 N NaOH (**Figure 3**, lane 3). The solubilized sample was filtered and then loaded into the IMAC column (**Figure 4**a). During loading, D4S2 bound to the column through its histidine residues, and other unbound materials including DNA were passed through the column (**Figure 3**, lane 4). The column containing bound D4S2 was washed with 3 column volume (equivalent to 16.5 mL) of the equilibrium buffer to further remove unbound materials from the column (**Figure 3**, lane 5). D4S2 can then be eluted from the column using elution buffer containing high concentration of imidazole (25 mM sodium phosphate, 1.2 M NaCl, 500 mM imidazole, pH 7.5) (**Figure 3**, lane 6). To remove salts in the eluted fractions of the IMAC, desalting chromatography using G-25 column was used (**Figure 4**b). After the desalting process, a final yield of D4S2 protein of approximately 7 mg with DNA concentration lower than 2 ng DNA/mg D4S2 was obtained (**Figure 5**).

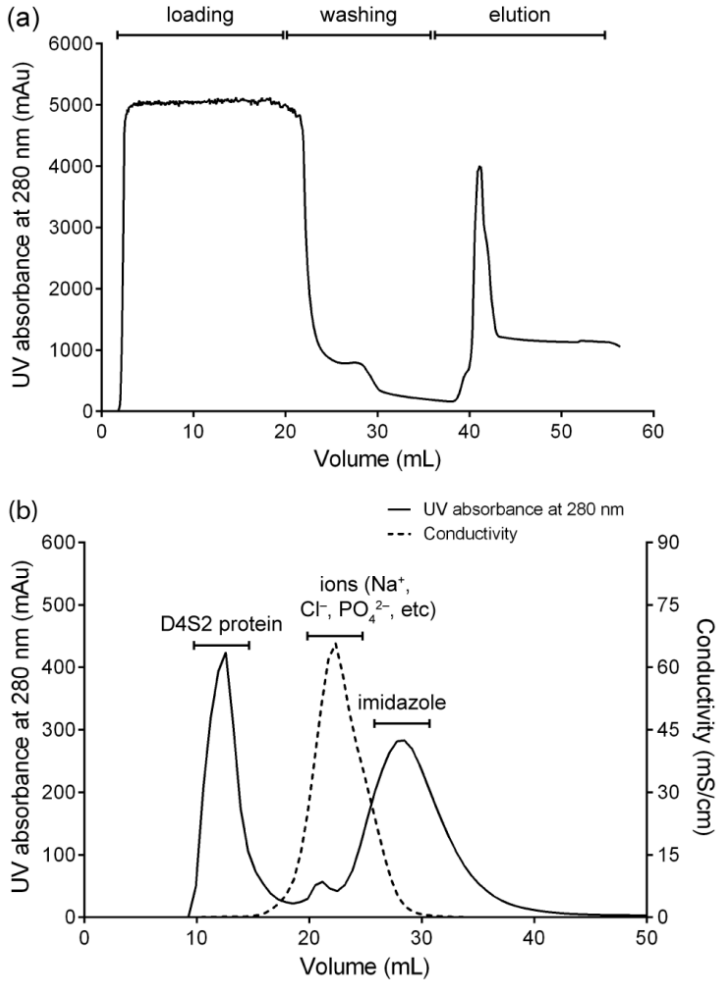

Figure 4. Representative chromatography profiles of D4S2 purification. a) Immobilized-metal affinity chromatography. b) Desalting chromatography.

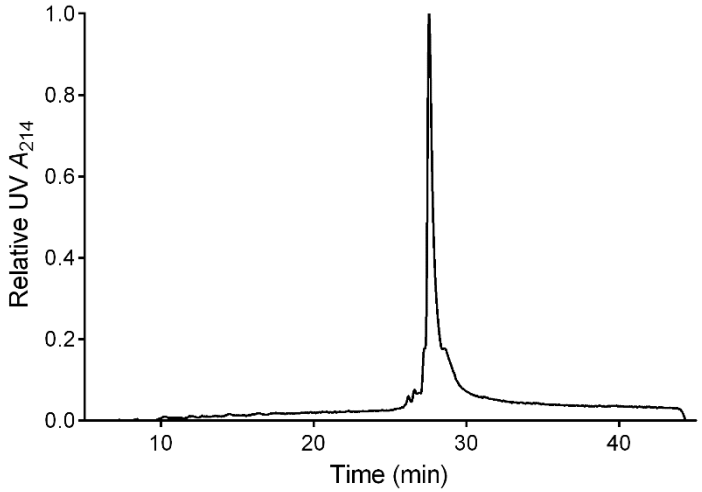

Figure 5. Characterization of D4S2 using reversed-phase high-performance liquid chromatography (RP-HPLC) showing high purity of D4S2.

In this study, fipronil was dissolved in Miglyol® 812 at a concentration of 10 mg/mL (**Figure 6**). The fipronil-loaded oil (0.3 mL) was mixed with HEPES buffer (25 mM, pH 7.5) in the presence of D4S2 protein (3 mL) *via* sonication, and the nanoemulsions were obtained due to the presence of the surface active module in the emulsifying protein (**Figure 7**). As much as 50 mL of the nanoemulsions were combined and then reacted with silica precursor tetraethoxysilane (TEOS) (96 µmol) to form silica shell encasing the nanoemulsion core at near-neutral pH and room temperature without using any toxic chemicals (**Figures 7 and 8**). The biosilicification process at the oil–water interfaces was due to the catalytic role of densely packed cationic arginine (R) and lysine (K) residues of biosilicification-active module as well as polar residues of surface-active module exposed toward the bulk aqueous solution that can induce hydrolysis of TEOS and interfacial polycondensation of the hydrolysis products. Morphology of the silica nanocapsules was visualized by using transmission electron microscopy (TEM) which showed a core–shell structure (**Figure 8**). The measured shell thickness, as determined by using TEM, of the silica nanocapsules was 57 ± 9 nm, while the outer diameter was 302 ± 16 nm.

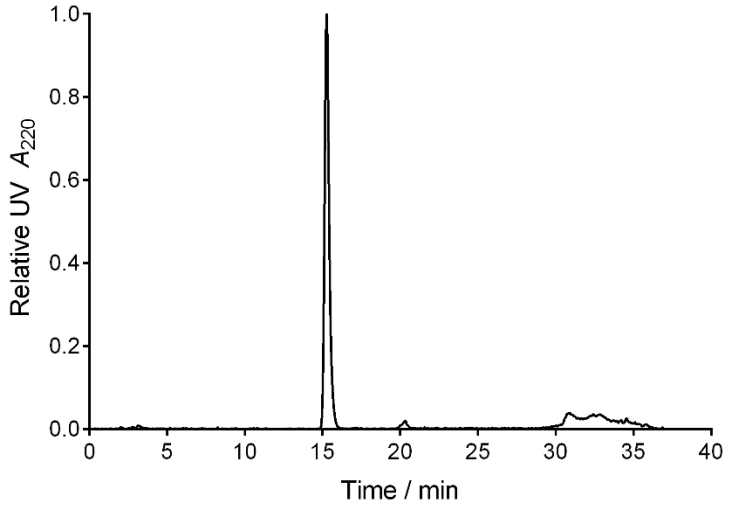

Figure 6. Reversed-phase high-performance liquid chromatography (RP-HPLC) analysis of fipronil-saturated Miglyol® 812 oil that was mixed with acetonitrile 60 v/v%. Miglyol® 812 oil was saturated with fipronil, and the oil was then centrifuged. The collected supernatant (2 µL) was mixed with acetonitrile 60 v/v% (998 µL) until it became homogeneous and then loaded into RP-HPLC (C_{18} column). Phosphoric acid 0.1 v/v% (A) and 90 v/v% acetonitrile, 0.1 v/v% phosphoric acid (B) were used as the mobile phases. A linear gradient from 50 to 70% B in 20 min at a flow rate of 1 mL/min was used with a monitoring wavelength set at 220 nm.

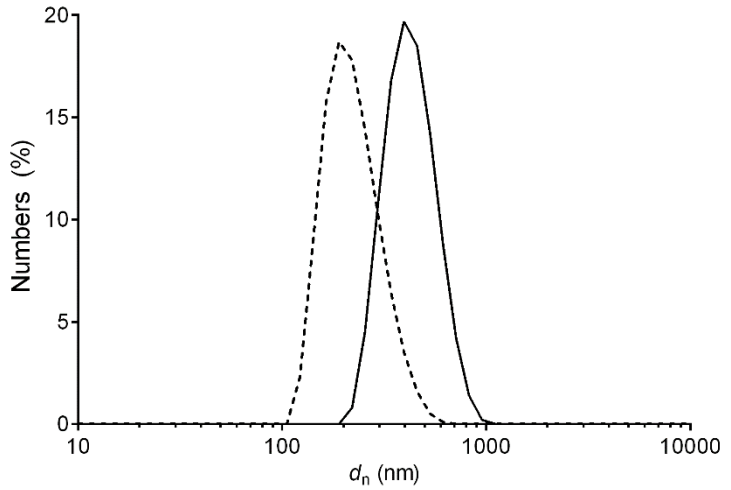

Figure 7. Representative size distribution profiles of nanoemulsions and silica nanocapsules encapsulating fipronil insecticide as measured by using dynamic light scattering. Fipronil-loaded nanoemulsions (-----) and fipronil-encapsulated silica nanocapsules (——).

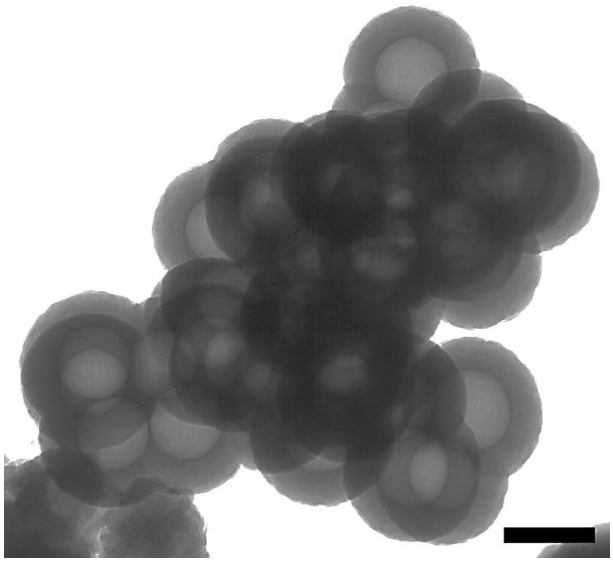

Figure 8. Representative transmission electron microscopy (TEM) image of fipronil-encapsulated silica nanocapsules formed using bifunctional modular D4S2 protein. Scale bar is 200 nm.

6.3.2 Termite field trial

Three treatment-units containing the treated baits (i.e., mixture of α-cellulose and fipronil-encapsulated silica nanocapsules) were placed separately and connected to three mounds (Mounds 4–6) *via* plastic conduits. At the side of each treatment-unit, a monitoring-unit containing untreated bait was also installed. It is generally agreed that follow-up monitoring of a site is usually necessary to ensure that a baiting program is successful [48]. Therefore, termite activities were inspected weekly.

At the first inspection (6 December 2014), live termites were seen in at least one unit in each mound. The termites were actively feeding on the baits in which ≤50% of the baits in each unit were consumed within 9 days. This was important as neither the conduits nor the vials appeared to be “sealed-off” from the mound suggesting that the termites responded well to the baits.

At the second inspection (10 December 2014), termites were actively moving in plastic conduits attached to Mounds 4 and 6 as indicated by Termatrac device. Live termites were also observed in the treatment- and monitoring-units placed in these mounds. The baits in the two treatment-units and one monitoring-unit were almost completely consumed by the termites as minimum amount of the baits were noticed in the units. There was little additional bait removal in the remaining monitoring-unit. In Mound 5, termites were not active in plastic conduit as indicated by Termatrac device, but termites were found in the treatment- and monitoring-units. Additional bait removal from

both of the units (Mound 5) was minimal. Mud materials built by the termites were also visible at the inside of most units. To monitor colony activity inside the mounds, two holes (22 mm) were drilled into each mound, and a plastic conduit (300 mm x 20 mm) and a timber dowel (400 mm x 19 mm) were inserted into one hole, while the other hole was left open.

At the third inspection (15 December 2014), termites were active in both plastic conduits attached to Mounds 5 and 6, as indicated by Termatrac, and live termites were seen in the treatment-units. The drill-hole in the mounds was filled and the dowel secured suggesting that the termite colonies in the mounds were alive. In Mound 5, little additional bait was removed before the termites plugged the conduit. In Mound 4, termites were not active in either plastic conduit, as indicated by Termatrac, and there were no live termites observed in the treatment-unit. The drill-hole in the mound had not been filled but the dowel secured suggesting that the termite colonies were alive. New drill-holes were made in Mounds 4–6.

The inspections were continued on weekly basis. At six week after installation of the treatment-units, all mounds with the treated baits (Mounds 4–6) contained active termite populations. Unlike laboratory experiments, many variables can affect the viability of a termite colony at the field site, including seasonal weather patterns, the number of alternative food sources available nearby the mound [49], presence of predation (e.g., ants [15]), population density or age of colony [50], and different castes of termites that have difference susceptibility on insecticide [51]. Due to these challenges and the cryptic lifestyle of subterranean termites [52], many baiting programme can take up to nine months (e.g., 3–9 months [14], 7 months [53], 3–7 months [54]). In our case, a consistently significant reduction in consumption of the treated baits from the treatment-units was observed during the six weeks of treatments which leaded to removal of the entire baits by the termites in Mounds 4 and 6 within three weeks of treatments, while most treated baits still remained in the treatment-units in Mound 5.

6.4 Conclusion

In this chapter, D4S2 was produced at approximately 1.4 g by biological expression in *E. coli* and then purified using precipitation- and chromatography-based purification processes. Prior to emulsification using D4S2, fipronil (≈0.9 g) was dissolved in Miglyol® 812 oil at a concentration of 10 mg/mL. D4S2 (1.53 mg/mL) was then used to emulsify the fipronil-loaded oil (10 v/v%), and the resulted nanoemulsions were reacted with silica precursor tetraethoxysilane to form fipronil-encapsulated silica nanocapsules having outer diameter of 302 ± 16 nm and shell thickness of 57 ± 9 nm. In termite field trial, the nanocapsules were mixed with α-cellulose baits placed in three treatment-units, in which the units were then attached separately to three mounds of termite *C. lacteus* in northern Queensland, Australia. At three week of the treatments, the result showed that

the treated baits were removed by the termites from the treatment-units, with no evidence of repellence. At six week of the treatments, the termite colonies in the three mounds are still alive, thus the field trial was continued and is still on-going. The time required for elimination of the colonies would be difficult to be predicted as it relies on the seasonal weather patterns, the number of alternative food sources available nearby the mound, presence of predation, population density or age of colony, and different castes of termites that have difference susceptibility on the insecticide. Nevertheless, the preliminary result indicated that the termites responded well to the treated baits as they readily removed the baits from the treatment-units within three weeks of treatments, providing a chance that the baits would be transmitted to other termites within the mounds through horizontal transfer which could then lead to potential elimination of the termite colonies.

References

1. Verma, M., S. Sharma, and R. Prasad, *Biological alternatives for termite control: a review.* Int. Biodeter. Biodegr., 2009. **63**(8): p. 959–972.
2. Rouland-Lefevre, C., *Termites as Pests of Agriculture*, in *Biology of Termites: A Modern Synthesis*, D.E. Bignell, Y. Roisin, and N. Lo, Editors. 2011, Springer: London. p. 499–517.
3. Broadbent, S., *A Stand-Alone Termite Management Technology in Australia*, in *Urban Pest Management: An Environmental Perspective*, P. Dhang, Editor. 2011, CAB International: London. p. 145–155.
4. Rust, M.K. and N.-Y. Su, *Managing social insects of urban importance.* Annu. Rev. Entomol., 2012. **57**(-): p. 355–375.
5. Hu, X.P., *Liquid Termiticide: Their Role in Subterranean Termite Management*, in *Urban Pest Management: An Environmental Perspective*, P. Dhang, Editor. 2011, CAB International: Oxfordshire. p. 114–132.
6. Gahlhoff, J.E. and P.G. Koehler, *Penetration of the eastern subterranean termite into soil treated at various thicknesses and concentrations of Dursban TC and Premise 75.* J. Econ. Entomol., 2001. **94**(-): p. 486–491.
7. *Termite protection: available treatments and hazard information about termiticides*. Chemical Review and International Harmonisation Section (Office of Chemical Safety, Therapeutic Goods Administration) and Janet Salisbury Last Update Date: 7 March 2007.
8. Peters, B.C. and C.J. Fitzgerald, *Developments in termite management in Queensland, Australia: life after cyclodienes (Isoptera).* Sociobiology, 2007. **49**(3): p. 231–249.
9. Boyd, A.M., et al., *Environmental effects of currently used termiticides under Australian conditions*. 2002, National Research Centre for Environmental Toxicology: Brisbane.
10. Su, N.Y. and R.H. Scheffrahn, *A review of subterranean termite control practices and prospects for integrated pest management programs.* IPM Rev., 1998. **3**(-): p. 1–13.

11. Esenther, G.R. and R.H. Beal, *Attractant-mirex bait suppresses activity of Reticulitermes spp.* J. Econ. Entomol., 1974. **67**(1): p. 85–88.
12. Gautam, B.K. and G. Henderson, *Escape behavior of the Formosan subterranean termite (Isoptera: Rhinotermitidae) in response to disturbance.* J. Insect Behav., 2012. **25**(1): p. 70–79.
13. Henderson, G., *Practical considerations of the Formosan subterranean termite in Louisiana: a 50-year-old problem.* Sociobiology, 2001. **37**(2): p. 281–292.
14. Su, N.Y., *Field-evaluation of a hexaflumoron bait for population suppression of subterranean termites (Isoptera, Rhinotermitidae).* J. Econ. Entomol., 1994. **87**(2): p. 389–397.
15. Peters, B.C. and C.J. Fitzgerald, *Field evaluation of the bait toxicant chlorfluazuron in eliminating Coptotermes acinaciformis (Froggatt) (Isoptera : Rhinotermitidae).* J. Econ. Entomol., 2003. **96**(6): p. 1828–1831.
16. Rojas, M.G. and J.A. Morales-Ramos, *Field evaluation of nutritionally-based bait matrix against subterranean termites (Isoptera : rhinotermitidae).* Sociobiology, 2003. **41**(1A): p. 81–90.
17. Cabrera, B.J. and E.M. Thoms, *Versatility of baits containing noviflumuron for control of structural infestations of formosan subterranean termites (Isoptera : Rhinotermitidae).* Fl. Entomol., 2006. **89**(1): p. 20–31.
18. Wang, Z.Y., et al., *Control of dam termites with a monitor-controlling device (Isoptera : Termitidae).* Sociobiology, 2007. **50**(2): p. 399–407.
19. Huang, Q.Y., C.L. Lei, and D. Xue, *Field evaluation of a fipronil bait against subterranean termite Odontotermes formosanus (Isoptera : Termitidae).* J. Econ. Entomol., 2006. **99**(2): p. 455–461.
20. Grace, J.K. and N.Y. Su, *Evidence supporting the use of termite baiting systems for long-term structural protection (Isoptera).* Sociobiology, 2001. **37**(2): p. 301–310.
21. Pawson, B.M. and R.E. Gold, *Evaluation of baits for termites (Isoptera: Rhinotermitidae) in Texas.* Sociobiology, 1996. **28**(3): p. 485–510.
22. Wang, C. and G. Henderson, *Evaluation of three bait materials and their food transfer efficiency in Formosan subterranean termites (Isoptera: Rhinotermitidae).* J. Econ. Entomol., 2012. **105**(5): p. 1758–1765.
23. Evans, T.A. and P.V. Gleeson, *The effect of bait design on bait consumption in termites (Isoptera : Rhinotermitidae).* Bull. Entomol. Res., 2006. **96**(1): p. 85–90.
24. Neoh, K.-B., N.A. Jalaludin, and C.-Y. Lee, *Elimination of field colonies of a mound-building termite Globitermes sulphureus (Isoptera: Termitidae) by bistrifluron bait.* J. Econ. Entomol., 2011. **104**(2): p. 607–613.
25. Evans, T.A., *Rapid elimination of field colonies of subterranean termites (Isoptera: Rhinotermitidae) using bistrifluron solid bait pellets.* J. Econ. Entomol., 2010. **103**(2): p. 423–432.

26. Schoknecht, U., D. Rudolph, and H. Hertel, *Termite control with microencapsulated permethrin.* Pestic. Sci., 1994. **40**(1): p. 49–55.
27. Buczkowski, G., C.W. Scherer, and G.W. Bennett, *Toxicity and horizontal transfer of chlorantraniliprole in the eastern subterranean termite.* J. Econ. Entomol., 2012. **105**(5): p. 1736–1745.
28. Buczkowski, G., C. Wang, and G. Bennett, *Immunomarking reveals food flow and feeding relationships in the eastern subterranean termite, Reticulitermes flavipes (Kollar).* Environ. Entomol., 2007. **36**(1): p. 173–182.
29. Vargo, E.L., *Genetic structure of Reticulitermes flavipes and R. virginicus (Isoptera : Rhinotermitidae) colonies in an urban habitat and tracking of colonies following treatment with hexaflumuron bait.* Environ. Entomol., 2003. **32**(5): p. 1271–1282.
30. Myles, T.G., *Development and evaluation of a transmissible coating for control of subterranean termites.* Sociobiology, 1996. **28**(3): p. 373–457.
31. Ghormade, V., M.V. Deshpande, and K.M. Paknikar, *Perspectives for nano-biotechnology enabled protection and nutrition of plants.* Biotechnol. Adv., 2011. **29**(6): p. 792–803.
32. Gogos, A., K. Knauer, and T.D. Bucheli, *Nanomaterials in plant protection and fertilization: current state, foreseen applications, and research priorities.* J. Agric. Food Chem., 2012. **60**(39): p. 9781–9792.
33. Kah, M., et al., *Nanopesticides: state of knowledge, environmental fate, and exposure modeling.* Crit. Rev. Env. Sci. Technol., 2013. **43**(16): p. 1823–1867.
34. Kah, M. and T. Hofmann, *Nanopesticide research: current trends and future priorities.* Environ. Int., 2014. **63**: p. 224–235.
35. Kumari, A. and S.K. Yadav, *Nanotechnology in agri-food sector.* Crit. Rev. Food Sci., 2014. **54**(8): p. 975–984.
36. Mulqueen, P., *Recent advances in agrochemical formulation.* Adv. Colloid Interface Sci., 2003. **106**(-): p. 83–107.
37. Pérez-de-Luque, A. and D. Rubiales, *Nanotechnology for parasitic plant control.* Pest Manag. Sci., 2009. **65**(5): p. 540–545.
38. Oberdörster, G., E. Oberdörster, and J. Oberdörster, *Nanotoxicology: An emerging discipline evolving from studies of ultrafine particles.* Environ. Health Perspect., 2005. **113**(7): p. 823–839.
39. Nel, A., et al., *Toxic potential of materials at the nanolevel.* Science, 2006. **311**(5761): p. 622–627.
40. Albrecht, M.A., C.W. Evans, and C.L. Raston, *Green chemistry and the health implications of nanoparticles.* Green Chem., 2006. **8**(5): p. 417–432.
41. Hull, M.S., et al., *Sustainable Nanotechnology: A Regional Perspective*, in *Nanotechnology Environmental Health and Safety: Risks, Regulation, and Management*, M. Hull and D. Bowman, Editors. 2014, Elsevier: Oxford.

42. Hill, R.F., *Termites (Isoptera) from the Australian Region*. 1942, Melbourne, Australia: CSIR.
43. Evans, T.A., M. Lenz, and P.V. Gleeson, *Estimating population size and forager movement in a tropical subterranean termite (Isoptera : Rhinotermitidae).* Environ. Entomol., 1999. **28**(5): p. 823–830.
44. Holdaway, F.G. and F.J. Gay, *Temperature studies of the habitat of Eutermes exitiosus with special reference to the temperatures within the mound.* Aust. J. Council Sci. Res., series B., 1948. **1**(4): p. 464–493.
45. Korb, J. and K.E. Linsenmair, *The effects of temperature on the architecture and distribution of Macrotermes bellicosus (Isoptera, Macrotermitinae) mounds in different habitats of a West African Guinea savanna.* Insectes Soc., 1998. **45**(1): p. 51–65.
46. Lüscher, M., *Air-conditioned termite nests.* Sci. American, 1961. **205**(1): p. 138–145.
47. Peters, B.C., *Personal communication*. 2014.
48. Thorne, B.L. and B.T. Forschler, *Criteria for assessing efficacy of stand-alone termite bait treatments at structures.* Sociobiology, 2000. **36**(1): p. 245-255.
49. Forschler, B.T. and J.C. Ryder, *Subterranean termite, Reticulitermes spp (Isoptera: Rhinotermitidae), colony response to baiting with hexaflumuron using a prototype commercial termite baiting system.* J. Entomol. Sci., 1996. **31**(2): p. 143–151.
50. Jones, S.C., *Effects of population density on tunneling by formosan subterranean termite (Isoptera: Rhinotermitidae) through treated soil.* J. Econ. Entomol., 1990. **83**(3): p. 875–878.
51. Ibrahim, S.A., G. Henderson, and H.X. Fei, *Toxicity, repellency, and horizontal transmission of fipronil in the formosan subterranean termite (Isoptera : Rhinotermitidae).* J. Econ. Entomol., 2003. **96**(2): p. 461–467.
52. Getty, G.M., et al., *Response of Reticulitermes spp. (Isoptera : Rhinotermitidae) in northern California to baiting with hexaflumuron with sentricon termite colony elimination system.* J. Econ. Entomol., 2000. **93**(5): p. 1498–1507.
53. Tsunoda, K., H. Matsuoka, and T. Yoshimura, *Colony elimination of Reticulitermes speratus (Isoptera : Rhinotermitidae) by bait application and the effect on foraging territory.* J. Econ. Entomol., 1998. **91**(6): p. 1383–1386.
54. Su, N.Y., P.M. Ban, and R.H. Scheffrahn, *Control of Coptotermes havilandi (Isoptera : Rhinotermitidae) with hexaflumuron baits and a sensor incorporated into a monitoring and baiting program.* J. Econ. Entomol., 2000. **93**(2): p. 415–421.

Chapter 7

Conclusions and future work

This thesis aims to discover and develop new methods and knowledge for the manufacture of biocompatible oil-core silica-shell nanocapsules. The novelty of the approach developed in this thesis is to design bifunctional modular biomolecules (i.e., peptide and protein), in lieu of conventional chemical surfactants, which are designed at the amino-acid level to contain surface-active module and biosilicification-active module. The modular design has enabled an environmentally-friendly (i.e., near-neutral pH, ambient temperature and pressure without using any of toxic organic solvents), sustainable and scalable approach for the synthesis of silica nanocapsules. This thesis also demonstrates the application of the silica nanocapsules for encapsulation and release of fipronil insecticide in a controlled manner in the context of termite control.

7.1 Summary of research findings

Through various strategies in biomimetic silicification, researchers have found ways to transfer the biological principles into synthetic processes to invent biomimetic approaches for the synthesis of silica-based nanomaterials under benign conditions. The use of biomolecules has the advantages of high biodegradability as well as a likely high biocompatibility. An additional advantage of using biomolecules is the ability to be produced renewably at large scale and relatively low cost using microbial cell-factory *Escherichia coli* (*E. coli*) [1, 2].

Silica-based nanomaterials having various morphologies have been fabricated based on the self-assembly of peptides in bulk aqueous solutions and at solid–liquid interface [3-5] (**Figure 1**). Yet, there is no current biomimetic approaches for making silica nanocapsules having oil-core silica-shell morphology. Although there is a number of peptides that are able to facilitate formation and stabilization of oil-in-water (O/W) nanoemulsions [6], they have never been demonstrated capable of inducing formation of silica at the oil–water interfaces.

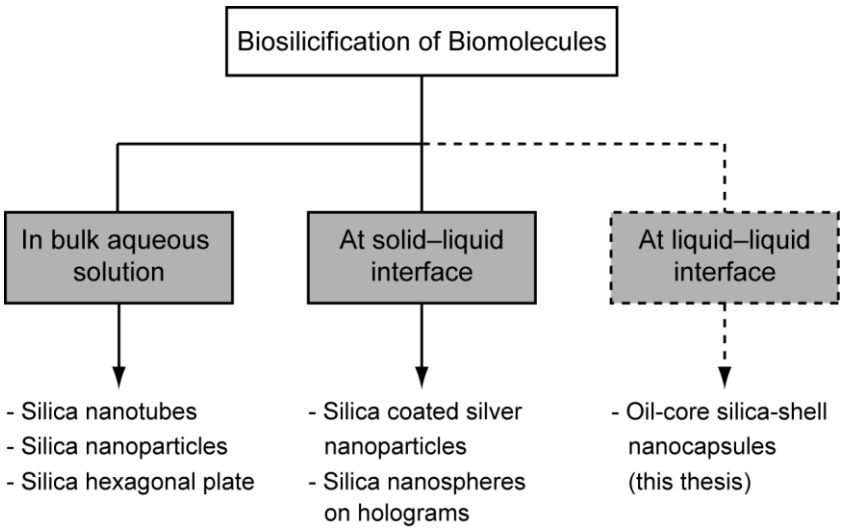

Figure 1. Applications of biosilicification of biomolecules. Solid lines represent the flow of research that has been conducted to date from biosilicification of biomolecules in bulk aqueous solution (to yield silica nanotubes [7-9], silica nanoparticles [10-12], silica hexagonal plate [13]) and at solid–liquid interface (to yield silica coated silver nanoparticles [14] and silica nanospheres on holograms [15]). Dashed lines represent researches that have not been done prior to this PhD thesis.

Figure 1 indicates a missing link of the biosilicification of biomolecules at liquid–liquid interface. This PhD thesis is aimed to bridge this gap, by designing bifunctional modular biomolecules comprising of surface-active module and biosilicification-active module. The design enables the designed biomolecules to facilitate formation and stabilization of nanoemulsion and to direct nucleation and growth of silica on the surface of the nanoemulsion under environmentally-friendly conditions. Therefore, a novel emulsion and biomimetic dual-templating approach has been developed in this thesis for the synthesis of biocompatible oil-core silica-shell nanocapsule. Furthermore, the silica nanocapsule was examined as a biocompatible nanocarrier of insecticide for agricultural applications, utilizing fipronil and subterranean termite as model insecticide and insect, respectively.

There are four specific key points addressed through experimental work in this thesis:

(1) Design of a bifunctional modular peptide (**Chapter 3**) – this study showed that modularization of a surface-active module with a biosilicification-active module in the designed bifunctional modular peptide was essential for the effective formation of silica at oil–water interfaces. The mechanistic actions of the dual-functionality of the designed peptide were discussed, including for stabilizing nanoemulsions core and directing interfacial biosilicification forming silica shell with tunable shell thickness.

(2) Application of silica nanocapsules to encapsulate and release fipronil insecticide for termite control in a laboratory scale (**Chapter 4**) – this study demonstrated facile encapsulation of fipronil with high-capacity loading in silica nanocapsules synthesized using the bifunctional modular peptide. The controllable releases of the insecticide *in vitro* in water and *in vivo* against termites in a laboratory scale were highlighted.

(3) Design and microbial-production of a bifunctional modular protein (**Chapter 5**) – the bifunctional modular peptide was re-designed by joining its biosilicification-active module with a variant of DAMP4 protein module [16]. The modular combination design allowed the protein to be produced via *E. coli* expression system. The expression and purification processes to obtain the protein were evaluated. The dual functionalities of the protein to synthesize oil-core silica-shell nanocapsules were tested.

(4) Large-scale production and field application of fipronil-encapsulated silica nanocapsules for termite field trial (**Chapter 6**) – this study was conducted to produce the bifunctional modular protein through *E. coli* in a large scale to synthesize fipronil-encapsulated silica nanocapsules which could then be used for termite field trial.

The following sections discuss the key research findings of this project in more detail.

7.1.1 Design of a bifunctional modular peptide

(1) Peptide having surface activity is insufficient for effective formation of oil-core silica-shell nanocapsules

Peptide surfactant AM1 (Ac-MKQLADS LHQLARQ VSRLEHA-$CONH_2$) [17] known for its ability to facilitate formation and stabilization of nanoemulsions [18] was used to test whether it could accelerate hydrolysis and condensation of silica precursor tetraethoxysilane (TEOS) at oil–water interfaces. The biosilicification reaction between TEOS presence in bulk solutions and AM1 peptide molecules located at the surfaces of oil droplets compromised the ability of AM1 to stabilize the nanoemulsions. Silica nanocapsules could not be efficiently formed without a significant formation of bulk silica precipitates as the surface activity of AM1 is sacrificed when this module was used for inefficient interfacial biosilicification. Therefore, a bifunctional modular peptide was designed by modularizing part of AM1 sequence with a specialized sequence specific to silica.

(2) Design of a bifunctional modular peptide comprising a surface-active module and a biosilicification-active module is necessary to effectively form silica nanocapsules

Based on the results of AM1 on the interfacial biosilicification, SurSi peptide (Ac-*MKQLAHS VSRLEHA* RKKRKKRKKRKKGGGY-$CONH_2$) was designed by modularizing part of the peptide surfactant AM1 for surface activity [17] (Sur module, *MKQLAHS VSRLEHA*) with a sequence for biosilicification (Si module, RKKRKKRKKRKKGGGY). Sur was designed based on heptads of AM1 (MKQLADS VSRLEHA), except that aspartic acid (D) at position 6 was replaced by histidine (H). Si module contained densely packed cationic lysine (K) and arginine (R) residues derived from high-yield TiO_2-precipitating dTi-1(RKK) peptide (RKKRKKRKKRKKGGGW) [19] except that the hydrophobic amino acid tryptophan (W) was replaced with tyrosine (Y). SurSi peptide has been demonstrated capable of facilitating formation and stabilization of nanoemulsions through amphiphilic nature of the Sur module. While hydrophobic residues in the Sur module faced toward oil phase, hydrophilic residues oriented away from the oil phase with the Si module projecting toward bulk aqueous phase. SurSi peptide was also shown capable of directing nucleation and growth of silica at the oil–water interfaces through Si module having the capacities to promote hydrogen-bonding and electrostatic interactions with silica species. Hypothetically, based on the literature, polar amino acid residues within SurSi, including serine (S), tyrosine (Y), histidine (H) and glutamine (Q), promote nucleophilic attack on the silicon atom within TEOS [20, 21] and thus facilitate its hydrolysis to produce silanol and negatively-charged silanolate. Positively-charged arginine (R) and lysine (K) residues interact electrostatically with silanolate at near-neutral pH, while the hydroxyls of serine (S) and tyrosine (Y) promote hydrogen bonding with silanol [10], which in turn act as nucleation sites to direct silica growth through polycondensation of the silica species at the interface. As a result of the synergistic actions of these functionalities, SurSi peptide was able to facilitate formation and stabilization of nanoemulsions (comprising 2 v/v% Miglyol® 812 oil) and direct nucleation and growth of amorphous silica shells surrounding the nanoemulsion cores.

(3) Silica shell thickness is tunable

The silica shell thickness could be tuned simply by controlling reaction pH, reaction time and silica precursor tetraethoxysilane (TEOS) concentration. Reaction of SurSi-based nanoemulsions and TEOS having concentrations of 8 µmol, 16 µmol and 32 µmol in 25 mM HEPES buffer pH 7.5 for 30 h resulted in the formation of nanocapsules having silica shell thicknesses of 5 ± 1 nm, 10 ± 2 nm and 16 ± 3 nm, respectively.

(4) Reaction conditions for making silica nanocapsules are environmentally friendly, and the resulting nanocapsules are composed of biocompatible components

The key ingredient for the synthesis of oil-core silica-shell nanocapsules is the designed SurSi peptide. The use of SurSi peptide has enabled the synthesis process to be conducted under entirely benign reaction conditions, including at near-neutral pH, room temperature, and ambient pressure in the absence of toxic organic solvents. In addition, the resulted silica nanocapsules were composed of biocompatible components, including pharmaceutically-grade Miglyol® 812 oil, the peptide, and amorphous silica shell in which synthetic amorphous silica is categorized as a "Generally Recognized As Safe (GRAS)" material by the U.S. Food and Drug Administration [22].

(5) Silica nanocapsules can be used to easily encapsulate fipronil insecticide with high loading-capacity (up to 10 mg/mL) and to slowly release fipronil to aqueous phase

In **Chapter 3**, applications of the silica nanocapsules were investigated by encapsulating an insecticide fipronil. Approximately 10 mg fipronil could be directly dissolved in 1 mL of Miglyol® 812 oil and then, upon sonication, fipronil-loaded nanoemulsions could be formed. Addition of silica precursor tetraethoxysilane (TEOS) to the nanoemulsions induced reaction of TEOS with the peptide residing at the oil–water interfaces which then directed the growth of silica shell encapsulating the fipronil-loaded nanoemulsions. *In vitro* release studies of fipronil from the silica nanocapsules in water showed a decreased release rate with increasing shell thickness (i.e., 8–44 nm) indicating that the controlled release of fipronil in water from the silica nanocapsules was tunable through control of the silica shell thicknesses. These results suggested that biosilicification reaction occurred preferentially at the oil–water interface, and thus the intact structure of the oil droplets could be preserved and used to encapsulate hydrophobic actives. On the other hand, the silica shell could serve as a diffusion barrier for the controlled release of active molecules in a sustained manner.

7.1.2 Controlled-release applications of silica nanocapsules

In **Chapter 4**, biocompatible oil-core silica-shell nanocapsules developed in **Chapter 3** were investigated in a more detail as nanocarriers for controlled release of fipronil insecticide *in vitro* and *in vivo*. The loading of fipronil in the oil core prior to biomimetic growth of a layer of silica shell surrounding the core, as demonstrated in **Chapter 3**, is known as a pre-loading technique. This pre-loading technique is beneficial as to reduce the possibility of attachment of fipronil at the external surfaces of the shells, thus increasing the high-loading capacity and flexibility to protect and release the actives. To demonstrate efficacy of the fipronil-encapsulated silica nanocapsules, the nanocapsules were used to treat termites – a model insect used in this thesis.

(1) Fipronil-encapsulated silica nanocapsules show *in vivo* efficacy against termites by slowly releasing fipronil at a rate that depends on the silica shell thickness which in turn controlling killing rates of the termites

Fipronil at concentrations of 0.5 and 1 mg/mL in Miglyol® 812 oil could be encapsulated in the silica nanocapsules having different shell thicknesses (i.e., 8–44 nm), with encapsulation efficiency as high as 73%. *In vivo* efficacy of fipronil-encapsulated silica nanocapsules was tested against termites by using two different treatment-methods, i.e. direct treatment and feeding treatment. Direct treatment experiments were applied by dropping silica nanocapsules on the dorsal thorax of worker termites, in comparison with fipronil-loaded nanoemulsions (having no silica shells) and commercial Termidor® containing fipronil. Direct treatment using silica nanocapsules having three different shell thicknesses (8 nm, 25 nm and 44 nm) demonstrated that the time interval between the application of the nanocapsules and the occurrence of the termite mortality could be prolonged in a way dependent on silica shell thickness. Further, the *in vivo* efficacy of 44 nm-shell nanocapsules against orphaned groups of ≈1500 worker and soldier termites was tested by feeding treatment. The treatment used α-cellulose mixed with fipronil-encapsulated silica nanocapsules as feeding baits that were placed in vials. The vials were connected via clear plastic tubes to the boxes containing the groups of termites. The treatment results showed that the baits could be taken up from the vials by foraging workers, transmitted to recipient termites in the groups, probably through horizontal transfer, and eventually caused 100% mortality of the termite groups in 6 days after the applications which were 3 days longer than the commercial Termidor®. The more delaying insecticidal effect demonstrated by the silica nanocapsules as compared to the commercial fipronil formulation would be highly desirable as it increases the likelihood of horizontal transfer of fipronil, and hence allowing improved area-wide control of larger populations of termite colonies.

7.1.3 Design and microbial-production of a bifunctional modular protein

Results presented in **Chapter 3** have demonstrated design of the SurSi peptide that was able to stabilize nanoemulsion core and form silica shell surrounding the core. The SurSi peptide-based silica nanocapsule was used as a biocompatible nanocarrier of fipronil insecticide for its controlled release as shown in **Chapter 4**. The successful use of the silica nanocapsules certainly opens opportunities to other applications that demand biocompatibility, minimal environmental-risks, high-capacity loading, and controlled-release properties, including for biomedical and agricultural applications. Aligned with this, sustainable and scalable productions of the peptide are required. The peptide developed in **Chapter 3** is useful for research but limiting for large-scale applications as it is technically difficult and too costly for large-scale production [23] using current method which is based on solid-phase chemistry [24]. An alternative way to produce functional biomolecule as in SurSi peptide in sustainable and scalable manners is thus the objective of **Chapter 5**.

(1) Bifunctional modular proteins comprising a surface-active module and a biosilicification-active module can be designed to allow production of the proteins via microbial cell-factory *E. coli*

Recombinant DNA technology offers a method to synthesize proteins by designing a synthetic DNA encoding for proteins, and then linked the recombinant DNA to bacterial DNA and inserted into bacterial cell factory system. In this regards, *E. coli* expression systems are commonly used to express the recombinant proteins due to its low-cost of fermentation and ease of cultivation. However, expression of short recombinant peptides, though possible, is very challenging as it may be unstable in *E. coli* [25-27], and thus would significantly reduce the expression yields. To addresses these challenges, a bifunctional modular protein, D4S2 (M *DP*S MKQLADSLHQLARQVSRLEHA *DP*S MKQLADSLHQLARQVSRLEHA *DP*S MKQLADSLHQLARQVSRLEHA *DP*S MKQLADSLHQLARQVSRLEHA EPS RKKRKKRKKRKKGGGY), having 116 amino acid residues was rationally designed in **Chapter 5**. D4S2 was designed by modularizing DAMP4 variant module (M *DP*S MKQLADSLHQLARQVSRLEHA *DP*S MKQLADSLHQLARQVSRLEHA *DP*S MKQLADSLHQLARQVSRLEHA *DP*S MKQLADSLHQLARQVSRLEHA EPS) with Si peptide module (RKKRKKRKKRKKGGGY). Si peptide rich in cationic amino acid side chains known for its biosilicification activity was derived from SurSi peptide (**Chapter 3**). The DAMP4 variant module was derived from a four-helix bundle protein DAMP4 (MD(PS MKQLADS LHQLARQ VSRLEHAD)$_4$) [16] known for its surface activity except that the aspartic acid (D) residue at *C*-terminal DAMP4 was replaced with glutamic acid (E) residue followed by addition of proline (P) and serine (S) residues in order to provide molecular flexibility to the Si module projecting toward the bulk aqueous phase. The modular combination design of D4S2 allowed the protein to be synthesized in *E. coli*. D4S2 could be extracted from the cells by heating and mixing with high concentration of Na_2SO_4 to disrupt the cells releasing the intracellular protein and to precipitate most protein contaminants but maintain D4S2 solubility. The stability properties of D4S2 to high temperature and chemical denaturant were related to its four-helix bundle structure in bulk [28], as designed. Further purification via chromatography was necessary to obtain high purity of D4S2 (*M* 13308.2 Da). Culturing *E. coli* BL21(DE3) expressing D4S2 protein in 800 mL-media and then purifying the D4S2 using precipitate- and chromatography-based purification processes could yield approximately 7 mg D4S2.

(2) Presence of DNA in solutions at some concentrations can inhibit biosilicification reaction

As aforementioned, purification of D4S2 involved a two-step process based on precipitation (i.e., heating/cell lysis, contaminant precipitation, and dilute precipitation) and then followed by chromatography (i.e., immobilized-metal affinity chromatography and desalting chromatography). After the precipitation-based purification step, D4S2 protein solution contained high levels of DNA at a concentration of approximately 63 ng DNA/mg D4S2, which could be derived from either the

expression construct or the genomic DNA [29]. Protein and DNA may form non-covalent complexes via electrostatic interactions between anionic phosphate groups on the DNA and cationic functional groups on protein at physiological pH [30, 31]. When the D4S2 was used to form nanoemulsions, the nanoemulsions were negatively charges, probably because the anionic DNA residues were still present in an amount sufficient to cover the cationic protein side chains at the oil–water interfaces. Therefore, chromatography-based purification step was conducted. Thereafter, D4S2 solutions contained DNA concentration of less than 2 ng DNA/mg D4S2. At this concentration, positively-charged nanoemulsions could be produced and thus, upon biosilicification reaction with silica precursor tetraethoxysilane, silica shell could be formed.

(3) The bifunctional modular protein produced in *E. coli* demonstrates surface activity and biosilicification activity which can be used to synthesize oil-core silica-shell nanocapsules

Surface activity of D4S2 was evidenced as it substantially lowered the dynamic interfacial tension of freshly formed Miglyol® 812 oil droplet upon interfacial adsorption. Thin film of D4S2 demonstrated stability against rupture when compressed at increasing pressure likely due to high electrostatic repulsion of D4S2 at the pH that imparted mechanical resistance to the film. With the surface activity demonstrated by D4S2, D4S2 was then used for making oil-core silica-shell nanocapsules. D4S2 was shown able to facilitate formation and stabilization of nanoemulsions (comprising 10 v/v% Miglyol® 812 oil in D4S2 protein solutions) through its surface-active module and, upon addition of silica precursor tetraethoxysilane (TEOS), direct nucleation and growth of a silica layer encasing the nanoemulsion core through its biosilicification-active module under near-neutral pH and ambient temperature without using any toxic organic solvents. The outer diameter and shell thickness of the nanocapsules as measured by TEM were 249 $\pm$ 29 nm and 26 $\pm$ 2 nm.

7.1.4 Large-scale production and field application

In this thesis, the recombinant bifunctional modular protein, D4S2, was produced at approximately 1.4 g using the expression and purification processes developed in **Chapter 5**. D4S2 was used for stabilizing fipronil-loaded nanoemulsions, which comprised 10 v/v% Miglyol® 812 oil loaded with fipronil (≈0.9 g) at a concentration of 10 mg/mL, and inducing silica shell formation surrounding the nanoemulsions. The resulting fipronil-encapsulated silica nanocapsules—having outer diameter of 302 ± 16 nm and shell thickness of 57 ± 9 nm—were then used for termite field trial by mixing the nanocapsules with α-cellulose bait placed in three treatment-units which were then attached separately to three mounds of *Coptotermes lacteus* in Beerburrum (Queensland, Australia). The preliminary result showed that the treated baits were removed by the termites from the treatment-units within three weeks after treatment-units installation, with no evidence of repellence. The termite colonies are still alive after six weeks of treatments, thus the field trial was continued and is still on-

going. The time required for elimination of the colonies in mounds would be difficult to be predicted as it relies on the seasonal weather patterns, the number of alternative food sources available nearby the mound, presence of predation, population density or age of colony, and different castes of termites that have difference susceptibility on the insecticide. Nevertheless, the preliminary result indicated that the termites responded well to the treated baits as they readily removed the baits from the treatment-units within three weeks of treatments, providing a chance that the baits would be transmitted to other termites within the mounds through horizontal transfer which could then lead to potential elimination of the termite colonies.

7.2 Future work

This thesis has contributed to the development of bifunctional modular peptide and protein comprising a surface-active module and a biosilicification-active module capable of stabilizing nanoemulsion core and forming silica shell under room temperature and nearly neutral pH without using any toxic chemicals. This synthesis method offers biocompatibility and environmentally-friendly processes with an additional advantage of renewability and scalability for large-scale production of the biomolecules using biological expression [1, 2]. Furthermore, this emulsion and biomimetic dual-templating approach offers easy pre-loading of active components by simple dissolution in the oil phase with a high loading-capacity without the need for template removal, thus increasing the flexibility to protect and release the active. These research outcomes collectively show the potential of designed peptide/protein as a platform for making silica nanocapsules. However, the realization of the platform requires further study:

(1) The design of protein in **Chapter 5** allowed the protein to be synthesized in microbial cell-factory *E. coli*, promising for scalability and sustainability processes. To further demonstrate the scalability of D4S2, high-cell-density pH-stat fed-batch fermentation culture in *E. coli* [32] could be developed for large-scale production of D4S2 achieving process scale-up.

(2) **Chapter 5** has demonstrated that DNA could be problematic for the D4S2 functionality as DNA attachment on the protein could alter the charge of the protein, and thus negatively affects biosilicification reaction with the silica precursor. In this case, DNA could be removed by using immobilized-metal affinity chromatography. To achieve lower production cost, purification process to remove DNA might be optimized probably by utilizing cationic chemicals like polyethyleneimine (PEI) that could bind to DNA through electrostatic interactions [33].

(3) Following the fed-batch fermentation of *E. coli* producing D4S2 and optimized DNA removal for D4S2 purification process aforementioned, cost analysis of D4S2 production could be evaluated using a process simulation package, SuperPro Designer [34, 35]. This analysis could provide a

quantitative data of the possible economics of process scale-up of D4S2 proteins in comparison with SurSi peptide (**Chapter 3**), which was commercially produced based on solid-phase chemistry [24], for making silica nanocapsules.

(4) The use of silica nanocapsules as a biocompatible nanocarrier in agricultural applications, as demonstrated in **Chapter 4**, could be extended for biomedical applications to demonstrate the robustness and flexibility of the nanocapsules platform. For example, encapsulation of model antigen ovalbumin in silica nanocapsules and injection into mice could be conducted to investigate whether the presence of silica shell could control release of the antigen in a sustained manner thus inducing immune response of the mice.

(5) Size of nanoemulsions could be increased by decreasing the D4S2 concentrations using the same ultrasound energy, as demonstrated in **Chapter 5**. By changing the nanoemulsion size, the size of nanocapsules could also possibly be tuned to achieve micro-sized capsules. Silica microcapsules have found many applications especially for encapsulation and controlled release of fragrance and flavour in perfume and food industries [36]. Therefore, the feasibility of bifunctional modular biomolecules to synthesize silica microcapsules could be tested for future work.

(6) As reviewed in **Chapter 2**, peptides have unique sequence-specific self-assembly and recognition properties to silica material thus play critical roles in controlling the mineralization of silica nanostructures. There are also particular amino acid residue sequences that are specific to various inorganic materials beyond silica [3], e.g., FDFDFDFD that is able to direct mineralization of calcium carbonate [37]. Using the design principles of bifunctional modular biomolecules developed in **Chapter 3**, the work contained in this thesis could be extended to manufacture a calcium carbonate nanocapsule composed of an oil core and calcium carbonate shell. The nanocapsules could be useful in food industries for the encapsulation and release of flavour [38].

7.3 Concluding thoughts

Nature's ability to form silica with controlled structure and properties as in diatoms, sponges, and plants [39] under aqueous conditions at ambient temperatures and pressures, near-neutral pH in the absence of toxic organic solvents [40] have great impact from the intersection of molecular and inorganic chemistry. The biological principle in biosilicification has been an inspiration to direct "bottom-up" synthesis of silica-based nanomaterials *in vitro* by mimicking functionality of the mineralizing proteins in the living organisms [41]. Although a lot of research has directed to use peptide/protein to form silica-based nanomaterials based on bulk reaction and at solid–liquid

interfaces, there is no current biomimetic approach at oil–water interfaces to make silica nanocapsules having oil-core silica-shell architecture. Thus, this thesis has contributed to the development of a novel dual-templating biomimetic approach and new design of modular peptide/protein, SurSi peptide and D4S2 protein, for biosilicification at oil–water interfaces, offering opportunities to develop nanocarriers of various hydrophobic actives having biocompatibility, high encapsulation-efficiency, and controlled-release properties. Both biomolecules have similar concept of design, that is, linking a surface-active module and a biosilicification-active module, thus enabling stabilization of nanoemulsion core and formation of a silica shell for making oil-core silica-shell nanocapsules. Furthermore, the use of D4S2 protein taking advantage of the bioprocessing production route through *E. coli* expression systems has opened opportunities for sustainable, scalable and environmentally-friendly processes to produce silica nanocapsules, and thus making the platform developed in this thesis suitable for large-scale applications of the silica nanocapsules in fields of biomedical and agricultural applications.

References

1. Kyle, S., A. Aggeli, E. Ingham, and M.J. McPherson, *Production of self-assembling biomaterials for tissue engineering.* Trends Biotechnol., 2009. **27**(7): p. 423–433.
2. Morreale, G., E.G. Lee, D.B. Jones, and A.P.J. Middelberg, *Bioprocess-centered molecular design (BMD) for the efficient production of an interfacially active peptide.* Biotechnol. Bioeng., 2004. **87**(7): p. 912–923.
3. Chen, C.-L. and N.L. Rosi, *Peptide-based methods for the preparation of nanostructured inorganic materials.* Angew. Chem., Int. Ed., 2010. **49**(11): p. 1924–1942.
4. Dickerson, M.B., K.H. Sandhage, and R.R. Naik, *Protein- and peptide-directed syntheses of inorganic materials.* Chem. Rev., 2008. **108**(11): p. 4935–4978.
5. Patwardhan, S.V., *Biomimetic and bioinspired silica: recent developments and applications.* Chem. Commun., 2011. **47**(27): p. 7567–7582.
6. Dexter, A.F. and A.P.J. Middelberg, *Peptides as functional surfactants.* Ind. Eng. Chem. Res., 2008. **47**(17): p. 6391–6398.
7. Yuwono, V.M. and J.D. Hartgerink, *Peptide amphiphile nanofibers template and catalyze silica nanotube formation.* Langmuir, 2007. **23**(9): p. 5033–5038.
8. Altunbas, A., N. Sharma, M.S. Lamm, C. Yan, R.P. Nagarkar, J.P. Schneider, and D.J. Pochan, *Peptide–silica hybrid networks: biomimetic control of network mechanical behavior.* ACS Nano, 2010. **4**(1): p. 181–188.
9. Wang, S., X. Ge, J. Xue, H. Fan, L. Mu, Y. Li, H. Xu, and J.R. Lu, *Mechanistic processes underlying biomimetic synthesis of silica nanotubes from self-assembled ultrashort peptide templates.* Chem. Mater., 2011. **23**(9): p. 2466–2474.

10. Kröger, N., R. Deutzmann, and M. Sumper, *Polycationic peptides from diatom biosilica that direct silica nanosphere formation.* Science, 1999. **286**(5442): p. 1129–1132.
11. Naik, R.R., P.W. Whitlock, F. Rodriguez, L.L. Brott, D.D. Glawe, S.J. Clarson, and M.O. Stone, *Controlled formation of biosilica structures in vitro.* Chem. Commun., 2003(2): p. 238–239.
12. Knecht, M.R. and D.W. Wright, *Functional analysis of the biomimetic silica precipitating activity of the R5 peptide from Cylindrotheca fusiformis.* Chem. Commun., 2003. **-**(24): p. 3038–3039.
13. Bellomo, E.G. and T.J. Deming, *Monoliths of aligned silica-polypeptide hexagonal platelets.* J. Am. Chem. Soc., 2006. **128**(7): p. 2276–2279.
14. Graf, P., A. Mantion, A. Haase, A.F. Thuenemann, A. Mašic, W. Meier, A. Luch, and A. Taubert, *Silicification of peptide-coated silver nanoparticles—a biomimetic soft chemistry approach toward chiral hybrid core–shell materials.* ACS Nano, 2011. **5**(2): p. 820-833.
15. Brott, L.L., R.R. Naik, D.J. Pikas, S.M. Kirkpatrick, D.W. Tomlin, P.W. Whitlock, S.J. Clarson, and M.O. Stone, *Ultrafast holographic nanopatterning of biocatalytically formed silica.* Nature, 2001. **413**(6853): p. 291–293.
16. Middelberg, A.P.J. and M. Dimitrijev-Dwyer, *A designed biosurfactant protein for switchable foam control.* ChemPhysChem, 2011. **12**(8): p. 1426–1429.
17. Dexter, A.F., A.S. Malcolm, and A.P.J. Middelberg, *Reversible active switching of the mechanical properties of a peptide film at a fluid–fluid interface.* Nat. Mater., 2006. **5**(6): p. 502–506.
18. Chuan, Y.P., B.Y. Zeng, B. O'Sullivan, R. Thomas, and A.P.J. Middelberg, *Co-delivery of antigen and a lipophilic anti-inflammatory drug to cells via a tailorable nanocarrier emulsion.* J. Colloid Interface Sci., 2012. **368**(1): p. 616–624.
19. Dickerson, M.B., S.E. Jones, Y. Cai, G. Ahmad, R.R. Naik, N. Kröger, and K.H. Sandhage, *Identification and design of peptides for the rapid, high-yield formation of nanoparticulate TiO2 from aqueous solutions at room temperature.* Chem. Mater., 2008. **20**(4): p. 1578–1584.
20. Cha, J.N., K. Shimizu, Y. Zhou, S.C. Christiansen, B.F. Chmelka, G.D. Stucky, and D.E. Morse, *Silicatein filaments and subunits from a marine sponge direct the polymerization of silica and silicones in vitro.* Proc. Natl. Acad. Sci. U. S. A., 1999. **96**(2): p. 361–365.
21. Cha, J.N., G.D. Stucky, D.E. Morse, and T.J. Deming, *Biomimetic synthesis of ordered silica structures mediated by block copolypeptides.* Nature, 2000. **403**(6767): p. 289–292.
22. U.S. Food and Drug Administration's Website, *GRN No. 321: Synthetic amorphous silica*. Available from: http://www.accessdata.fda.gov/scripts/fcn/gras_notices/GRN000321.pdf. Cited 21 May 2014.
23. Latham, P.W., *Therapeutic peptides revisited.* Nat. Biotechnol., 1999. **17**(8): p. 755–757.
24. Merrifield, R.B., *Solid phase peptide synthesis. 1. Synthesis of a tetrapeptide.* J. Am. Chem. Soc., 1963. **85**(14): p. 2149–2154.

25. Itakura, K., T. Hirose, R. Crea, A.D. Riggs, H.L. Heyneker, F. Bolivar, and H.W. Boyer, *Expression in Escherichia coli of a chemically synthesized gene for hormone somatostatin.* Science, 1977. **198**(4321): p. 1056–1063.
26. Goeddel, D.V., D.G. Kleid, F. Bolivar, H.L. Heyneker, D.G. Yansura, R. Crea, T. Hirose, A. Kraszewski, K. Itakura, and A.D. Riggs, *Expression in Escherichia coli of chemically synthesized genes for human insulin.* Proc. Natl. Acad. Sci. U. S. A., 1979. **76**(1): p. 106–110.
27. Shine, J., I. Fettes, N.C.Y. Lan, J.L. Roberts, and J.D. Baxter, *Expression of cloned β-endorphin gene sequences by Escherichia coli.* Nature, 1980. **285**(5765): p. 456–461.
28. Dimitrijev-Dwyer, M., M. Brech, L. Yu, and A.P.J. Middelberg, *Intensified expression and purification of a recombinant biosurfactant protein.* Chem. Eng. Sci., 2014. **105**(-): p. 12–21.
29. Gregory, C.A., G.P. Rigg, C.M. Illidge, and R.C. Matthews, *Quantification of Escherichia coli genomic DNA contamination in recombinant protein preparations by polymerase chain reaction and affinity-based collection.* Anal. Biochem., 2001. **296**(1): p. 114–121.
30. Harrison, S.C. and A.K. Aggarwal, *DNA recognition by proteins with the helix-turn-helix motif.* Annu. Rev. Biochem., 1990. **59**: p. 933–969.
31. Kalodimos, C.G., N. Biris, A. Bonvin, M.M. Levandoski, M. Guennuegues, R. Boelens, and R. Kaptein, *Structure and flexibility adaptation in nonspecific and specific protein-DNA complexes.* Science, 2004. **305**(5682): p. 386–389.
32. Lee, S.Y., *High cell-density culture of Escherichia coli.* Trends Biotechnol., 1996. **14**(3): p. 98–105.
33. Dai, Z. and C. Wu, *How does DNA complex with polyethylenimine with different chain lengths and topologies in their aqueous solution mixtures?* Macromolecules, 2012. **45**(10): p. 4346–4353.
34. Chuan, Y.P., N. Wibowo, L.H.L. Lua, and A.P.J. Middelberg, *The economics of virus-like particle and capsomere vaccines.* Biochem. Eng. J., 2014. **90**: p. 255–263.
35. Lee, G.H., D. Cooney, A.P.J. Middelberg, and W.S. Choe, *The economics of inclusion body processing.* Bioproc. Biosyst. Eng., 2006. **29**(2): p. 73–90.
36. Ciriminna, R., A. Fidalgo, V. Pandarus, F. Béland, L.M. Ilharco, and M. Pagliaro, *The sol–gel route to advanced silica-based materials and recent applications.* Chem. Rev., 2013. **113**(8): p. 6592–6620.
37. Volkmer, D., M. Fricke, T. Huber, and N. Sewald, *Acidic peptides acting as growth modifiers of calcite crystals.* Chem. Commun., 2004. **-**(16): p. 1872–1873.
38. Wang, X.L., W.Z. Zhou, J. Cao, W.C. Liu, and S.P. Zhu, *Preparation of core–shell $CaCO_3$ capsules via Pickering emulsion templates.* J. Colloid Interface Sci., 2012. **372**(-): p. 24–31.
39. Patwardhan, S.V., S.J. Clarson, and C.C. Perry, *On the role(s) of additives in bioinspired silicification.* Chem. Commun., 2005. **-**(9): p. 1113–1121.
40. Mann, S., *Biomineralization and biomimetic materials chemistry.* J. Mater. Chem., 1995. **5**(7): p. 935–946.

41. Mann, S., *Biomineralization: Principles and Concepts in Bioinorganic Materials Chemistry*. 2001, New York: Oxford University Press.

Appendix A

Experimental set-up for termite control experiments in a laboratory scale

The following Appendix contains several photographic images describing method section, *in vivo* study against termites, in **Chapter 4**.

Figure A1. Photographic images of the collection of *Coptotermes acinaciformis* from Esk, Queensland, Australia. a–c) Technique to collect termites: trench was constructed and filled with timbers (a); moist woods covered with insulating material were placed in plastic containers and then secured with soil (b); and the plastic containers (lid off) were inverted and placed onto the

timber-filled trench (c). d, e) Difference in physical appearance of the moist woods: before (d) and after (e) termite infestations. f–h) Termites isolated from the infested woods: Magnification figure of the infested wood shows the presence of galleries built by the termites (f); collected worker and soldier termites by gently tapping them out from the infested woods (g); actively moving worker termites were carefully selected from the colonies and placed in a petri dish containing a filter paper for direct treatment (h)—this figure shows a piece of the filter paper consumed by the worker termites which demonstrated that the filter paper could be utilized as a food source for termites during direct treatment. i) *Nasutitermes magnus* mound materials used for feeding treatment.

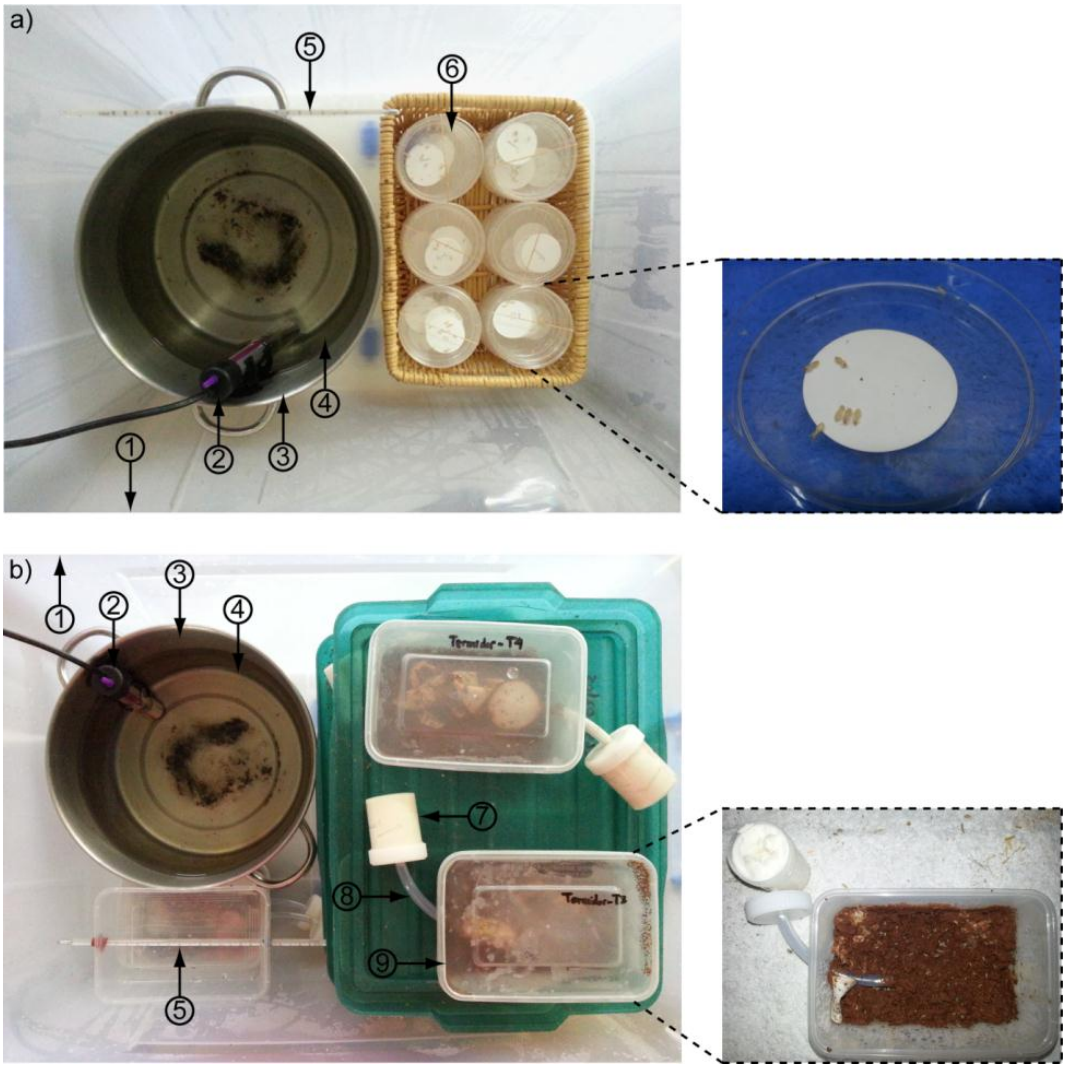

Figure A2. Experimental units for *in vivo* efficacy test of nanocapsules against termites on direct treatment (a) and feeding treatment (b). 1) Chamber; 2) Heater; 3) 11.5-L metal container; 4) Water; 5) Thermometer; 6) Petri dish containing a filter paper and 10 *Coptotermes acinaciformis* worker termites; 7) Feeding vial containing moist α-cellulose bait, 8) Vinyl tubing, and 9) Container containing mound materials, water and ≈1,500 *Coptotermes acinaciformis* worker and soldier termites.